Delamination of Cross-laminated timber and its impact on fire development

Focusing on different types of adhesives

Eric Johansson
Anton Svenningsson

Division of Fire Safety Engineering
Lund University, Sweden

Brandteknik
Lunds tekniska högskola
Lunds universitet

Report 5562, Lund 2018
Examensarbete på Civilingenjörsprogrammet i Riskhantering

Delamination of Cross-laminated timber and its impact on fire development | Focusing on different types of adhesives

Eric Johansson
Anton Svenningsson

Lund 2018

Titel
Delaminering av korslimmat trä och dess inverkan på brandförloppet | Med fokus på olika limtyper
Title
Delamination of Cross-laminated timber and its impact on fire development | Focusing on different types of adhesives

Authors
Eric Johansson
Anton Svenningsson

Report 5562
ISSN: 1402-3504
ISRN: LUTVDG/TVBB—5562—SE

Number of pages: 182
Illustrations: Eric Johansson and Anton Svenningsson unless otherwise stated

Keywords
CLT, cross-laminated timber, X-lam, delamination, engineered timber, adhesive, glue

Sökord
KL-trä, korslimmat trä, X-lam, delaminering, limträ, bindemedel, lim

Abstract
In the recent decade, the interest of building taller all-timber structures using engineered timber materials such as cross-laminated timber (CLT) has increased substantially. On the other hand, there's also a significant resistance and fear concerning the fire safety of buildings with wood-based load-bearing structures. In this report, the aim is to investigate the potential deviations of the fire performance of CLT. More specifically the occurrence of losing entire layers due to fire exposure, delamination, and how this might affect the fire development. Fire tests were performed in a standard testing furnace with specimens of CLT manufactured with five different adhesives. For these tests, the fire conditions of a previous full-scale test were attempted to be replicated. After evaluating the results, it was concluded that the type of adhesive used, could have a significant impact on whether a CLT-element delaminates or not. Furthermore, delamination also has a severe impact on the fire development, increasing the temperatures and extending the duration of the fire. CLT as a future building material still faces a lot of challenges, and further research is needed to optimise the composition of the material and investigate complications other than fire performance as well.

Brandteknik
Lunds tekniska högskola
Lunds universitet
Box 118
221 00 Lund

www.brand.lth.se
Telefon: 046 - 222 73 60

Division of Fire Safety Engineering
Faculty of Engineering
Lund University
P.O. Box 118
SE-221 00 Lund
Sweden

www.brand.lth.se
Telephone: +46 46 222 73 60

Preface

This report is a part of the final examination from Lund University and the Master of Science Engineering programme in Risk Management and Fire Safety Engineering. Executed experiments in this report is part of a project by the National Fire Protection Association (NFPA). The NFPA-report (Brandon & Dagenais, 2018), can be found on the NFPA website.

This report is a result of months of hard work and many hours spent at Lund University and the RISE facility in Stockholm. Through good and bad times, we have tackled problems together and gained a lot of new experience along the way. It has truly been an amazing journey and we are proud of have been a part of it.

During the progress of this report, there are some people for whose support and guidance we are very grateful, and we would like to especially thank the following:

Håkan Frantzich, *researcher at the Division of Fire Safety Engineering at Lund University,* for being our head supervisor during this project with your guidance and support.

Daniël Brandon, *scientist at Research Institutes of Sweden, RISE,* for being our supervisor at RISE and giving us the opportunity to make this report possible.

Alar Just, *researcher at Research Institutes of Sweden, RISE,* for your knowledge and assistance during the experimental parts of this project, and your exceptional skills in controlling the furnace.

Mattia Tiso, *PhD-student at Research Institutes of Sweden, RISE,* for your assistance during the final experiments and your valuable input.

Barry Lewis, *yttre befäl at Storstockholms brandförsvar, SSBF*, for assisting us with accommodation and giving us the opportunity to learn more about your organisation. Thanks for making our stay in Stockholm a great experience.

Erik Nilsson, *Student at the Risk Management and Safety Engineering programme,* for your proofreading of this report and your valuable input.

Executive Summary

Cross-laminated Timber, or CLT, is an engineered timber product, were the disadvantages of single wood components are mitigated by gluing timber boards together in layers perpendicular to each other. The result are pre-fabricated elements which have a high strength to weight ratio and can be used as load-bearing walls as well as joist floor structures. Research and relaxation of building regulations continues to push the boundaries of what is possible for timber structures, and in the last decade there has been an ever-growing interest to construct taller and taller all-timber buildings.

However, there's also a significant fear of the use of timber as load-bearing components in high-rise structures, especially from a fire safety perspective. On one hand, wood materials are credited for their slow and predictable fire performance, as the material forms a protective char layer while burning and the remaining fresh wood maintains some level of load-bearing capacity. On the other hand, by introducing wood to the load-bearing structure, the overall total fire load is increased substantially. It's also not entirely clear how glued engineered timber elements actually performs in fire, and any deviation from the fire behaviour of solid wood could mean serious complications.

In recent years extensive research into the fire performance of engineered timber elements have been conducted. As a part of the NFPA project *Fire Safety Challenges of Tall Wood Buildings*, a full-scale test involving CLT elements was carried out in 2017. In this test, it was observed that for some elements, the first and second lamella of the CLT fell off entirely due to the fire exposure, a phenomenon termed delamination. Previous research had also suggested that the type of adhesive used could have a significance as to whether or not delamination of CLT occurred.

The purpose of this report has been to, within the frame of the continuing NFPA project, examine the occurrence and effect of delamination of CLT elements in regard to the adhesive type used. As full-scale testing can be very costly and it's unreasonable to limit the experiment to just one single phenomena at that scale, it was decided to attempt to recreate the fire conditions of the full-scale test in a standard test furnace at the RISE facility in Stockholm.

A total of ten tests were performed with two sets of specimens manufactured with five different adhesives, were two of the specimens had been cut directly from leftover elements from the original full-scale test. Measurements were made directly or calculated, to indicate and study the effects of delamination, including: the temperature profile inside the specimen, charring rate and heat flux. Additionally, the furnace temperature and oxygen level were chosen as target parameters for the task of replicating the fire behaviour of the full-scale test.

Out of all the specimen only the two original full-scale test specimen exhibited complete delamination, which in turn verified the results of the full-scale tests to some extent. The delamination severely impacted the fire development, as the underlying layer was instantaneously ignited. It also became apparent that if delamination occurred, the task of controlling the target fire conditions became far more difficult.

It became clear that the adhesive type used could have a major impact on the fire development, and that the preference should be for CLT elements to perform similarly to solid wood when exposed to fire. This in turn means that delamination should be avoided at all cost by choosing the most optimal adhesive.

CLT as a building material shows great potential for future sustainable structures, but also faces a lot of challenges. There's still a lot of questions that needs answering in order to objectively evaluate the extent to which CLT and engineered timber material can be used in future structures. The final goal being a future with reliable and safe timber structures.

Sammanfattning

Korslimmat trä, eller KL-trä, är en form av limträprodukt, där träpaneler limmats ihop tillsammans med vartannat lager lagt rätvinkligt mot det föregående. Grundkonceptet är att defekter i de enskilda, ingående träkomponenterna blir av mindre betydelse och materialet blir mer homogent. Resultatet blir pre-fabricerade element med hög styrka i förhållande till deras vikt, vilka kan användas som såväl bärande väggar som hela golvbjälklag. Forskning och lättnader i byggreglementen fortsätter att driva utvecklingen framåt för användningen av limträprodukter och under det senaste årtiondet har intresset för att bygga höga hus helt i trä ökat markant.

Det finns dock ett tydligt motstånd mot det ökande användandet av trä i lastbärande konstruktioner, och då framförallt ur ett brandskyddsperspektiv. Trämaterial beskrivs förvisso uppvisa ett långsamt och förutsägbart brandbeteende, då de förkolnar och kollagret bildar en form av isolerande lager. Det trä som inte ännu påverkats av förkolningen bibehåller dessutom en del av dess lastbärande kapacitet. Det går däremot inte att bortse ifrån det faktum att den totala brandbelastningen ökar avsevärt då även det bärande stommaterialet utgörs av ett brännbart material som trä. Det är även inte helt utrett exakt hur alla typer av limträprodukter beter sig vid brand och avvikelser från det normala brandbeteendet för obehandlat trä, kan ha stor betydelse.

De senaste åren har omfattande forskning bedrivits för att undersöka hur limträprodukter presterar vid brand. Som en del av projektet *Fire Safety Challenges of Tall Wood Buildings* som drivs av NFPA, utfördes 2017 ett fullskaleförsök med KL-trä. Under detta test observerades att för en del av KL-trä-elementen lossnade det första och andra lagret helt till följd av brandpåverkan, ett fenomen som kallas delaminering. Tidigare forskning hade även påvisat limmets betydelse för om delaminering kunde tänkas ske.

Syftet med detta examensarbete har varit att inom ramen för NFPA-projektet undersöka förekomsten och effekterna av delaminering, med fokus på olika limtyper. Ett fullskaleförsök kan innebära mycket höga kostnader och då det i en sådan kontext kan vara orimligt att enbart studera ett enskilt fenomen, togs beslutet att försöka återskapa förhållanden i branden från fullskaleförsöket, i en mindre standardförsöksugn på RISE-anläggning i Stockholm.

Totalt tio försök genomfördes med två uppsättningar av provkroppar tillverkade med fem olika limtyper, varav två av provkropparna hade skurits direkt från kvarvarande element från det ursprungliga fullskaleförsöket. Mätningar och beräknade värden från försöken grundade sig i att kunna indikera förekomsten och effekterna av delaminering, vilket inkluderade: temperaturprofiler inne i provkropparna, förkolningshastighet och värmeflöde. Utöver detta användes även mätningar av ugnstemperaturen och syrenivån för att kunna styra ugnen och återskapa de aktuella brandförhållandena.

Av alla provkroppar så var det enbart de två från fullskaleförsöken som uppvisade fullständig delaminering, vilket till viss utsträckning bekräftade resultatet från fullskaleförsöket. Delamineringen hade en betydande inverkan på brandförloppet, till följd av att det efterliggande lagret antände ögonblickligen. Det blev även mycket tydligt att om delaminering inträffade så blev det betydligt svårare att styra brandförhållandena i ugnen. Därav stod det klart att valet av lim kan ha en avsevärd påverkan på hur brandförloppet kan tänkas utvecklas, och att målet bör vara att KL-trä ska bete sig som solitt trä vid brand. Det betyder med andra ord att delaminering bör undvikas till varje pris genom att välja det mest lämpade limmet.

KL-trä uppvisar stor potential som byggnadsmaterial för framtida konstruktioner, med står även inför många utmaningar. Många obesvarade frågor återstår innan en helt objektiv bedömning kan göras för att fastställa till vilken utsträckning KL-trä kan tillämpas i framtidens säkra och hållbara byggnader.

Abbreviations

CLT - Cross-laminated timber

LVL - Laminated Veneer Lumber

NFPA - National Fire Protection Association

NIST - National Institute of Standards and Technology

RISE - Research Institutes of Sweden

LCA - Life Cycle Analysis

GHG - Green House Gases

PUR - Poly-urethane

MF - Melamine Formaldehyde

EPI - Emulsion Polymer Isocyanate

PRF - Phenol Resorcinol Formaldehyde

RCSM - Reduced Cross-Section Method

ZSL - Zero Strength Layer

ISO - International Organization for Standardization

ASTM - American Society for Testing and Materials

CPR - Construction Products Regulations

BBR - Boverkets Byggregler

EKS - Europeiska Konstruktionsstandarder

ANSI - American National Standards Institute

TC - Thermocouple

PT - Plate Thermometer

Table of content

1 Introduction

1.1 Background

In the last decade, the use of engineered, heavy timber products such as Cross-Laminated Timber (CLT) has seen a significant increase in Europe as well as the rest of the world. Utilising the anisotropy of wood to its advantage, CLT is constructed by glueing timber boards together in layers rotated perpendicular to one another. This innovative solution has shown great potential, and elements of CLT can be utilised as load-bearing walls as well as joist floor structures.

CLT-elements have a high load-bearing capacity in relation to their weight, providing good thermal and acoustic insulation as well as making construction easier and quicker (Yeh, et al., 2013). Updates of fire regulations around the world and modern architectural trends have resulted in an increased interest in taller buildings comprised by only engineered timber elements (Emberley, et al., 2017).

First introduced in Austria and Germany in the 1990s, CLT was developed through the combined effort of academia and industry in Austria. In the beginning of the new millennium, the interest for CLT in the construction of mid-rise (5-10 storeys) buildings in Central Europe greatly increased, establishing CLT as an efficient, heavy construction system in Europe (Gagnon, et al., 2013). For a long time, restrictions in national building regulations severely limited the use of timber in load-bearing structures, and in particular in regard to high-rise constructions. As extensive research of the fire performance of timber products was conducted and relaxations of regulations followed, engineered timber products such as CLT saw a renaissance all over Europe and North America (Östman, et al., 2017).

In Sweden, an update of the restriction regarding number of storeys for timber buildings changed the building codes in 1994. Introducing novel timber materials like CLT meant that the construction of higher timber structures became a real possibility (Brandskyddsföreningen, 2017). For a country like Sweden, with a prominent and large timber industry, this most certainly sparked an interest. In the last decades, an increasing number of multi-storey buildings with timber load-bearing structures has been constructed. Buildings as the eight-storey structure of Limnologen in Växjö and Strandparken in Sundbyberg, Stockholm, with its nine storeys. The future might hold even more impressive timber structures such as the 34-storey tall HSB Västerbroplan in Stockholm, the winning contribution of HSB architectural competition for their 100th anniversary in 2023 (C.F. Möller, 2013). This development has particularly benefitted from the general perception of wood as a sustainable and renewable material, which makes for key arguments in many initiatives (Brandon & Östman, 2016).

Yet, there is still a considerable resistance to all-wood structures considering fire protection, moisture resistance and if wood-based building materials truly are as sustainable as claimed by producers. The sustainability of wood materials all comes down to how calculations are performed and mistakes in the construction of wood structures could result in severe moisture-related damages. The fire resistance aspect, however, is of particular significance as it concerns the very safety of residents and the emergency rescue services. The fact remains that wood is a combustible material, and in using such materials for the entire load-bearing structure, the total potential fire load increases substantially.

In the context of designer methods like reliability-based fire design and more specifically the uncertainties concerning fire design of timber structures, there are countless parameters affecting the true reliability of the final structure. The building codes of today present relatively high safety factors, this in combination with a lack of knowledge about the actual behaviour of materials could result in a view that absolute safety can be achieved, which is not the case (Thoft-Christensen & Baker, 1982). However, it's important to remember that the true goal is to recognize the risks and find the acceptable level of tolerance.

What is an acceptable level of tolerance, and what does it mean for the future of tall timber structures? For the future development of taller timber structures, novel engineered timber products will be crucial, and as such the reliability of such elements becomes a priority. This, in turn, means that in order to find an acceptable level of tolerance, the knowledge gap needs to be bridged concerning engineered timber products like CLT, which is achieved through continuous research.

A great amount of research has been done to study the fire-related properties of CLT, a substantial amount of this research has been executed within research projects such as the *Fire Safety Challenges of Tall Wood Buildings*, organized by the National Fire Protection Research Foundation (NFPA). Other great examples are the research by Bartlett et al. (2017) and Emberley et al. (2017) on the conditions for self-extinction of fire in CLT-elements.

When it comes to the fire resistance properties of CLT one of the main concerns is the risk of entire layers losing bond strength and falling off, which is known as delamination. In previous full-scale experiments by Medina Hevia (2014) and McGregor (2013), the occurrence of delamination has been observed, and even more importantly an immediate ignition of the underlying layer, resembling a second flash-over. The results of Medina Hevia (2014) also suggested that the adhesive used to bond the CLT together could have a significant impact on the occurrence of delamination.

In the beginning of 2017 as part of the second phase of the NFPA project *Fire Safety Challenges of Tall Wood Buildings*, a full-scale test involving CLT elements was carried out in Canada with the assistance of the National Institute of Standards and Technology (NIST). During these NIST-tests, the phenomena of delamination were observed as well (Su, et al., 2017), highlighting the complications of what this could mean for the fire performance of certain CLT-materials. It became apparent that this was a subject in need of further investigation. Previous research concerning CLT and delamination had all been full-scale fire tests or standardised furnace tests, but in order to verify these results, a different approach was suggested. What if the fire conditions of Su et al. (2017) could be replicated to a satisfactory extent within the more controllable environment of a standard furnace?

Not only are furnace tests less costly than full-scale testing, but it would also present the opportunity of investigating if the procedure of simulating a natural fire in a furnace is practically possible. If so, it could not only be applied to verify the full-scale results, but also for future stand-alone testing with more realistic fire exposure, as standard fires, in reality, have very little to do with real fire conditions. It was decided that this type of experiment was to be attempted at the RISE-facility in Stockholm (former Trätek), and part of the outcome of these experiments comprise the foundation of this report.

1.2 Purpose & objectives

The main purpose of this report is to expand the knowledge and understanding of the process of delamination of CLT, and to which degree the adhesive used effects this process. This information will be evaluated in a reliability-based fire design context, and from this, conclusions concerning the future potential of the material will be formulated.

The following research questions will constitute the foundation of this report:

- What effect do different adhesives have on the occurrence, and process of delamination of CLT-elements?
- If delamination of a CLT-element occurs, what are the effects on the fire conditions?
- What meaning could the results possibly have for future research projects involving engineered timber elements?

1.3 Methodology

This section presents a brief description of the different phases and methodology that was performed to accomplish this report.

1.3.1 Start-up

In the start-up phase of this report all the major practical details with RISE as well as with the Division of Fire Safety Engineering at Lund University had to be managed. This phase mainly consisted of networking with contacts at RISE as well as our supervisor at Lund University. A project plan was made to get the report started including purpose, objectives and question formulation of the report.

1.3.2 Preparations & pilot tests

After the start-up phase was completed preparations for the upcoming experimental trials were to begin. Initially, this involved obtaining more information about the subject in general and discuss the experimental methodology with RISE which resulted in a trial plan. A substantial part of this preparational phase was spent with literature studies and other research, in order to increase the knowledge about the fire properties of CLT and wood-based materials.

A couple of simple pilot tests were conducted in order to practice the experimental procedure and verify that the replication of the full-scale fire could be performed as intended.

1.3.3 Experimental phase

The experiments were performed at the RISE fire testing facility in Stockholm (former SP Trätek). Samples of CLT was manufactured with different types of adhesives and were exposed to a one-dimensional fire load in a furnace setup. The focus of the experiments was to gather data that could determine the occurrence of delamination.

1.3.4 Data analysis

When the experimental phase was over, analysis of the data began. Important measurements and calculations are presented for further discussions. Output data has been sorted and structured in a more readable manner in the form of graphs and tables.

1.3.5 Discussion and conclusions

In the final phase, the result of the data analysis was discussed and evaluated based on the formulated questions and a risk point of view. From this discussion and the knowledge from the early research and literature studies, a set of conclusions was formulated to summarise the outcome of this report and to present suggestions for further research.

1.4 Limitations & Delimitations

This report is based on a limited set of experiments which were originally planned by RISE. This being the case, the possibility of adjusting and changing experiment parameters has been considerably limited. In summary, these are the main limitations and delimitations of this report:

<u>Limitations</u>

- To the fullest possible extent, the fire conditions will be replicated from previously performed full-scale experiments (Su, et al., 2017). Since a standard fire is not used, the result can be difficult to compare to previous or future small-scale tests.
- The specimens used in the experiments will be manufactured off-site at FP-innovation in Canada. This means that the authors will have very little control of aspects concerning the manufacturing and possible limitations therein.

- Only one of each kind of adhesive will be studied, except for the Poly-Urethane (PUR) – adhesives. Earlier research indicates that the difference in performance even between different brands of the same adhesive type can be significant (Klippel, 2014).

Delimitations

- Only one-dimensional fire impact on a horizontal specimen will be studied, this could be compared with a floor/ceiling element being affected by a fire from below.
- The adhesive will be the only differentiating parameter between specimens.

2 Wood as a building material

2.1 Characteristics of wood

In contrast to other building materials utilised in load-bearing structures, wood is rather unique in respect to it being a completely natural, organic material. When stored, used and treated correctly it's a strong, but light material, with supreme elasticity and good insulation properties, all while being aesthetically pleasing (Zhang, 2011).

It's a fibrous material consisting mainly of cellulose with a given direction and internal organization (Zhang, 2011). Cellulose, which comprises the main component of all high plant life, is a condensation polymer with a linear structure forming bundles which provide stability for the cell walls of the plant (Drysdale, 2011). From a macroscopic perspective, the tree consists of a central pith followed by the heartwood, sapwood, cambium, and finally the inner and outer bark. This structure can primarily be described by three main directions: the fibre/grain direction, radial direction and tangential direction, see fig. 2-1. The non-homogenous structure and different properties along these directions, result in wood being a highly anisotropic material (Burström, 2007).

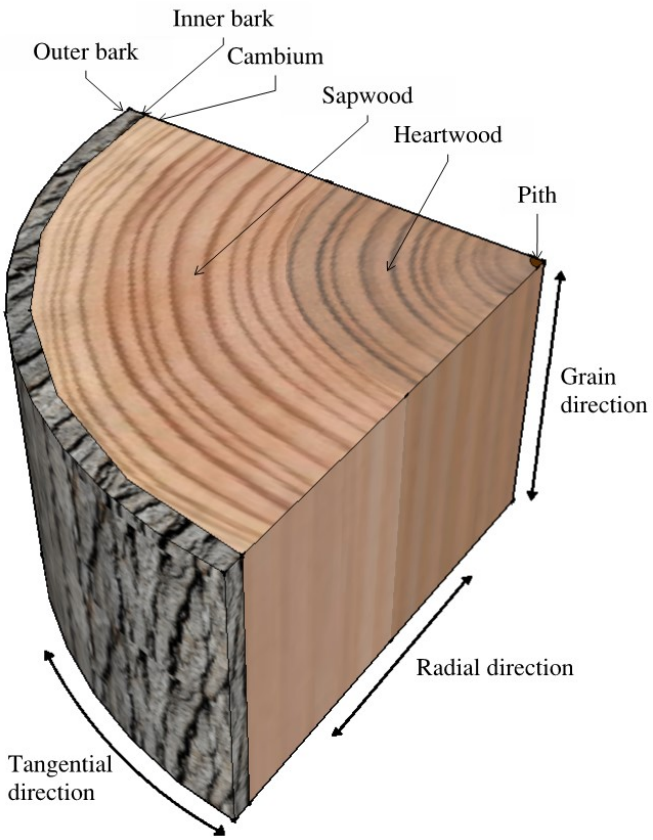

fig. 2-1. Cross-section sketch of a wood sample

When considering the strength of wood, as wood is an anisotropic material, the strength parallel to the grain and perpendicular to the grain are very different. The highest level of strength is exhibited through tensile strength in the grain direction, compression in this direction yields only half of this strength, as the fibres bend (Burström, 2007). The strength perpendicular to the grain can vary greatly, and tangential static bending of flawless specimens are used when grading wood strength. Characteristic values far lower than the actual strength are used, as there are numerous deviations and factors that affect the strength (Zhang, 2011).

From a holistic perspective, the primary production of wood is represented by the growth of the tree followed by lumbering, temporary storage in the forest and ultimately transportation to a sawmill for further processing. During all of these processes, a wide variety of defects can arise in the wood, such as forming of knots and splits, grain disorder, curving, decay, as well as rot and impact of fungi and pests (Zhang, 2011), see fig 2-2. Additionally, most properties of wood are affected by the moisture content, as all wood species bond and absorb water to a high extent (Burström, 2007), see section 2.2.

fig.2-2. Examples of different defects in wood.

This, in turn, has the effect that the degree of control over material quality is lower for wood than for materials produced through a completely industrial process. In the end, it becomes a matter of choosing wood of sufficient quality for construction applications. Heavy timber products are therefore divided into different classes based on their performance and strength, limiting the available supply of quality load-bearing massive timber products further. However, the development of engineered timber products based on waterproof adhesive methods has made this less of a problem (Burström, 2007), the product as a whole compensates for individual deficiencies in each component, see section 2.4.

2.2 Wood and moisture

As an organic material, wood can hold substantial amounts of water. The cell walls of wood consist of bundles of cellulose fibres, it's these fibres that can absorb water until the fibre saturation point is reached (Nevander & Elmarsson, 1994), this point is generally from 25 to 35 % of the mass (Zhang, 2011). Still, this is not freely available water, and the fibre saturation point represents an approximate moisture equilibrium of the wood. In other words, additional water can be absorbed by the wood in the form of free water storage in the spaces in between the cells (Burström, 2007).

The main reason why this aspect is relevant concerns the potential damage large amounts of water could have on wood as a building material. In particular, within the frame of this report, this becomes an issue when water is used for extinguishing purposes in the context of fire. This is most commonly the case in traditional fire-fighting efforts, as well as when a sprinkler system is activated. When the amount of water used widely exceeds the amount actually needed in order to control or extinguish a fire, water damages of organic building materials such as wood can become a serious problem (Särdqvist, 2013).

It's not only a question of generally reduced characteristic properties of wood as a result of higher moisture content, but secondary effects of moisture also affect the material. Wood-based materials are subject to moisture-related movement, when the moisture content is high, the wood swells and when moisture content is low it begins to shrink. These movements are most pronounced in the radial direction of the wood, see fig 2-1, but the moisture transport in the material is highest in the grain direction (Zhang, 2011), the material might swell as much as 2 to 14 % in the radial direction (Särdqvist, 2013).

An excessive moisture content also contributes to an increased risk for a biological attack of the wood (Särdqvist, 2013). Microorganisms like fungi, algae and bacteria can get a hold and start growing. The fungi feeds off of the sugars in the wood, and mostly don't affect the structural integrity of the material. However, rot fungi completely degrade the cells of the wood and can thereby critically affect the load-bearing capacity (Nevander & Elmarsson, 1994).

Water damages to buildings and structures can become a costly problem and if statistics from Swedish insurance companies are any indication, the costs have increased during the last decade, while the occurrence of water damages appears seemingly stable, see fig 2-3.

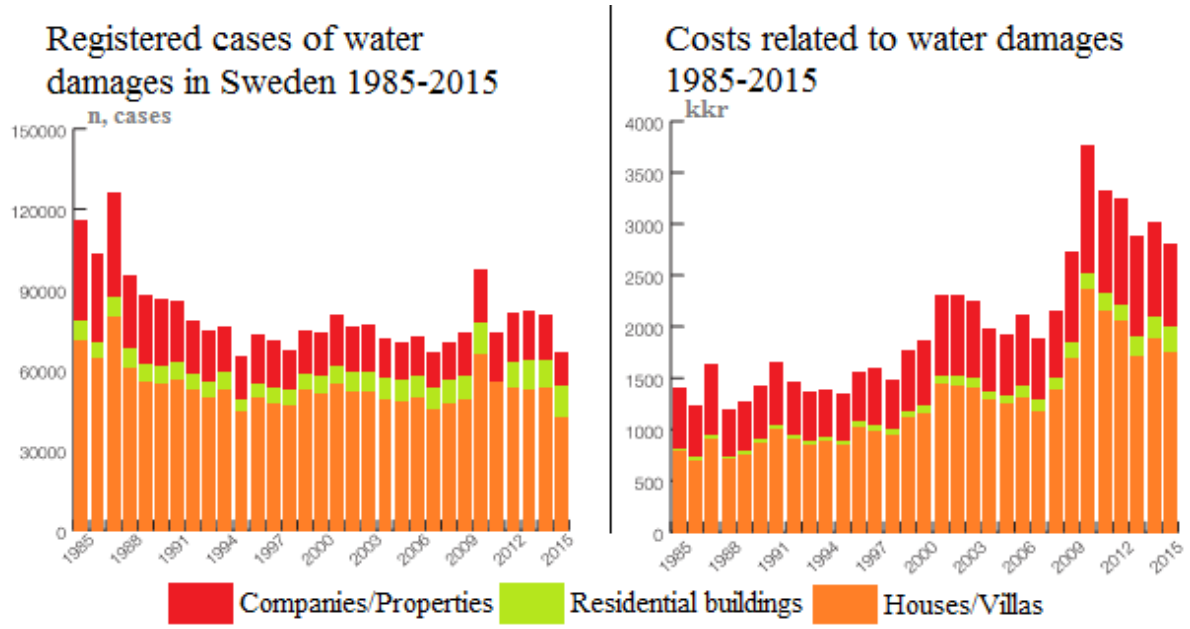

fig. 2-3. Statistics for water damages in buildings based on diagrams from (Vattenskadecentrum, 2016)

Worth noting is that these statistics do not include water damages caused by fire-fighting efforts by emergency services or sprinkler activation (Vattenskadecentrum, 2016). For consideration, if a mounted water cannon with a water flow of 1500 liter per minute is used during firefighting operations, a total of 90 m^3 of water will be consumed within an hour (Särdqvist, 2013). The required volume of water for a sprinkler system in a one-family home is according to NFPA 13 approximately 182 gallons (approximately 689 liter), and the total amount required for completely extinguishing that building type, amounts to 30,000 gallons (114 m^3) (The Fire Protection Research Foundation, 2012). With these figures in mind, it's not hard to imagine the complications this can cause for load-bearing structures made entirely out of wood products, as well as the challenge of drying such amounts of water.

2.3 Wood as a sustainable material

In response to the challenge of climate change, an increasing number of industries all over the world are looking to bio-materials, such as forest resources, in order to lower their climate impact (Peæaloza, et al., 2016). Globally the building sector is identified as one of the biggest contributors, accounting for up to 33 % of the Green House Gas (GHG) - emissions, and as a result, the effects of increased usage of pre-fabricated wood elements are being studied across the globe
OBJ

The standard and internationally recognised method for evaluating climate change impact is by Life Cycle Analysis (LCA), where the in- and output is measured for the different phases of a products' lifetime, including the production, construction, usage phase and end-of-life phase (Brege, et al., 2017). A substantial amount of LCAs of wood products have been performed, with a wide range of results. One explanation for these varying results is the controversy concerning the aspect of taking into account the carbon sequestration of wood. By doing so, the total carbon footprint of a building material can be reduced significantly. In order to actually make this assumption several factors such as the original tree life, growth time and the complete lifetime of the building, have to be considered (Peæaloza, et al., 2016). For buildings constructed with a higher content of timber products, a time horizon longer than 100 years has to be considered in order to be able to account for carbon sequestration in the buildings life cycle (Peæaloza, et al., 2016).

However, both Brege et al. (2017) and Hoxha et al. (2017) reported that timber materials in construction are superior to concrete from an LCA-perspective. Still, Hoxa et al. (2017) also reported that timber materials and specifically non-structural wood had a far greater impact on the uncertainty of the LCA results.

2.4 Engineered timber elements

In the last decades, the development of engineered wood elements has had a great impact on how wood can be used for construction (Burström, 2007). In the building sector of today, a wide range of different products are used. Some of these are Glued laminated timber (Glulam), Laminated Veneer Lumber (LVL) and Cross-Laminated timber (CLT) (Buchanan & Abu, 2017), where the main focus in this report is on the latter.

Glulam is the one element-type that is most similar to CLT in the build-up with thickness and format of lamellas as well as manufacturing. The material was one of the first modern engineered timber products and consists of high-quality timber panels glued together (Swedish Wood, 2016). The lamellas are positioned with fibres in the axial direction while CLT has every other layer rotated perpendicular to each other (Buchanan & Abu, 2017), see section 2.4.1 for further description of CLT. LVL consists of wood veneer sheets glued together, each with a thickness of about 3 mm, in the fibre direction. The total thickness of those elements are approximately 20 to 90 mm (Swedish Wood, 2016). For visual examples of the engineered timber products mentioned, see fig. 2-4 below.

fig.2-4. Examples of engineered timber products. Top left: Glulam, top right: LVL and bottom: CLT. Courtesy of Stora Enso.

The use of these types of elements have many advantages, besides the easy use in the construction process (Yeh, et al., 2013), the so-called *lamella effect* is a factor that promotes the material as well. The lamella effect increases the overall stability and durability of the material by reducing the weaker links and minimise the risk that weaker spots in the material will be stocked on top of each other, mitigating the fact that a wood-based material is not stronger than its weakest point. (Svenskt Limträ AB, 2007)

In line with the increase of the pre-fabrication products in the industry, the use of different adhesives has also changed. Using the material in different environments has laid the foundation for the use of different adhesives (Svenskt Limträ AB, 2007). Therefore, adhesives of different types will be further presented in section 2.4.2.

2.4.1 Cross-laminated timber definition

The modern engineered timber products have in the last couple of years increased in popularity as a building material, and cross-laminated timber is one of these types of materials (Wiesner, et al., 2017).

Cross-laminated timber, also called CLT, is a prefabricated laminated based material that consists of several layers of plane, high-quality timber panels that are stacked together cross-wise (Yeh, et al., 2013), see fig 2-5 below. The shifting directions of the panels in the wood-based product are to increase the strength, rigidity and stability. In comparison with solid timber, this reduces the influence of defects, as well as the degree of anisotropic properties in the material (Sikora, et al., 2016).

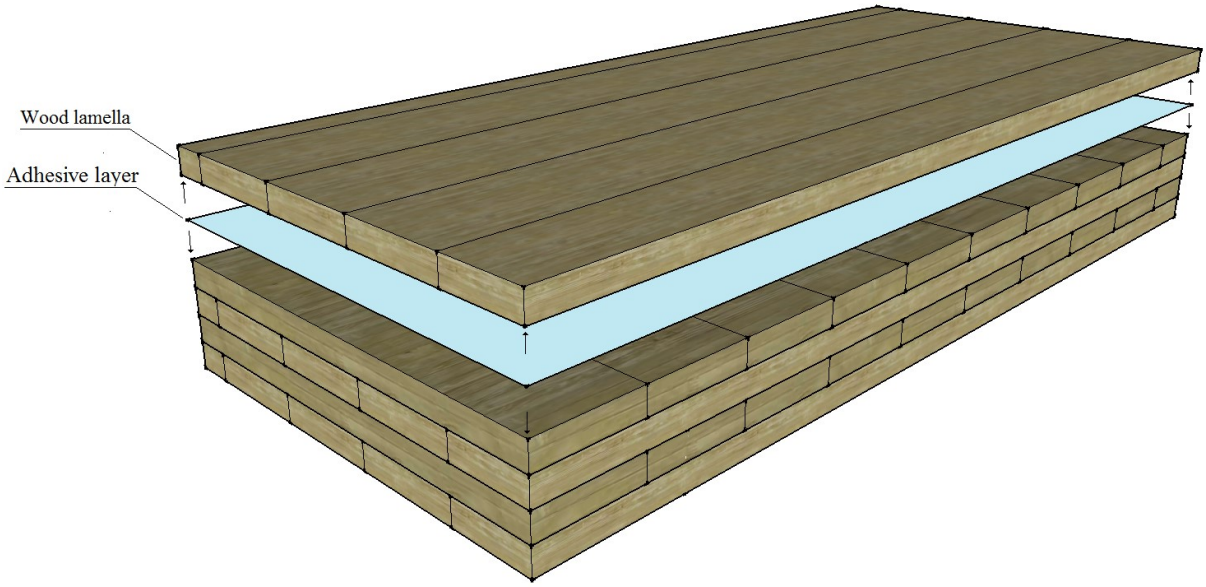

fig. 2-5. Sketch of CLT element and it's composition.

Attaching the cross-wise stacked panels to each other is most commonly done by using an adhesive. Most popular is the use of a one-component Polyurethane adhesive, but other options of glue can be offered, as well as non-adhesive options such as nails or wooden dowels (Buchanan & Abu, 2017). The number of layers that are stacked together can differ and so can the thickness of each layer. Normally between three to nine layers of lamellas with a variety of thicknesses are used (Yeh, et al., 2013). CLT-elements are used both as load bearing and non-load bearing structures and therefore thickness often change from case to case.

Manufacturing details regarding sizes and construction can differ internationally, but overall the final products are similar. Two Scandinavian manufactures of CLT, Stora Enso (Stora Enso, 2017) and Martinsons (Martinsons, 2016), use a total thickness of elements that varies from 60 mm to 320 mm, where each lamella varies with a thickness of 20 mm to 45 mm. Stora Enso also acts internationally, with wood production in Europe as well as Russia and Australia (Stora Enso, 2017). In Canada and USA, the thickness of lamellas varies between 16 to 51 mm, with a total thickness of up to 508 mm (Yeh, et al., 2013). What often limits the sizes of elements are standards, the ANSI/APA PRG 320-standard used in America set the maximum thickness to 508 mm because transportation and production of elements should not be limited.

CLT is a relatively young building material that has its roots in Austria in the mid-1990‘s and was primarily used in the countries around that region. At that time, the product was not as widespread compared with today. After a few years of slow growth on the market the material got a boost in the beginning of the new millennium (Yeh, et al., 2013), and today it’s becoming more and more common to build mid- to high-rise buildings using CLT.

The reason why the material has increased so much in popularity is the many advantages that goes with it. Cross-laminated timber is generally prefabricated and is therefore delivered to site as ready-to-use modules. Prefabrication and the strength to weight ratio of timber allow for a rapid and easier construction phase (Wiesner, et al., 2017). The strength to weight ratio makes the material more adaptable to work with in comparison to other prefabricated elements such as concrete.

CLT also has excellent properties of thermal insulation and airtightness. Therefore, the use of solid timber panels contributes to reducing the risk of fire spread through cavities, compared to a light timber frame for example. However, solid timber panels contribute to increasing the fuel load in the room (Fontana, et al., 2009), but the performance of timber structures during fire are generally

predictable and the charring layer forms a sort of protection (Wiesner, et al., 2017). Further presentation of fire behaviour of wood and CLT will be presented later in section 3: Fire behaviour of wood.

2.4.2 Adhesives

The primary method of bonding the layers together in CLT-elements is by application of an adhesive between each layer. For manufacturers of CLT, some of the properties that are of importance concerning the adhesives are wood to wood bonding strength, production-related properties such as curing times and spread rates, moisture resistance, temperature resistance and environmental- as well as sustainability aspects (Pizzi & Mittal, 2003). As adhesives generally show decreased strength with increasing temperature, it's crucial that the adhesive satisfy a reliable functionality during a specified time of fire exposure (Klippel, 2014).

The most commonly used adhesives for CLT production in Europe are Poly-urethane (PU)- and Melamine Formaldehyde (MF)-based adhesives. In this report, experiments will be performed with samples manufactured with these adhesive, and comparative tests will be performed for the following adhesive types: Emulsion Polymer Isocyanate (EPI) and Phenol Resorcinol Formaldehyde (PRF). See below for a brief description of each of the adhesive types.

Poly-urethane (PU)

Poly-urethane adhesives is a glue with a wide range of modification possibilities. It is most commonly used as one-component glue, but due to the chemical combinations, different types appear on the market. The one-component based versions of the glue are the ones most used since it can be applied instantaneously without any premixing phase as needed with a two-component glue (Strobech, 1990).

In Europe, the PU-adhesive is the most commonly used when manufacturing CLT-elements, and it is popular for the fast curing time at ambient temperature. Excluding the short hardening process that generally is between one to three hours, the adhesive is also popular because it is free from formaldehyde and needs no mixing with other components before application (Fontana, et al., 2009). The adhesive is also preferred for architectural reasons since it provides a colour free bondline. (Kemmsies, 1999).

Variabilities within the adhesive spectra makes it hard to determine a temperature when the adhesive will start to lose strength. The adhesive is generally known to have poor fire resistance, the extent of variabilities varies between different types of chemical composition of the material. (Klippel, 2014)

Melamine Formaldehyde (MF)

Introduced in the 1970's Melamine Formaldehyde (MF)-adhesives was a successor to the early Urea Formaldehyde (UF)- and Phenolic-Resorcinol-Formaldehyde (PRF)-adhesives (Klippel, 2014). One of the main characteristics of MF-adhesives in comparison to previous adhesive types is the high moisture resistance, as well as shorter hardening times. As the component Melamine in MF-adhesives is quite expensive most of the MF-adhesives used have been cheapened by adding Urea to some extent, resulting in a MUF-adhesive (Pizzi & Mittal, 2003).

MF/MUF-adhesives are considered thermosetting adhesives which work well for engineered wood-composites like glulam and CLT. In addition, the Melamine component in the adhesives causes the compound to form a network structure, increasing the thermal resistance of the adhesive (Zhou, et al., 2017). However, MF/MUF-adhesives are fairly brittle and the Formaldehyde-component in the adhesives are harmful to humans and the environment, making it considerably less attractive for future use in the industry.

Emulsion Polymer Isocyanate (EPI)

The types of adhesives known as Emulsion Polymer Isocyanate (EPI) are two-component adhesives, where a water-based emulsion is cured with a cross-linker of isocyanate. EPI-adhesives show great wood to wood bonding properties and because they are cold curing, moisture resistant and doesn't require long pressing times, they are used in a wide variety of engineered wood products (Grøstad & Pedersen, 2010).

In Europe, EPI-adhesives' are generally not used to bond lamellas together in CLT-elements. However, some manufacturers, such as Stora Enso, uses an EPI-adhesive to extend elements in production, applying it on the narrow sides of the elements (Stora Enso, 2013).

The knowledge of EPI-adhesives' fire resistance properties is limited, due to the fact that these adhesives are still in an introduction phase for use in layer-bonding in CLT-manufacturing (Grøstad & Pedersen, 2010). Still, isocyanate-adhesives have been shown to manage temperatures over 300°C before significant degradation of bonds occurred (Umemura, et al., 1998).

Phenol Resorcinol Formaldehyde (PRF)

Phenol Resorcinol Formaldehyde, also known as PRF is a dark brown adhesive commonly used in North America when manufacturing glulam beams. The adhesive has been popular on the market due to many factors, it has good structural performance, long-term duration time and good properties when exposed to higher temperatures and fires (Yeh, et al., 2013). PRF is also one of the cheaper adhesives used within the structural industry of glulam manufacturing (Sikora, et al., 2016).

The adhesive has been tested in long-term heating in temperatures of 220℃ and it fulfilled the structural requirements of loaded finger joints. A negative part of the PRF resistance to fire is that during the manufacturing, large air gaps can appear between the lamellas after curing. This makes it easier for a potential fire to spread in between the lamellas. (Klippel, 2014)

3 Fire behaviour of wood

In this section, the characteristics of fire behaviour of wood will be presented. Wood is known as a combustible material, but it can still perform relatively well during a fire in terms of resistance (Östman, et al., 2012). Fire performance of solid wood and CLT-element are similar, but still there are some deviations. These depend on the special composition that CLT has and will be further presented in section 3.2 and 3.3.

The initial stage of fire-exposed wood is the heating phase. When heating of wood occurs, a thermal breakdown of the material begins, also known as pyrolysis. The pyrolysis makes a combination of combustible vapours and moisture start moving, both in the direction of the fire as well as the opposite (Tsantaridis, 2003). Therefore, timber often shrinks when exposed to fire, moisture will evaporate or be transported to a place in the material where the temperature is below 100℃, while the combustible vapours will become additional fuel to the fire at the exposed surface. (Kodur & Harmthy, 2002)

Along with the increase of heat and the fire exposure, the material forms a charcoal layer at the surface exposed to the fire, see fig. 3-1. The charring and pyrolysis process continues, and when temperatures at the surface are high enough the material will ignite. The higher the radiation levels are, the faster the material will ignite. It is hard to determine a specific temperature when auto-ignition occurs, according to (Östman, et al., 2012) it varies between 200℃ and 530℃. The range of auto-ignition temperature depends on a multitude of parameters, the level of radiation, density, moisture content, wood species and shape of the wood matter (Structural Timber Education Programme, 1995). In contrast, when a pilot flame is present on the surface, the ignition temperature varies between 300℃ to 360℃ (Östman, et al., 2012), while ignition for larger, solid timber members will require temperatures on the surface to be around 400℃ (Structural Timber Education Programme, 1995).

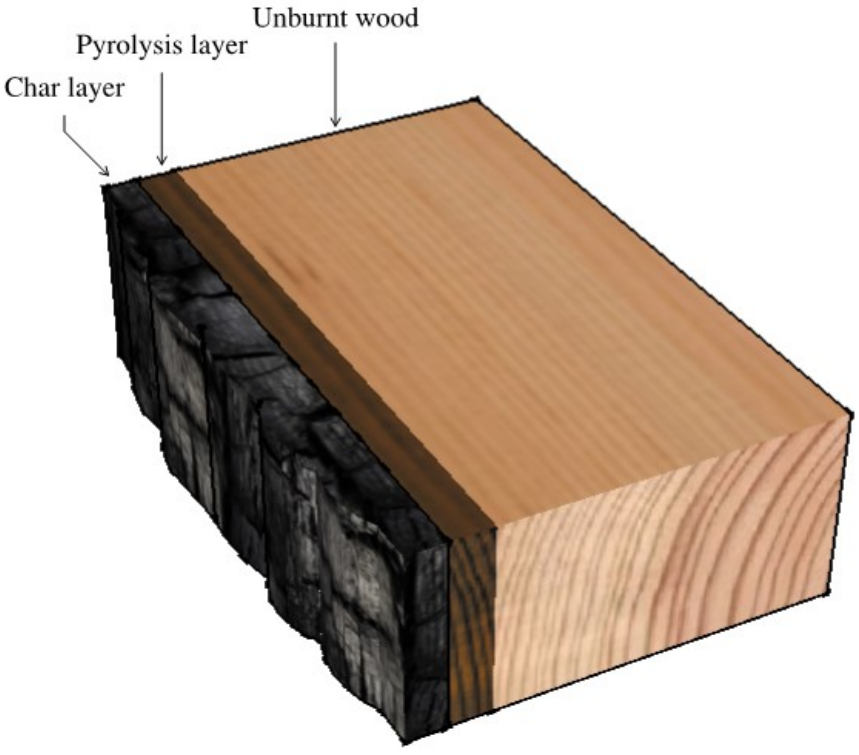

fig. 3-1. Sketch of a wood element after fire exposure, with its different resulting zones.

The density and the face of the surface are factors that influence the ignition and spread of fire. The higher the density of the timber, the longer the time to ignition will be. The surface of the timber can contribute to spreading the fire faster, as well as lower the ignition temperature (Structural Timber Education Programme, 1995). A structure that results in a less favourable fire behaviour has, for example, a coarse surface and sharp edges. Different types of shakes and cracks can also impact the fire behaviour in an undesired way.

As the fire continues, the charring layer builds up and creates a protective layer on the wood surface. Depending on the fire conditions and the room properties, the growth of the fire might rapidly reach a fully developed fire through complete combustion of all room surfaces, also called flashover (Karlsson & Quintiere, 2000). When flashover is reached, burning will continue for a time before the decay phase begins. This phase is dependent on the amount of available fuel and air in the room, and the fire will eventually go towards self-extinction, see fig 3-2.

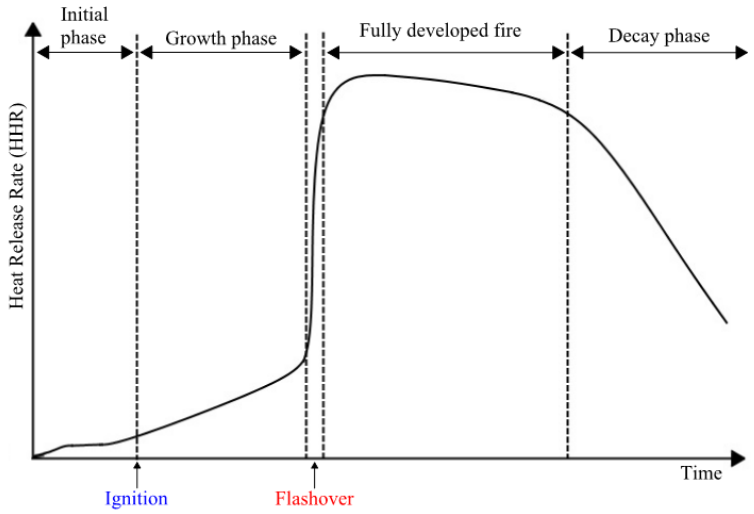

fig. 3-2. Example of a fire development within an enclosure including the main phases of a fire based on the stages presented in Selecting design fires by Leif Staffansson (2010).

3.1 Standard and parametric fire

In order to perform fire design calculations for the load-bearing capacity and performance of structural components, information about the thermal exposure from a relevant fire source is necessary. This is most commonly done by describing a fire by a temperature-time curve and performing furnace tests for structural components based on these curves (Karlsson & Quintiere, 2000). The majority of standards for structural fire design has calculation methods based on the results from furnace tests, where the temperature exposure was based on nominal fire curves such as the European ISO 834 or the American ASTM E119 (Buchanan & Abu, 2017), see fig. 3-3.

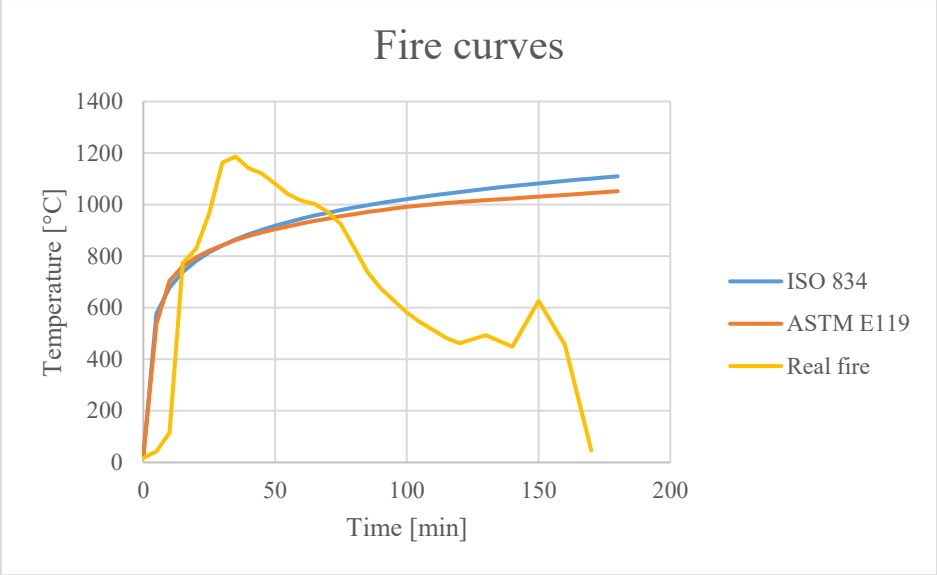

fig. 3-3. Comparison of standard fire curves (ISO 834 and ASTM E119) and a more realistic temperature curve. The real fire temperature curve is based on plate thermometer data from the full-scale tests of (Su, et al., 2017).

Since standard curves have been widely used in numerous tests all over the world, a greater amount of results is comparable to some extent. However, the relevance of these fire curves has been questioned, since their representation of real fire exposure is lacking to say the least (Drysdale, 2011).

In order to account for aspects like ventilation conditions, enclosure geometry, thermal properties of surface materials and fire load, parametric fire-representations have been developed. One of the most popular ones were developed by Magnusson and Thelandersson and consists of a set of gas-temperature curves dependent on, and distributed by the fire load, opening factors and thermal properties of enclosure surfaces (Karlsson & Quintiere, 2000), see fig. 3-4.

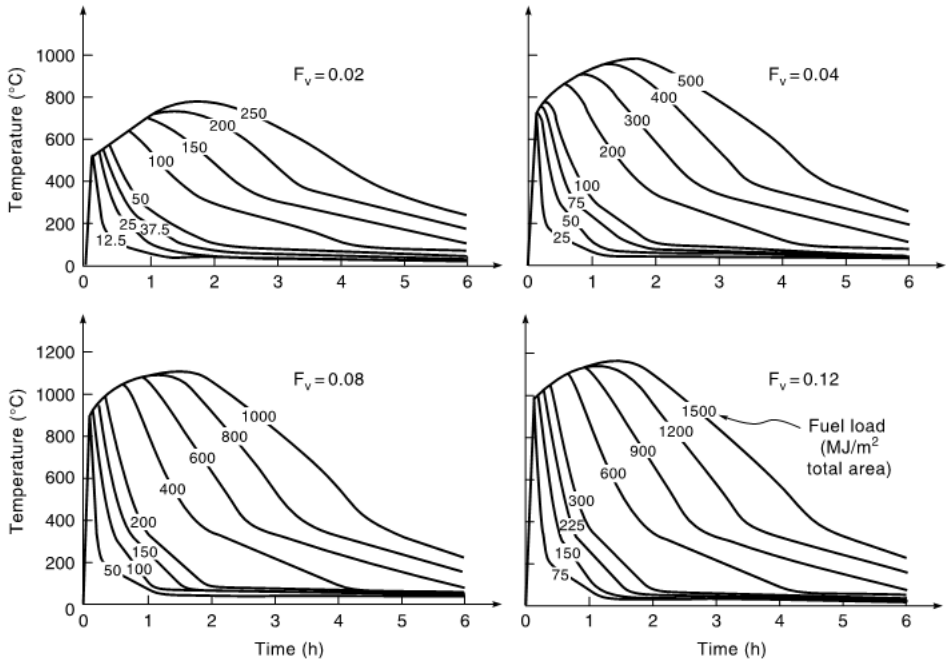

fig. 3-4 Representing the correlation between temperature and time with different ventilation factors as well as fuel loads. Curves are a representation based on Magnusson and Thelandersson (1970) with permission by Fire Safety Engineering Department, Lund University.

The utilisation of these fire curves when designing parametric fire curves has been substantial, and it's known as the Swedish method. They better represented a real fire post-flashover and has been compared with a lot of full-scale experiment results, with good agreement (Walton & Thomas, 2002). Magnusson and Thelandersson used a numerical computer model to solve the general heat equation, and thereby made it possible to derive more realistic temperature-time curves for the full duration of a fire scenario (Karlsson & Quintiere, 2000).

Still, the representation of a real natural fire is far from perfect, as a uniform temperature is assumed for the inside of the enclosure for the full duration. Additionally, complete combustion is assumed and heat transfer to boundaries are one-dimensional with a constant heat transfer coefficient (Karlsson & Quintiere, 2000).

In other words, to represent the fire exposure of an enclosure fire when performing small-scale testing, is no easy feat. In the experimental work within this report, this will be attempted using a more direct approach. The temperature and oxygen levels from a previous full-scale experiment (Su, et al., 2017) will act as moderating parameters, in order to replicate those fire conditions and verify the delamination results on a small scale. The procedure could in some way be considered an empirical small-scale simulation of the original fire, where the fire development is directly controlled to the practically fullest extent. The fire conditions used in this report is further explained in section 5.3.

3.2 Charring of wood

When exposed to high enough temperatures, CLT, as well as all wood products, burn in the outer layers and these are converted to char. The char layer and the healthy remaining wood form a distinctive moving boundary as the burning continues, and the pyrolysis zone moves through the material. This boundary corresponds to a temperature of about 300℃ (Buchanan & Abu, 2017), and typically represents the charring front.

The charring procedure can be expressed in both one-dimensional as well as two-dimensional charring. The two-dimensional procedure is used when expressing and calculating heat transfer for corners, where the heat will approach from two directions at the same time. In this report, the studied heat transfer and charring will be one-dimensional, and the char depth, $d_{char,0}$, can be expressed as follows (FireInTimber, 2010):

$$d_{char,0} = \beta_0 \cdot t$$

Parameters included in the formula are:

β_0: One-dimensional charring rate [mm/min]

t: Time of fire exposure [min]

The charring rate is dependent on a multitude of different aspects, some of these are wood species, density, and moisture content. Eurocode 5 presents a couple of characteristic values for the charring rate, based on wood species and density. For glulam, a charring rate of 0,65 mm/min is given, but a value for CLT-products is yet to be presented (International Organization for Standardization, 1995). These characteristic values for the charring rate are only valid for a standard fire (ISO 834). The standard rates should therefore only be applied when performing small-scale standard tests, and not a natural fire since that representation is very far from realistic (Drysdale, 2011).

Charring rates for CLT-elements depends on both the thickness of the layers and the used adhesive. In the case of one or more layers falling off, an increase in charring rate is to be expected. With thicker lamellas, the charring behaves similarly to a homogenous solid timber panel and a charring rate of 0,65 mm/min can be assumed (VY Wong & Fah Tee, 2017). For CLT-elements with thinner layers of lamellas, a different behaviour arises. The charring is faster and behaves similarly to plywood with a

charring rate of 1.0 mm/min (VY Wong & Fah Tee, 2017). A summary of the overall average charring rates from research between elements with a different number of layers and thicknesses can be observed in table 3-1.

Table 3-1. Overall average charring rates measured in different research experiments using CLT, for a different number of layers and thickness of lamellas.

	Charring rate*	Number of layers	Thickness	References
Average	0.85	3	35-35-35	(McGregor, 2013)
Average	0.99	5	20-20-20-20-20	(Wiesner, et al., 2017)
Average	0.85	3	33-34-33	(Wiesner, et al., 2017)
Average	0.85	3	35-35-35	(Li, et al., 2015)

**Disclaimer: Differences in the performance of the tests could have had significant influence on the result. The authors take no responsibility of comparing them with each other.*

With time, the charring layer serves as a protective surface for the underlying timber. This verification- and analysis design for the fire resistance is called the Reduced Cross Section Method, RCSM. The method is currently used for massive timber structural elements and assumes that the char layer created on the fire-exposed side of the timber will have a protective function. This in a manner that it will work as an insulating layer and therefore forms a protective and insulating surface. The sacrificed char layer on the fire-exposed surface of the timber will slow down the increase of the internal temperature in the timber as well as the deterioration of the load carrying capacity of the elements (Wiesner, et al., 2017). Not only does the charcoal layer form a protective layer against the fire, wood is a relatively poor conductor of heat. This also favours the materials' heat resistance properties, as the inner unburnt wood can be protected from the heat for a longer period of time (Structural Timber Education Programme, 1995).

The mechanical properties of wood elements change when exposed to a fire. The sacrificed char layer is assumed to have no mechanical strength and a certain depth in the element will suffer reduced mechanical properties as well. This particular depth is beneath the char layer and is thermally affected, the properties of this zone change due to the heating process. According to the reduced cross-section method, this portion beneath the char layer is assumed to be lumped together as the thermally affected zone and is called the 'zero strength layer', ZSL. This zone is assumed to have no load-bearing capacity and has been generalised to be 7 mm deep. (Wiesner, et al., 2017)

3.3 CLT and fire

Cross-laminated timber behaves not much differently from solid timber when exposed to fire. As long as the lamellas stay intact with the element, the properties of a fire remain very similar (Buchanan & Abu, 2017). Since CLT is a heavy timber element a large amount of energy is needed to ignite the surface. The large amount of mass of solid timber makes the material able to absorb a large amount of energy, therefore temperature rise is slower because of the scattered energy into the thick wood panel (Medina Hevia, 2014). Different thicknesses of lamellas may influence the behaviour of charring and burning. Drysdale observed a difference between thermally thin and thick pieces of wood. Thicker pieces of wood self-extinguish while smaller pieces kept burning. (Drysdale, 2011)

Research shows that self-extinction of CLT and solid timber occurs (Emberley, et al., 2017), this since the charcoal layer builds up a form of insulating protective layer. In order to determine the self-extinction of CLT elements, mass loss rate or radiant heat flux can be used. Reduction in heat flux, or mass loss rate for that matter, will result in a slower burning rate and will after a while reach a point where the combustion will stop (Bartlett, et al., 2017).

Additionally, CLT can behave differently if the thickness and number of lamellas changes. It is suggested by (Frangi, et al., 2008) that CLT-elements with the same total thickness with 3 lamellas instead of 5 showed a reduced risk of delamination and that effective charring rate decreased. The difference in charring rates can also be observed in table 3-1 above with different thickness and number of lamellas on different CLT-elements.

Even though CLT behaves similarly to solid wood when exposed to fire, a difference in charring rate as well as charring depth is observed and confirmed. The charring properties of CLT-elements are more difficult than for solid timber, mainly because of the built-up design with multiple wood panels glued together, where the adhesives behave differently when the temperature rises. If the adhesive maintains its bonding ability and the panels are intact, the CLT-element is expected to burn as natural solid sawn timber (Medina Hevia, 2014).

3.3.1 Delamination

The phenomenon of delamination is the event when the outermost lamella of a CLT-element detaches from the underlying lamella, because of fire exposure. This could occur locally at specific points, or entire boards or lamellas could detach at once (Bartlett, et al., 2017). The reduction of the insulating char layer because of delamination results in an increased heat-flux into the CLT-element and is also characterized by a large peak in the mass loss rate (Emberley, et al., 2017). This mass loss is mostly due to larger pieces of char and wood falling off, but Medina Hevia (2014) also observed a significantly higher charring rate following the delamination event. This being an effect of the loss of the insulating and protective char layer, exposing fresh wood to the fire (Medina Hevia, 2014), a process resembling that of loss of protective cladding described in Eurocode 5: 1-2.

Bartlett et al. (2017) and Emberley et al. (2017) both observed that after delamination, the fire went from a steady-state to a transient state. During this transient state, the mass loss was elevated, and it remained so until the forming char layer was deep enough to reduce the heat flux (Emberley, et al., 2017). This process led to increased energy release rates that prolonged the fire duration. In other words, if a CLT-element delaminate, it can have a significant impact on the fire development and the available fire load (McGregor, 2013).

The delamination does not exclusively have to refer to the detaching of char, as the falling of layers of unburnt timber has been observed as well. This is most likely a result of sufficient thermal penetration through the unburnt wood to affect the adhesive in the bondline (McGregor, 2013). It is therefore of great interest to examine the effect of a variety of adhesives, preferably with different melting points than the defined charring front temperature of 300°C (Medina Hevia, 2014).

3.3.2 Second flashover

The phenomena of second flashover is often mentioned when speaking in terms of delamination. The second flashover occurs most commonly during the decay phase of the fire when parts, or whole lamellas falls off from a glued laminated element, such as CLT. This is because the fire will get access to previously non-exposed wood and the sudden exposure to very high temperatures enable reignition (Brandon & Östman, 2016).

Second flashover doesn’t always need to be a result of a falling lamella. Studies have shown that situations with falling protective cladding, such as gypsum boards, can also cause a second flashover. McGregor and Medina Hevia have previously performed and reviewed compartment tests to determine the contribution of CLT to compartment fires in combination with failure of protection. Medina Hevia (2014) observed delamination in two tests where two out of four walls were unprotected, in both these instances the underlying ply was exposed and the second flashover followed.

McGregor (2013) concluded that CLT-elements protected by fire-rated gypsum boards did not contribute to the duration nor the intensity of the fire, as long as failure of the protection did not occur. When the failure of the gypsum boards occurred and the CLT surface was exposed, it led to an increased intensity of the fire, as well as a second flashover in the compartment. The whole process resembling a second flashover due to delamination of a CLT element. (McGregor, 2013)

The increased intensity mentioned above is partly explained in the Eurocode 5 regarding protective cladding falling off. In Eurocode 5 part 1-2 it's explained that the charring rate increases initially after the fire protection has fallen off. This was due to the surface getting exposed to high temperatures with the absence of a protective char layer or external protective material. The increased charring rate continues until the charring has reached a depth of 25 mm. After exceeding this depth, the charring rate will be reduced to a similar value as for an unprotected element. (FireInTimber, 2010)

4 Fire design of timber structures

Buildings based on timber structures concerns many areas. During construction of a building, many different aspects of the fire design need to be evaluated. In Sweden, function-based, prescriptive regulation is utilized in the majority of cases, but for more complex constructions an analytical approach has to be applied. This section gives a brief description of the standards for these analytical design calculations concerning timber structures, and some background for reliability-based design.

4.1 Standards and regulations

In Europe, there are general building regulations that were developed to make the buildings safer. The regulations of today started as a directive but were updated and modified in the year of 2013, now called Construction Products Regulations (CPR). In these regulations, seven main requirements are mentioned, and fire safety is one of them. The fire safety regulations dictate that a structure shall be constructed after following instructions:

1. Loadbearing capacity for a building can be presumed to be intact for a certain amount of time.

2. Rise and spread of fire and smoke within the building should be limited.

3. Spread of fire to an adjacent building should be limited.

4. Occupants within a building should be able to leave the building or be rescued in any matter.

5. Consideration of safety for the rescue service personnel shall be taken.

These rules are to be considered through prescriptive design and/or functional based engineering. The prescriptive rules are different from country to country.

In order to assist the prescriptive national building codes in Europe, the European Union has developed their own standardised design rules. These are called the Eurocodes and are divided into different areas within the field of structural engineering. Design of timber structures is covered in chapter 5 where design calculation methods for timber structures and verification are presented. These presented methods are based on a semi-probabilistic design concept with partial safety coefficients. The semi-probabilistic approach allows for fire design based on tabular values and a more general calculation approach to optimise the protection from fire (FireInTimber, 2010).

In Sweden, a prescriptive based national building code called Boverkets Byggregler also known as BBR is used. These prescriptive rules are not well adapted for CLT as a structural building component specifically, or for timber as a building material in general. The regulations cover timber as a cladding material and to a certain degree, different product classifications that can be obtained (Östman, et al., 2012). Instead, Sweden added a body of law called European construction standards (Europeiska konstruktionsstandarder, EKS). These prescriptions and general advices were introduced to clarify how the Eurocodes were supposed to be defined and interpreted in Sweden (Boverket, 2011).

4.2 Reliability-based fire design

A majority of building codes are deterministic in nature, continually changing with new discoveries in the field of structural engineering and the introduction of new building materials. The Eurocodes however, are more scientific in nature and as such they account for a degree of uncertainty for quantities involved in engineering calculations (Thoft-Christensen & Baker, 1982). There are mainly three types of uncertainties that must be taken into account, namely:

- Physical: material properties, quantified through sample tests.
- Statistical: Lack of information, insufficient sample size.
- Model: theoretical, empirical models, simplified assumptions.

The Eurocodes are not based on a complete method of reliability analysis, but uncertainty is represented in the form of partial safety coefficients. These partial coefficients, in turn, correlates to calculated characteristic values resulting in design values for relevant variables, be it the strength of building components or the applied load.

As the Eurocodes are based on a semi-probabilistic design concept, the partial coefficients for building components and simple structures are developed using stochastic variables. In short, if a structures' load-bearing capacity, *r* and applied load, *s*, vary in a statistically known, random way, they can both be described as stochastic variables: *R* and *S*. The difference between *r* and *s* can be expressed as a safety margin:

$$m = r - s$$

$m > 0$: Construction deemed reliable

$m < 0$: Construction will fail

However, when described statistically with stochastic variables the probability of failure, P_f, or in this case the reliability, P_r, can be described using probability distributions and probability density functions for *R* and *S*:

$$P_r = P(R - S > 0) = 1 - P_f = 1 - \int_0^{+\infty} F_R(x) f_S(x) dx$$

Where:

$F_R(x)$: Probability distribution for values of the load-bearing capacity.

$f_S(x)$: Probability density function for values of applied loads.

(Björkenstam, 1992)

In this report, the focus is primarily on the load-bearing capacity, R_d, of the studied CLT-elements, as a result of a reduced cross-section following fire exposure. The cross-section of the CLT-element is a geometrical quantity and is referred to as a basic variable, governing the load-bearing capacity of that element (Thoft-Christensen & Baker, 1982). The basic variables together comprise an n-dimensional space and this space can be divided into two areas: a safe region, where the variables resulting in a reliable structure are found, and a failure region where the variables resulting in failure are found (Björkenstam, 1992).

The border between the two regions is known as the failure surface or limit state, this surface can be hard to represent graphically when more than two basic variables are used to describe the load-bearing capacity. If the stochastic set of basic variables are normally distributed, it can be compared to the failure surface after variable transformation (Björkenstam, 1992).

In a normalized coordinate system the shortest distance from the origin to the failure surface can be defined by a safety index, β. An example of this safety index is Cornell's definition:

$$\beta_C = \frac{\mu_M}{\sigma_M}$$

Where:

μ_M: Mean value of the safety margin

σ_M: Standard deviation of the safety margin

(Thoft-Christensen & Baker, 1982)

In this simplified case where the safety margin can be described with a single stochastic variable that is normally distributed, the safety index, β_C and the reliability of the structure, $\mathcal{R}$, can be expressed as:

$$\beta_C = -\Phi^{-1}(P_f)$$

$$\mathcal{R} = 1 - \Phi(-\beta_C)$$

Where:

Φ^{-1}: The inverse of the normal distribution

P_f: The probability for failure

(Björkenstam, 1992)

If the reliability of the structure, $\mathcal{R}$, is defined and acceptable, the safety index, β and its direction vector in the n-dimensional space, α, is known for a design point on the failure surface, partial coefficients, γ_i, can be calculated:

$$\gamma_i = \frac{x_{s_i}}{x_{d_i}}$$

Where:

x_{s_i}: Specific value from the set *i* of basic values describing the load-bearing resistance.

x_{d_i}: Comparable design value for a basic value design point on the failure surface.

(Thoft-Christensen & Baker, 1982)

The partial coefficient can be utilized as partial safety factors to account for a diversity of probabilistic factors, and even be combined to form combination coefficients, Ψ_i, to account for synergy effects (Pettersson & Jönsson, 1988). Together with distributions of characteristic values, C_i a final design value for the load-bearing capacity, R_{dn} can be expressed as:

$$R_{dn} = \frac{1}{\gamma_i} R_d \cdot C_i$$

Where:

R_d: The lowest value of the ultimate load-bearing capacity.

(Pettersson & Jönsson, 1988)

For an example of how the process of reliability-based fire design might look, see fig. 4-1, on the following page. This illustration shows a multitude of aspects that influence the reliability-based fire design that all have their own level of uncertainty. However, all of these uncertainties can't be represented in a single image.

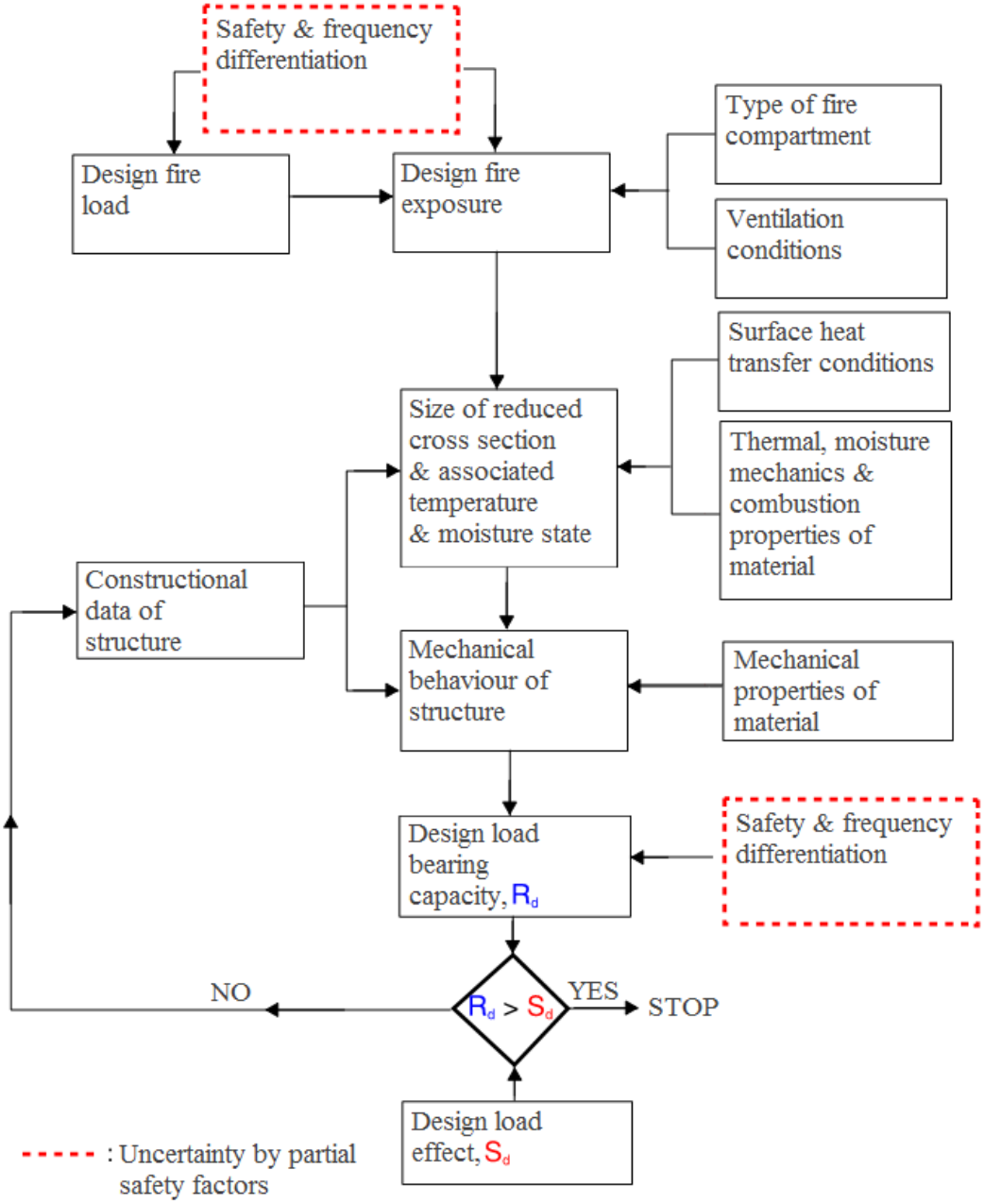

fig. 4-1. Flow chart for a reliability-based fire design procedure, based on an illustration from (Pettersson & Jönsson, 1988).

5 Experimental method

In this section aspects and details concerning the experimental procedure will be explained, this includes the experimental setup, information about the test specimens, the equipment and measurement devices used as well as what output data these will produce.

5.1 Experimental setup

The experiments were performed at the testing facility of RISE (previous SP Trätek) in Stockholm. The complete procedure was divided into a set of tests with different specimens, and for these tests a model-furnace was used. The furnace has the inner measurements of 1.0 x 1.0 x 1.0 m, with outer metal cladding surrounding the inner walls of ceramic insulation, see fig. 5-3. The specimens were placed at an opening on top of the furnace, exposing a 1.0 x 0.6 m area of the specimen to the fire conditions inside the furnace.

Four burners at the furnace walls will provide heat for the tests in order to replicate the most severe fire conditions of previous full-scale experiments (Su, et al., 2017). At the bottom, there was an exhaust with a damper and an analysis point for oxygen levels inside the furnace. One of the furnace sides had an air inlet connected to a supply of oxygen and nitrogen gas. By measuring the oxygen levels in the exhausts, the oxygen concentration and thereby the fire conditions could be adjusted in real time by adding additional oxygen or nitrogen through the air inlet. In proximity to the specimen placement at the furnace top, plate thermometers and a thermocouple were mounted on a thin rod. On the opposite wall, the furnace is equipped with a sensor registering air pressure, as well as an observation tube for direct observation of the specimen. Approximately 50 percent of the exposed specimen was visible through this observation tube. An air-cooled camera was mounted inside this observation tube for visual recordings of the delamination process during the experiments. For a section overview of the furnace setup, see fig. 5-4.

fig. 5-3. Testing furnace at the RISE facility, Stockholm.

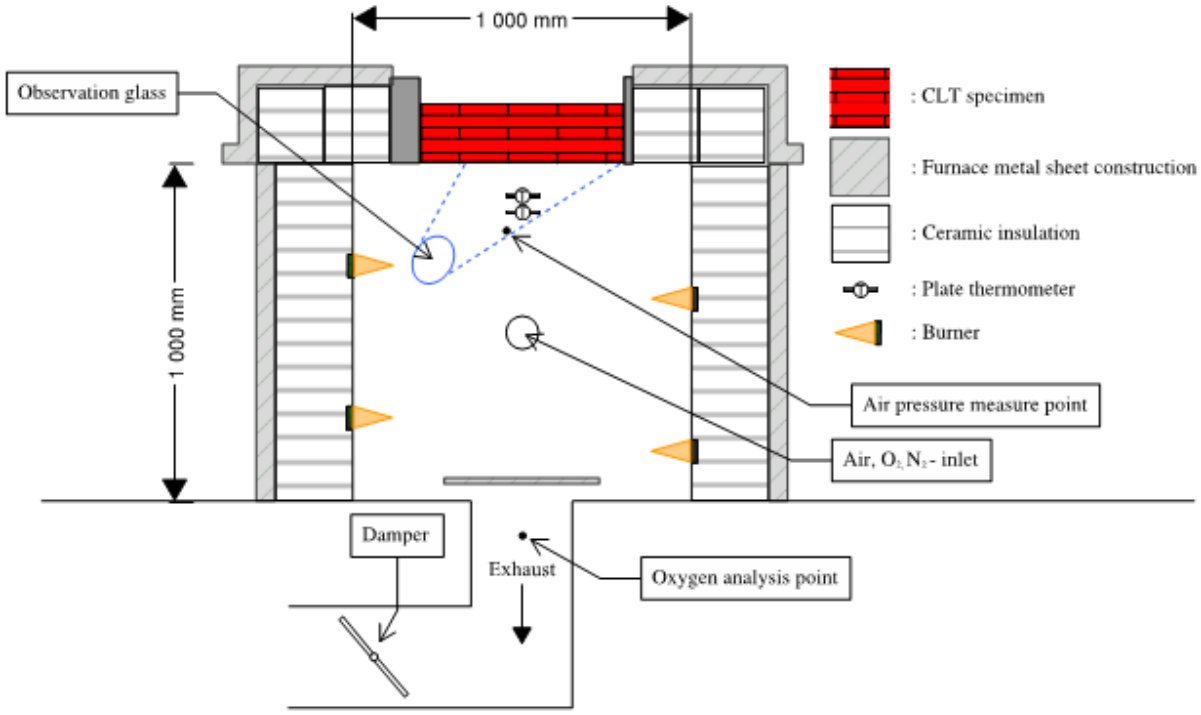

fig. 5-4. Section sketch of furnace setup.

5.2 Specimens

A collection of five different specimens made in two copies were tested. Each specimen had the same dimensions of 1400 x 600 mm with a thickness of 175 mm, five layers of lamellas each 35 mm thick. The CLT-elements were comprised of the same wood species, Black Spruce, as the elements used in previous full-scale experiments. Eight of the total ten specimens used in the experiment were prepared and manufactured in accordance with the standard ANSI PRG 320, by FP-Innovation in Canada. The other two consists of leftover CLT-elements from the full-scale test, these specimens were included for direct evaluation of reproducibility of the previous experiments.

The specimens were manufactured using four different adhesive types including: Poly-Urethane (PUR), Melamine Formaldehyde (MF), Emulsion Polymer Isocyanate (EPI) and Phenol Resorcinol Formaldehyde (PRF). The CLT-specimens from the previous full-scale experiments were originally manufactured using a standard PUR-adhesive commonly used in CLT manufacturing. A second set of specimens comprised of a different Poly-Urethane adhesive, manufactured at FP-Innovation was also included. This adhesive was fairly new to the industry and considered top of the line. For an overview of the different specimens and adhesives used, see Table 5-1 below.

Table 5-1. Description of the different specimens that will be used in the experiments.

Type of adhesive	**Abbreviation**	**Specimens**	**ANSI PRG 320**	**Production**
Poly-urethane (Full-scale product)	PUR Type A	2	Yes	Industrial manufacturer
Poly-urethane (Newer type)	PUR Type B	2	Yes	FP-Innovation
Emulsion Polymer Isocyanate	EPI	2	Yes	FP-Innovation
Melamine Formaldehyde	MF	2	Yes	FP-Innovation
Phenol Resorcinol Formaldehyde	PRF	2	Yes	FP-Innovation
	Σ:	10		

All prefabricated specimens were prepared during manufacture with thermocouples inserted 100 mm deep in the bondlines, with a vertical distance of 35 mm between each of the three lowest lamellas. This procedure was carried out at FP-Innovation in Canada. The thermocouples were placed in four groups of three and in a horizontal position to limit the thermal conduction along the line of measurement, in accordance with the standard EN 1363-1 (2012).

When arriving at the RISE testing facility in Stockholm, the specimens were stored in a controlled environment at a temperature of 20℃ and a relative humidity of 65%. The prefabricated thermocouples in the bondlines were complemented with additional thermocouples inserted in the three lowest lamellas from the side of the specimen to complete each of every series, see fig. 5-6. In total, there were four identical series of six thermocouples, two on each side of the specimen, located according to fig. 5-5 and 5-6. To complement as well as validate the horizontal measuring series two additional series of three thermocouples were mounted at the top of the specimen according to fig. 5-5.

The non-prefabricated thermocouples were manually drilled in 2 mm-diameter holes on the designated depth and insertion of 75 mm. The thermocouples in the side series were drilled in at a height of 20 mm, 50 mm and 87,5 mm from the fire-exposed side, see figure 5-6. While the top thermocouples were positioned 125 mm from the edge of the specimen, located on the same level as the three lowest placed thermocouples in the side series. In total 30 thermocouples were mounted on the specimen, for a comprehensive overview of the thermocouples placement see fig. 5-5 to 5-7.

In order to allow potential delamination to occur freely during the experiments, each specimen was prepared with saw cuts at RISE, Stockholm. These saw cuts were made along the short sides in the border of the exposed and supported areas based on where the specimen rested on the furnace during the test. The cuts were approximately the depth of two lamellas, and to prevent fire spread through the saw cuts during the experiment they were filled with ceramic paper. For the location of the saw cuts refer to the dotted lines in figure 5-5 and markup in figure 5-7.

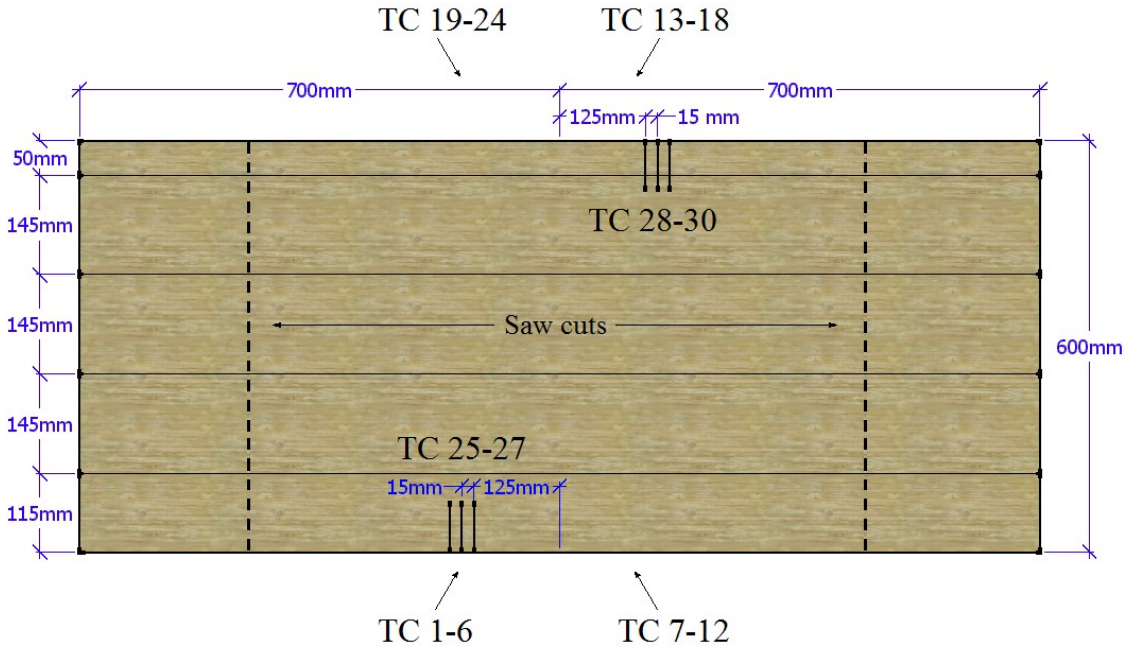

fig. 5-5. Top view of ready CLT sample with the positioning of thermocouples and dimensions. The dotted line representing saw cuts on the fire-exposed side.

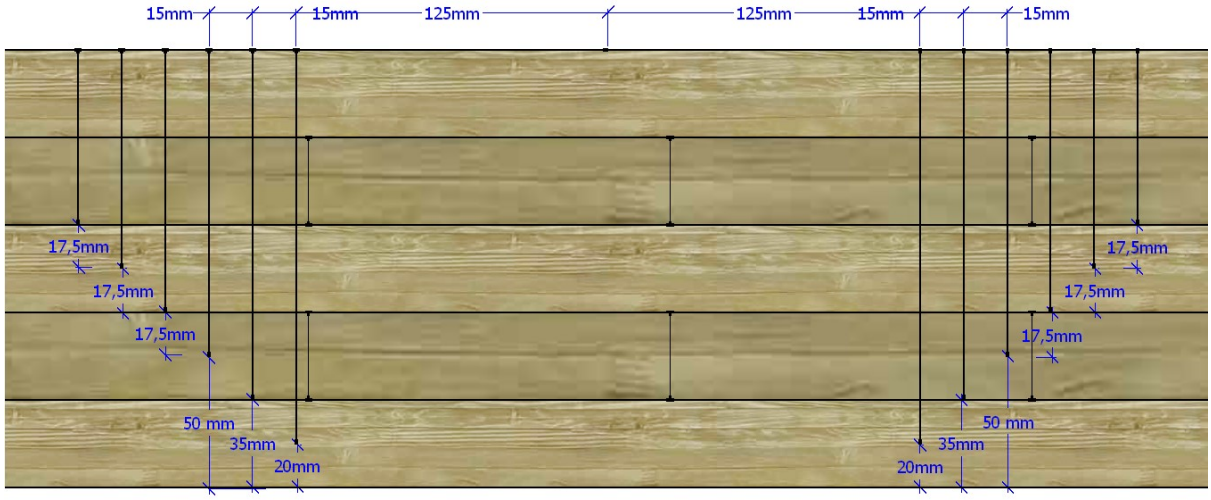

fig. 5-6. Side view of the specimen (front/back), with the positioning of thermocouples.

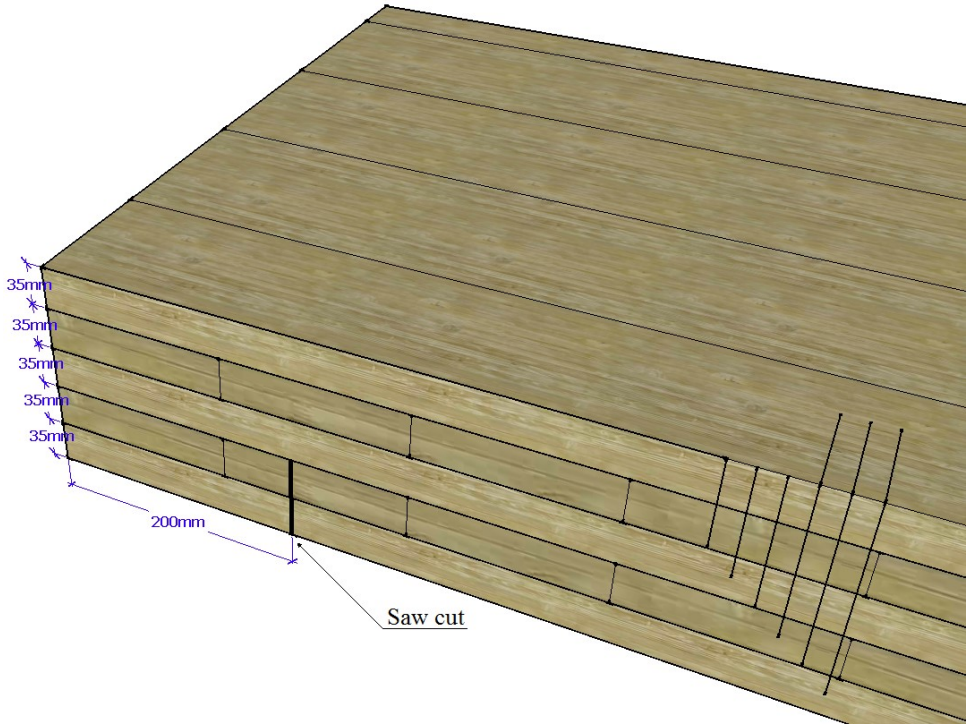

fig. 5-7. CLT sample with mark-ups for positioning of thermocouples and approximate placement of one of two saw cuts.

5.3 The target fire conditions

For the fire exposure of the experiments, a natural fire resembling that of the full-scale test (Su, et al., 2017) is the goal. In order to achieve this, the fire conditions of that test need to be replicated to some extent within the standard furnace, see fig. 5-8. For that reason, the furnace temperature and oxygen levels are chosen as representative parameters to be monitored and controlled during the experiments.

Regarding the furnace temperature, plate thermometer data measured at ceiling level in the original full-scale test are used as target values. As it would be impossible to replicate the temperature perfectly due to the constant flux, a simplified temperature curve based on mean values had to be derived. To account for tests where no delamination occurs, the registered peak towards the end of the original full-scale test is not included in the target curve. Instead an uninterrupted decay phase has been approximated. Limitations of the furnace, such as a critical temperature limit of 1200°C also had to be accounted for when deriving this curve. See fig. 5-8 below for the target temperature curve and the reference temperature.

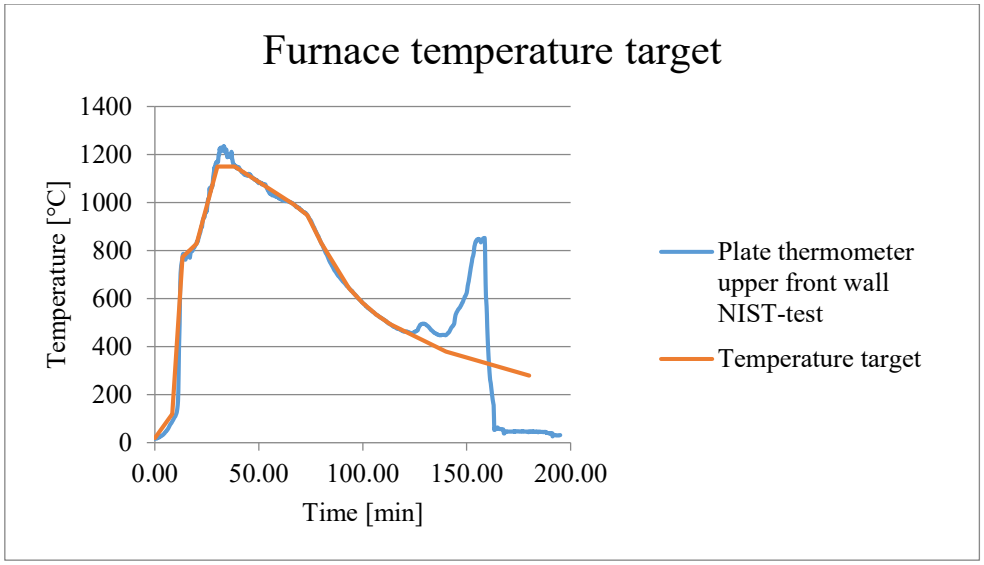

fig.5-8. Temperature target curve and original thermoplate data.

The same methodology is used when deriving the target oxygen curve, with data from the oxygen measurements from the full-scale test. This curve was also adjusted, mainly in order to compensate for the fact that some of the test specimens might not delaminate as the full-scale test specimen did, which impacts the oxygen levels. The drop in the oxygen level towards the end of the original full-scale test was due to delamination and this is not included in the target curve. See fig. 5-9 below for the target oxygen curve.

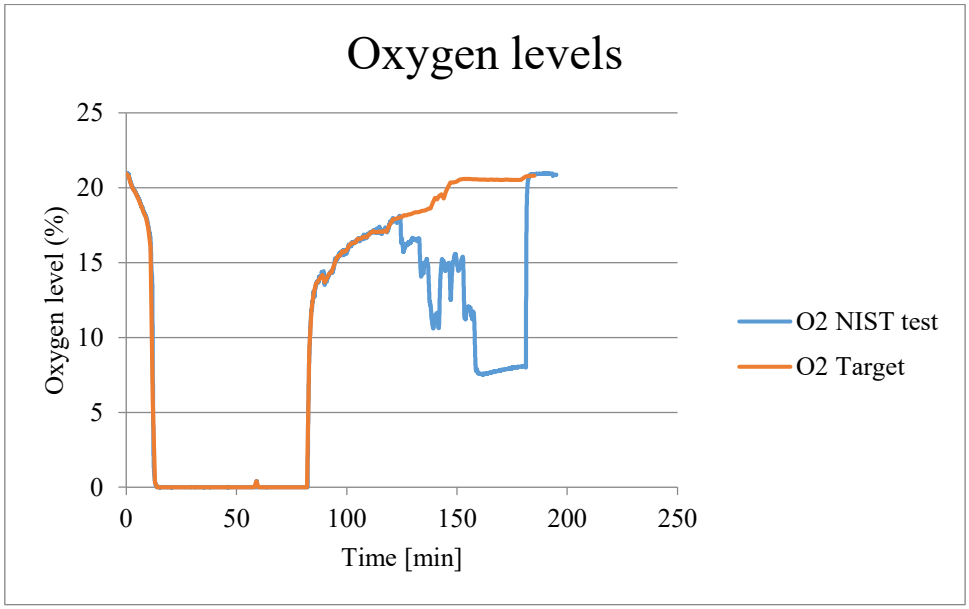

fig.5-9. Oxygen level target curve and original oxygen level data.

For details concerning the practical execution of attempting to follow these target curves, see the following sections.

5.4 Instrumentation & output

A variety of instruments were used to gather the required data. Some of the results were based on directly measured data from each test, while some had to be analysed and calculated further. As the main focus of the experiments was the occurrence and effect of delamination, the setup of measuring devices was primarily used to track and measure this phenomenon. See Table 5-2 for an overview and summary of all the measuring devices used in each test and their output.

Table 5-2. Overview of measuring devices, output and handling of data for the experiment.

Device	**Quantity**	**Output**	**Data handling**
Thermocouples (inside CLT-specimen)	30	Temperature profile inside CLT-specimen and in the bondlines	Track the charring front (300°C) and calculate the charring rate.
Plate thermometers	2	Adiabatic surface temperature of specimen	An average of the two thermometers were calculated. This was also used to calculate the incident heat flux.
Thermocouple (near specimen surface)	1	Temperature of gas layer in proximity to the plate thermometers	Raw data as well as a component in calculating the incident heat flux.
Heat flux meter (water-cooled)	1	Radiative heat flux near the specimen surface	Was used once in order to calculate constant parameters of the heat flux.
Manometer	1	Air pressure inside top layer of furnace	Used to control the furnace damper during the experiment.
Gas analyser	1	Oxygen content in the exhaust	Raw data and the measurements were also used in real time as an indicator for adjusting the air inlet.
Video camera	1	Recordings of the fire exposed specimen.	The recordings of the delamination process were used as complementing material in the analysis
Electrical resistance moisture meter	1	The moisture content of specimen prior the experiments.	Used in combination with values of weight before and after to calculate the total mass loss of specimen.

5.4.1 Thermocouples
Additional to the plate thermometers, a thermocouple of type K were placed in proximity to the plate thermometers. The thermocouple as a measuring device is not as sensitive to radiation and is therefore used to measure the gas temperature close to the plate thermometers. It is also the measuring device of choice for measuring the temperature of the specimen, as they are compact and small. The charring rate was calculated based on data of temperature readings inside the test-sample. Using the reference value of 300°C, the charring front in the material could be tracked, and thus the rate could be calculated.

5.4.2 Plate thermometers
Plate thermometers that gathered data of the temperature caused by radiation and convection inside the furnace were used. In order to determine the temperature of the gas layer closest to the specimens, plate thermometers were located 100 and 150 mm away from the specimens.

5.4.3 Incident heat flux meter
The water-cooled heat flux meter was only used for measurements during the last test, this since its robustness is very limited and should not be used for heat levels exceeding 200 kW/m^2. However, using the data from the plate thermometers and the nearby thermocouple, the heat flux could be calculated for the remaining tests, the data from the heat flux meter was used to derive the constant values used in the calculation of the heat-flux, see Appendix A.

5.4.4 Gas analyzer
For measurements of the oxygen levels in the exhaust of the furnace, a gas analyser was used. Not only will this data be used to analyse the occurrence and effects of delamination, but also as an indicator for adjusting the air flow to the furnace in real time. This was a critical function in order to succeed in replicating the fire conditions of previous full-scale tests. For the decay phase, the air inlet was instead used to cool down the furnace in a structured and controlled manner since the temperature inside the furnace was prioritised before the oxygen level.

5.4.5 Video camera
The video camera was mounted in the observation tube of the furnace, covering a view of approximately 50 percent of the exposed surface of the specimen. An estimated 180 minutes of the material was recorded for each test.

5.4.6 Moisture meter
Prior to each test, each specimen was scaled and the moisture content was measured by the means of electric resistance, a moisture meter. By doing this, the dry weight of the specimen before each test could be estimated. After a test is performed the specimen will be left to dry in an oven at 120℃ before being weighed a final time. By comparing the weight before and after, the total mass loss caused by the fire exposure can be calculated. This mass-loss is however not presented in this report due to time limitations.

5.5 Experimental procedure
The complete experiment was divided into a series of tests involving different specimens, each test, in turn, consisted of a multitude of different tasks and actions. A substantial amount of time was consumed preparing and calibrating equipment for measurements.

In fig. 5-10 on the following page a graphical overview of the process and management of the output is presented.

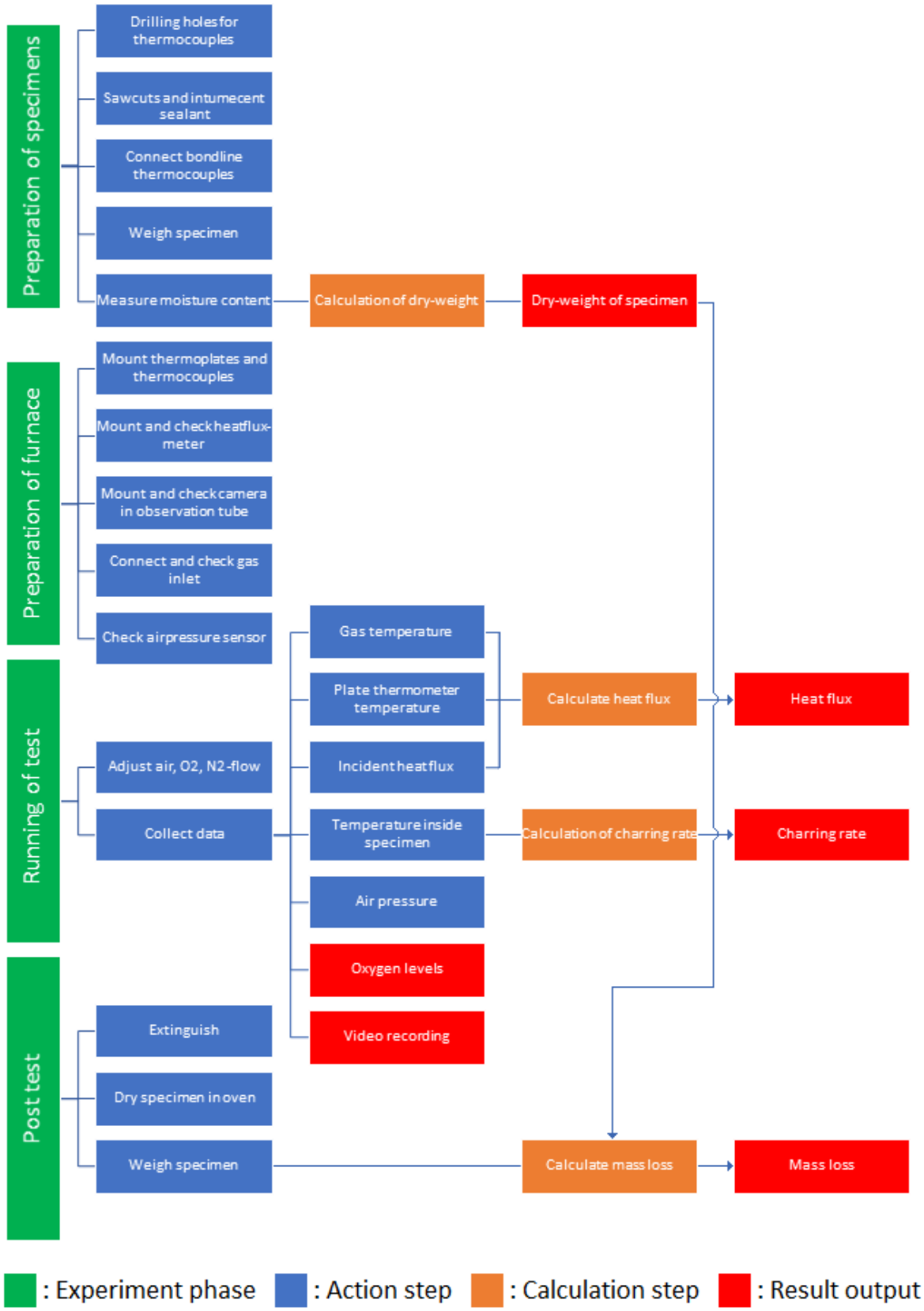

fig. 5-10. Flowchart of the test process of an experiment, with the resulting output.

5.6 Pilot tests

Before the actual experiments, two pilot tests were performed in order to observe and to ensure a successful management of the furnace. This chapter will further present potential aspects that could impede the experiments as well as the outcome. Finally, this is presented as a short summary in this section, that served as material for a checklist that was used when executing the main tests, see Appendix B.

5.6.1 Controlling the fire conditions

Some critical aspects were identified before the pilot tests which required additional measures to ensure the accuracy of the real tests. In the bullet list below the possible complications are mentioned and what aspects make them critical.

- Oxygen content:
  During the test, the oxygen content level needed to be controlled to make sure the oxygen levels inside the furnace matched the measurements from original full-scale test. To be able to manage this, nitrogen was applied to support gas products produced by the fire (such as carbon dioxide) in the lowering process of the oxygen content.

- Temperature:
  The temperature was controlled by regulating the furnace burners. It was ramped up to match the temperature curve of the replicated full-scale fire.

- Insulation:
  Potential openings and gaps between the specimen, furnace and closing elements need to be ensured that they are well insulated. This in order to have control of the air entering the enclosure, as well as to prevent the fire spreading out of the furnace.

- Saw cuts:
  The saw cuts were observed to see if it contributes to the fire spreading up in the element faster than if there were no saw cuts.

- Video recording:
  During the test, a video recording was made to detect delamination of the specimen through observation. The focus during the pilot tests was to ensure that a good angle of the camera was used so that as much as possible of the specimen was visible in the recording.

5.6.2 Outcome and complications

A compilation, and the outcome of the tests are presented in the bullet points below.

- Oxygen content:
  Regarding the oxygen content it is a parameter that is hard to control. Oxygen and nitrogen are manually injected into the furnace to support the lowering or increasing the amount of oxygen in the furnace, but there were some complications that were discovered during the pilot tests. One tank and inlet of nitrogen was not sufficient enough. For the real tests, more inlets of nitrogen, as well as more tanks, will be added to have enough gas. This will make it possible for a faster injection of nitrogen and a more rapid lowering of the oxygen content inside. Stronger tubes and connections will also be added to allow for increased transport of nitrogen.

  To control the oxygen content better, it was discovered that the damper in the exhaust could help in bringing down the oxygen content level. This by having the damper slightly open when applying nitrogen to the furnace.

It was concluded that during the main tests, communication between involved persons needed to be improved to be able to better follow the oxygen curve. This involves the person controlling the damper, the person managing the flow of nitrogen/oxygen and the person controlling the level of oxygen content. During the first pilot test communication between involved persons were lacking, but this improved slightly during the second test.

- Temperature:
  In the first pilot test, the temperature was pushed to the furnace limit and was above 1200℃. The furnace is not made for these types of experiments and can't handle temperatures above 1200℃. For the next pilot test and for further experiments the temperature was to be held below 1200℃, for the main tests the temperature was limited to approximately 1150℃.

- Insulation:
  During both of the pilot tests, the insulation failed to some degree. It was concluded that when executing the main tests, precautionary measures needed to be taken to ensure that the integrity of the furnace is properly maintained. Minimizing the space between furnace, closing elements and the specimen as much as possible, to not let air in or for flames to spread out. Rockwool in combination with gypsum boards should be used as insulation to minimize this space.

- Saw cuts:
  No complications with the saw cuts were observed during the pilot tests. The prediction was that the fire might spread through the saw cuts and travel faster up in the lamella layers, but this was not the case and no further actions were taken.

- Video recording:
  The task of achieving a correct angle and positioning of the camera in order to record a sufficient portion of the element, did not pose any problems. A couple of minutes into the first test, the recording stopped due to a limited hard drive space on the computer. A sufficient amount of hard drive space on the computer was, therefore, an aspect that needed to be ensured during the main tests.

5.6.3 Lessons learned

The final conclusions from these pilot tests are that there are many small and simple details that required solving to improve the final results. The control of oxygen and nitrogen content were the most critical parameters, but actions to mitigate the risks could be taken. In Appendix B, a checklist is presented that summarises the actions for the main tests. This checklist is a direct consequence of the outcome and lessons learned from these pilot tests and was developed to guarantee that the complications from these pilot tests would be taken into account.

6 Results

For the result section of this report, the main focus has been the occurrence and effect of delamination. The main reason why this needs to be clarified is to explain the selective handling of the results. Due to a large amount of output data, and the limitations and scope of this report, the results had to be carefully selected depending on relevance to the formulated objectives of the report.

With this in mind, the results were divided into different result categories like direct measurements such as temperatures and oxygen levels, calculated results such as charring rates and heat flux, as well as visual observations like pictures and observational timelines. Most results are presented in a comparative manner, where selected datasets from each specimen is presented together for comparison.

If output data was considered less relevant to the posed objectives, this material was comprised in an appendix, see Appendix A-G. In the case of significant deviations in the presented results, additional data material has been presented, in order to serve as explanatory material to the deviation in question and is further handled in the discussion. For some of the results, all specimen could not be presented in a reasonable comparable way. For these sections, the most extreme results have been selected together with one or two examples of specimen presenting more moderate results. The results that are considered moderate in this regard are results that appear similar between the majority of tested specimens. As a reminder of the sets of specimens see table 6-1, in this table the moisture content of each specimen that was measured before each test, is also presented.

Table 6-1. Overview of all the specimens used in the tests, with measured initial weight and moisture content.

Denomination	**Adhesive type**	**Origin**	**Moisture content (%)**
PUR-A1	Poly-Urethane A	Leftover from original full-scale NIST- test	14,5
PUR-A2	Poly-Urethane A	Leftover from original full-scale NIST- test	-*
PUR-B1	Poly-Urethane B	FP-Innovation	18,0
PUR-B2	Poly-Urethane B	FP-Innovation	15,3
PRF-1	Phenol Resorcinol Formaldehyde	FP-Innovation	16,3
PRF-2	Phenol Resorcinol Formaldehyde	FP-Innovation	14,6
EPI-1	Emulsion Polymer Isocyanate	FP-Innovation	16,3
EPI-2	Emulsion Polymer Isocyanate	FP-Innovation	16,3
MF-1	Melamine Formaldehyde	FP-Innovation	-*
MF-2	Melamine Formaldehyde	FP-Innovation	-*

**Note: Moisture content were measured before tests, due to limited time and resources, some measurements were not collected for the specimens, and these are presented with a horizontal line.*

6.1 Measurement of test performance

In order to replicate the full-scale fire conditions of (Su, et al., 2017) the oxygen levels- and furnace temperature curves presented in section 5.3 was used as target curves. In this section, the measured oxygen levels and furnace temperatures of each test are presented in graphs. In these graphs, the target curves have been included for comparison, to give an indication as to how well the target fire conditions were replicated for each test, see fig. 6-1 to fig. 6-6.

A selection of three graphs has been chosen for the result section. These graphs include the two most extreme cases, where delamination was observed, and the specimen for which the matching of the furnace temperature and the oxygen level was considered to be the best. The rest of the graphs presented more similar and moderate results and are therefore not included, these can be found in Appendix C.

For the PUR-A1 results, the NIST-target curve for the oxygen levels was the intended target curve, as it accounts for the occurrence of delamination. The result is a bit different from the targeted curve, this because the furnace temperature and oxygen-level were in some cases hard to balance.

The temperature inside the furnace for PUR-A1 is presented in fig. 6-1 where the furnace temperature can be seen to be slightly above the target at the beginning of the decay phase. While towards the end of the curve, it deviates more and more, peaking just before the end of the test.

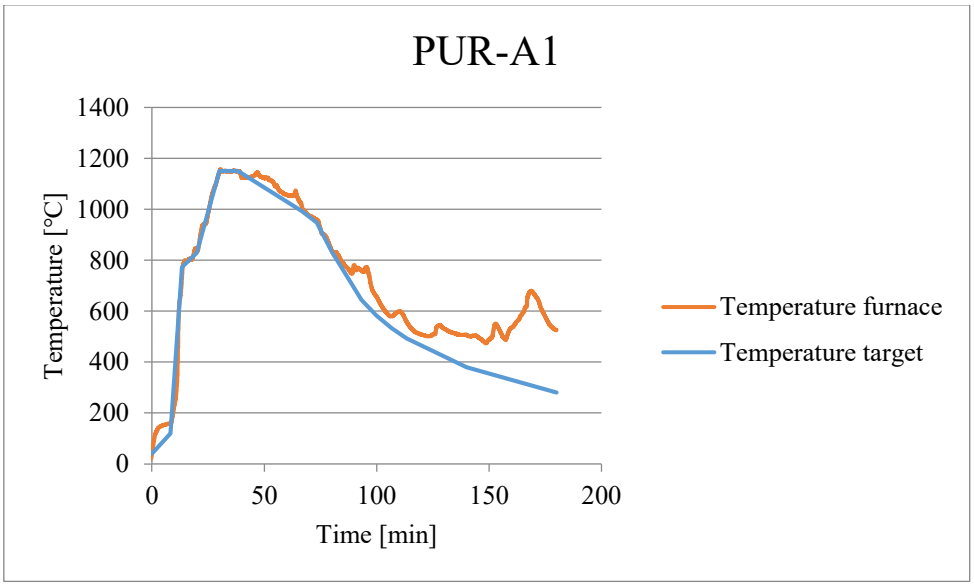

fig. 6-1. Temperature profile of the furnace in comparison with the expected target for PUR-A1.

During the initial 80 minutes of the PUR-A1 test, the oxygen-curve followed the NIST-test curve quite well. In the following phase of rapid increase, the oxygen level is far below the expected NIST-test curve, and above the curve towards the end.
see fig. 6-2.

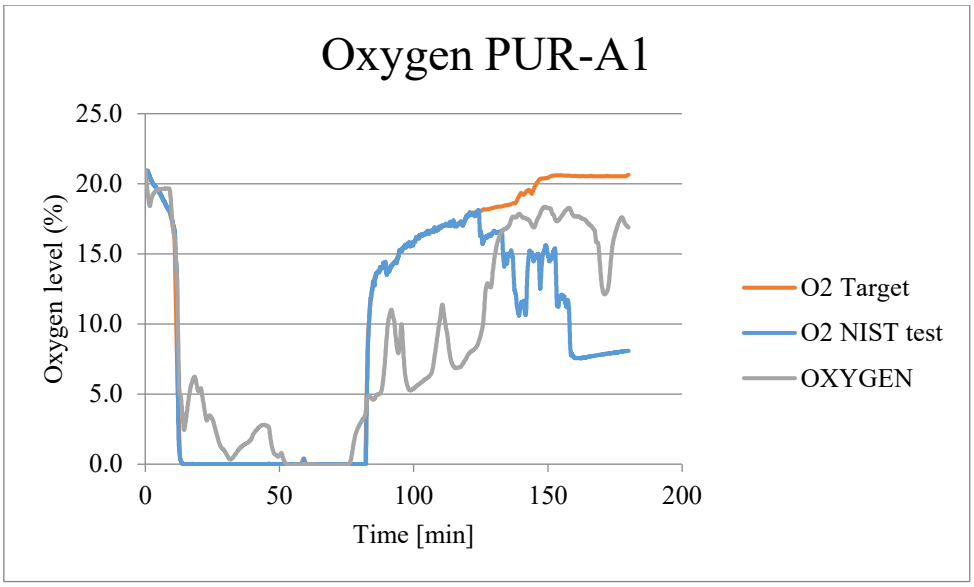

fig. 6-2. Visual graphs of the oxygen levels inside the furnace during the test for specimen PUR-A1.

The furnace temperature of the PUR-A2 specimen matched the target temperature quite well and did not deviate to the same extent as the PUR-A1 specimen towards the end of the test, see fig. 6-3.

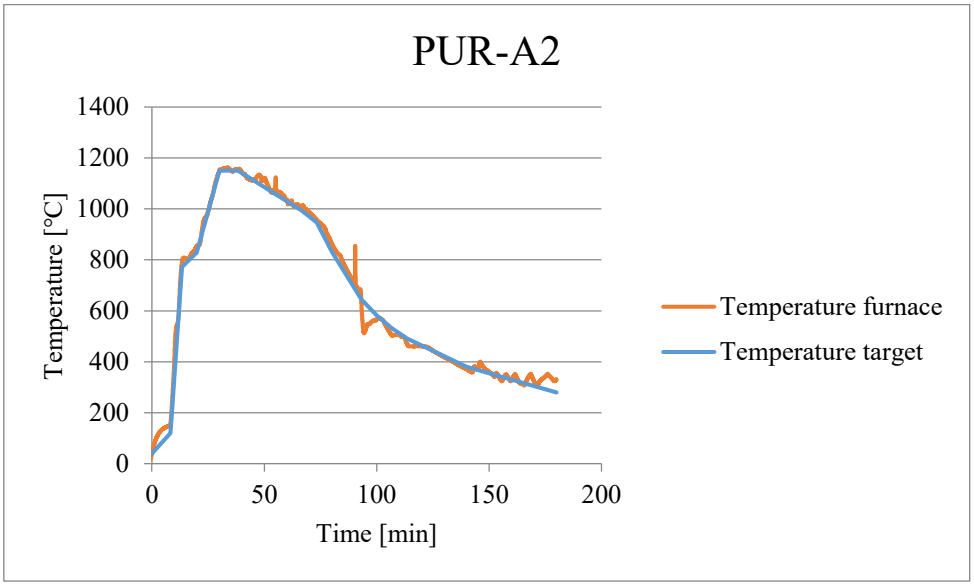

fig. 6-3. Temperature profile of the furnace in comparison with the expected target for PUR-A2.

Similar to the PUR-A1 test, the PUR-A2 test follows the expected oxygen curve rather well in the beginning, with minor deviations from the target during the lowest- and rapid increase phases, see fig. 6-4.

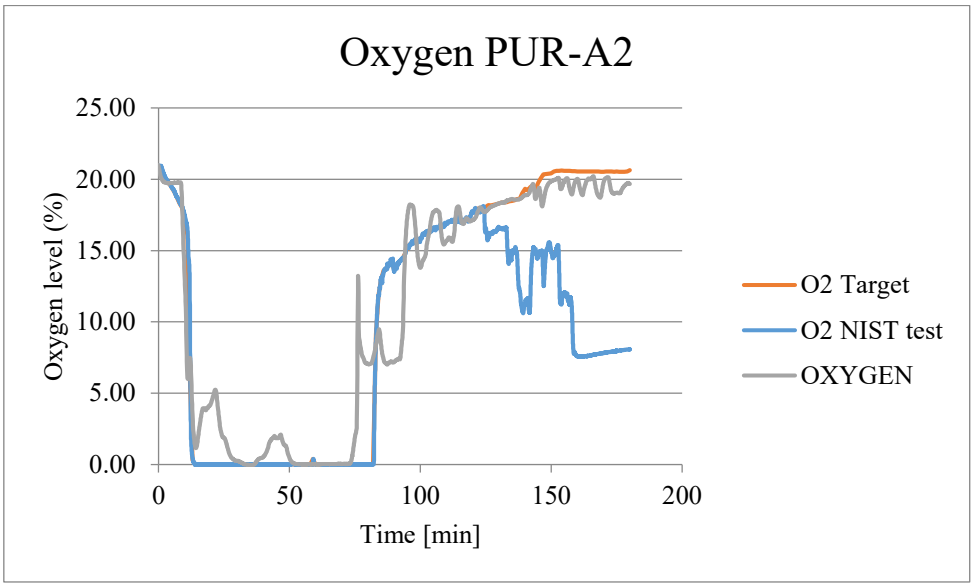

fig. 6-4. Visual graphs of the oxygen levels inside the furnace during the test for specimen PUR-A2.

The test with EPI-2 specimen was one of the tests where the performance of replicating the target curves was superior. Both the furnace temperature and oxygen levels matched the target curves very well, see fig. 6-5. and fig. 6-6. The furnace temperature curve only deviates from the target curve ever so slightly. Oxygen levels only deviate significantly during the zero-level phase, which was the case for all performed tests. Most test performances were very similar to this test, with only minor deviations, the rest of the graphs can be found in Appendix C.

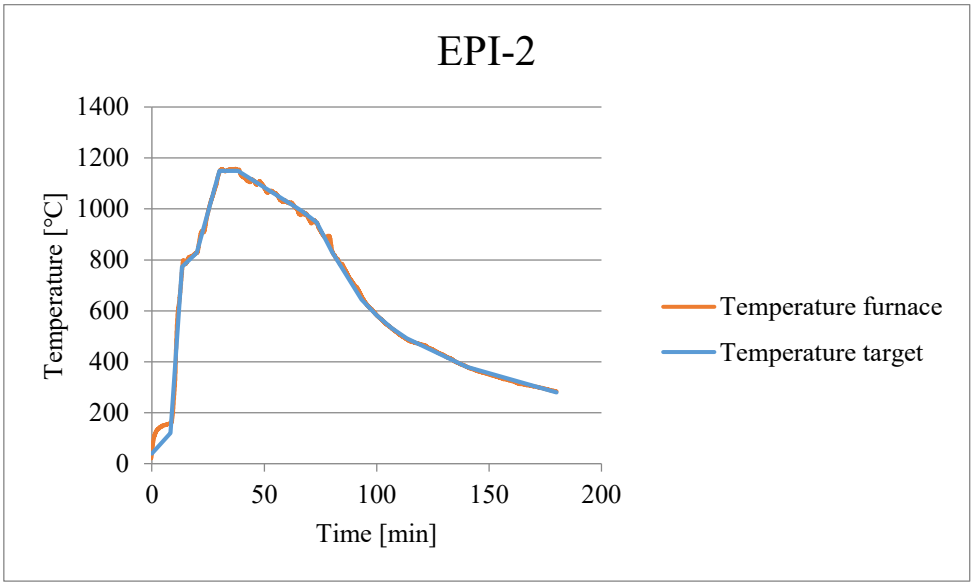

fig. 6-5. Temperature profile of the furnace in comparison with the expected target for EPI-2.

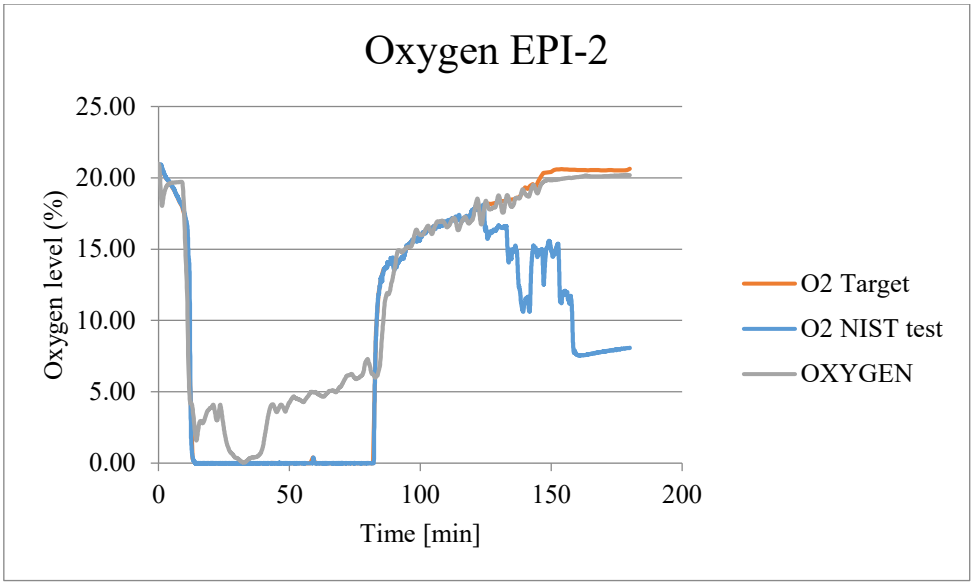

fig. 6-6. Visual graphs of the oxygen levels inside the furnace during the test for specimen EPI-2.

6.2 Temperature profiles

The temperature at specific depths was measured during the tests and is here presented as raw data over time. Measurements were made at six different depths from the side, at four different positions of the specimen, as well as three different depths from the top at two different positions. The depths of the top series (25-30) correspond to the first three lowest placed thermocouples in the side series (1-3 and 13-15). See fig 6-7 for an overview of the thermocouple numbering, and section 5 for more details concerning thermocouple placement.

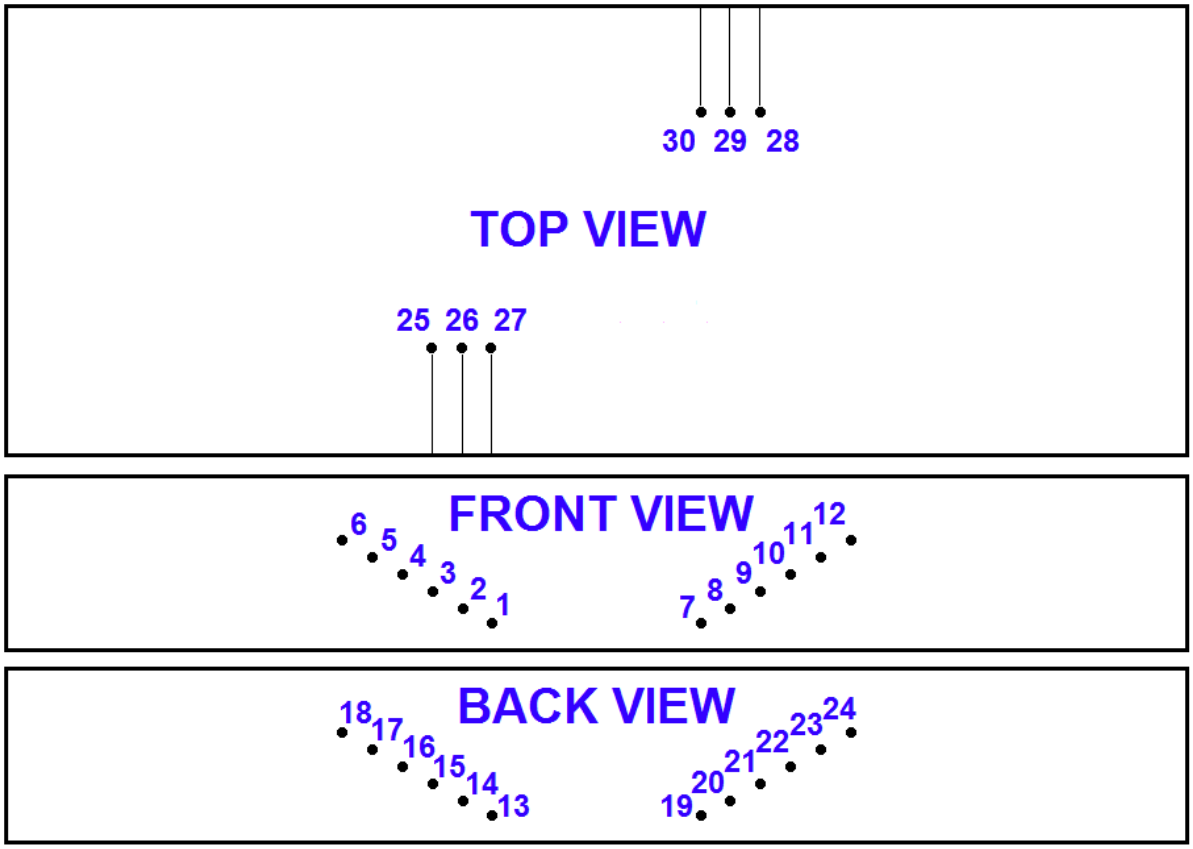

fig. 6-7. Sketch of thermocouple numbering and approximate placement in specimen.

Below, the temperature development in each specimen over time is presented. The specimens have been divided into their respective set of duplicates, and specific depths that have significance in analysing the occurrence of delamination, has been chosen. The thermocouples on the depth 35 mm correspond to the first bondline between the first and second lamella, the 50 mm approximately the middle of the second lamella and the 70 mm the second bondline between the second and third lamella. As measurements at all depths were repeated in four different series on the sides (see fig. 6-7), the data sets became very large. Therefore, in order to remain conservative, only the highest registered temperature reading at the depth of interest for each specimen has been chosen, see fig. 6-8 to 6-11. For all individual temperature profiles, including all depths and thermocouples, see appendix D.

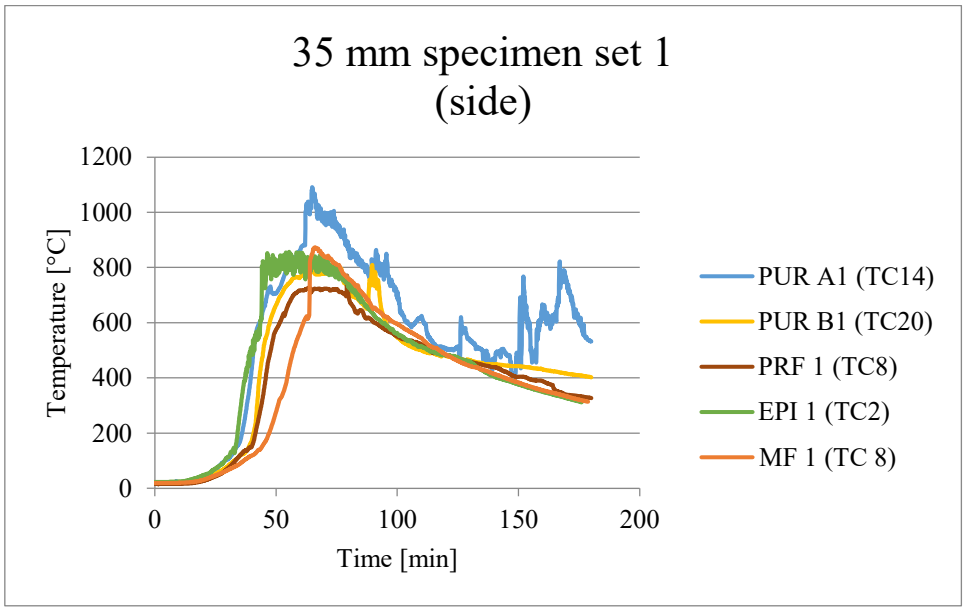

fig. 6-8. Top registered temperatures of specimen set 1 from the side series, at the depth 35 mm (bondline).

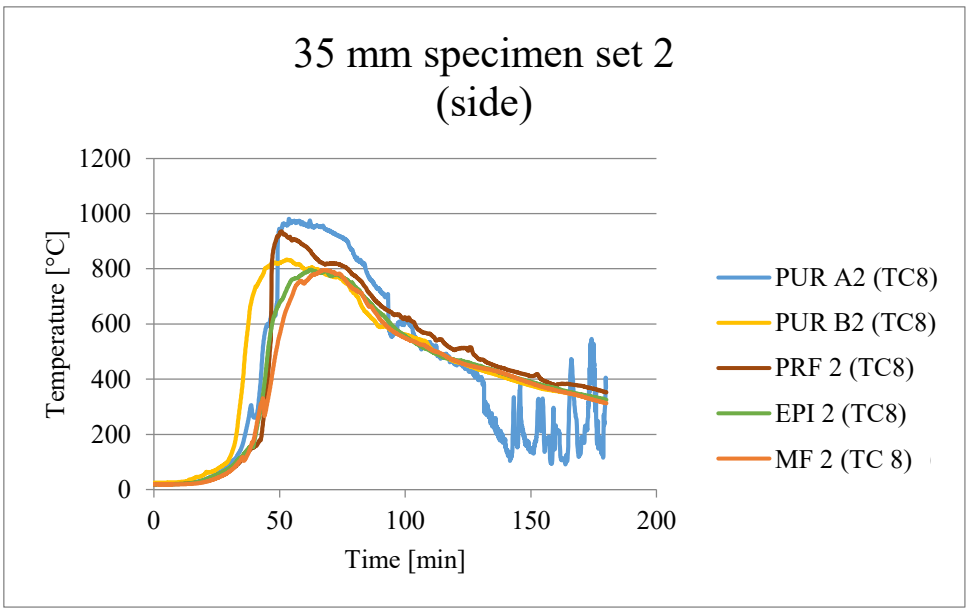

fig. 6-9. Top registered temperatures of specimen set 2 from the side series, at the depth 35 mm (bondline).

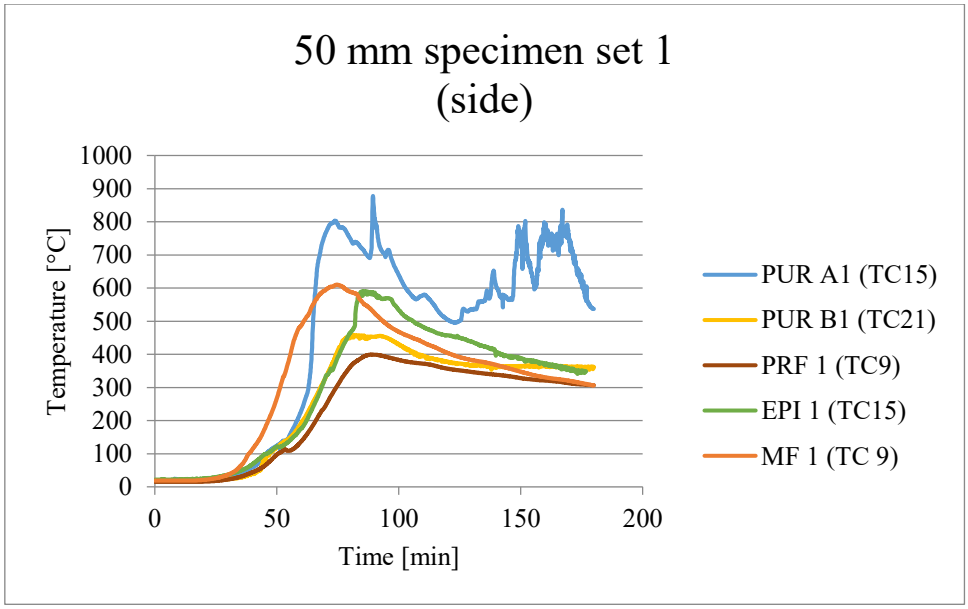

fig. 6-10. Top registered temperatures of specimen set 1 from the side series, at the depth 50 mm.

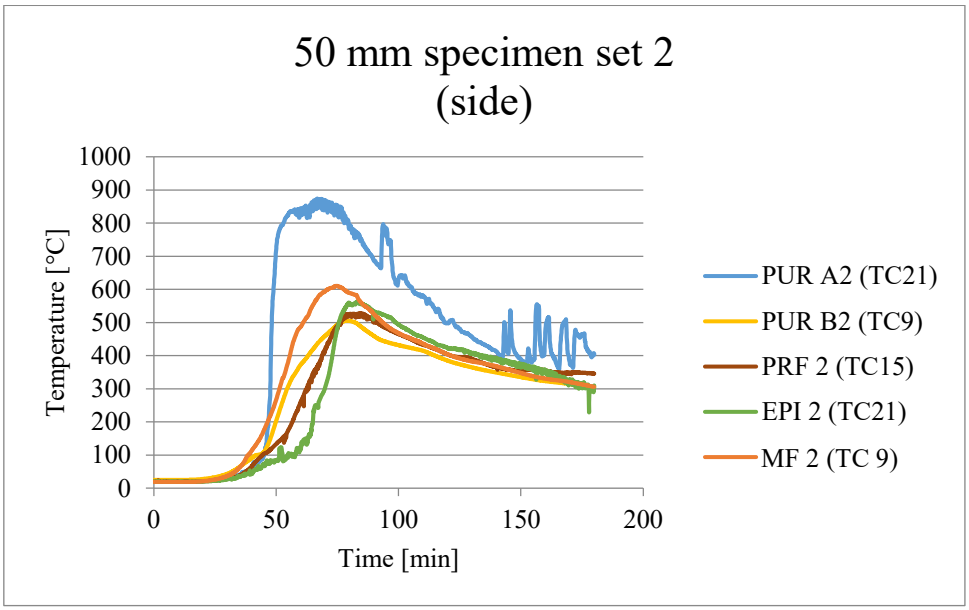

fig. 6-11. Top registered temperatures of specimen set 2 from the side series, at the depth 50 mm.

The temperature development in the first bondline (35 mm) and the following lamella (50 mm), appears fairly similar for most specimen and between the two sets, with the exception of the two full-scale test specimens (PUR-A1 and-A2) in each set and the PRF-2 in set 2. Overall the temperatures appear to have peaked at around 800°C at the 35 mm depth for most specimens, while the temperatures registered in the PUR-A1 and -A2 were closer to 1000°C. At the following depth of 50 mm, peak temperatures of approximately 600°C were registered for all specimens but the PUR-A1 and -A2, which registered top temperatures of around 800°C.

As the temperature measurement of 35 mm for PRF-2 clearly deviated from the rest in fig. 6-9 the individual temperature profiles for all thermocouples at 35 mm and 50 mm for PRF-2 are presented below, see fig 6-12 and 6-13.

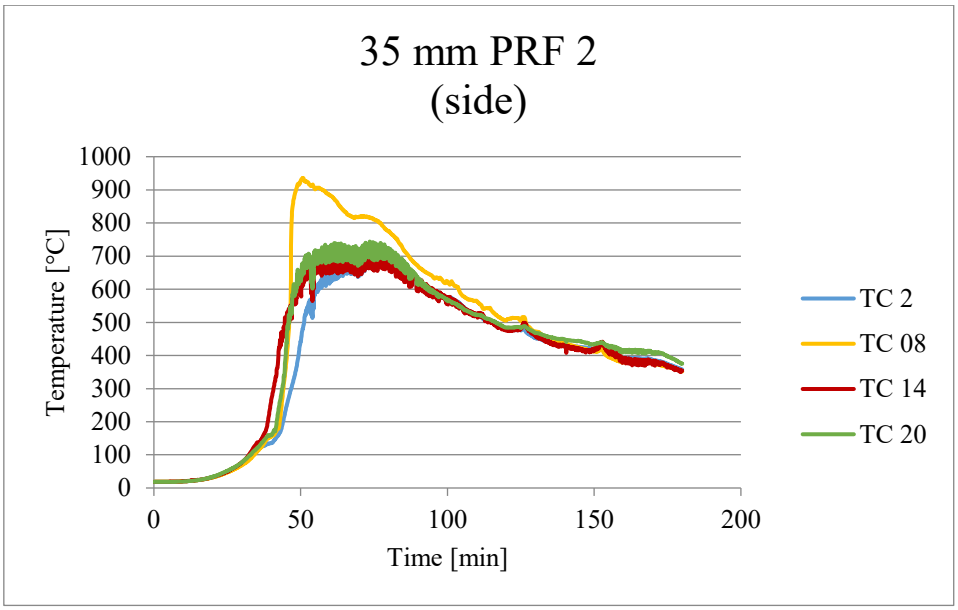

fig. 6-12. All thermocouple temperatures at the depth 35 mm (bondline), for the PRF 2 specimen.

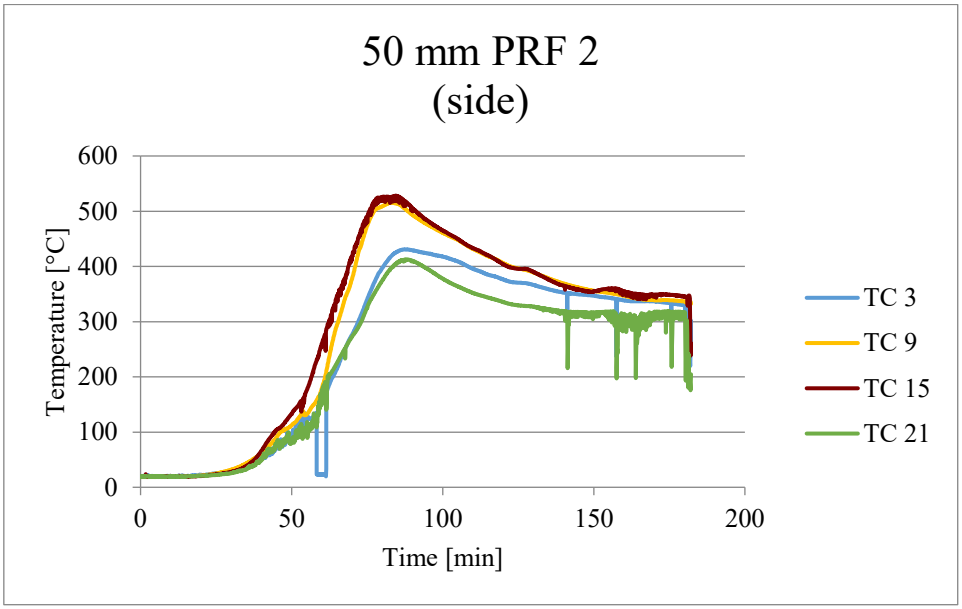

fig. 6-13. All thermocouple temperatures at the depth 50 mm, for the PRF 2 specimen.

The chosen measurement data for PRF-2 at the depth 35 mm (TC8) was indeed the highest registered temperature measurement for that depth series, see fig 6-12. Following TC 8 at the depth 50 mm was TC 9, which peaked at approximately 500°C, see fig 6-13.

Next depth of interest is 70 mm as it corresponds to the second bondline, see fig. 6-14 and 6-15 for the highest registered temperatures for each specimen at this depth.

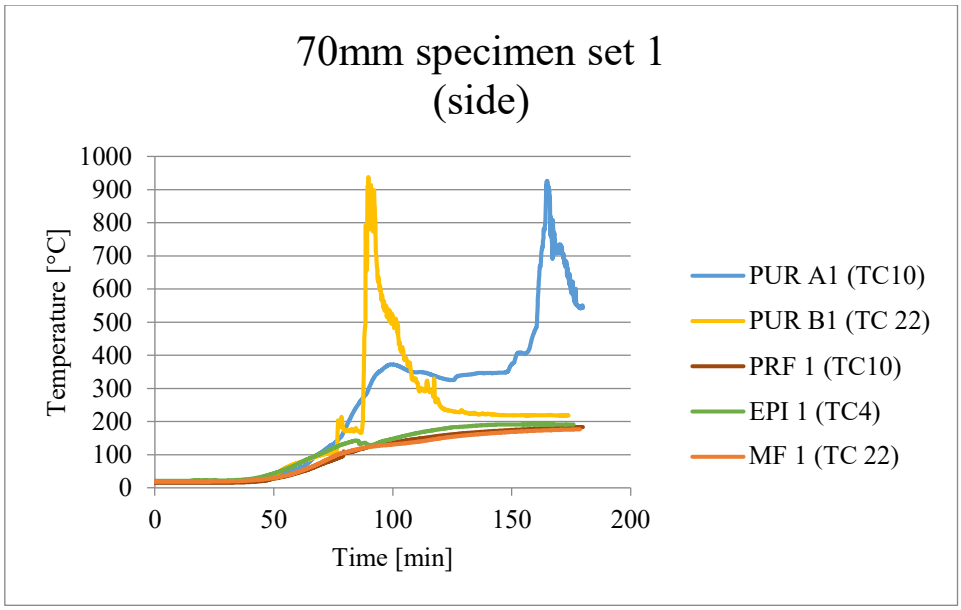

fig. 6-14. Top registered temperatures of specimens set 1 from the side series, at the depth 70 mm (2nd bondline).

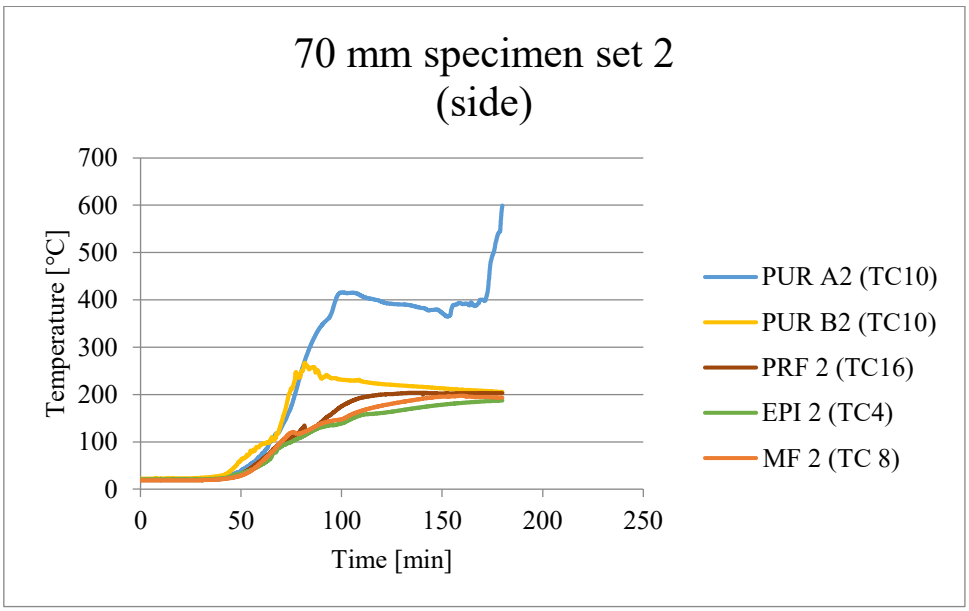

fig. 6-15. Top registered temperatures of specimens set 2 from the side series, at the depth 70 mm (2nd bondline).

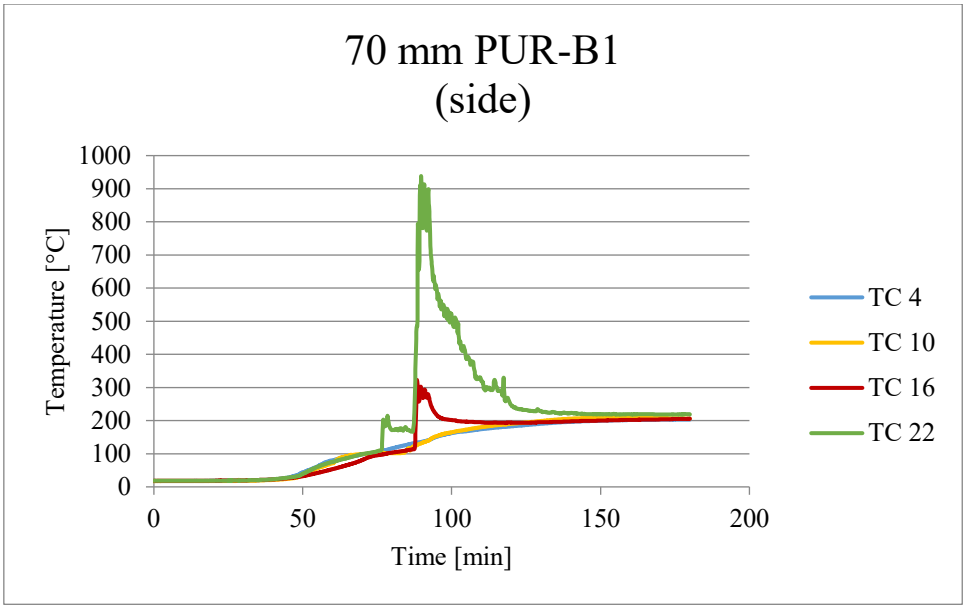

fig. 6-16. All thermocouple temperatures at the depth 70 mm, for the PUR-B1 specimen.

For most specimens, the temperature development at 70 mm started slowly and levelled out at approximately 200°C. However, this was not the case for the PUR-A specimens and the PUR-B1 specimen. The PUR-A specimens increased to around 400°C, and towards the end rapidly increased to 600 or 900°C, depending on set. The top registered temperature for the PUR-B1 specimen on the other hand, was reached after just 80 minutes, peaking at 900 ºC.

As this result was somewhat deviating, the individual temperature profile for the PUR-B1 specimen at the 70 mm depth, with all the thermocouple readings, was included in the result, se fig. 6-16.

6.3 Charring rate

The charring rate of each specimen was calculated using the assumption that the charring front corresponds to the characteristic temperature of 300°C, see section 3. In fig. 6-17 and 6-18 below, the calculated average charring rate over time for each specimen is presented, divided into the first and second set of duplicate specimens. The calculated charring rates are based on the temperature measurements of the four side-series of six thermocouples each, see section 5.3. The data points in the diagrams corresponds to the time it took to reach a temperature of 300°C for the thermocouples at a particular depth, and the calculated charring rate at that specific point. It's important to point out that each data point in the diagrams is presented as a calculated average of the measurements from the four side-series of thermocouples on the same level of depth. This being the case, local deviations of the charring rate are to be expected.

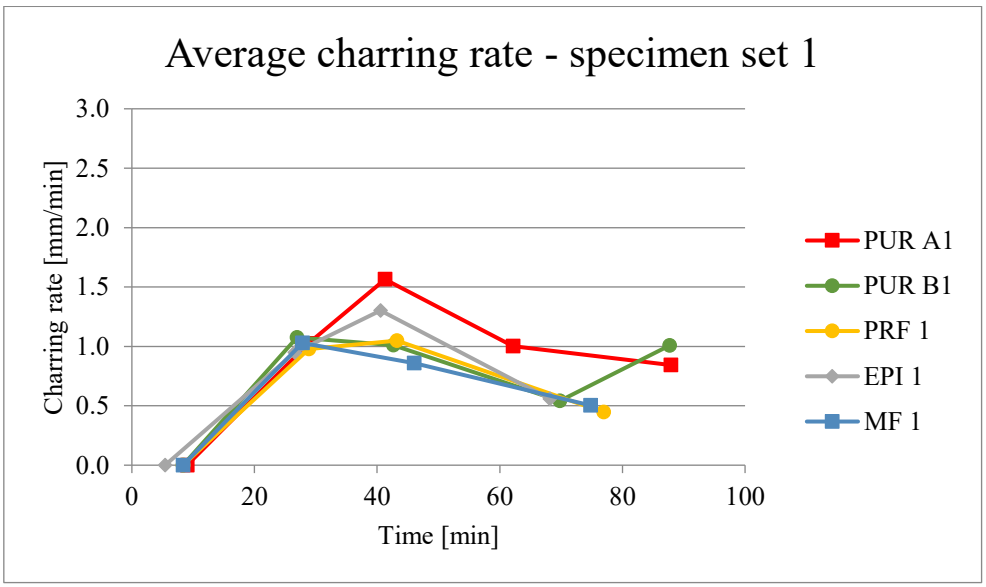

fig. 6-17. Calculated average charring rate over time for specimen set 1.

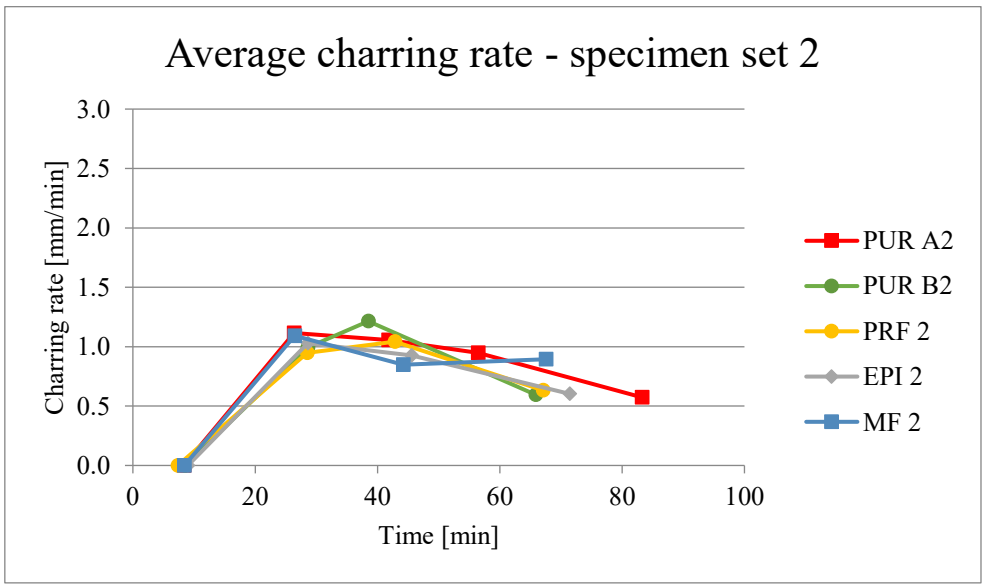

fig. 6-18. Calculated average charring rate over time for specimen set 2.

The charring rates over time are generally very similar from specimen to specimen and set 1 and 2, apart from PUR-A1 and EPI-1 in set 1, as well as MF-2 in set 2. PUR-A1 and EPI-1 being significantly higher than the overall set, and MF-2 slightly lower. Below, the individual diagrams for these specimens and the PUR-A2 are presented. In these diagrams the minimum and maximum values of the calculated charring rates of each data point are also shown as red intervals, see fig. 6-19 to 6-22. This selection was considered the most interesting due to the large uncertainty intervals, and a complete presentation of all individual charring rates over time is presented in Appendix E to limit the length of the result section.

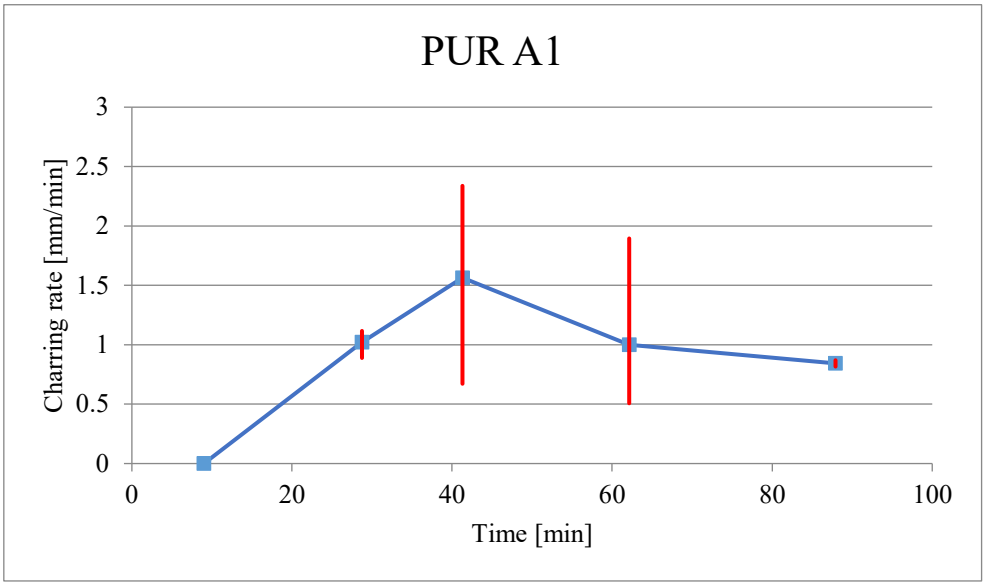

fig. 6-19. Average charring rate over time for the PUR-A1 specimen. minimum and maximum intervals of each calculated average are marked in red.

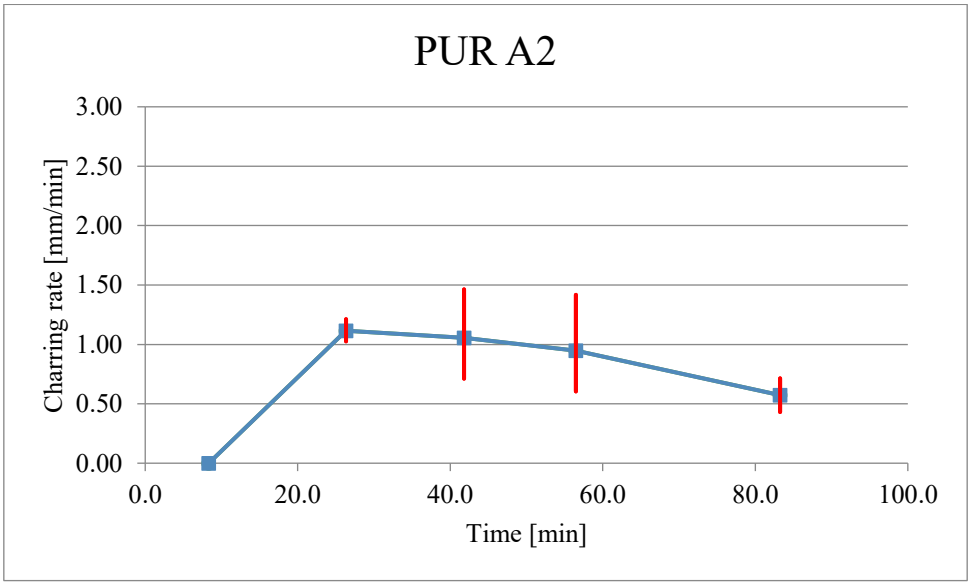

fig. 6-20. Average charring rate over time for the PUR-A2 specimen. minimum and maximum intervals of each calculated average are marked in red.

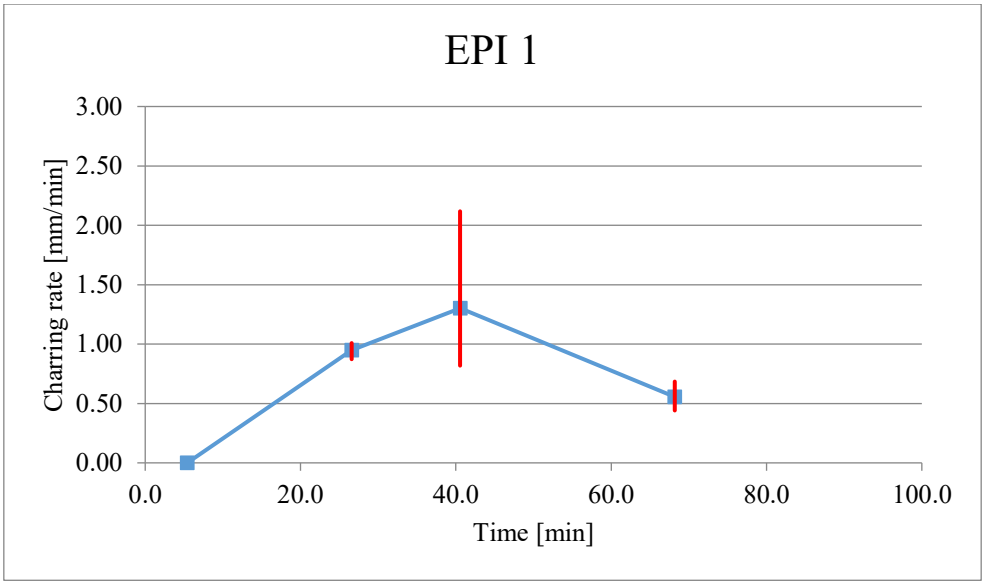

fig. 6-21. Average charring rate over time for the EPI-1 specimen. minimum and maximum intervals of each calculated average are marked in red.

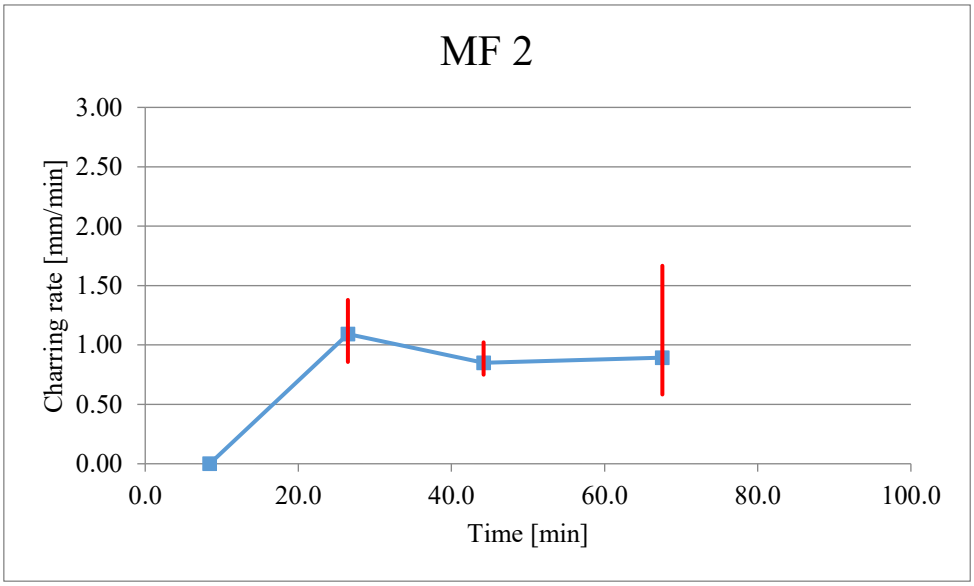

fig. 6-22. Average charring rate over time for the MF-2 specimen. minimum and maximum intervals of each calculated average are marked in red.

For individual diagrams of the charring rate over time and tabulated values for all specimens, see Appendix E.

6.4 Heat flux

The heat flux for each of the tests was determined through calculations based on the temperatures from the plate thermometers, according to section 5 and Appendix A. Constant values for these calculations were derived by measuring the actual heat flux for periods of time during the final test, which was the PUR-B1 test. A comparison of the measured and calculated heat flux for the PUR-B1 test is shown below in fig. 6-23. For the measured heat flux, the period for which the heat flux meter had to be removed from the furnace due to its limited robustness, can be observed in fig. 6-23.

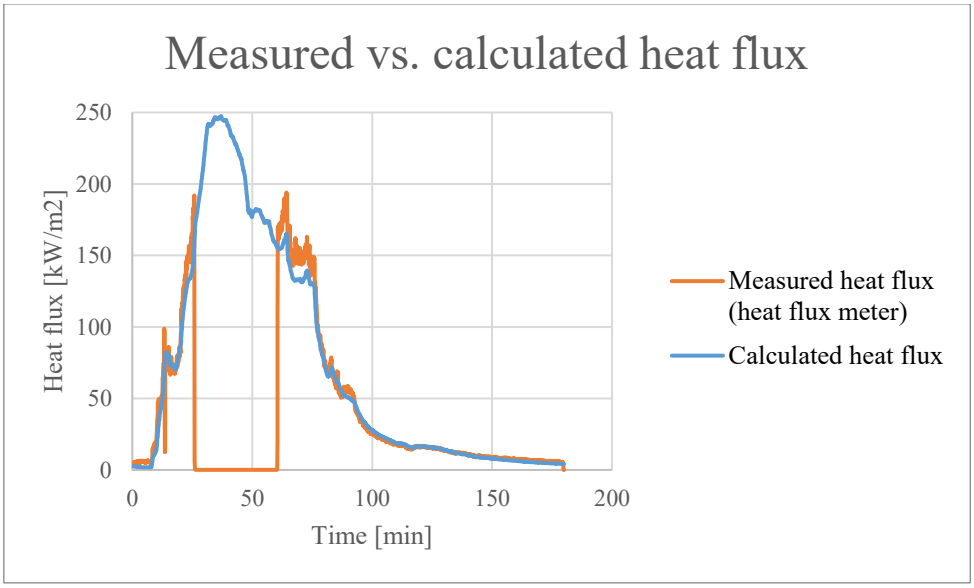

fig. 6-23. Comparison of the measured and calculated heat flux for the PUR-B1 test. Measured heat flux drops down to zero due to limited robustness of the device that was taken out as a protective measure when exposed to very high temperatures.

The PUR-A1 as well as the PUR-A2 presented a minor increase and fluctuations at around 48 minutes just before the start of the decay phase, see fig. 6-24. After approximately 92 minutes PUR-A2 exhibited a major drop in heat flux. However, PUR-A1 rose slightly at the same time. The end phase also differs somewhat for the two tests, the PUR-A1 exhibits an increase up to just below 50 kW/m^2, while the PUR-A2 continues to decay.

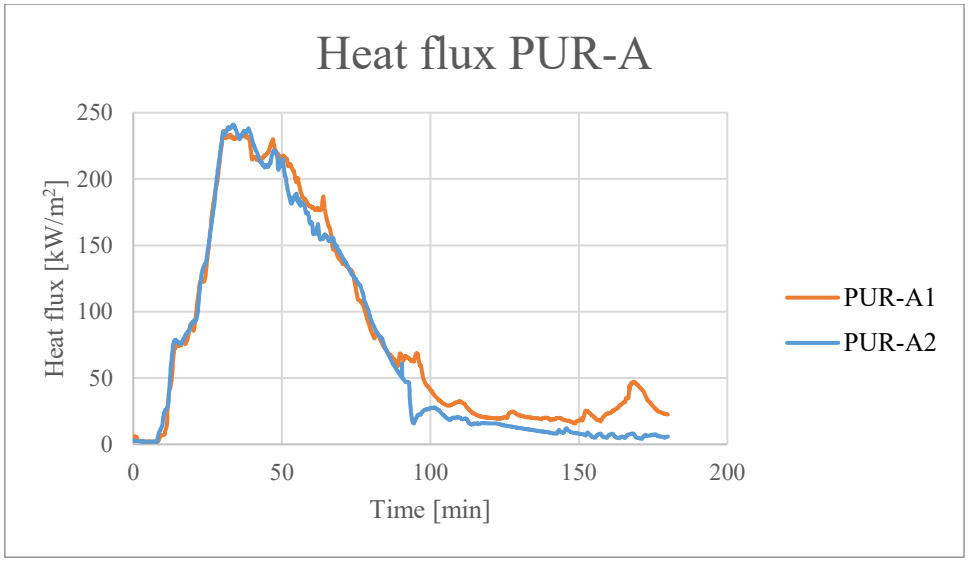

fig. 6-24. Comparison of heat flux between PUR-A1 and PUR-A2.

Regarding the test results of heat flux for the PUR-B as well as the PRF specimen the heat flux is similar between each specimen manufactured with the same adhesive. Small fluctuations in the measurements can be observed in general for all the tests, especially during the decay phase in some cases, see fig. 6-25 and 6-26.

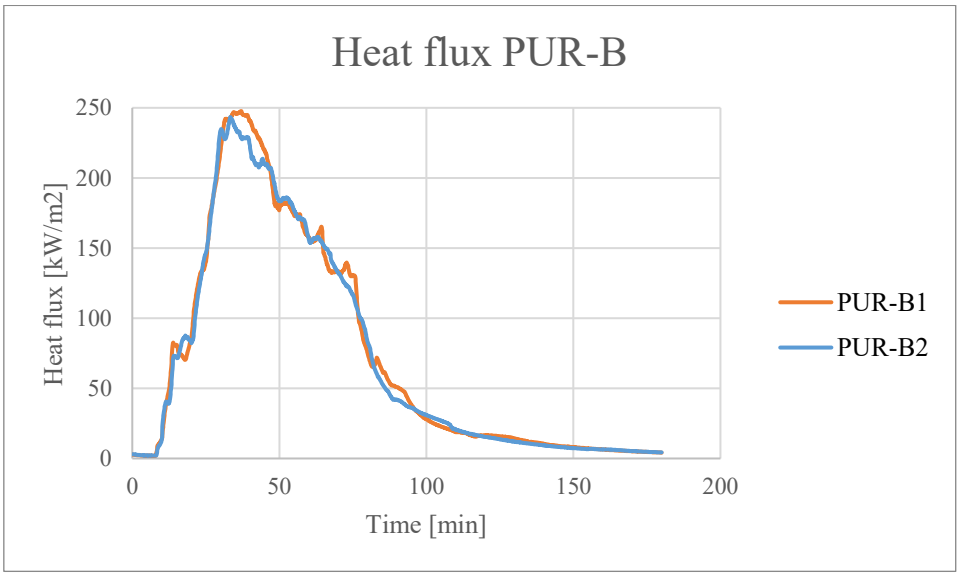

fig. 6-25. Comparison of heat flux between PUR-B1 and PUR-B2.

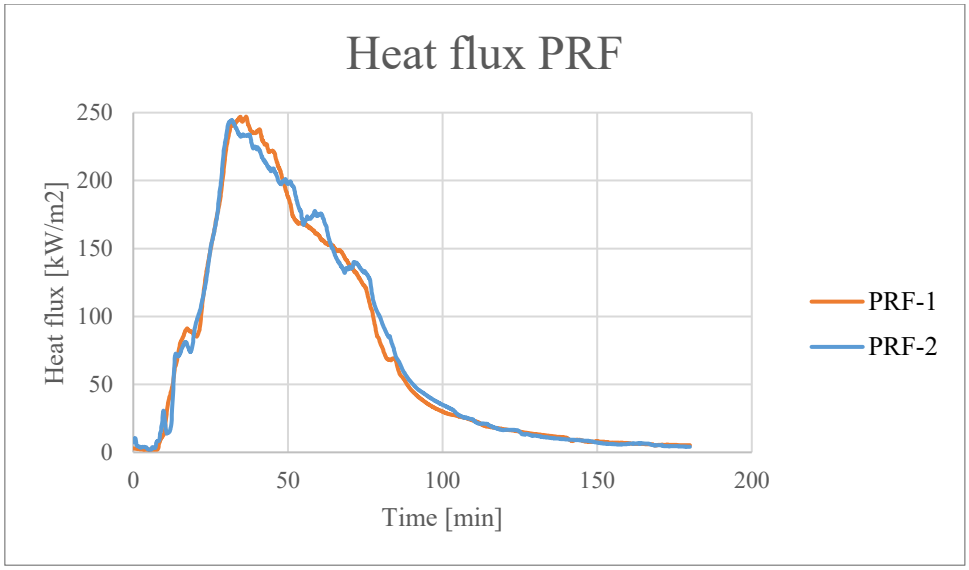

fig. 6-26. Comparison of heat flux between PRF-1 and PRF-2.

Earlier mentioned fluctuations are visible also for the EPI-1, where the decay phase differs between the two tests, see fig. 6-27. Comparison between the two MF tests shows that the change in heat flux acts quite similar, see fig. 6-28.

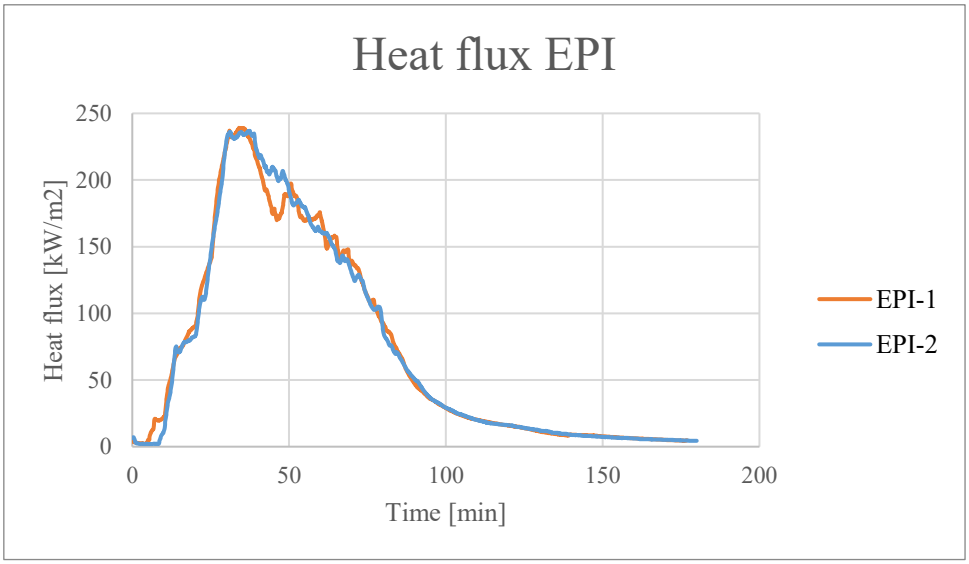

fig. 6-27. Comparison of heat flux between EPI-1 and EPI-2.

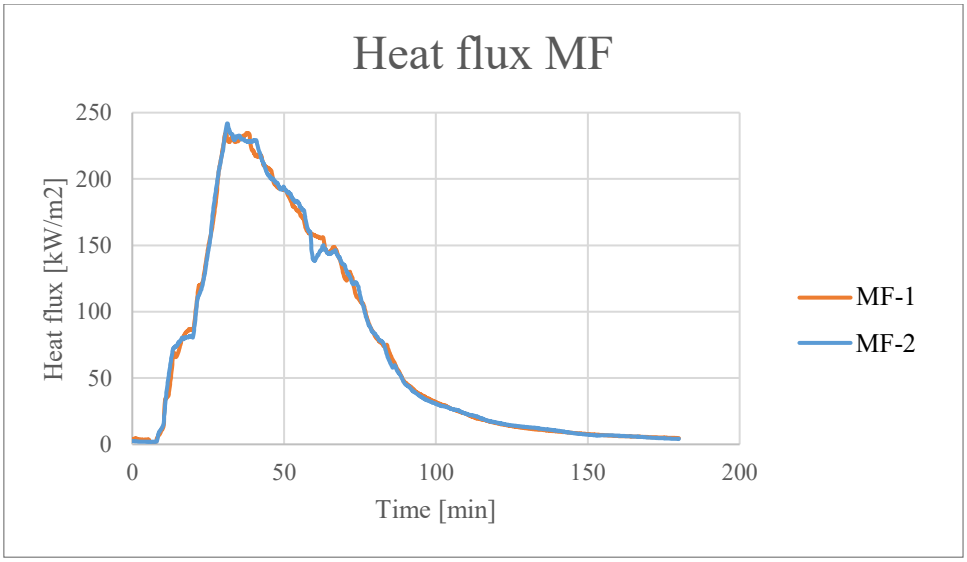

fig. 6-28. Comparison of heat flux between MF-1 and MF-2.

6.5 Observational timeline

For each test, visual observations of the specimen were achieved by recording video material with a camera mounted in the observational tube of the furnace. In this section timelines for three tests have been chosen in order to maintain a reasonable length of the result section. The selected tests are PUR-A1, PUR-A2 and EPI-2, as theses tests differed noticeably in measurements in comparison to the rest in terms of observed activity and significant events, such as delamination.

An overview of the observations regarding delamination can be found in table 6-2 below.

Table 6-2. Visual observations regarding delamination and times until said observation.

Specimen	**Observed Delamination?**	**Comments**	**Time until visually observed delamination [**min**]**
PUR-A1	YES	Complete delamination of first and second lamella	52 min (first lamella) 2 h, 43 min (second lamella)
PUR-A2	YES	Complete delamination of first lamella, partial delamination of the second lamella	50 min (first lamella) 2h, 58 min (second lamella)
PUR-B1	NO	-	-
PUR-B2	NO	-	-
PRF-1	NO	-	-
PRF-2	NO	-	-
EPI-1	NO	-	-
EPI-2	Partial	Larger part fell off towards the end, no ignition of the underlying layer	1h, 24 min (parts of first lamella)
MF-1	NO	-	-
MF-2	NO	-	-

For more details concerning the observations for PUR-A1, PUR-A2 and EPI-2, see the observational timelines on the following pages. Observational timelines for all ten executed tests are found in Appendix F.

Timeline for PUR-A1

Initial stage of delamination

Image of the first lamella in the initial stage of the fire after 16 minutes.

The test with PUR-A1 started to show signs of delamination when a smaller part delaminated after approximately 51 minutes and within a minute later a major part of the first lamella delaminated.

First delamination

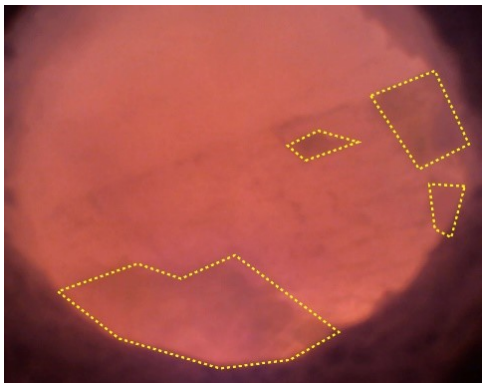

Reignition

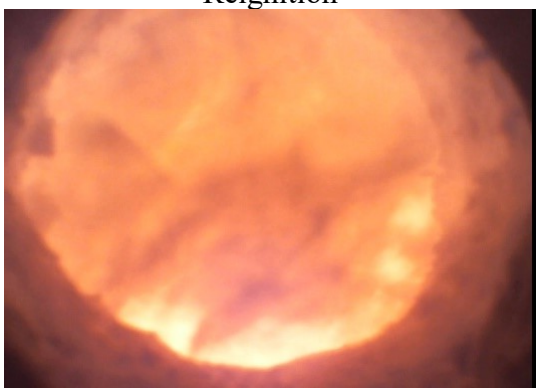

Shortly after the first delamination the intensity of smoke and flames increases inside the furnace and reignition of the wood was shown.

Second delamination

After approximately 2 hours and 43 minutes a second layer of the specimens are delaminating from the element.

Timeline for PUR-A2

Initial stage

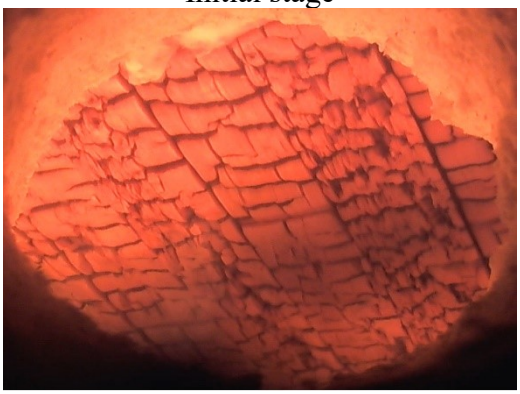

Initial stage of the first lamella before any major changes occurred. This picture represents the beginning of the test after approximately 17 minutes.

First delamination

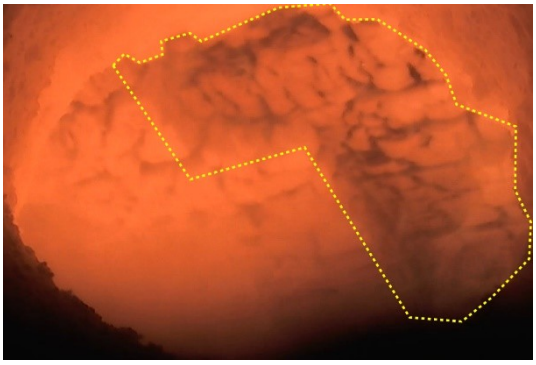

After approximately 42 minutes smaller parts of lamellas are falling off, and 2 minutes later a larger part of the first lamella falls off as well. After this an increase in flames occurred as well as turbulence of gases.

After 48 minutes further delamination of the first lamella occurred. Shortly after this an increased intensity of smoke and flames occurred and more parts of the first lamella were gone.

Second delamination

After a while of low activity on the screen, small parts of the second lamella fell off at around 2 hours and 48 minutes. The newly exposed wood in the furnace began to burn, causing flames and increased glowing of the wood.

After 2 hours and 58 minutes a highly increased intensity of light, glowing parts as well as flames occurred after a period of darkness. On the specimen way up from the furnace observations showed that a larger part delaminated in the down left corner of the picture.

Second delamination

Timeline for EPI-2

Initial stage

The initial stage of the charcoal and fire after approximately 17 minutes.

First stage of delamination

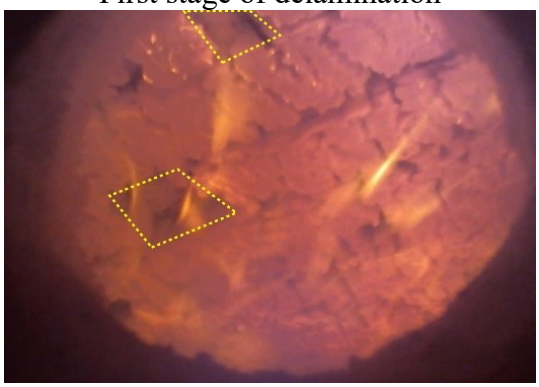

Small and local parts of the first lamellas started to fall off around 1 hour and 16 minutes.

Second stage of delamination

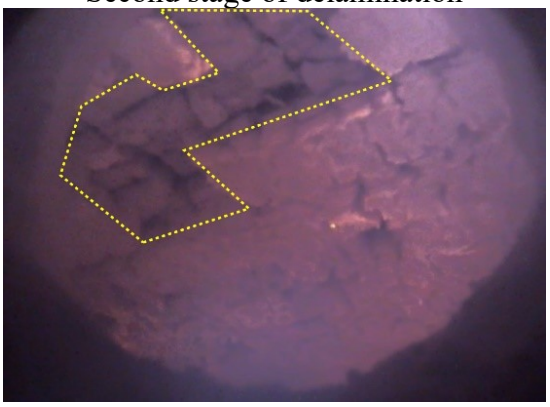

Approximately 1 hour and 30 min into the test a larger part delaminated in the first lamella. This was the last visible stage caught on camera before it became too dark in the furnace.

7 Discussion

In this section, the results will be evaluated and discussed in detail as well as in a broader context. Details concerning the performance of the tests will be the initial subject of discussion, to evaluate how well the target full-scale fire (Su, et al., 2017) was replicated. Following this are discussions regarding the different measurements and the visual observations through the video material. These measurements include temperature profiles and calculations of charring rate for the specimens, as well as heat flux inside the furnace. The topic thereafter, are the potential sources of errors that the authors have identified. Finally, future potential and challenges of CLT as a building material are discussed, based on the results and the evaluation of these.

7.1 Test performance

During each fire test, target temperatures and oxygen levels were supposed to be replicated, which was done by controlling the furnace burners and manually adjusting the oxygen levels through the input of nitrogen. This procedure proved quite difficult to perform, but the overall results were satisfactory. A distinct experience concerning the performance of the tests was that the task of matching the furnace temperature and the oxygen levels with the desired target curves, became significantly more difficult if delamination occurred during a test.

For the adhesives PRF, PUR-B and MF no major signs of delamination were observed, so these tests progressed with no major complications, see graphs in section 6.1 and Appendix C as well as observational timelines in section 6.5 and Appendix F. Even with specimens manufactured with the EPI adhesive where partial delamination occurred, no major difficulties arose. In contrast, when delamination occurred for the PUR-A based specimen, it resulted in a fire development that was harder to control due to the rising temperatures that followed.

The delamination resulted in an immediate ignition of the underlying lamella, resembling a flashover. During this period, the oxygen level inside the furnace dropped rapidly and in most instances, went all the way to zero for period of time. This, in turn, was beneficial when it came to replicate the original full-scale NIST-fire, as no nitrogen had to be used during this phase to meet the target criteria. However, the rising temperatures soon proved problematic, as the furnace temperature following delamination for these tests became significantly higher than the target temperatures. In order to cool the furnace during this phase, a variety of methods were tried, such as adding large amounts of nitrogen, opening up the top of the furnace and/or adjusting the pressure.

It became apparent that if delamination occurred during a test, it would be very hard to control the furnace temperature and the oxygen level at the same time in the phase following delamination. Certain periods of time, large amounts of nitrogen needed to be applied to reach the target value of the oxygen level or furnace temperature. During the experiment with PUR-A1, we experienced that the application of nitrogen required a lot of resources, and that the current approach was not sustainable in the long run. Since only a finite amount of resources were available for the experiments, a specific amount of nitrogen per test was set. In order to not exceed this amount, it was decided to keep the oxygen level below a maximum of 5% during the zero-level phase, as a sufficent criteria for this phase.

Some actions proved somewhat counter-productive in terms of replicating the full-scale NIST-fire. For example, sometimes adding more nitrogen cooled the furnace, but it also lowered the oxygen level below the target level. For the second test with an original NIST-test Poly-urethane specimen (PUR-A2), a working combination of measures had been developed. For this test, the whole furnace door was opened slightly and used to regulate the cooling of the furnace, while a moderate amount of nitrogen was injected to lower the oxygen levels. The original idea for this was that this procedure would better replicate the ventilation conditions of a real compartment fire and cool the furnace more efficiently. A concept that proved accurate in the end.

Based on the overall results, the authors believe it's fully possible to replicate something close to a real fire scenario in a standard furnace, but events such as delamination significantly aggravate this process. It's possible that this procedure could be improved and even automated, given more time and resources. This is something that we consider should be investigated further in the future.

7.2 Occurrence and effects of delamination

As the main focus of the report has been the event of delamination, the bulk of the presented results were chosen to evaluate and study either the indication of delamination or the following effects, see section 6. For some of these results, the difference was very clear, while some material was far from conclusive. In order to maintain a coherent structure in the evaluation of the results, the visual observations of the delamination in the form of the video material (see section 6.5), has been used as a foundation in the discussion of individual results.

Below follows the discussion of results divided into each respective category of measurements or calculations.

7.2.1 Temperature profiles

The choice of including the highest registered temperatures of the depths of 35 and 70 mm in the result section felt natural as these depths corresponds to the first and second bondline of each specimen and should therefore be of significance when studying delamination. The first thing one notices when observing the temperature diagrams of the 35 mm depth (see fig 6-8 and 6-9 in section 6.2), is that the temperatures overall are high, and most specimens see a rapid increase in temperature after around 30-40 minutes. Both in set 1 and 2, the PUR-A1 and -A2 showed the highest registered temperatures, peaking at approximately 1000°C or slightly over. This is interesting since these two specimens were the only ones where complete delamination was observed (see section 6.5).

One can also observe that the PRF-2 specimen in set 2 also registered a high peak temperature, which sets it apart from the rest since it didn't show any sign of delamination during testing. However, we believe this to be a local irregularity caused by defects in the specimen at that particular measurement point, possibly a crack or cavity. This wouldn't be surprising as the overall quality of the specimens was quite poor, see Appendix G for images. To somewhat verify that this deviation wasn't caused by local delamination, the individual temperature profiles for the PRF-2 specimen for the 35 and 50 mm depths were included in the result, which includes all thermocouple series of that specimen (see fig 6-12 and 6-13). When studying fig. 6-12 one can confirm that the thermocouple that was chosen (TC8), indeed deviates from the rest. The following thermocouple in that series is TC 9 and as shown in fig. 6-13 it registered a higher peak temperature than most thermocouples at 50 mm. Still, when compared to the peak temperatures of the delaminating specimen PUR-A1 and -A2 at the 50 mm depth (see fig. 6-10 and 6-11), this temperature is more than 300°C lower, suggesting that it's a question of a local deviation rather than delamination.

For the rest of the specimen at the 35 mm depth, although lower in peak temperature (around 800°C), they still registered very high, considering that no complete delamination was observed for these specimens. Another interesting point is that delamination was visually observed at around 50 minutes for PUR-A1 and -A2 (see section 6.5), which in turn should mean that the characteristic charring front temperature of 300°C should be reached around this time or slightly before.

This, however, does not seem to have been the case. Both of the delaminating specimens were from the original full-scale test and manufactured with the same type of Poly-urethane adhesive, an adhesive suggested to have a critical thermal degrading temperature of approximately 200°C, suggesting that delamination should have occurred even earlier. Yet, this was still not the case, and this is why the additional temperature diagrams of the 50 mm depth were included in the results

(see fig. 6-10 and 6-11). At the 50 mm depth, the difference between the delaminating PUR-A specimens and the rest becomes more apparent. The PUR-A specimens rapidly reaches temperatures of approximately 800°C at around 50 minutes or somewhat after, while the rest of the specimens peaks at around 600°C at approximately the same time. The extremely rapid increase in temperature for the PUR-A specimens at around 50 minutes corresponds better to the observed time of delamination for the 50 mm depth than the actual bondline depth of 35 mm.

What does this really tell us? It would seem that if the previously mentioned characteristic value for the charring front temperature of up to 300°C is applicable in this case, and the observed time for delamination was correct, the charring front had moved past the bondline at the time when delamination was observed. The high temperatures at the 35 mm depth for the specimens that delaminated are reasonable since the thermocouples at that particular depth would be left in part, or fully unprotected and exposed to the upper gas layer of the furnace.

This doesn't explain the high temperatures of the rest of the specimen, which didn't delaminate, and still registered temperatures up to 800°C. We believe this to be a result of the formed char layer still being quite thin at this time, meaning that at this particular charring depth, the temperatures would still be quite high due to the limited insulating capability of the initial char layer. In turn, this would also explain the extremely rapid increase in temperature at the 50 mm depth for the PUR-A specimens at the observed time of delamination, as a whole insulating, charred lamella was lost instantaneously and the charring had already progressed into parts of the second lamella.

The final results presented in the temperature profile results are the 70 mm depth data. The reason for this is that this depth corresponds to the second bondline, and secondly, that after this depth no measurement exceed 300°C during any test. The results at this depth appears far clearer than at the lower depths, with the delaminating PUR-A specimen rising to a steady 350 - 400°C and increasing rapidly towards the end of the test.

The temperature for the PUR-B1 specimen also differed noticeably, as thermocouple 22 registered an extremely rapid temperature increase at approximately 80 minutes, peaking at 900 ºC, see fig. 6-14. It's our theory that this was not the result of localized delamination, but rather a faulty thermocouple reading, as no significant activity was observed around this time mark, see appendix G. This theory is enforced when comparing thermocouple 22 to the rest of the thermocouples at the 70 mm depth for PUR-B1, as it's clearly deviating, see fig. 6-16. Additionally, if delamination or any other mechanism had exposed the thermocouple to the hot gases of the furnace, the temperature would have stayed high and not decreased back down to the same level as the rest of the thermocouples.

The second delamination of PUR-A1 was visually observed at around 163 minutes into the test (see section 6.5), which is in good agreement with the heat peak at approximately 165 minutes for the 70 mm bondline-depth, see fig. 6-14. For the PUR-A2 specimen complete delamination of the second lamella was not observed during the full duration of the test (see section 6.5). Still, when studying the bondline temperature of PUR-A2 (see fig.6-15) it seems that the temperature increase towards the end of the test could indicate delamination, although delayed.

Towards the end of this test smaller parts fell off and the underlying lamella ignited, resulting in visual flames across the specimen (see section 6.5). Afterwards, when the test was terminated and the specimen was lifted off the furnace, a large middle piece fell off, exposing fresh, unburnt wood underneath (see fig. G-10 in appendix G). It's, therefore, our conclusion that complete secondary delamination most likely would have occurred for PUR-A2 if the test had been running for a bit longer.

The temperature at the 70 mm depth for the rest of the specimens levelled out at the quite low temperature of 200°C and stayed at this level throughout the remainder of the test. The PUR-B

specimens differed somewhat, with a more rapid increase in temperature and a slight peak before levelling out (see fig. 6-14 to 6-16). We believe that this might have something to do to with the properties of the adhesive as the PUR-B is manufactured with a Poly-urethane adhesive, like the delaminating PUR-A specimen, albeit a more recent, and in this case better performing one. The Poly-urethane adhesives overall might be more prone to quicker heating due to their composition. In the end, this doesn't seem to have affected the final outcome for the PUR-B specimens, and they performed well.

7.2.2 Charring rate

In terms of charring rate, the calculated average values over time for each test looked very similar, but there were some exceptions. For instance, the PUR-A1 specimen presented very high calculated values, peaking at around 1.5 mm/min, see fig. 6-17. One could speculate that this would be the result of delamination, as this was observed for the PUR-A1 specimen (see section 6.5). This theory, however, is something we're prepared to dismiss, as when comparing the average charring rate over time for PUR-A1 to that of PUR A2 in set 2, which also delaminated, PUR A2 is nowhere near as extreme (see fig. 6-17 and 6-18).

Furthermore, when studying the individual diagrams of the average charring rate over time for PUR-A1 and PUR-A2 (see fig. 6-19 and 6-20), one also notices the very large intervals of deviation from the average values for PUR-A1. This appears to be a trend in the overall charring rate results, where specimens that presented the most extreme values also presented the greatest intervals of uncertainty in the individual average values. This is confirmed for the EPI-1 and MF-2 specimens, which both presents somewhat deviating results as well, see fig 6-21 and 6-22 and Appendix E for all individual charring rates. It's therefore difficult to conclude anything certain about the impact and occurrence of delamination in regard to the charring rate in this case.

This is in stark contrast to what we expected, as the basis for these calculations were the temperature data, and the temperature profile results were quite conclusive at this point. One would expect to see a rise in the charring rate for all measuring series around the time of observed delamination. For example, Eurocode 5 suggests that the charring rate should be doubled following the loss of protective cladding, like gypsum boards and the like. A concept believed by some, to be applicable as a rule of thumb for the event of delamination as well. This is not something we can confirm with our results, as measurements for individual series differ greatly, giving rise to high uncertainty.

The local extreme values of the materials are most likely the result of uneven charring across the specimen, irregularities in the wood and/or potentially faulty readings from thermocouples. This is supported by the temperature profile data (see appendix D), which makes sense when considering the applied definition of the charring front of 300°C for the charring rate calculations. One fact that we can confirm though, is that for the specimen that did delaminate, the calculated charring front went further into the specimen, see fig. 6-17 and 6-18, as well as Appendix E.

Another observation is that the average values of the charring rates were overall relatively high for all the specimens (see appendix E), at least when compared to the recommended standard value of 0,65 mm/min for glulam in Eurocode 5. However, one has to keep in mind that this standard value is based on furnace testing with the ISO 843-fire, which has very little in common with a real full-scale fire, which was the intended target for replication. In any case, we still believe that this is an aspect that should be considered in future updates of designer guidelines for CLT and timber structures in general, such as the future revision of Eurocode 5.

7.2.3 Heat flux

When considering the correlation between heat flux and the occurrence of delamination it can be hard to come to any definitive conclusions. If delamination occurs, one should be able to see a rise in heat flux, as previously unexposed wood ignites and contributes to this increase. We will further discuss three of the specimens where complete or partial delamination was observed in the video material (see section 6.5), these are PUR-A1, PUR-A2 and EPI-2. By only observing the heat flux graphs in section 6.4 it is hard to get any indication of whether delamination occurs or not. It is hard to determine whether a rise in heat flux is a consequence caused by delamination or an error in terms of calculations, measurement data or some other phenomena. Mainly because the graphs in general fluctuate a lot. For example, the heat flux of PRF-2 shows small increases during the decay phase that could have been a sign of delamination, but there's no indication of this in the video material or temperature measurements.

With the PUR-A1 test, the delamination of the second lamella appear to have resulted in a quite distinct increase in heat flux after 2 hours and 43 minutes. This is in the period when delamination occurred according to the observational timeline in section 6.5. The occurrence of the first delamination in the PUR-A1 test occurred after 51 minutes according to the observational timelines in section 6.5, this event can't be seen as clearly in the heat flux graph in fig. 6-24. A small increase in heat flux can be seen, but it's not significant enough to be able to confirm that it is an actual indication or effect of delamination. Changes of heat flux occur in similar ranges as the first delamination, that doesn't necessarily mean that delamination occurred. Therefore, it might be hard to always determine when delamination occurs by only observing heat flux.

A similar discussion can be made regarding the test with PUR-A2. In this test, delamination of the first layer started after 42- 44 minutes according to the observational timeline (see section 6.5) and a larger part delaminated after approximately 48 minutes. Increases in the heat flux graph can be observed during this period and effects of delamination can be spotted as well, see fig. 6-24, which is verified when compared with the video material. However, the increase even in this test is not completely significant but differ more than the individual fluctuations. The second delamination only occurred partly in this test during the duration of the test, and it's not possible to observe in the graph in the same way as with the PUR-A1 where the effect was quite clear.

When considering the PUR-A tests, to determine delamination through the rise in heat flux, we believe that the current heat flux or temperature at that moment indeed has an impact. For the results of PUR-A1 as well as PUR-A2, the first delamination can possibly be observed as a small increase, but at the same time, it is harder to separate that peak from other fluctuations in the heat flux. While at the end of the PUR-A1 test, when the second delamination occurred, a distinct rise can be seen in the heat flux, see fig. 6-24. This is probably because the difference in temperature was much larger compared to the first delamination when the temperature inside the furnace was still quite high.

The last test where delamination was observed through video material was EPI-2, where the first lamella delaminated partially. No signs of delamination can be seen in the heat flux graph of this test, which might have a reasonable explanation. The first major delamination in this test occurred after 1 hour and 16 minutes according to the video material in section 6.5. At this time, the temperature inside the furnace had been decreasing for a while, and the most intense phase of the fire was over. No reignition of the underlying timber was observed. This is likely a result of how far the charcoal front had moved into the second lamella. According to temperature profile data, the charcoal front defined by the characteristic temperature of 300°C reached the end of the first lamella already at 42 minutes, see Appendix D, and after that continued to char the second lamella. Due to this no increase in heat flux was registered and the fire continued towards self-extinction in the absence of fuel.

7.3 Sources of error

In experiments like these, there are many factors that can influence and change the result. One of these is the moisture content of the specimens. The measured moisture content differed quite a lot between each specimen (see table 6-1 in section 6), and for most of them, it was above the recommended standard value of 16 % (Svenskt Trä, 2017). The difference in moisture content could have affected the results, since a specimen with higher moisture content would be more fire resistant than a specimen with less moisture.

When unpacking the specimens, notes where taken on the elements build-up and on their design. The quality of the specimen was far below expectations. Cracks and gaps of several millimetres were found in many of the wooden elements and the surfaces were quite coarse. Additionally, several layers of lamellas were not placed in perfect position on top of each other which made most of the elements somewhat uneven. We believe that a reason for this might be incorrect manufacturing procedures, since the specimens were made by a research organisation, instead of a manufacturer of CLT.

Normally, manufactured timber products use an individual moisture content between 6 and 15 % (Svenskt Trä, 2017). It's possible that the Canadian manufactured specimens deviated from this and was not allowed to dry fully before assembly. This resulted in moisture-related movements of the wood during transport, because of the change of storing conditions. Possibly this contributed to widen the cracks and gaps, as well as making some sides slightly non-perpendicular. For a couple of examples of these defects see Appendix G.

The poor quality of the specimens may have resulted in some inaccuracy in the measurements and might have changed the outcome of some tests, having similar specimen behave differently during testing. When comparing the two specimens manufactured with the EPI adhesive, one of them showed partial and local delamination, while one of them remained more or less intact. The causes of these differences could be many. Apart from the aforementioned moisture-content differences, the overall design of the specimen is of importance, gaps, cracks, cavities, glue amount and the quality of timber panels to mention a few. These parameters can influence the spread of fire in a multitude of ways in the wood element. External errors like the proficiency of steering the furnace correctly, is also a factor that may have influenced the final outcome of the results, as the fire conditions might have been different at specific time marks of importance.

In some of the experiments, smaller parts of charcoal fell off from the lamellas. These local losses of char are hard to determine the cause off, but it might be an indirect cause of some type of cavity between lamellas or in the wood. This can reduce the contact area between the two layers of lamellas and in turn affect the bonding capability between the two. Additionally, a cavity can result in direct contact between the adhesive and the fire, or hot gases, accelerating the thermal breakdown process, and thereby reducing the bonding strength.

Not only are there errors regarding the quality of the specimens, several potential sources of error can be mentioned when considering the measurements and the calculation of heat flux. To begin with, the location of the heat flux meter can be discussed. The heat flux meter would ideally be positioned in line with the centre of the fire-exposed surface, to correctly represent the exposure of the specimen. In reality, the measurements were performed when the device was located in the centre line but right next to the specimen, see Appendix G. This gives a small source of error because of the improper placement of the device, and the heat flux may change because of incident radiation between different locations.

The measurement itself had a limit, as the heat flux meter could only resist a maximum of 200 kW/m^2 exposure. This meant that the device couldn't be inside the furnace when the heat flux was above this value. To determine the heat flux during this time a constant during the other stages was derived and

then used to calculate the heat flux during the unknown time, for the calculation methods see Appendix A. This constant was further used to calculate the heat flux for rest of the tests. It's questionable how reliable these types of measurements and the calculation methods itself really are in between different tests were conditions might differ.

No further analysis regarding reliability and uncertainties of the heat flux formula has been considered. But conclusions can be made that there are properties that do influence it. The convective constant and emissivity that are used as a constant are the same for each test, even though the heat related conditions could very well differ from test to test. However, the assumption to use the same constant for each test was in this case considered accurate enough for the intended purpose of studying relative differences in regard to delamination. Since the temperature of each test was supposed to follow the same target curve there are most likely no major changes to the thermal conditions inside the furnace for each test. Additionally, when comparing the measured and calculated heat flux in order to derive constant values mostly associated with the convection heat part, these constants had minimal impact. Therefore, we believe that the heat flux graphs can be considered a good estimate for each test for the intended purpose.

During the work of this report, the authors have tried to work after a due diligence approach. This means that throughout the work process, potential sources of errors have been noted and analysed in order to be averted. A trial plan was made to be prepared and to ensure that the experimental process was understood. Another reason for the development of the trial plan was to have something to rely upon during the tests, this trial plan can be found in Appendix A. Apart from the trial plan, a checklist was created to ensure that critical steps of the experimental procedure were not missed and potential errors avoided. More or less every critical step from the preparation of specimen to the preparation of the furnace, the execution of the test and post-test tasks, with potential failures and how to avoid them are included in this checklist. To observe the checklist see Appendix B.

Even though a mitigating approach was used in order to avoid experimental errors, errors were still not completely avoided. In total, ten experiments were conducted, where thermocouples were re-used several times, and replaced continually after observing faulty readings. This lead to that the more the thermocouples were used and exposed to fire, the higher the probability were for them to malfunction in the following test. In the last couple of tests, more thermocouples than usual malfunctioned as a result of continuous wear and tear and limited resources. A mitigating measure was taken before the experimental phase by using four thermocouples on each depth to compensate for the loss of data due to faulty thermocouples.

Since the experiments were manually controlled, the influence of human error could have had a significant impact. Human errors and their impact on the experimental environment, should not be underestimated. Communication during the experiment was a key function in order to balance the oxygen levels and furnace temperature. For example, the application of nitrogen was done by manually adjusting the flow through two gas regulators, each connected to a gas bottle of nitrogen. When one bottle was empty, a change to a new bottle had to be made. During this time only a limited amount of nitrogen could be used. Bad timing for this change resulted in a phase of less than optimal nitrogen outage, the influence can be seen in the result as a sudden increase of oxygen in most tests, see oxygen level graphs in section 6.1 and Appendix C.

7.4 Future potential and challenges

The results presented, and the interpretation of these results above presents a somewhat ambiguous image of the fire performance of CLT. On one hand, there are CLT specimens manufactured with one of the most common Poly-urethane adhesive types on the market that delaminate and behaves unpredictably when exposed to severe fire conditions. On the other hand, the rest of the specimens showed little to no signs of delamination and behaved more like elements of solid timber. It's clear to us that the composition and the adhesive type used, have an impact on the fire development, and that delamination to a high degree governs the predictability of the fire. What significance does this have from a reliability-based design perspective, and future design limitations?

Reliability-based fire design is all about trying to account for uncertainties and limitations of individual building components or joint functional structures and compare this to a reasonable level of fire exposure. This report highlights some parameters for CLT that give rise to uncertainties of the fire performance of the material. A major point of these results is that they are based on fire conditions more resembling a realistic fire than a standard fire, which in itself makes the data somewhat unique. Real fire conditions have been studied in several full-scale tests of CLT in the past, but in tests of such scale, one can't really afford to isolate and observe single parameters and occurrences like delamination only.

However, one has to be aware that it's unreasonable to view the results from a complete reliability-based design perspective. Mainly because only the fire properties of CLT was studied, as no loads of any kind were applied during the tests. One could connect the results to limitations of the load-bearing capacity of CLT, due to charring depth and reduced residual cross sections, but without accounting for loads this would only be speculation. We therefore believe that these results should be used for what they are, an evaluation of CLT manufactured with different types of adhesive. This information, in turn, says something about how the material should be comprised, in order to reduce the uncertainty of the fire performance. The goal is to have CLT elements that behave like solid timber while burning, so that previous research concerning timber fire performance can be applied. That means having an adhesive that doesn't allow for delamination to occur. Sadly, this does not seem to be the case for one of the most common types of Poly-urethane adhesives used in CLT manufacturing today. This is something we really hope that the CLT manufacturing industry takes to heart.

So, what could this mean for the future of CLT, and the construction of timber buildings in general? We believe that if CLT continues to be optimised as a building component and the quality is assured to the point that the material exhibits fire performance equal to solid timber, then CLT has great potential of being the future of timber buildings. When building larger structures, it's simply not possible to use single solid timber elements, as finding enough strength graded material of the required dimensions is near impossible. Here's were engineered timber elements such as CLT finds its role.

The advantage of having building elements that resemble prefabricated concrete elements but with only a fraction of the weight and quicker assembling times, as well as far better working conditions for the construction workers is invaluable at a construction site. The material is beautiful and warm and favoured by many architects as it doesn't necessarily need to be hidden for aesthetic reasons like concrete and steel. The notion of wood as a sustainable material due to its natural origin and the effects of carbon sequestration also helps the image of timber structures.

However, when considering the potential of CLT one must retain some sense of objectivity, and the mentioned advantages have to be taken with a grain of salt. Even if a CLT element doesn't delaminate and the fire performance equals that of a solid timber element, the fact remains that the timber load-bearing structure is contributing to the fire in a way that concrete and steel could not. It's possible that one could accredit the effects of auto-extinction of these elements when the char layer gets thick

enough, as researched by (Bartlett, et al., 2017). Still, to do so it needs to be assured that the level of heat contributed by external fuel is below a certain critical level.

This raises the question of the amount and type of fuel in the compartment. Fuel load in terms of furniture and installations will have an impact on the fire development and in turn the timber load-bearing structure. It's a two-way relationship and it's possible that the extent of the external fuel package of furniture is far more influential to the fire development than the additional fuel contributed by the load-bearing structure. However, if delamination occurs there's no point in considering this, as the impact on the fire development can be substantial, as demonstrated by the results of this report and the results of Su et al. (2017). We believe this to be of grave importance when considering the use of CLT in the load-bearing structures. Especially when viewed from the perspective of the rescue emergency services, as they would be the ones experiencing the highest risk when dealing with unpredictable fire behaviour.

Besides the more apparent risks concerning the fire performance of CLT- and timber structures overall, there are other problematic factors that one has to consider. Two of these are the resulting damages of fire and the aftermath of an extinguished fire in a timber structure. If the structure is still standing after a fire, how much could easily be repaired? It's not only a question of direct fire damages as charred wood, but also water damages following the extinguishing efforts of the rescue emergency services. The overall information and statistics of these types of damages are far from complete, and the information that do exist could use further interpretation. These are questions far beyond the scope of this report, but nevertheless, subjects that should be researched further in the future to be able to fully evaluate CLT and other timber products potential.

To summarise, it's our belief that CLT could have great potential for future all-timber structures and possibly high-rise buildings. It all comes down to ensuring that the fire performance of CLT doesn't deviate from that of solid timber. It's also essential to evaluate the advantages and disadvantages of wood as a material fully and objectively, which can only be done through further research. When considering high-rise structures, a reasonably safe number of storeys needs to be worked out, and the opinions and fears of the rescue emergency services need to be taken seriously. Overall CLT structures could be safe if properly assembled and protected, and for regions with prominent and rich foresting and timber industries like North America and Scandinavia they could be highly beneficial.

8 Conclusions

After compiling and evaluating the results of the report, a set of four general conclusions could be formulated. The background for these conclusions is the discussion in the previous section, and for more details concerning the line of thought and reasoning behind the conclusions see section 7. Below are the final conclusions:

- It's possible to replicate real fire conditions in a standard testing furnace. This opens up for the possibility of verifying the results from full-scale tests to some extent, while isolating single parameters and conditions.
- Most of the tested specimens exhibited a predictable and steady behaviour when exposed to fire. However, specimens manufactured with one of the markets most common Poly-Urethane adhesive showed a quite different result, where both the first and second lamella delaminated to some extent.
- Delamination of CLT elements could have a severe impact on the overall fire development, causing reignition of fresh wood, preventing auto-extinction and prolonging the fire duration.
- For future projects with engineered timber elements, considerations should always be made regarding how appropriate timber structures are for the intended purpose and the emergency rescue services intervention in case of fire.

From the overall experience of performing the tests and through a long series of trial and error in pilot testing, a sufficient level of control over single fire behaviour parameters was achieved. Given more time and resources it's clear that this process can be refined and expanded upon.

Even though not all results could fully indicate and confirm the occurrence of delamination, the results as a whole, coupled with the visual observations gave a very conclusive image. The main point in the end, is that the specimens where delamination was observed, differed noticeably in measurements in comparison to the rest of the specimens at specific time marks.

The interpretation of the effects following delamination is a question of relative extremes. Following delamination, the temperatures were higher, the charring was deeper and had a longer duration, heat flux peaked, and flames became visible once again. It's clear that delamination was not only temporary affecting the fire behaviour of CLT, but it could cancel the decay phase and extend the duration of the fire.

The advantages and disadvantages are many for CLT and timber structures overall. It's not really a question of whether or not it's the building material of the future or something to be avoided entirely. Timber materials definitely have a part in the development of future buildings and for larger timber structures, engineered timber elements such as CLT, really is the only option. It's a material with great potential, but is surrounded by many questions that still need answering. The research is still somewhat behind due to strict regulations grounded in the old fears of great timber city fires, the future will tell what a reasonable scale is, and what is not. In this quest, it's crucial that all relevant parties are involved, from researchers, architects and fire brigades to governments, the timber industry and individual organisations, to ensure a future of beautiful and sustainable, but most of all safe, timber buildings.

9 Further research

In order to validate and strengthen the results of the delaminating properties of different adhesives investigated in this report and other effects of delamination, further research is necessary. Potential areas that can be further evaluated for fire safety in modern timber buildings are the following:

- Different aspects that might impede the delaminating process. Aspects that might have an influence on the delaminating process could need further research, for example the thicknesses of the lamellas in CLT, as well as the of use of different types of wood species.
- An experimental analysis of simulating a full-scale fire using a standard furnace, considering the accuracy with experimental issues, as well as a comparison with a standard fire test and possibilities to automatize the process.
- Consideration of damages caused by a fire and the aftermath of an extinguished fire in a timber structure needs to be taken. To what extent is it possible to repair a timber structure after a fire? Such research should include both direct damages caused by the fire, as well as water damages from extinguishing efforts by the fire brigade.

References

Bartlett, A. I. et al., 2017. Auto-extinction of engineered timber: Application to compartment fires with exposed timber surfaces. *Fire Safety Journal,* Volume 91, pp. 407-413.

Björkenstam, U., 1992. *Probabilistisk dimensionering.* 2:nd ed. Göteborg, Sweden: The Institution for Marine Technology, Chalmers University of Technology.

BoatCraft Pacific Pty. Ltd., Collected 2017-09-25. *A single pack waterproof polyurethane adhesive,* Beverly Hills, NSW, Australia: DRIVE Marine Services.

Boverket, 2011. *BFS 2011:10 - EKS 8, Boverkets föreskrifter och allmänna råd om tillämpning av europeiska konstruktionsstandarder (eurokoder),* Sweden: Catarina Olsson.

Brandon , D. & Dagenais, C., 2018. *Fire Safety Challenges of Tall Wood Buildings – Phase 2: Task 5 – Experimental Study of Delamination of Cross Laminated Timber (CLT) in Fire,* Quincy, MA, USA : Fire Protection Research Foundation.

Brandon, D. & Östman, B., 2016. *Fire Safety Challenges of Tall Wood Buildings – Phase 2: Task 1 - Literature Review ,* Stockholm, Sweden : SP Technical Research Institute of Sweden.

Brandskyddsföreningen, 2017. *brandskyddsforeningen.se.* [Online]
Available at: https://www.brandskyddsforeningen.se/vart-arbete/trahus/
[Accessed 09 11 2017].

Brege, S., Nord, T. & Stehn, L., 2017. *Industriellt byggande i trä – nuläge och prognos mot 2025,* Linköping, Sweden: Linköpings universitet- Instutitionen för industriell ekonomi.

Buchanan , A. H. & Abu, A. K., 2017. *Structural Design for Fire Safety.* 2.a ed. University of Canterbury, New Zealand: John Wiley & Sons, Ltd.

Burström, P.-G., 2007. *Byggnadsmaterial-Uppbyggnad, tillverkning och egenskaper.* 2nd ed. Lund, Sweden: Studentlitteratur.

C.F. Möller, 2013. *HSB 2023 Västerbroplan.* [Online]
Available at: http://www.cfmoller.com/p/-sv/hsb-2023-vasterbroplan-i3048.html
[Accessed 22 11 2017].

Drysdale, D., 2011. *An Introduction to Fire Dynamics.* 3rd ed. University of Edinburgh, Scotland, UK: John Wiley & Sons Ltd.

Emberley, R., Do, T., Yim, J. & Torero, J. L., 2017. Critical heat flux and mass loss rate for extinction of flamingcombustion of timber. *Fire Safety Journal,* Volume 91, pp. 252-258.

Emberley, R. et al., 2017. Description of small and large-scale cross laminated timber fire tests. *Fire Safety Journal,* Volume (To be published), pp. 1-8.

FireInTimber, 2010. *Fire Safety in Timber Buildings - Technical Guideline for Europe.* Stockholm, Sweden: SP - Trätek.

Fontana, M., Hugi, E., Jöbstl, R. & Frangi, A., 2009. Experimental analysis of cross-laminated timber panels in fire. *Fire Safety Journal,* Volume 44, pp. 1078-1087.

Frangi, A., Fontana, M., Knobloch, M. & Bochicchio, G., 2008. Fire Behaviour of Cross Laminated Solid Timber Panels. In: *Fire Safety Science-Proceedings of The Ninth International Symposium.* Zurich: International Association For Fire Safety Science, pp. 1279-1290.

Gagnon, S., E.M. Ted, B., Lisa, P. & Crespell, P., 2013. Introduction to cross-laminated timber. In: F. &. B. S. L. Council, ed. *CLT Handbook U.S.* Canada: FPInnovations & Binational Softwood Lumber Council , pp. 1-44.

Grøstad, K. & Pedersen, A., 2010. Emulsion Polymer Isocyanates as Wood Adhesive: A Review. *Journal of Adhesion Science and Technology,* Volume 24, p. 1357–1381.

Hoxha, E. et al., 2017. Influence of construction material uncertainties on residential building LCA reliability. *Journal of Cleaner Production,* Volume 144, pp. 33-47.

International Organization for Standardization, 1995. *Eurocode 5: Design of timber structures – Part 1-2: General – Structural fire design,* Geneva, Switzerland: ISO.

Karlsson, B. & Quintiere, J. G., 2000. *Enclosure Fire Dynamics.* 2nd ed. Flordia, USA: CRC Press.

Kemmsies, M., 1999. *Comparison of bond lines in glulam beams adhered with a phenol-resorcinol-formaldehyde (PRF) and one-component polyurethane (PUR) after fire exposure.* Borås, SP Swedish national testing and resaerch institute.

Klippel, M., 2014. *Fire safety of bonded structural timber elements, Doctoral Thesis,* Zurich, Germany: ETH Zurich.

Kodur, V. K. R. & Harmthy, T. Z., 2002. Chapter 1-10: Properties of Building Materials. In: R. Andrau, ed. *SFPE Handbook of Fire Protection Engineering.* Quincy, Massachusetts, United States of America: National Fire Protection Association, Inc., pp. 1-155 - 1-180.

Li, X., Zhang, X. & Hadjisophocleous, G., 2015. Experimental Study of Combustible and Non-combustible Construction in a Natural Fire. *Fire Technology,* Volume 51, pp. 1447-1474.

Magnusson, S. E. & Thelandersson, S., 1970. *Temperature - TIme Curves of Complete Process of Fire Development,* Lund, Sweden: Lund Institute of Technology.

Martinsons, 2016. *Martinsons handbok i KL-trä.* 1:a ed. Bygdsiljum: Martinsons.

McGregor, C., 2013. *Contribution of cross-laminated timber panels to room fires. Master thesis.,* Ottawa, Ontario, Canada.: Department of Civil and Environmental Engineering Carleton University..

Medina Hevia, A. R., 2014. *Fire Resistance of Partially Protected Cross-Laminated Timber Rooms-Master Thesis,* Ottawa, Ontario, Canada: Carleton University .

Nevander, L. E. & Elmarsson, B., 1994. *Fukt handbok- praktik och teori.* 2nd ed. Stockholm, Sweden: Svensk Byggtjänst AB.

Peæaloza, D., Erlandsson, M. & Falk, A., 2016. Exploring the climate impact effects of increased use of bio-based materials in buildings. *Construction and Building Materials,* Volume 125, pp. 219-226.

Persson, L. & Sandberg , M., 2011. *Vikten av att välja rätt virke - Undersökning gällande förekomsten av skadat virke längst virkeskedjan, Examensarbete,* Lund: Ingenjörshögskolan, Campus Helsingborg, Lund University.

Pettersson, O. & Jönsson, R., 1988. *Reliability Based Design of Fire Exposed Timber Structures - State of Art and Summary Design Guide,* Lund, Sweden: Institute of Science and Technology, Department of Fire Safety Engineering.

Pizzi, A. & Mittal, K. L., 2003. Melamine-formaldehyde adhesives. In: M. D. Inc., ed. *Handbook Adhesive Technology: 2nd Edition, Revised and Expanded.* New York, USA: CRC Press.

Sikora, K. S., McPolin, D. O. & Harte, A. M., 2016. Shear Strength and Durability Testing of Adhesive Bonds in Cross-laminated timber. *The Journal of Adhesion,* 92(7-9), pp. 757-777.

Staffansson, L., 2010. *Selecting design fires,* Lund: Department of Fire Safety Engineering and Systems Safety, Lund University.

Stora Enso, 2013. *Questions and answers- CLT.* [Online]
Available at: http://www.clt.info/en/product/faq/
[Accessed 25 09 2017].

Stora Enso, 2017. *CLT standard designs.* s.l.:Stora Enso.

Stora Enso, 2017. *Stora Enso.* [Online]
Available at: http://buildingandliving.storaenso.com/products-and-services/australia
[Accessed 09 11 2017].

Strobech, C., 1990. Polyurethane adhesives. *Construction and Building Materials,* 4(4), pp. 214-217.

Structural Timber Education Programme, 1995. *Timber Engineering STEP 1.* First Edition ed. The Netherlands: Centrum Hout.

Su, J., Lafrance, P.-S., Hoehler, M. & Bundy, M., 2017. *Cross Laminated Timber Compartment Fire Tests for Research on Fire Safety Challenges of Tall Wood Buildings - Phase 2 (DRAFT),* Canada: National Reasearch Council.

Swedish Wood, 2016. *Design of timber structures: Structural aspects of timber construction Volume 1.* 2 ed. Stockholm: Swedish Forest Industries Federation.

Svenskt Limträ AB, 2007. *Limträ Guide.* 4 ed. Stockholm: Svenskt Limträ AB.

Svenskt Trä, 2017. *KL-trähandbok- Fakta och projektering av KL-konstruktioner.* 1 ed. Stockholm: Svenskt Trä.

Sveriges Träbyggnadskansli, n.d. *Limnologen Växjö.* [Online]
Available at: http://www.trabyggnadskansliet.se/inspiration/flervaningshus/limnologen-vaxjo
[Accessed 22 11 2017].

Särdqvist, S., 2013. *Vatten och andra släckmedel.* 3rd ed. Karlstad, Sweden: Myndigheten för samhällsskydd och beredskap .

The Fire Protection Research Foundation, 2012. *Fire Flow Water Consumption in Sprinklered and Unsprinklered Buildings: An Assessment of Community Impacts ,* Quincy, USA: The Fire Protection Research Foundation .

Thoft-Christensen, P. & Baker, M. J., 1982. *Structural Reliability Theory and It's Applications.* Berlin, Germany: Springer-Verlag.

Trätek, 1987. *Temabok Trä som material.* Sweden: Trätek.

Tsantaridis, L., 2003. *Reaction to fire performance of wood,* Stockholm: Byggnadsmaterial och Trätek.

Umemura, K., Takahashi, A. & Kawai, S., 1998. Durability of isocyanate resin adhesives for wood I: Thermal properties of isocyanate resin cured with water. *J Wood Sci,* Volume 44, pp. 204-210.

Walton , W. D. & Thomas, P. H., 2002. Chapter 3-6: Estimating Temperatures in Compartment Fires. In: R. Andrau, ed. *SFPE Handbook of Fire Protection Engineering.* Quincy, Massachusetts, United States of America: National Fire Protection Association, Inc., pp. 3-171 - 3-188.

Vattenskadecentrum, 2016. *Vattenskadeundersökningen 2016,* Stockhom, Sweden: Vattenskadecentrum.

Wiesner, F. et al., 2017. Structural response of cross-laminated timber compression elements exposed to fire. *Fire Safety Journal,* Volume 91, pp. 56-67.

VY Wong, B. & Fah Tee, K., 2017. Charring Rate for Fire Exsposed X-Lam. *IOF Conference Series: Materials Science and Engineering,* Volume 216, pp. 1-6.

Yeh, B., Kretschmann, D. & Wang, B. J., 2013. Manufacturing - Cross-laminated timber manufacturing. In: F. &. B. S. L. Council, ed. *CLT Handbook U.S.* Canada: FPInnovations & Binational Softwood Lumber Council, p. 572.

Zhang, H., 2011. *Building Materials in Civil Engineering.* 1st ed. Cambridge, UK: Woodhead Publishing.

Zhou, J. et al., 2017. Bonding performance of melamine-urea-formaldehyde and phenol-resorcinol-formaldehyde adhesives in interior grade glulam. *Journal of Adhesion Science and Technology,* 31(23), pp. 2630-2639.

Östman, B., Brandon, D. & Frantzich, H., 2017. IAFSS 12th Symposium 2017- Fire safety engineering in timber buildings. *Fire Safety Journal,* Volume 91, pp. 11-20.

Östman, B., König, J., Just, A. & Schmid, J., 2012. *Brandsäkra trähus: Den nordiska-baltiska handboken.* 3 ed. Stockholm: SP Trä,.

Appendix A – Trial plan

Trial plan

Eric Johansson
Anton Svenningsson

2017-09-27

Table of contents

1 Introduction

This document describes the procedure of the experiments on CLT scheduled from 2017-11-13 to 2017-11-20, including preparations and pilot tests from 2017-10-9 to 2017-10-13. The experiments are to be performed at Research Institute of Sweden, RISE (Former SP – Trä) in Stockholm. The results of these experiments are to be utilized and analyzed in the master thesis "*Delamination of CLT and its impact on the fire development, with focus on different kinds of adhesives*" by Eric Johansson and Anton Svenningsson. Performing, and mainly responsible for the experiments are Daniel Brandon (RISE) and Alar Just (RISE), accompanied by the authors mentioned above.

The background for the experiments is recent findings concerning delamination of CLT in fires. These findings suggest that delamination of CLT during a fully developed fire could have significant impact and effect on the fire development, and in some cases even result in a second flashover (Medina Hevia, 2014). The delamination process, in turn, is connected to the adhesive used and it has been shown in previous experiments that some types of adhesives are more fire resistant than others, and in some cases preventing delamination entirely (Frangi, et al., 2009). Therefore, there is a need to explore these aspects further and to closer examine the process of delamination of CLT in fires and the adhesives impact on this occurrence.

1.1 Purpose & Objectives

The main purpose of the experiments is to improve the understanding of the process and cause of delamination, as well as to which degree different adhesives effects the delamination.

For previous results and findings to be verified it is of utmost importance that the fire conditions of these experiments are replicated to a sufficient level. Previous experiments were performed in large scale, while the current experiments are to be performed in small scale, which presents a considerable challenge. Thus, the main objective of the experiments is to achieve this sufficient level of reproducibility to be able to correctly verify the results.

1.2 Question formulation

For the experiments, the following questions are formulated:

- Will delamination occur, and if so when, and what will the effect on the fire development be?
- What effects do different types of adhesives have on the occurrence and process of delamination?

2 Theory

Before executing the experiments, it is important to have a better understanding of the reaction of the specimens. The CLT-elements are mainly made of timber connected to each other with some type of adhesive. This chapter will therefore briefly explain the charring phenomena that occur when timber is exposed to fire and higher temperatures. The different ways one can determine, predict and estimate the delamination of the specimens by using different calculation methods will also be described.

2.1 Charring rate

CLT, as well as all wood burn in the outer layers and these are converted to char. The char layer and the healthy remaining wood form a distinctive moving boundary as the burning continues, and the pyrolysis zone moves through the material. This boundary corresponds to a temperature of about 300°C (Buchanan & Abu, 2017), and typically represents the charring front.

For one-dimensional charring, as will be the case in the current experiment, the charring can be expressed as follows (FireInTimber, 2010):

$$d_{char,0} = \beta_0 \cdot t$$

Parameters included in the formula are:

β_0: One-dimensional charring rate [mm/min]

t: Time of fire exposure [min]

The charring rate is dependent on a multitude of different aspects, some of these are wood species, density, and moisture content. Eurocode 5 presents a couple of characteristic values for the charring rate, based on wood species and density. For Glulam, a charring rate of 0,65 mm/min is given, but a value for CLT-products are yet to be presented (International Organization for Standardization, 1995).

These characteristic values for the charring rate are only valid for a standard fire (ISO 834), which will not be utilized in the current experiment. For this particular experiment, the charring rate will be calculated based on data of temperature readings inside the test-sample. Using the value of 300 °C mentioned earlier, the charring front in the material can be tracked, and thus the rate can be calculated.

2.2 Calculation parameters

Different calculation parameters than the charring rate will be used in the experiments. To determine when the timber will ignite and later delaminate, important aspects are the temperature in samples and the compartment, as well as the heat flux on the surface. Collecting of this data will be done with the help of thermocouples and thermometers inside the furnace. The heat flux of interest is that caused by radiation and the convective heat caused by this radiative heat flux. In order to calculate parameters such as the convective constant, h_c and the emissivity, ε_{PT}, a water-cooled incident heat flux meter will be used. Worth noting is that since it's the incident heat flux that is of interest in this case, a modified version of the one-dimension heat balance equation will be used. Presented below is the used equation for received heat flux through radiation and convection (Wickström , et al., 2017).

$$\dot{q}_{inc} = \frac{1}{\varepsilon_{PT}}\left[\varepsilon_{PT} \cdot \sigma \cdot T_{PT}^4 + h_c\left(T_g - T_{PT}\right)\right]$$

Parameters included in the formula are:

$\dot{q}_{inc}$: Incident heat flux [kW]

σ : Stefan Boltzmann constant [W/m^2·K^4]

T_{PT}: temperature measured by the plate thermometer [K]

T_g: gas temperature measured by thermocouples [K]

h_c: convection constant [W/K]

ε_{PT}: the emissivity [-]

The radiative temperature, $T_{rad.}$ will be calculated as per the equation below:

$$T_{rad.} = \sqrt[4]{\frac{\dot{q}_{inc}}{\sigma}}$$

Other ways to estimate when CLT will delaminate is by observing the mass loss and the heat release for the affected specimen. Mass loss rate and heat release increase as a result of the delamination (Brandon & Östman, 2016).

By weighing the specimen before the test and measuring the moisture content in several depths using an electrical resistance, moisture meter tool, one can estimate the dry weight of the specimen. After each test the specimen will be dried in an oven at 120° C, to evaporate the last moisture inside, to determine the true dry weight.

Estimation of the heat released will be done with the heat of combustion formula presented below:

$$Q_{CLT} = \Delta m_{dry} \cdot H_{wood}$$

Parameters included in the formulas are:

Δm_{dry} : difference of mass before and after test, excluding the mass of the moisture, it is the mass loss of the timber. [kg/s]

H_{wood}: Heat of combustion for dry wood will be used [kJ/kg]

3 Execution

In this section, the practical details concerning the experiment will be explained further. This includes more exhaustive information about the experimental setup, type of instruments and equipment that will be used during the tests, and also what type of specimens that will be used.

3.1 Experimental setup

Each test of the experiment will be performed in a model-scale furnace with the inner measurements of 1.0 x 1.0 x 1.0 m. The furnace is designed with surrounding ceramic insulation with outer metal cladding and an exhaust opening at the bottom. Burners mounted at the wall of the furnace will provide the heat output to replicate the most severe fire conditions registered at previous full-scale experiments.

The inside of the furnace will be outfitted with equipment such as plate thermometers, and sensors will register air pressure as well as oxygen levels in the exhaust. To control the fire conditions the oxygen supply will be controlled through an air inlet by adding nitrogen gas or additional oxygen gas.

The furnace comes equipped with a looking- glass opening allowing for direct observation of approximately 50 percent of the fire exposed sample. See Fig. 1 for a section overview of the test setup.

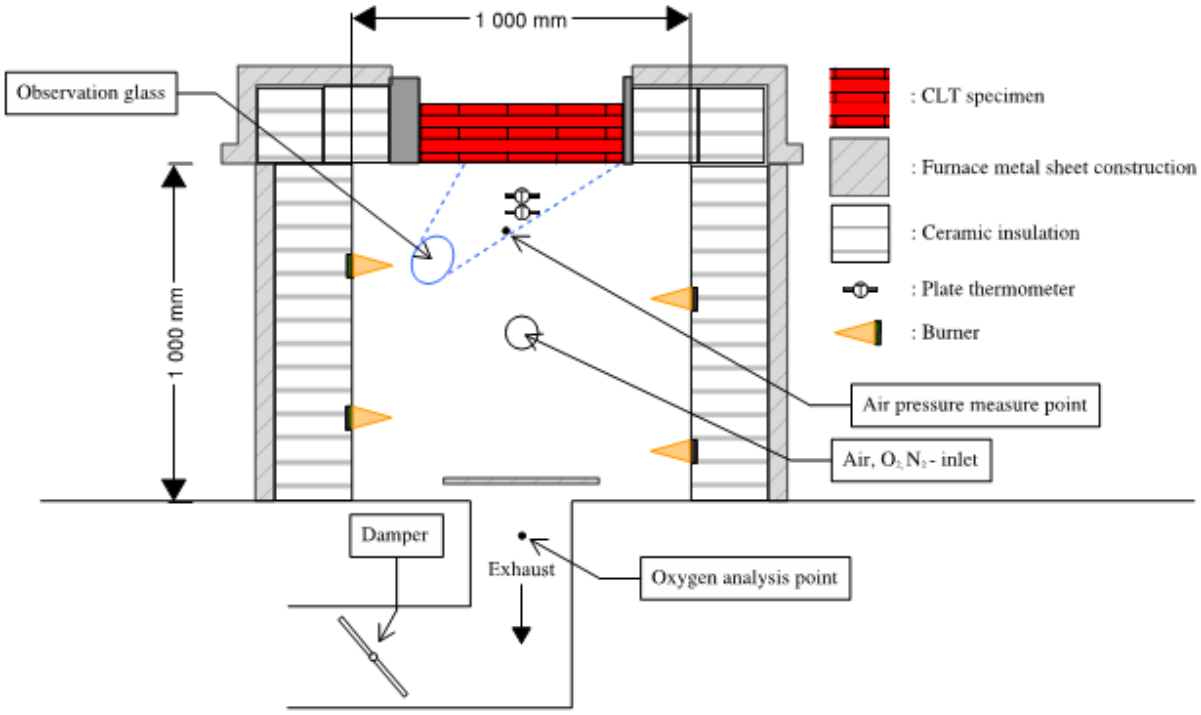

Fig. 1. Section sketch of furnace setup

3.2 Instrumentation & equipment

A variety of instruments and equipment will be used to perform the test and gather the required data. In the bullet list below the main instruments and equipment are listed:

- Plate thermometers – to measure the temperature inside the oven and on the surface of the CLT samples.
- Thermocouples – to measure the temperature both inside the furnace and inside of the CLT-element.
- Video camera – used for observation and recording of the test of delamination of CLT.
- Oxygen analysis – The oxygen content will be measured using a gas analyzer.

- Air pressure sensor – To measure air pressure inside the furnace

3.2.1 Plate thermometer

Thermometers are thin plates that gather data just in front of the surface, both radiation and convection. To determine the surface temperature on the CLT-element, plate thermometers will be located 100 and 150 mm away from the element.

3.2.2 Thermocouples

Additional to the plate thermometers, K-type thermocouples will be placed in a position close to the plate thermometers to measure the surrounding gas temperature in the compartment.

Thermocouples will also be in a fixed position inside of the CLT to determine the temperature profile, charring rates as well as the delamination of the CLT. The thermocouples will be placed in a horizontal position to limit the thermal conduction along the line of measurement, which is in accordance with standard EN1363-1 (2012). To be able to determine when delamination occurs, thermocouples will be placed in the bond line of the three lowest layers of lamellas. This was made during the construction phase of the specimens at FP Innovation, Canada.

Inserted in the CLT-element there will be four groups of six thermocouples each, see Fig. 2 down below. In each group, three out of six thermocouples are prefixed according to the procedure mentioned in the earlier paragraph. The other three thermocouples will be drilled and inserted at the testing facility at RISE, Stockholm. Each of these thermocouples will be inserted in holes with a diameter of 2 mm and in the center of the three lowest lamellas, the vertical distance between each thermocouple will be 17.5 mm, see Fig. 2. In total, there will be four groups with six thermocouples each, three measuring temperatures in the bond line and three measuring temperature in the center of each of the lamellas, see Fig. 3 for a top view of the sample.

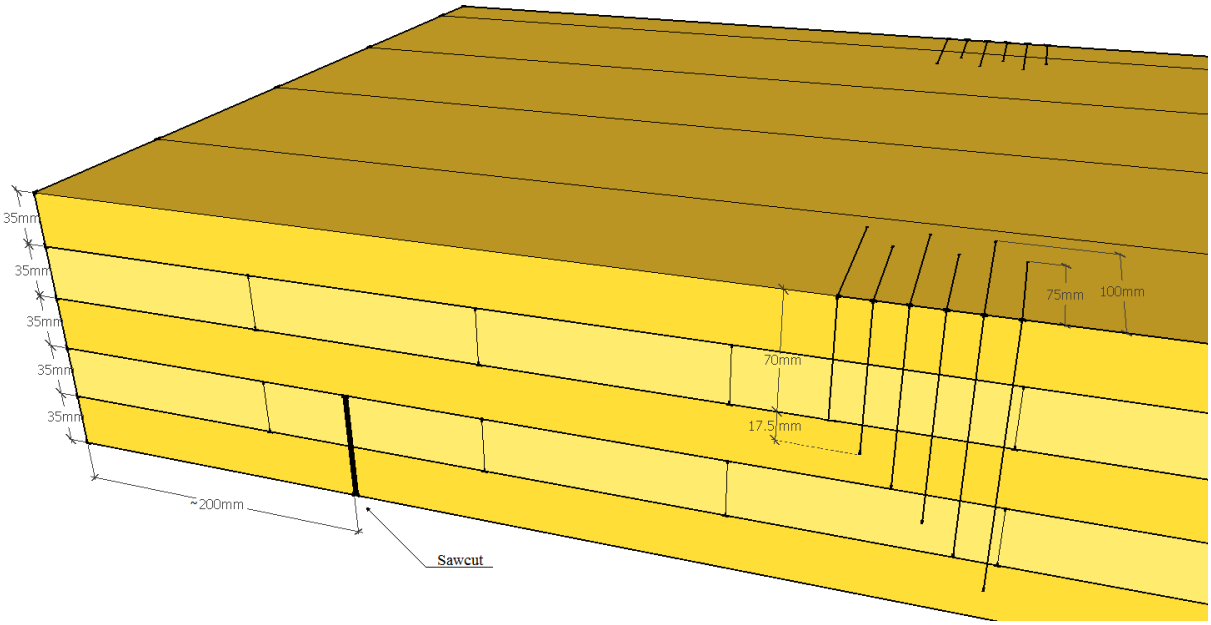

Fig. 2. CLT sample with mark-ups for positioning of thermocouples and approximate placement of one of two saw cuts.

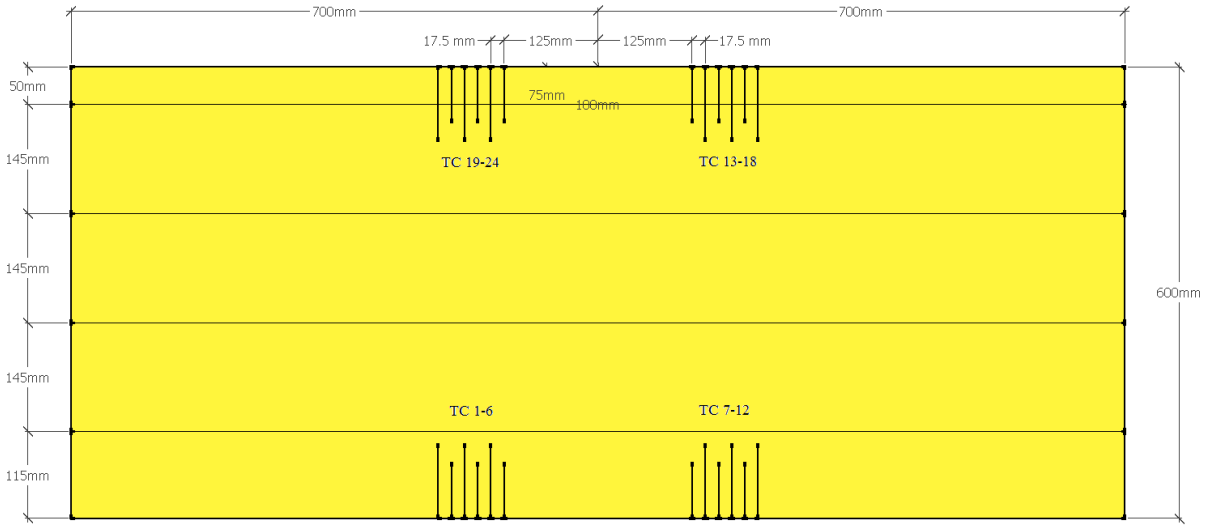

Fig. 3. Top view of ready CLT sample with the positioning of thermocouples and dimensions.

3.2.3 Incident heat flux meter

In order to be able to calculate the radiative heat flux near the specimen surface using the plate thermometers and thermocouples, a water-cooled heat flux meter will be used. A single measurement near the specimen surface will be performed in order to determine the value of the parameter, h_c / ε_{PT}. Since the instrument is relatively fragile, this measurement will not be repeated.

3.2.4 Video camera

An air-cooled video camera will be used to record the process of delamination inside the furnace. The recording will be through the observation tube and will cover approximately 50 percent of the CLT-surface. See observation glass in Fig. 1.

3.2.5 Gas analyzer

The oxygen content inside of the compartment will be controlled with the assistance of a gas analyzer to replicate the same amount of air as in the large-scale test earlier performed at NIST. This will be done by measuring the amount of oxygen leaving the furnace and adjust it by controlling the flow of air in and out. For the decay phase, the air inlet will be used to cool down the furnace in a structured and controlled manner. The rate of the cooling phase shall be prioritized instead of the inlet rate from the large-scale test.

3.3 Samples

Specimens for the tests are five different CLT-elements made in copies of two. They measure 1400 by 600 mm but only 1000 by 600 mm is the area that will be exposed in the furnace. Most of the specimens, eight out of ten, are produced by FP-Innovation in Canada in accordance with standard ANSI PRG 320. These eight elements are made of the same timber as the elements used in the full-scale compartment tests of this study. To compare the full-scale compartment test and the furnace test, there will be two specimens made of the same CLT as used in the previous full-scale model test.

Additional information about the specimen is that they are manufactured using different adhesives, these adhesives include Poly-urethane (PU), Melamine Formaldehyde (MF), Emulsion Polymer Isocyanate (EPI) and Phenol Resorcinol Formaldehyde (PRF). The specimen from the full-scale compartment test are also manufactured with Poly-urethane adhesive.

Type of adhesive	**Abbreviation**	**Specimens**	**ANSI PRG 320**	**Production**
Poly-urethane (Full-scale product)	PU Type A	2	Yes	Industrial manufacturer
Poly-urethane	PU Type B	2	Yes	FP-Innovation
Emulsion Polymer Isocyanate	EPI	2	Yes	FP-Innovation
Melamine Formaldehyde	MF	2	Yes	FP-Innovation
Phenol Resorcinol Formaldehyde	PRF	2	Yes	FP-Innovation
	∑:	10		

Saw cuts will be made in the CLT elements in the border of the supported area and the area of exposure. This will avoid prevention of the delamination due to pressure from the sides. This will make the middle part of the two lowest placed lamellas unsupported and if the adhesive softens, the CLT is free to delaminate without any further difficulties. To avoid fire spreading through the saw cuts, ceramic paper will fill the hollow space sealed with an intumescent sealant. Because of this, a pilot test will be made before the major tests to study possible edge effects near the saw cuts.

4. Execution plan

For easier handling of the experiment, a more overviewed execution plan is made. In this step-by-step guide, it will be possible to keep track of what is to be done and what is next to come in the experiment. A quick reference guide to make sure everything is done according to plan.

There will in total be ten fire tests performed in the furnace on four different types of adhesives. Same fire exposure will be used in all of the tests, a replication of the full-scale fire test at NIST. Output data will be collected for analysis through different types of measurements to determine behavior of the material.

As the occurrence and effects of delamination are the main focus of the experiments, there need to be ways of keeping track and observe this phenomenon. The following data output will be used in the experiments to indicate and measure delamination:

- Temperature development inside the specimen - thermocouples in bond lines
- Material overall temperature and charring rate – plate thermometers and calculations
- Total mass loss of the specimen after test – weighing before and after.
- Video recording of specimen surface during test – recorded during test
- Sudden peak of oxygen consumption – oxygen analysis point in exhaust
- Sudden peak of gas temperature – thermocouples in proximity to specimen surface

As mention above, some of the result output will be comprised of measured raw data from each test, while some will have to be calculated using experiment output and the theories described in section 2 (Theory).

For an overview of the experiment procedure and the resulting data output see Fig. 4 on the following page.

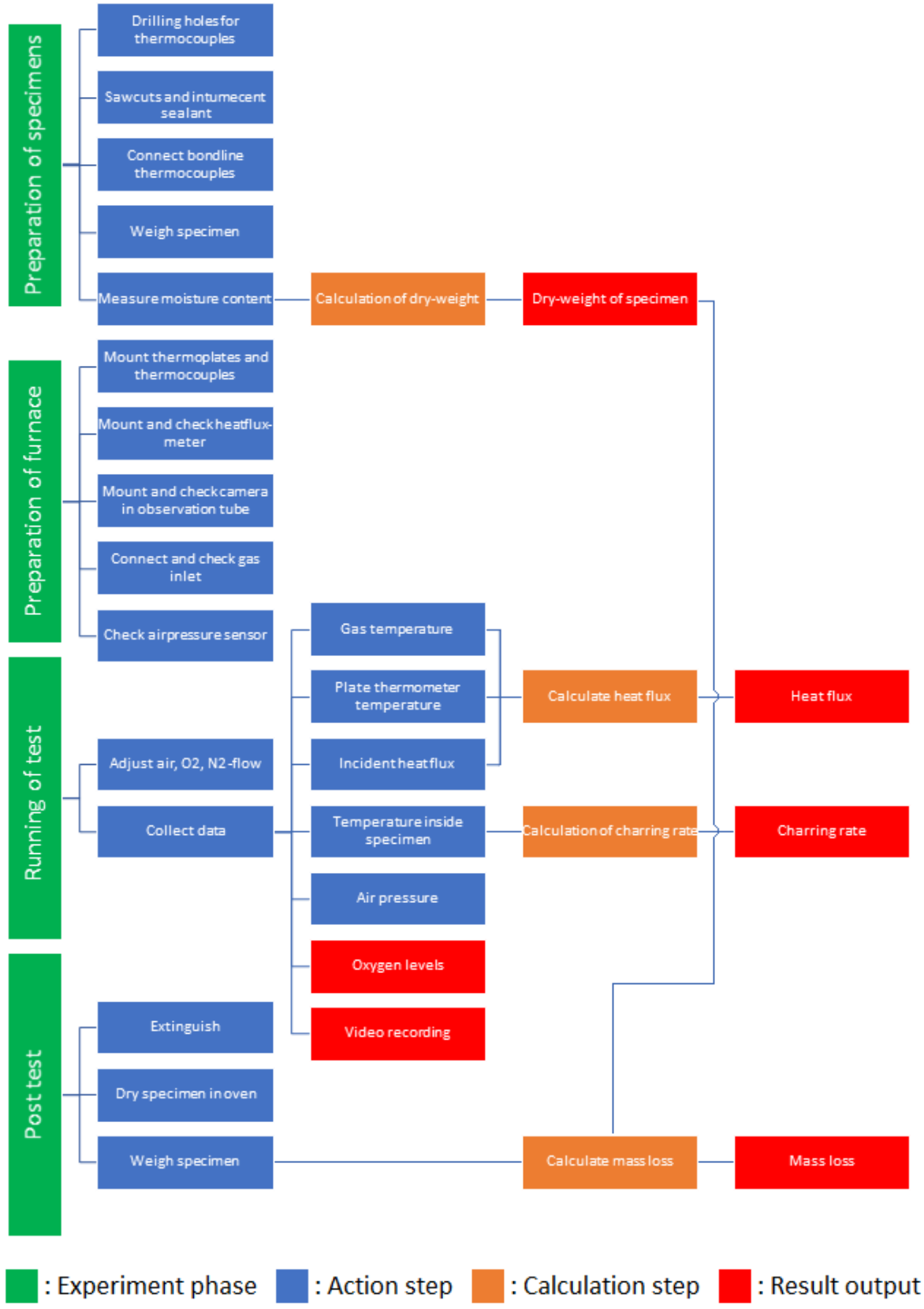

Fig. 4. Graphic illustrating the execution plan of the experiment, with the resulting outputs.

5. Expectations and predictions

This section briefly describes the authors' expectations and predictions to the level that is considered possible in the pre-experiment phase. This material can essentially be interpreted as an early composition of hypotheses.

5.1 Delamination occurrence

The CLT-samples produced with PU-adhesives should delaminate to some extent when exposed to the designed fire conditions. This has been the case in previously performed full-scale experiments, and the delamination might even occur before the char layer reaches the glue line, as a result of a lower melting point for the glue (Medina Hevia, 2014).

The fire resistance for CLT-samples with adhesives types other than PU is less known. However, previous experiments by (Frangi, et al., 2009) have shown that CLT-elements manufactured with Melamine Formaldehyde (MF) can prove quite resistant to delamination, and behave more like solid wood when burning. It's therefore reasonable to expect that the samples manufactured with MF-adhesive will perform better than those with PU-adhesive, and maybe even avoid delamination entirely.

The knowledge of Emulsion Polymer Isocyanate (EPI) -adhesives fire performance as a CLT bonding agent is limited, due to it still being in an introduction phase for use in layer-bonding in CLT-manufacturing (Grøstad & Pedersen, 2010). In a Dynamical Mechanical Analysis (DMA) performed by (Umemura, et al., 1998) Isocyanate- adhesives managed temperatures up to 300°C before any significant degradation of bonds was observed. This could suggest that the samples with EPI-adhesive will perform well in the current experiments. Based on this the authors predict that the EPI-adhesives will at least perform better than the PU-adhesive.

Phenol-Resorcinol-Formaldehyde (PRF) is known to exhibit high thermal stability, yet PRF-adhesives do not foam like PU during manufacturing of CLT-elements. This can result in air gaps in between the CLT lamellas, where heat and flames can spread more easily (Klippel, 2014). To what extent this might effect the results of the current experiments is hard to predict, but since the tests are designed to be one-dimensional and with fire exposure perpendicular to the adhesive layers, these effects are expected to be limited. The performance of the PRF-adhesive is therefore expected to be better than the PU-adhesive, but not as good as the MF-adhesive.

5.2 Second flash-over

If delamination occurs this will result in a rapid exposure of the following unburnt wood layer to some degree. If previous experiments, such as (Medina Hevia, 2014) and (McGregor, 2013) are any indication, this should result in a second flash-over. The effects of this second flash-over will be an increase in heat release, temperature and a higher consumption of oxygen in the fire compartment.

6. Risk analysis

When executing the experiments, there are factors that might fail or not work as expected. In this section, some potential risks that can occur during the experimental parts of these test are briefly discussed.

6.2 Input of gas

During the experiments, a certain amount of oxygen will fill the compartment to replicate the fire conditions of previous tests. Critical aspects that are possible to fail and influence the experiments are the wrong inflow of air as well as the exhaust of the air.

6.2 Failure of measurements

A lot of data are collected through different thermocouples and thermoelements. It's therefore important to take good care of the equipment and be gentle to make sure they log what's needed. Different and independent types of measurements are used to make sure that important data is collected.

6.3 Preparation of specimen

The specimens are assumed to be manufactured the same and according to specifications of the experiment. This is an important aspect to be able to compare the different adhesives. Only some holes for the thermocouples are made by hand through drilling at RISE, these need to be well made to measure temperature in the right place and depth.

The saw cut sealant that is supposed to fill the hollow space may fail if it is not executed well enough and change the result of the experiments. Because if a failure occurs the fire can reach the lamellas and adhesives from more directions than intended.

Material properties may be affected if specimens are not stored according to instructions. Instructions for the materials storage are 20°C and 65% humidity.

6.4 Loss of data

If systems for the gathering of data, such as data loggers, malfunction during tests the loss of data can be substantial. This in return could mean that a sample is wasted, as well as precious time. To avoid this, the use of several independent systems is recommended. That way if some data is lost, some form of backup results can be used.

6.5 Observation tube & camera equipment

The observation tube will mainly be used for mounting the camera that will record video material of the results. Poor visibility because of the smoke and gas layer may render some or most of the video material useless. The camera used will be air-cooled to protect it from extreme temperatures. If the cooling system malfunction, the camera equipment could get permanently damaged, resulting in loss of video material as well as expensive equipment.

6.6 Burner failure

Failure of one or more burners inside the furnace could occur and it could have a devastating impact on the experiment results. It's hard to take action against this when the test is running, therefore it's important to make sure before the tests start that the burners work as intended. If a burner brakes during a test, the experiment most likely needs to be stopped and that the specimen is wasted.

References

Brandon, D. & Östman, B., 2016. *Fire Safety Challenges of Tall Wood Buildings – Phase 2: Task 1 - Literature Review ,* Stockholm, Sweden : SP Technical Research Institute of Sweden.

Bryant, R., Womeldorf, C., Johnsson, E. & Ohlemiller, T., 2003. Radiative heat flux measurement uncertainty. *Fire Mater,* Volume 27, pp. 209-222.

Buchanan , A. H. & Abu, A. K., 2017. *Structural Design for Fire Safety.* 2.a ed. University of Canterbury, New Zealand: John Wiley & Sons, Ltd.

FireInTimber, 2010. *Fire Safety in Timber Buildings - Technical Guideline for Europe.* Stockholm, Sweden: SP - Trätek.

Frangi, A., Fontana, M., Hugi, E. & Jobstl, R., 2009. Experimental analysis of cross-laminated timber panels in fire. *Fire Safety Journal,* Volume 44, p. 1078–1087.

Grøstad, K. & Pedersen, A., 2010. Emulsion Polymer Isocyanates as Wood Adhesive: A Review. *Journal of Adhesion Science and Technology,* Volume 24, p. 1357–1381.

International Organization for Standardization, 1995. *Eurocode 5: Design of timber structures – Part 1-2: General – Structural fire design,* Geneva, Switzerland: ISO.

Klippel, M., 2014. *Fire safety of bonded structural timber elements, Doctoral Thesis,* Zurich, Germany: ETH Zurich.

McGregor, C., 2013. *Contribution of cross-laminated timber panels to room fires. Master thesis.,* Ottawa, Ontario, Canada.: Department of Civil and Environmental Engineering Carleton University..

Medina Hevia, A., 2014. *Fire resistance of partially protected cross-laminated timber rooms. Master thesis.,* Ottawa, Ontario, Canada : Department of Civil and Environmental Engineering Carleton University. .

Umemura, K., Takahashi, A. & Kawai, S., 1998. Durability of isocyanate resin adhesives for wood I: Thermal properties of isocyanate resin cured with water. *J Wood Sci,* Volume 44, pp. 204-210.

Wickström , U., Anderson, J. & Sjöström, J., 2017. *Measuring Incident Heat Flux and Adiabatic Surface Temperature with Plate Thermometers in Ambient High Temperatures,* Borås, Sweden: SP Technical Research Institute of Sweden.

Appendix B – Checklist

CHECKLIST: CLT-trials			
BEFORE TEST			
Object	**Task**	**Check?**	**Comments/value**
Specimen	Measure and mark drill holes		depth 75 mm, distance x: 15 mm y: 17,5 mm
Specimen	Mount lifting chains		As far out as possible, keep chains short
Specimen	Saw cuts		200 mm in, fill with ceramic paper and sealant
Specimen	Drilling holes (side)		2 mm drill
Specimen	Drilling holes (top)		4 mm drill, 25 mm above side holes
Specimen	Install thermocouples		Mark with connection numbers
Specimen	Weigh specimen		
Specimen	Measure moisture content		
Furnace	Prepare and control insulation		Isover adhesive
Furnace	Place beams and specimen		3 beams, tight, but preferably no clamps
Furnace	Check inside of furnace		If no light shines through insulation - OK
Furnace	Connect thermocouples		Use corresponding connection numbers
Furnace	Check thermal plates/couple		Adjust ceramic insulation on thermocouple
Furnace	Take pictures of furnace		Primarily inside before closing
Furnace	Close furnace		
Webcam	Mount and prepare webcam		Turn of Auto-focus and adjust manually
O2 Analy.	Check tube and connection		Use compressed air to clear tube.
Gas tanks	Check regulators and tubes		Prepare each tank for easy access during test
Furnace	Connect all gas tubes to inlet		If necessary connect extra tank of N2
Burners	Program test fire curve		Alar does this
Clock	Mount and reset clock		Set to 00:00:00
DURING TEST			
Burners	Start furnace burners		5 min delay, Alar handles the burners
O2 Analy.	Start air pump		
Clock	Start clock		Daniel does this after the 5 minute delay
Webcam	Start webcam		Eric does this after the 5 minute delay
Furnace	Open inlet for gas		Eric does this after the 5 minute delay
Computer	Check measurements		Look for faulty thermocouples and O2 content
Continually check and communicate the O2-levels, this is adjusted by adding N2 or additional O2-gas. Temperature is adjusted by controlling burners and opening the damper. Repetitively check and improve furnace insulation. Check gas levels and prepare new tanks for quick change. Communication!			
AFTER TEST			
Burners	Shut off burners		
Webcam	Turn off recording		
Specimen	Disconnect thermocouples		Be prepared to remove wires during lift
Gas tanks	Close all regulators		
Specimen	Connect chains and lift up		Use extra gloves and move fast
Specimen	Weigh specimen		Use chain connected scale
Specimen	Extinguish specimen		Water hose
Specimen	Remove thermocouples		Pull out and save the undamaged ones
Specimen	Carry specimen outside		
Specimen	Take pictures of specimen		Note char depth
Specimen	Carry specimen to oven for drying		120 degrees C

Appendix C – Oxygen levels and furnace temperatures

Presented in this Appendix are graphs of oxygen level and furnace temperature for all tested specimens.

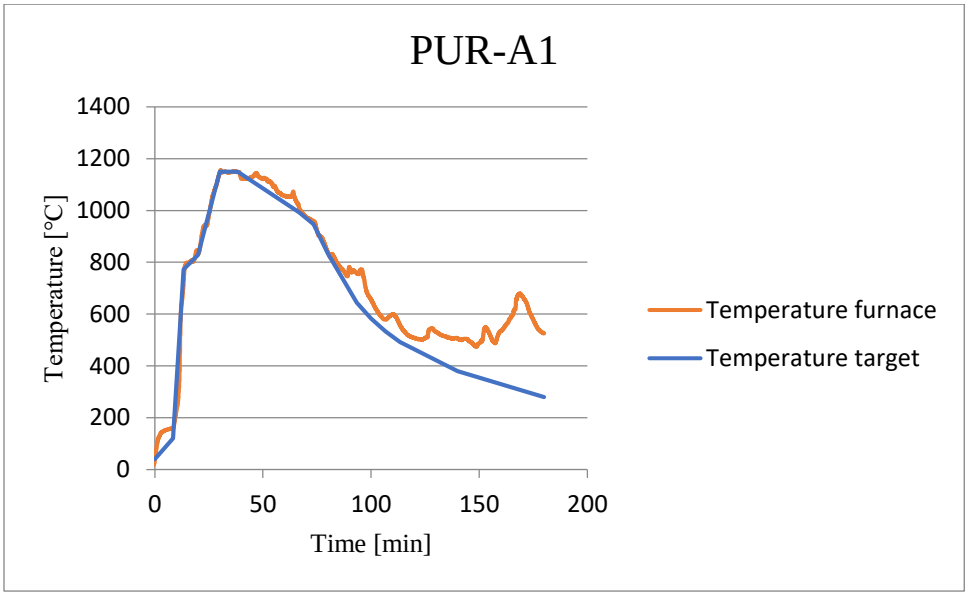

fig. C-5. Temperature profile of the furnace in comparison with the expected target for PUR-A1.

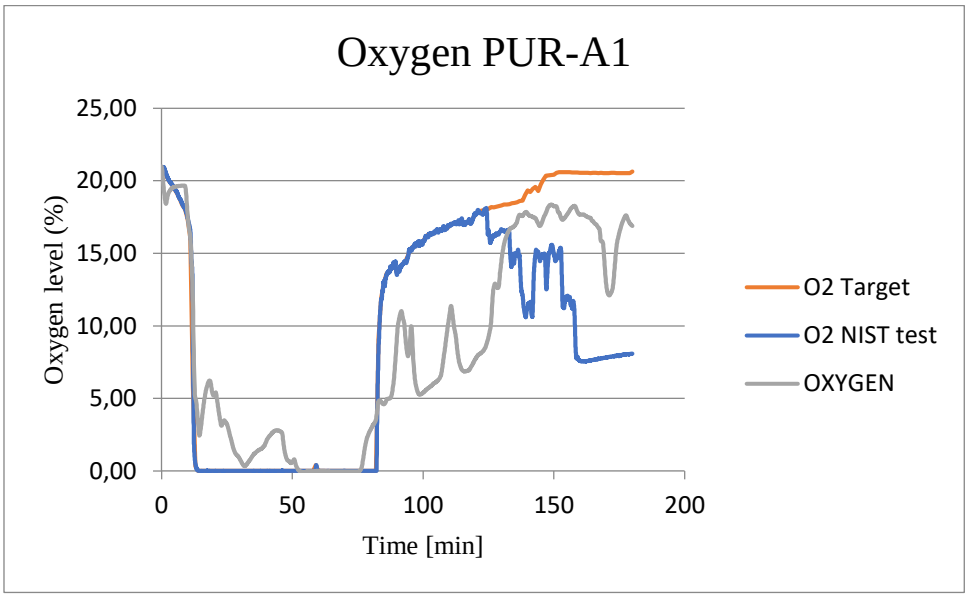

fig. C-6. Visual graphs of the oxygen levels inside the furnace during the test for specimen PUR-A1.

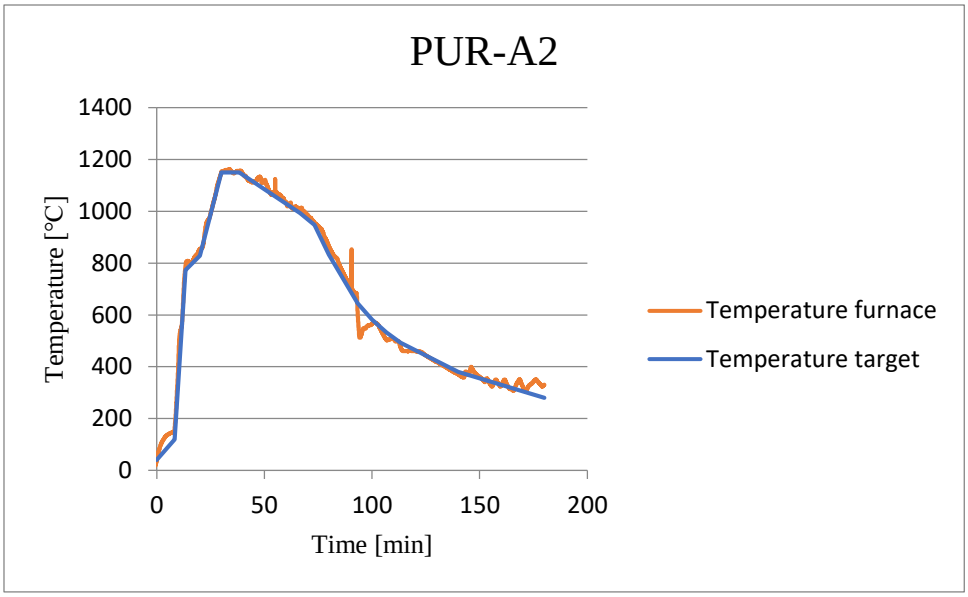

fig. C-7. Temperature profile of the furnace in comparison with the expected target for PUR-A2.

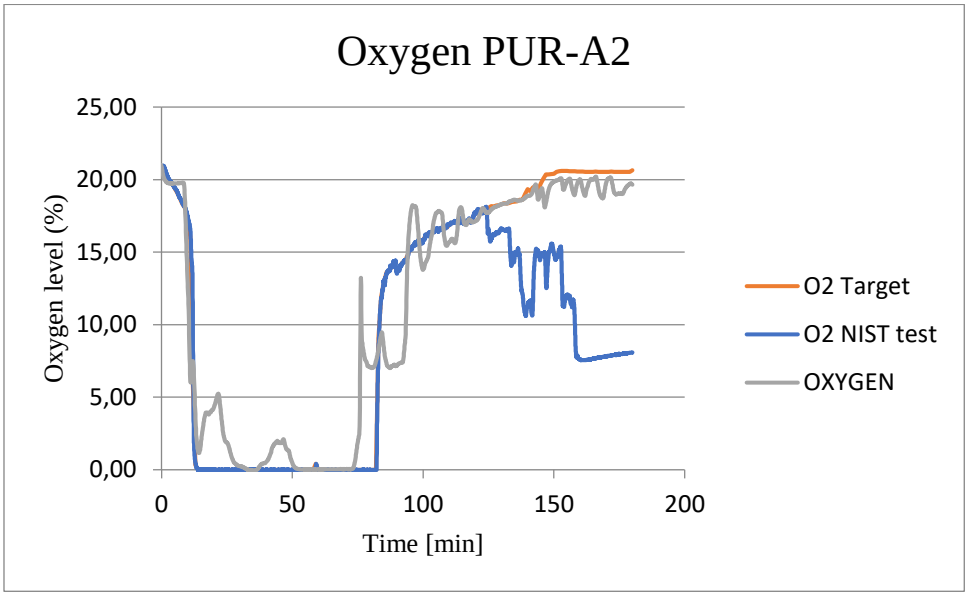

fig. C-8. Visual graphs of the oxygen levels inside the furnace during the test for specimen PUR-A2.

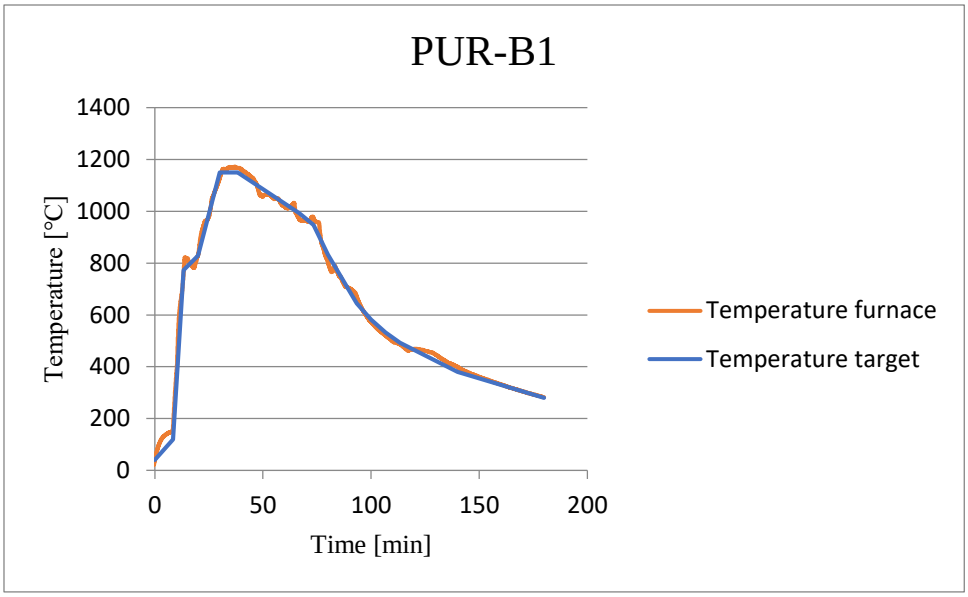

fig. C-9. Temperature profile of the furnace in comparison with the expected target for PUR-B1.

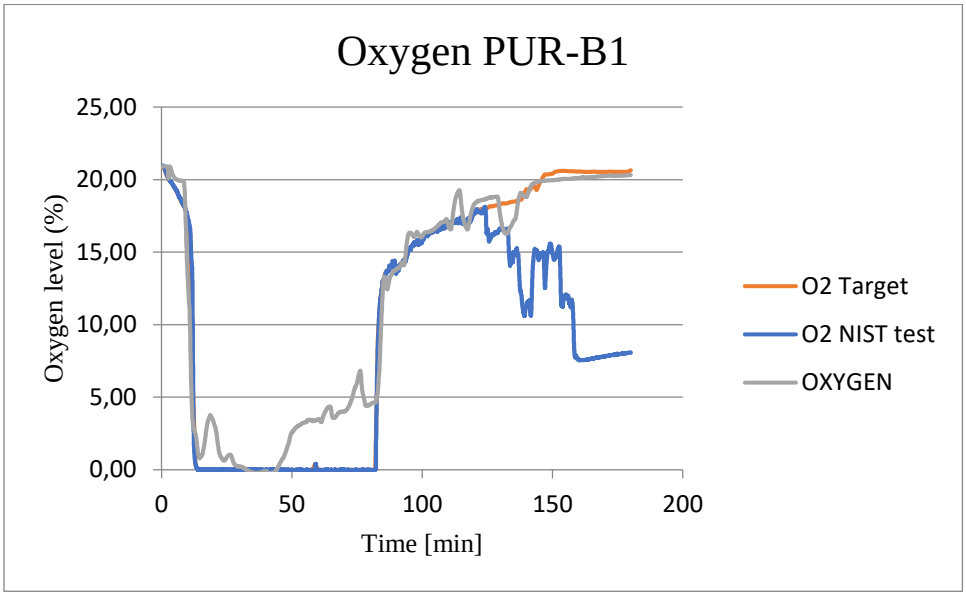

fig. C-10. Visual graphs of the oxygen levels inside the furnace during the test for specimen PUR-B1.

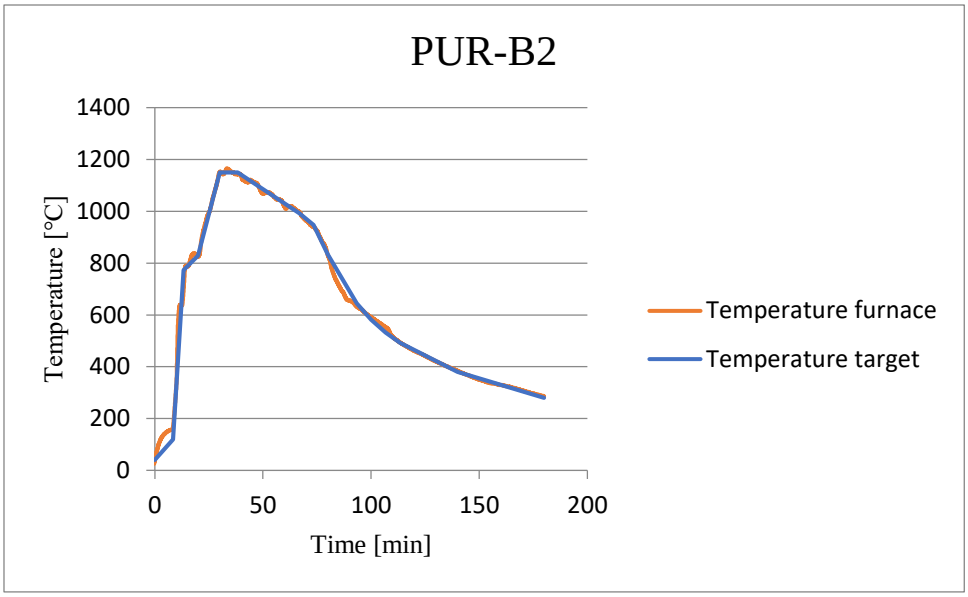

fig. C-11. Temperature profile of the furnace in comparison with the expected target for PUR-B2.

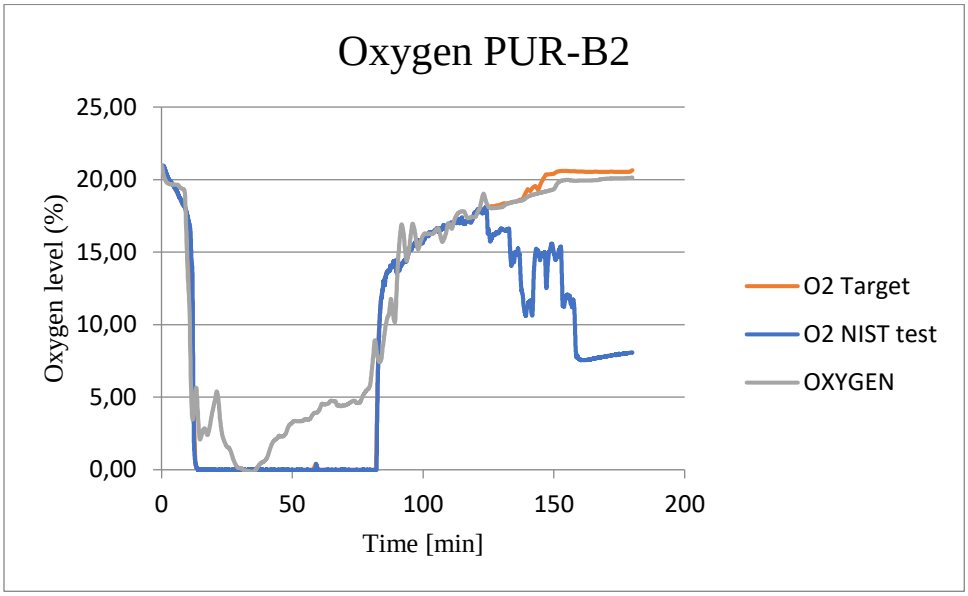

fig. C-12. Visual graphs of the oxygen levels inside the furnace during the test for specimen PUR-B2.

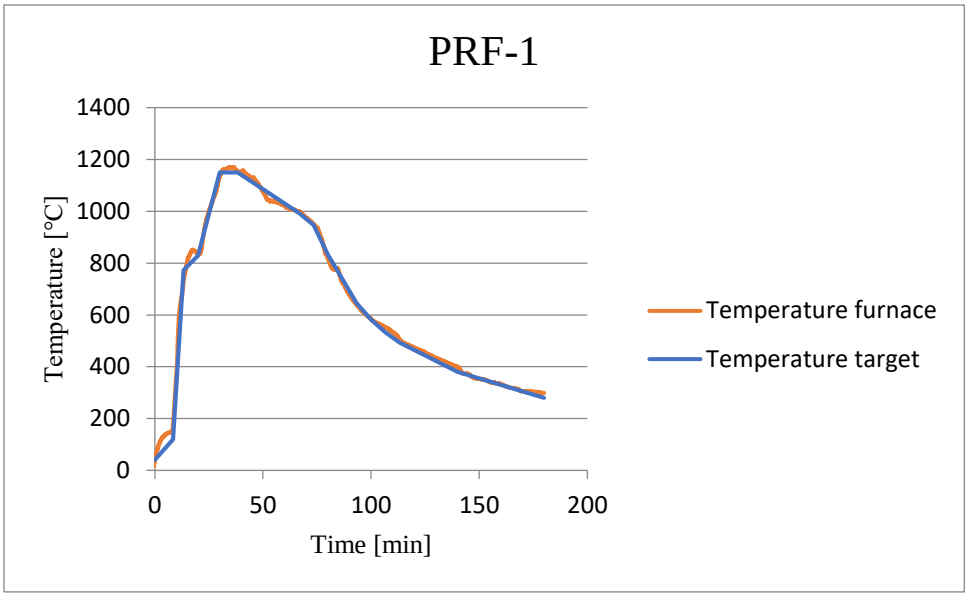

fig. C-13. Temperature profile of the furnace in comparison with the expected target for PRF-1.

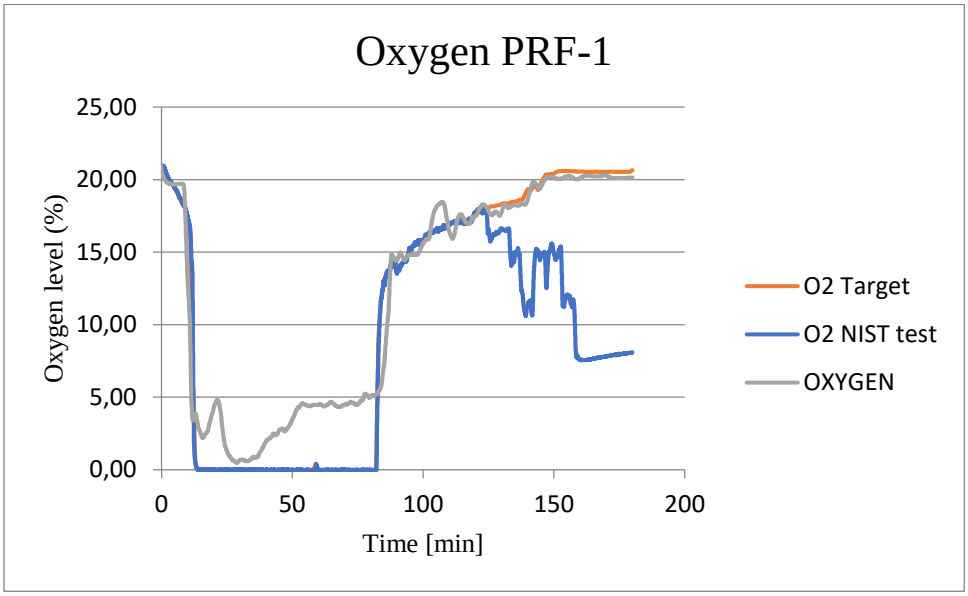

fig. C-14. Visual graphs of the oxygen levels inside the furnace during the test for specimen PRF-1.

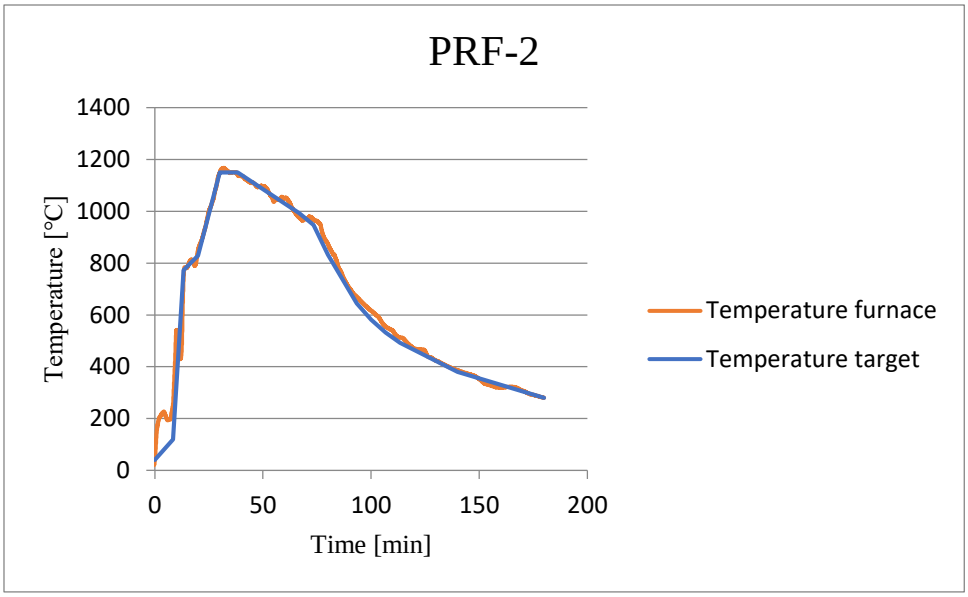

fig. C-15. Temperature profile of the furnace in comparison with the expected target for PRF-2.

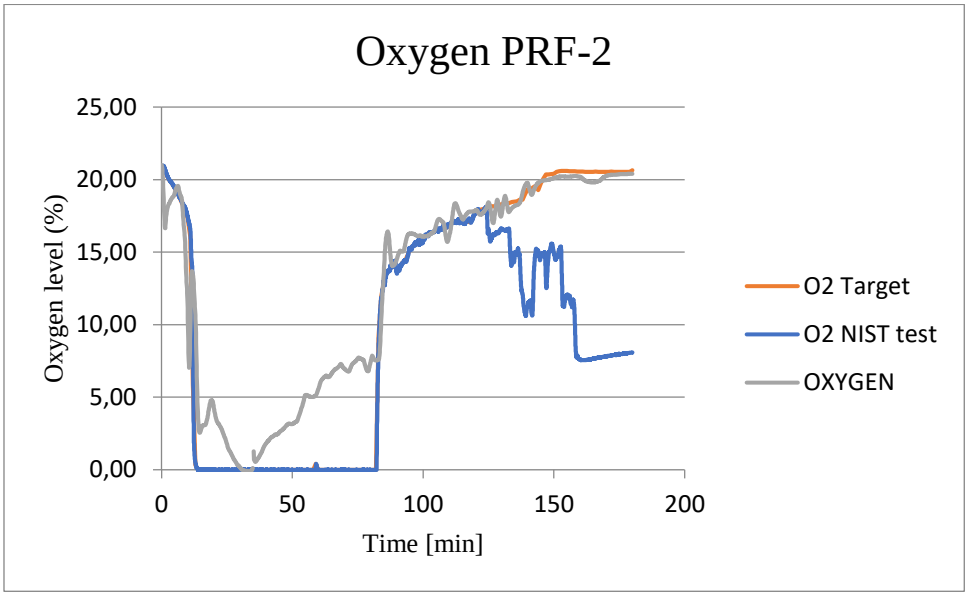

fig. C-16. Visual graphs of the oxygen levels inside the furnace during the test for specimen PRF-2.

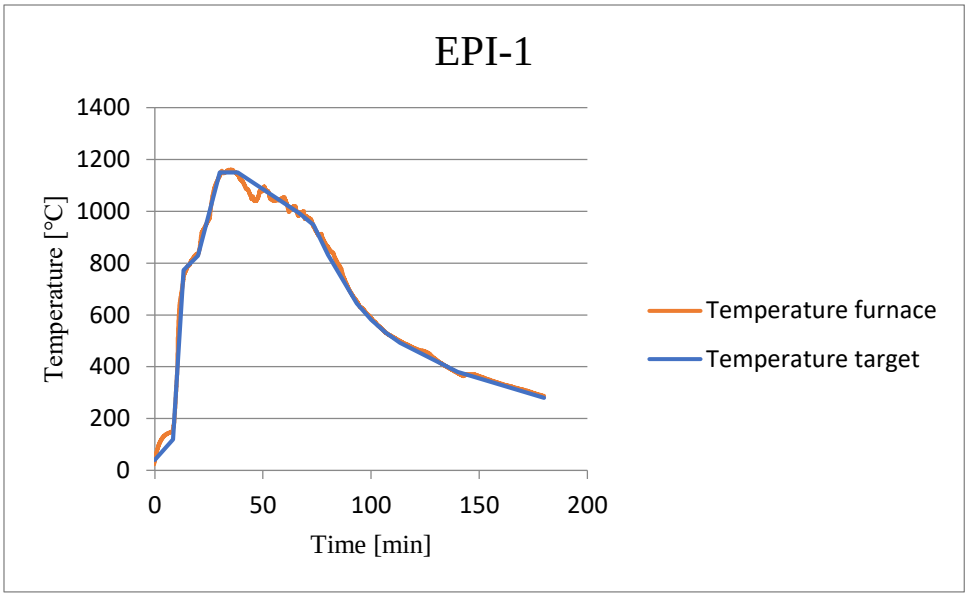

fig. C-17. Temperature profile of the furnace in comparison with the expected target for EPI-1.

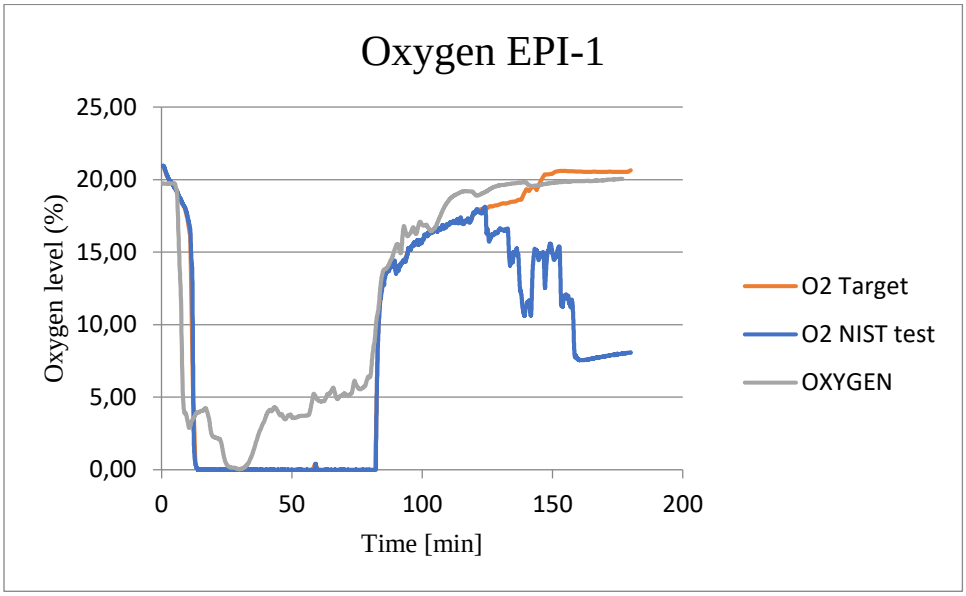

fig. C-18. Visual graphs of the oxygen levels inside the furnace during the test for specimen EPI-1.

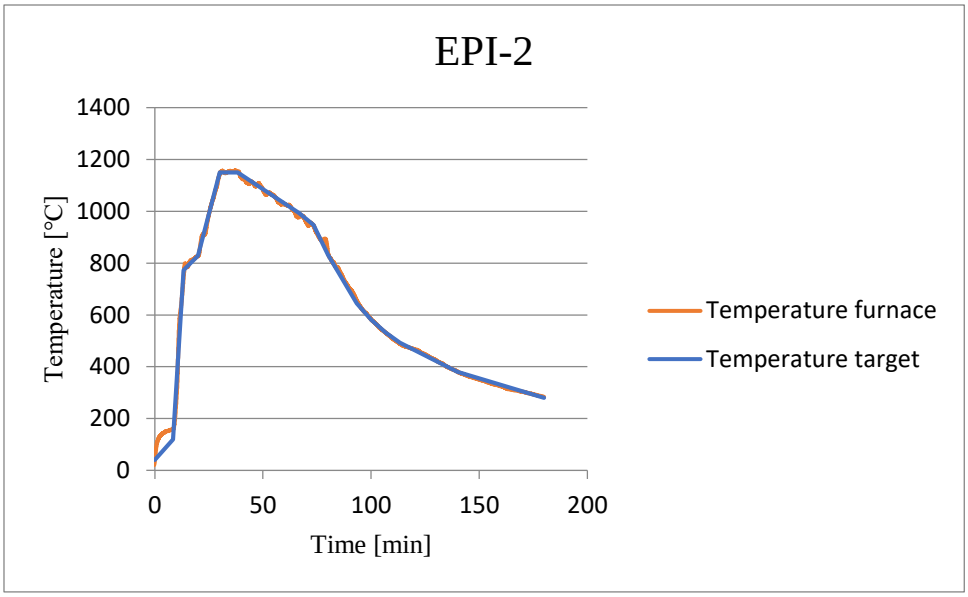

fig. C-19. Temperature profile of the furnace in comparison with the expected target for EPI-2.

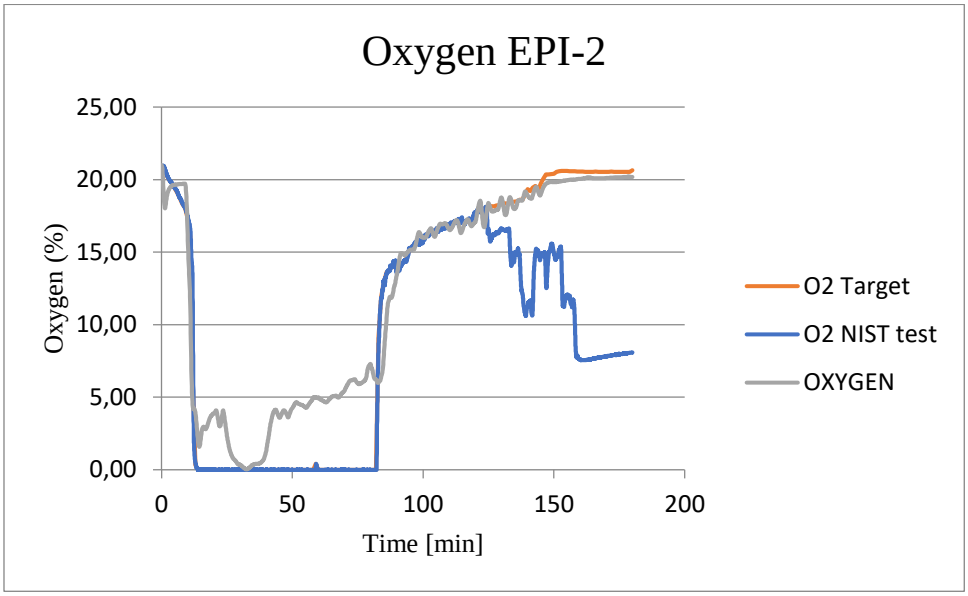

fig. C-20. Visual graphs of the oxygen levels inside the furnace during the test for specimen EPI-2.

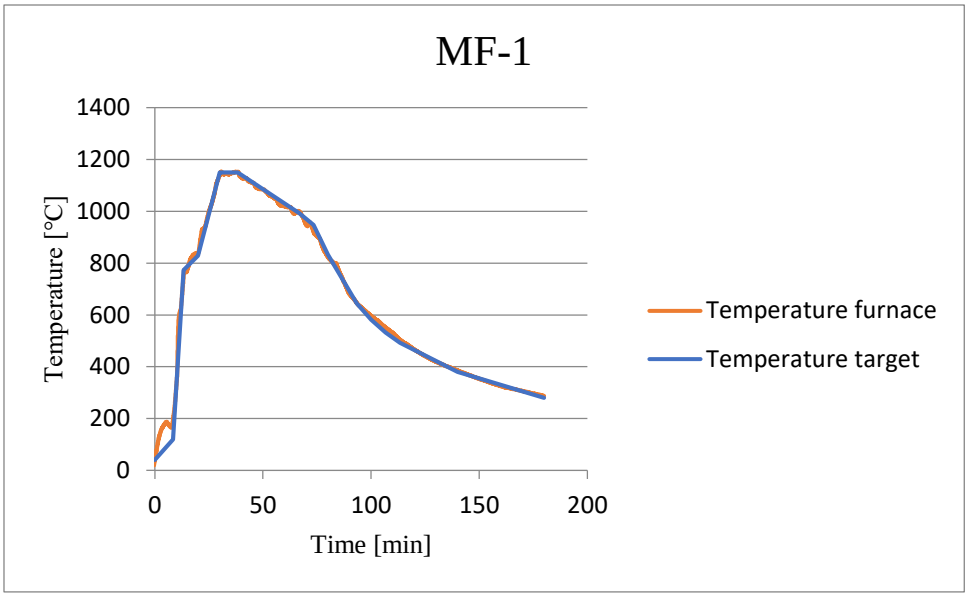

fig. C-21. Temperature profile of the furnace in comparison with the expected target for MF-1.

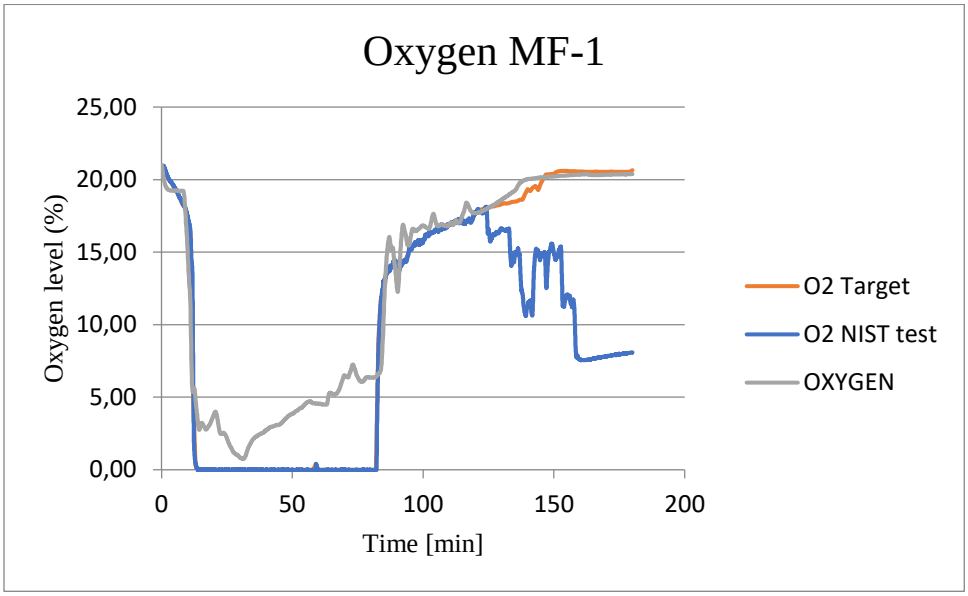

fig. C-22. Visual graphs of the oxygen levels inside the furnace during the test for specimen MF-1.

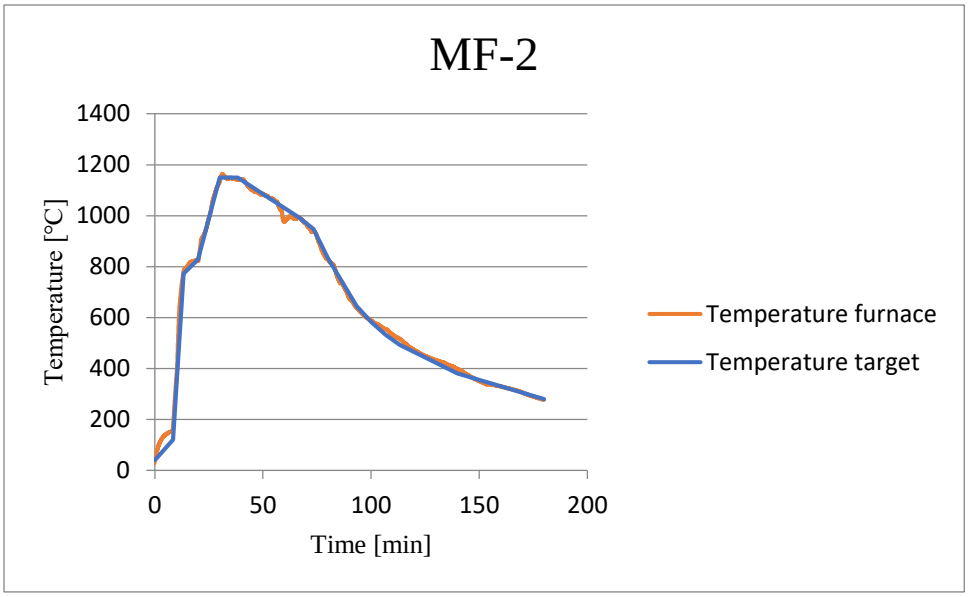

fig. C-23. Temperature profile of the furnace in comparison with the expected target for MF-2.

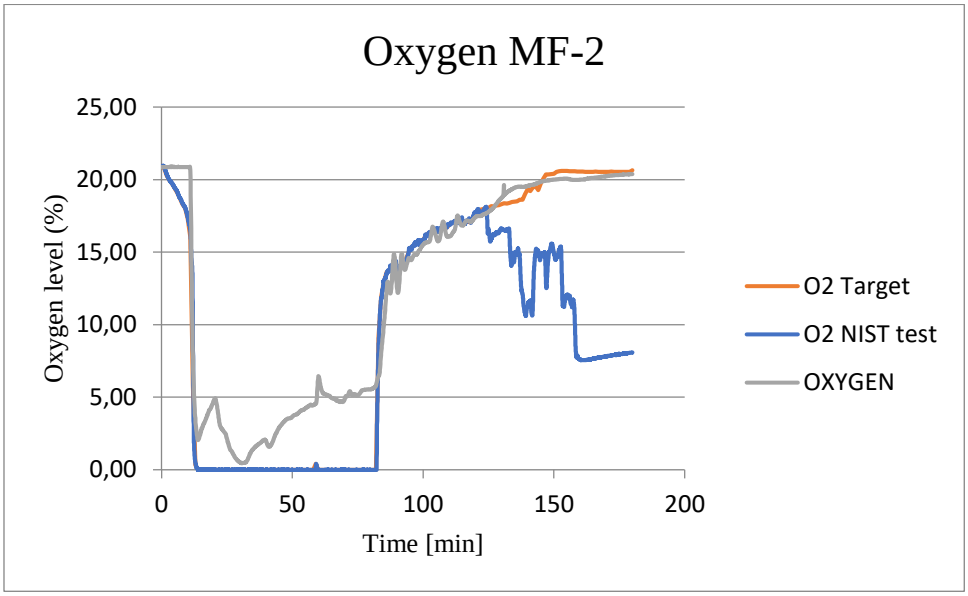

fig. C-24. Visual graphs of the oxygen levels inside the furnace during the test for specimen MF-2.

Appendix D – Temperature profiles

This Appendix presents all of the registered temperature profiles for each thermocouple series during the experiments. Only the first four lowest thermocouples of each side series are shown, as the rest of the thermocouples in each series never reached temperatures above 300°C. The comparative temperature curves from the full-scale NIST test (Su, Lafrance, Hoehler, & Bundy, 2017) are based on readings from thermocouples drilled in from the top of a ceiling element.

For an overview of the location of each thermocouple and their numbering see fig. D-1.

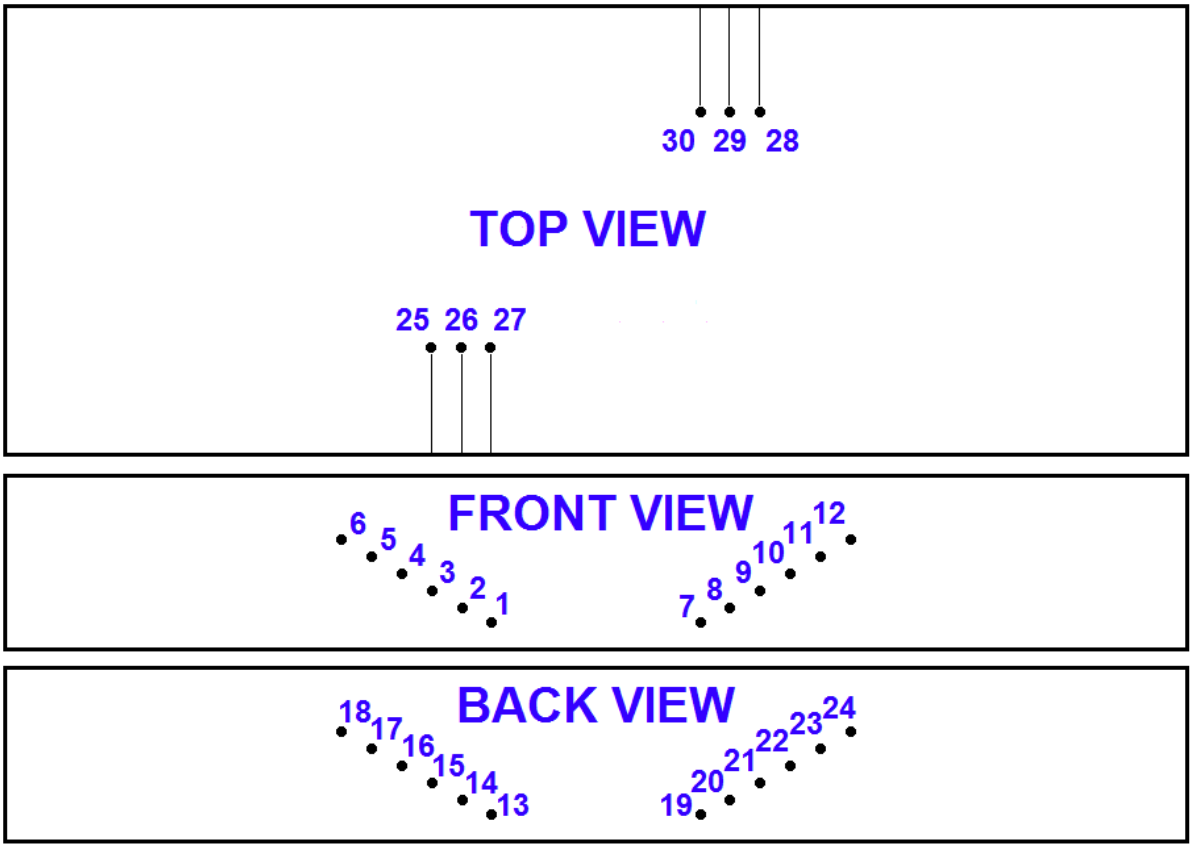

fig. D-25. Sketch of thermocouple numbering and approximate placement in specimen.

PUR-A1:

As the PUR-A specimen were cut from original pieces of the target full-scale test, the temperature profile of these specimen should correspond well to the original measurements (NIST). For PUR-A1, this seems to be the case of the 20 mm side-depth and the top series. Among the presented measurement of this test only TC 4 appears to have been malfunctioning.

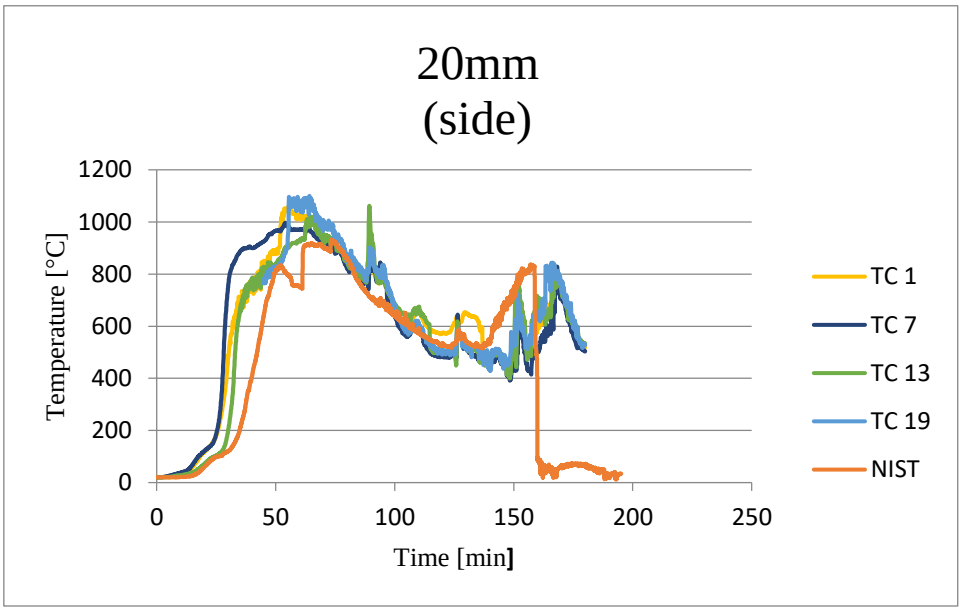

fig. D-26. All thermocouple temperatures at the depth 20 mm, for the PUR-A1 specimen.

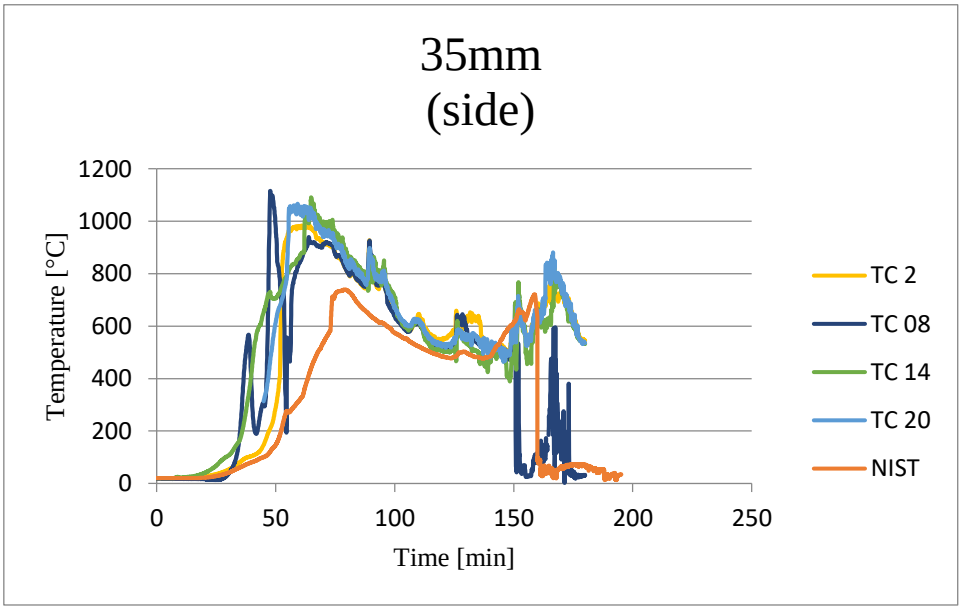

fig. D-27. All thermocouple temperatures at the depth 35 mm (bondline), for the PUR-A1 specimen.

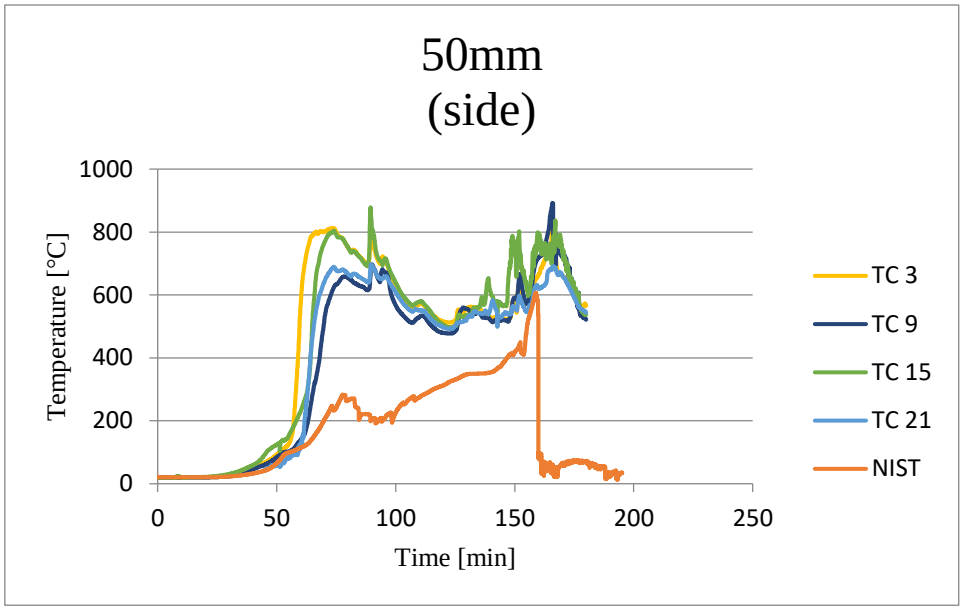

fig. D-28. All thermocouple temperatures at the depth 50 mm, for the PUR-A1 specimen.

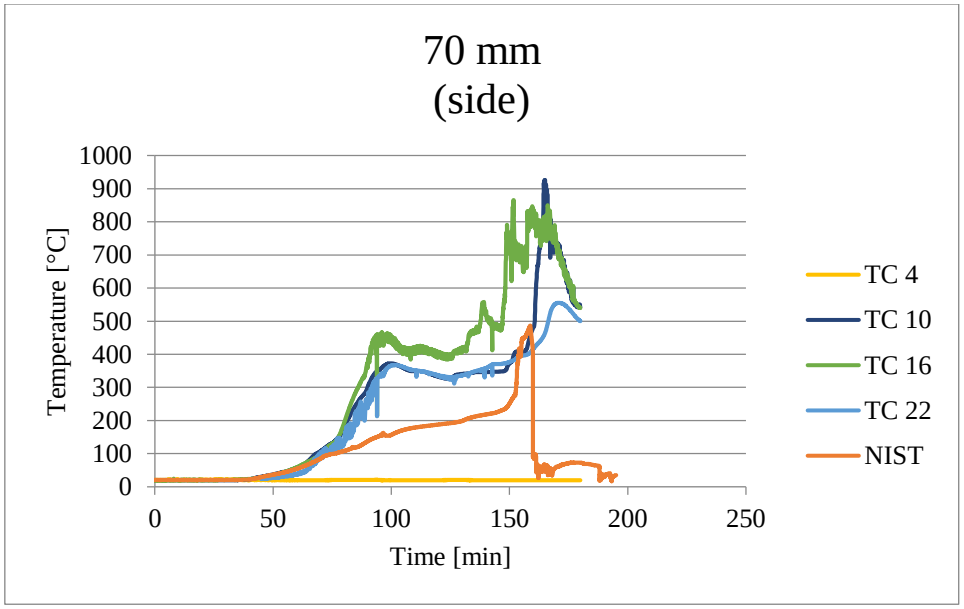

fig. D- 29. All thermocouple temperatures at the depth 70 mm (bondline), for the PUR-A1 specimen.

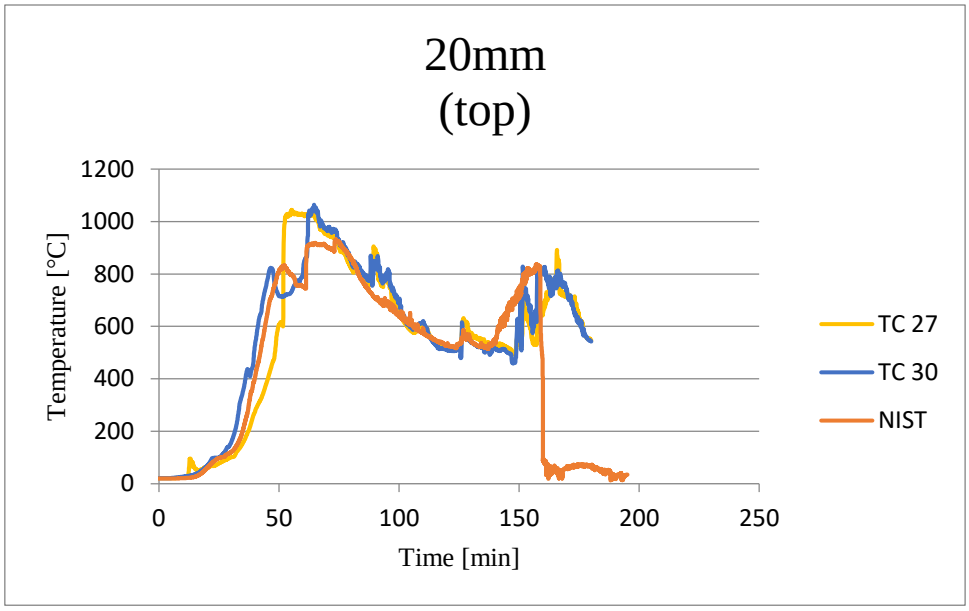

fig. D-30. All thermocouple temperatures at the depth 20 mm drilled from the top, for the PUR-A1 specimen.

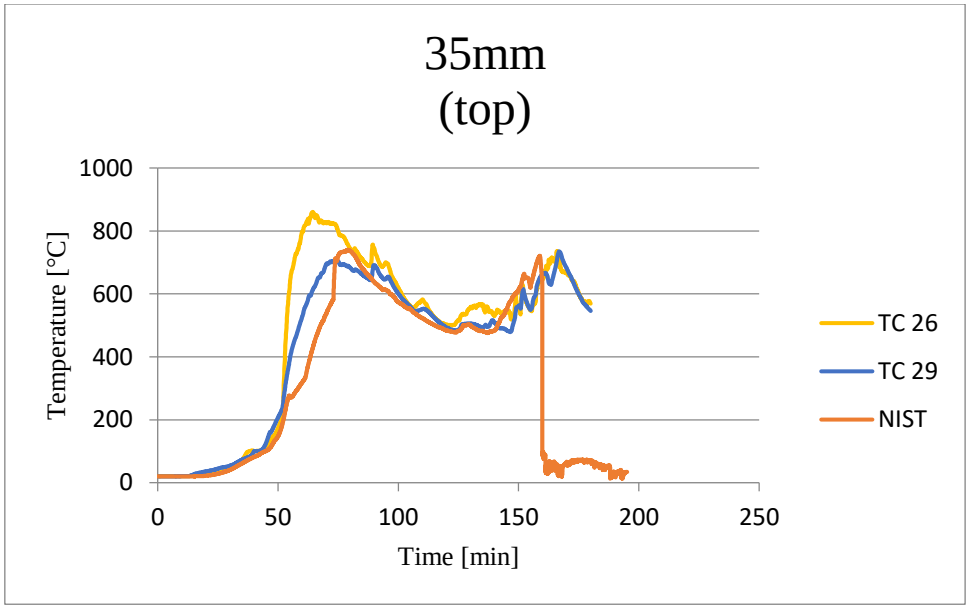

fig. D-31. All thermocouple temperatures at the depth 35 mm (bondline) drilled from the top, for the PUR-A1 specimen.

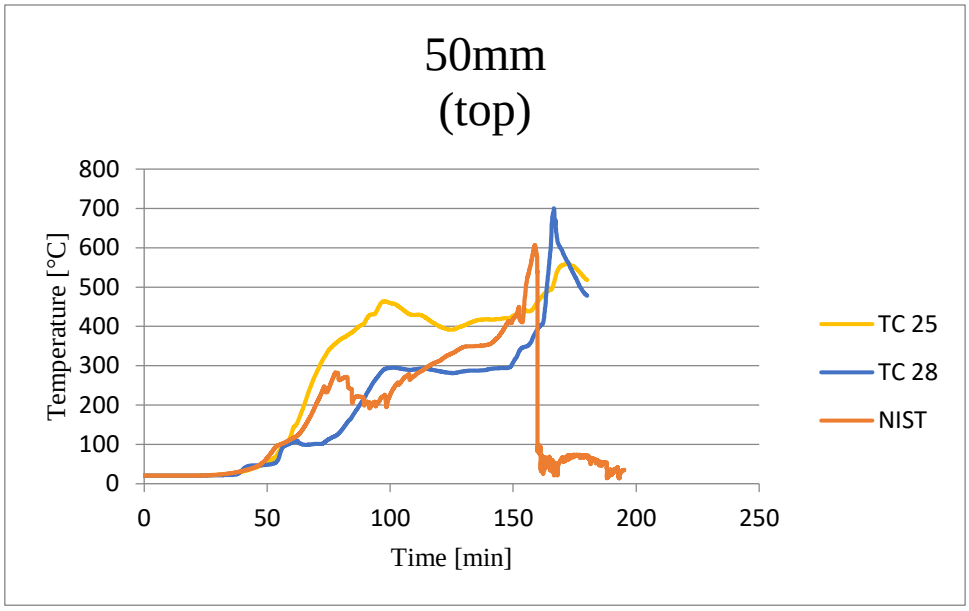

fig. D-32. All thermocouple temperatures at the depth 50 mm drilled from the top, for the PUR-A1 specimen.

PUR-A2

For the PUR-A2 specimen no significant errors with measurements or the thermocouples was registered during the test. The temperature profiles correspond well with the target (NIST) -test at the 20 mm depth for the side series. For the top series, this is also true up until the final stages of the test, toward the second delamination of the original test.

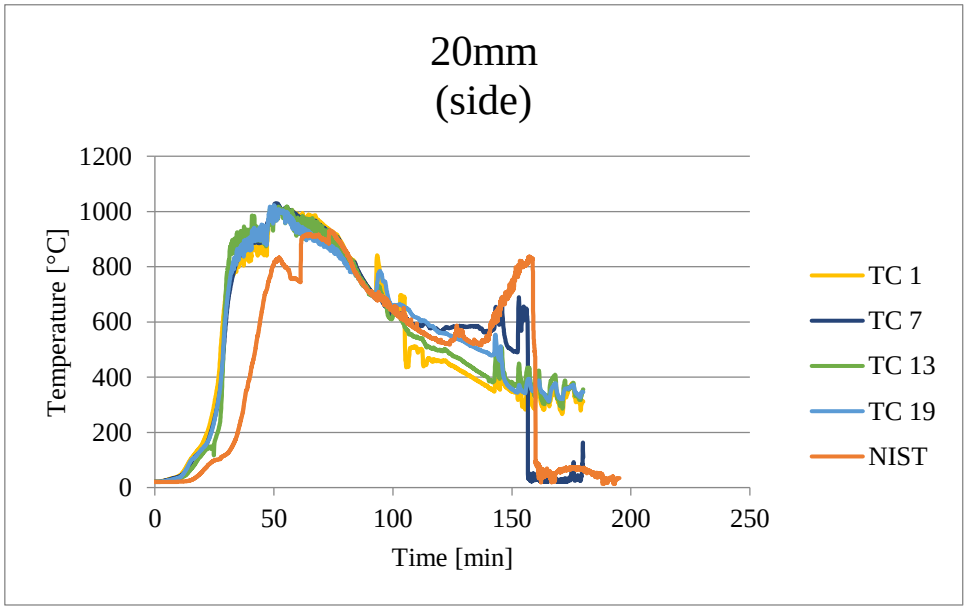

fig. D-33. All thermocouple temperatures at the depth 20 mm, for the PUR-A2 specimen.

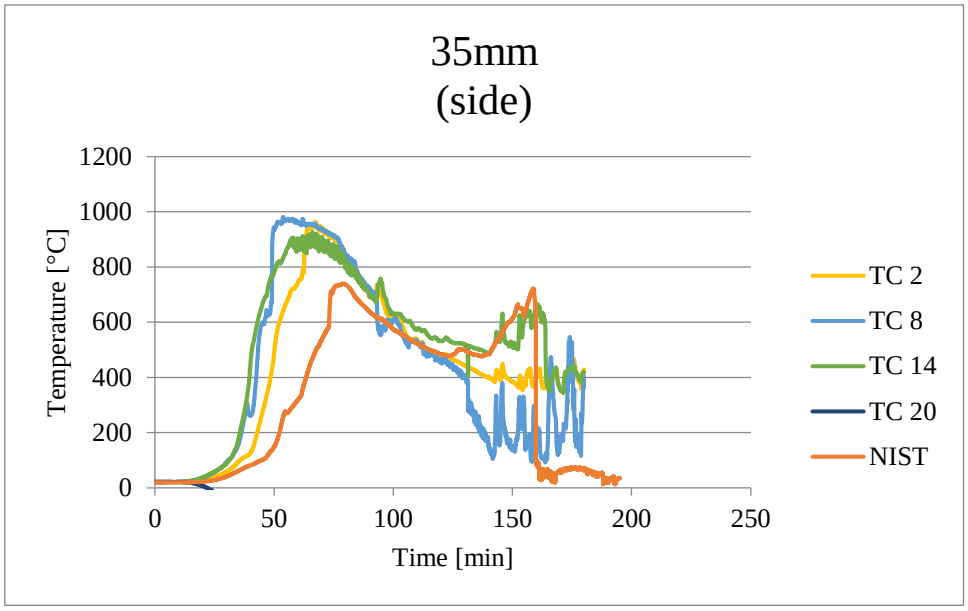

fig. D-34. All thermocouple temperatures at the depth 35 mm (bondline), for the PUR-A2 specimen.

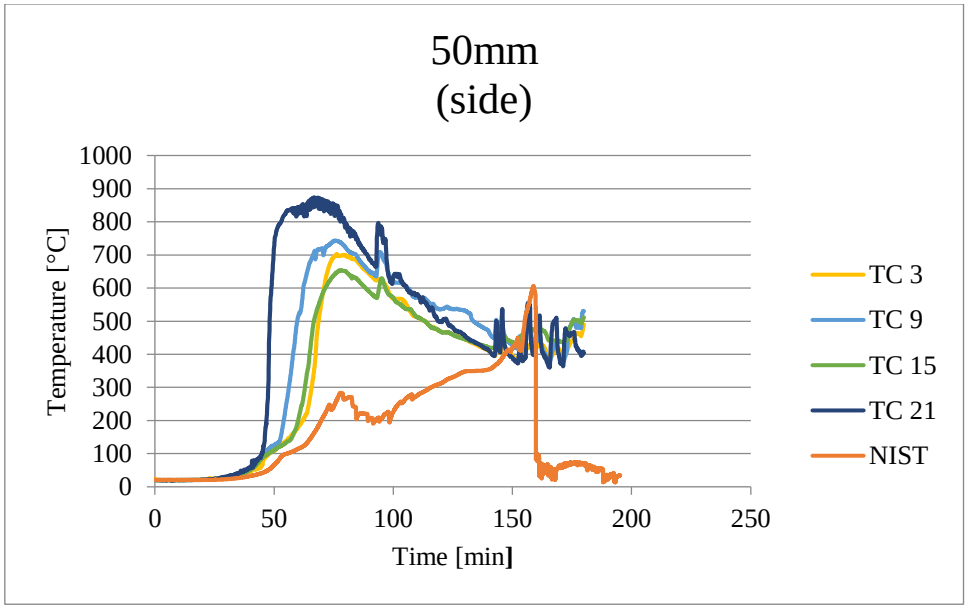

fig. D-11. All thermocouple temperatures at the depth 50 mm, for the PUR-A2 specimen.

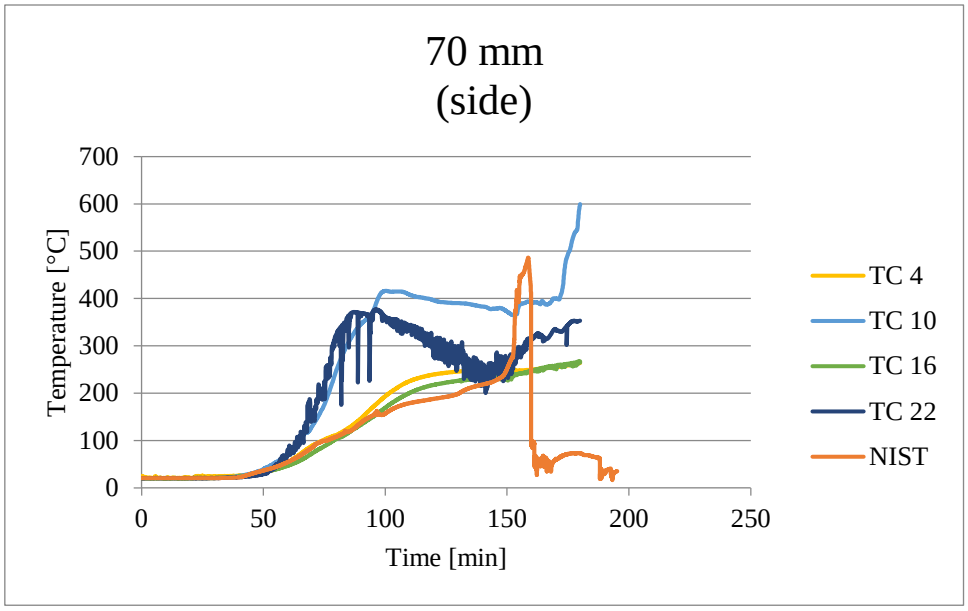

fig. D-35. All thermocouple temperatures at the depth 70 mm, for the PUR-A2 specimen.

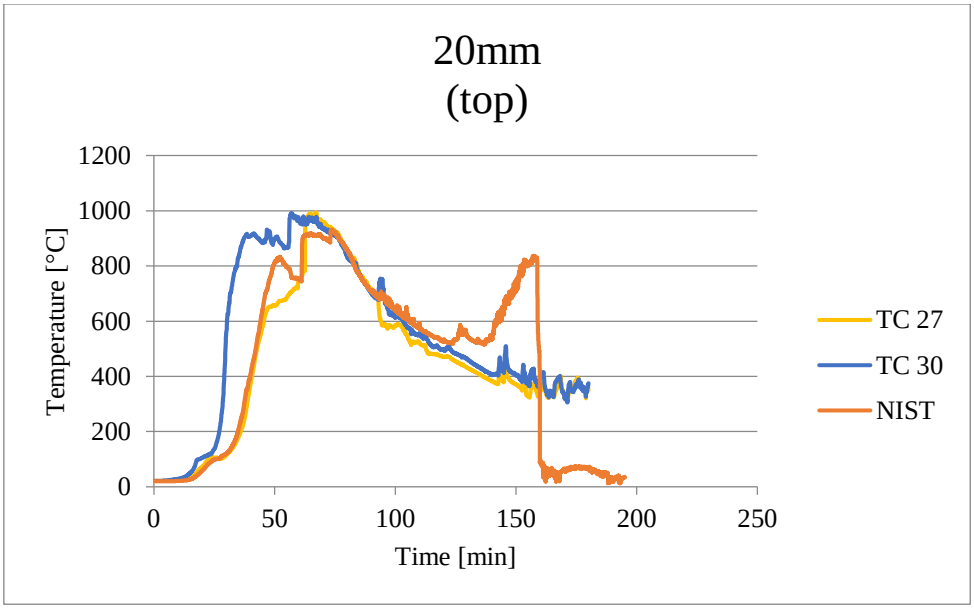

fig. D-36. All thermocouple temperatures at the depth 20 mm drilled from the top, for the PUR-A2 specimen.

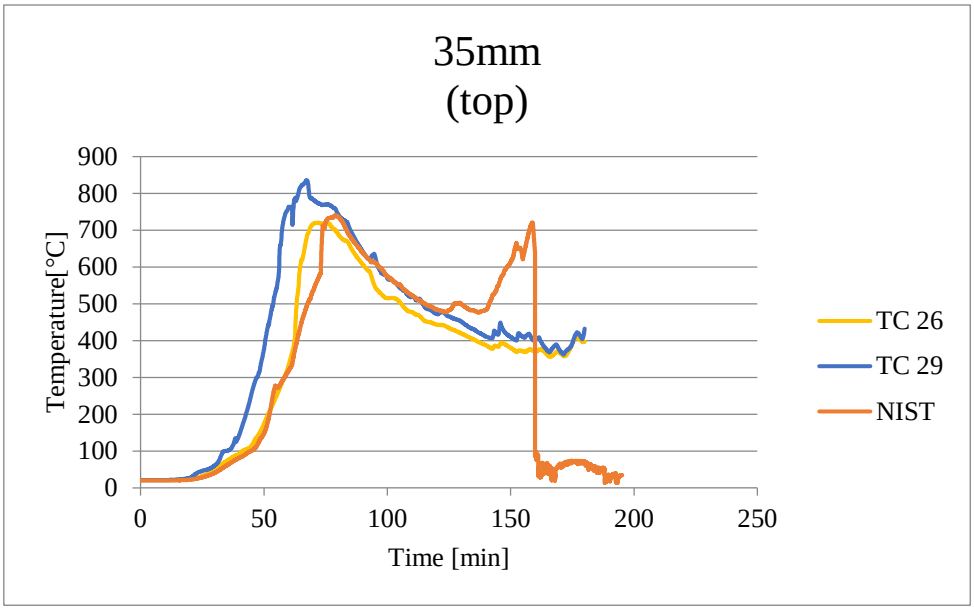

fig. D-37. All thermocouple temperatures at the depth 35 mm (bondline) drilled from the top, for the PUR-A2 specimen.

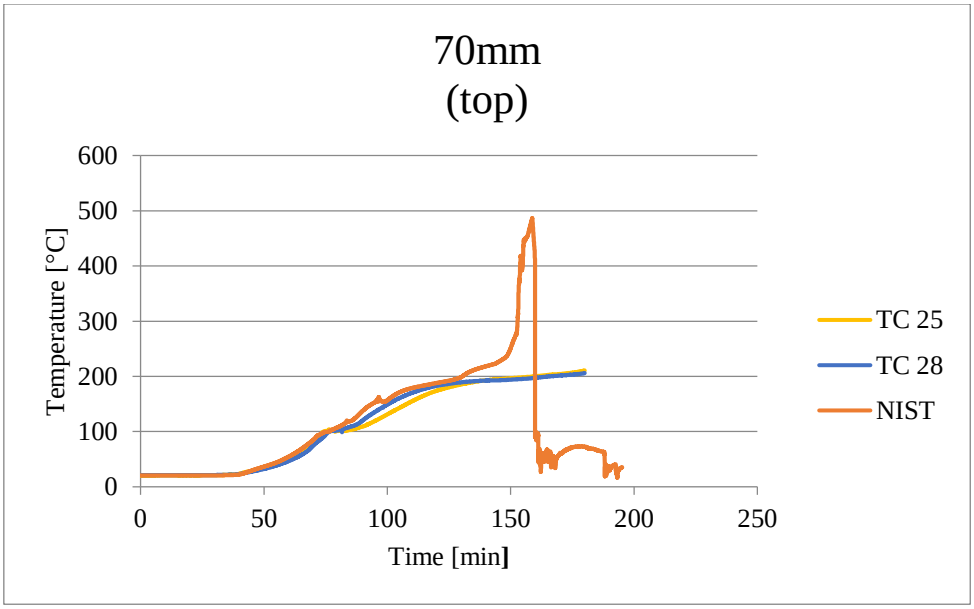

fig. D-38. All thermocouple temperatures at the depth 70 mm (bondline) drilled from the top, for the PUR-A2 specimen.

PUR-B1

During the PUR-B1 test two errors with thermocouples were registered, TC 15 on the 50 mm depth and TC 22 on the 70 mm depth, both in side series. More reasoning about TC 22 can be found in the discussion of the master thesis report.

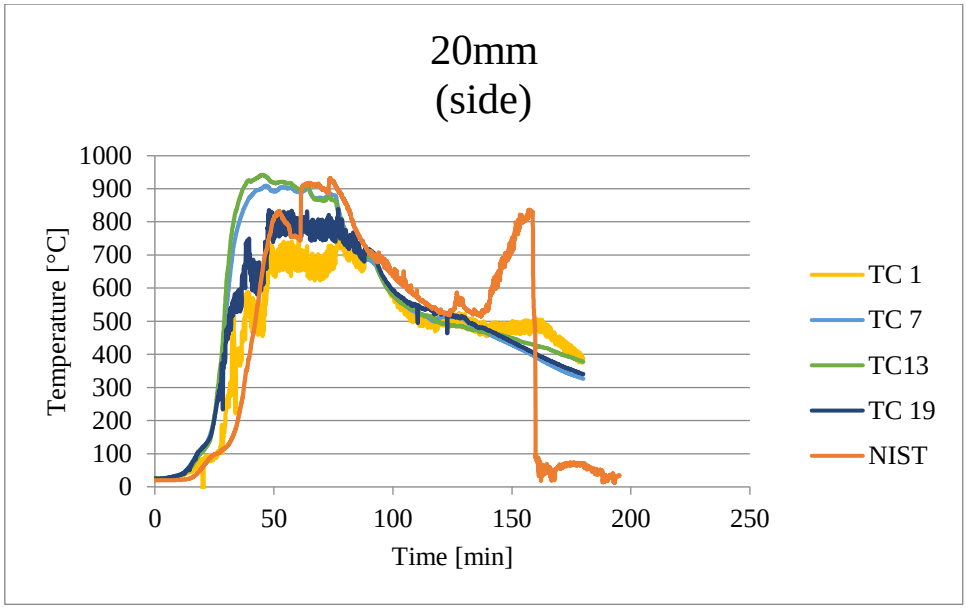

fig. D-39. All thermocouple temperatures at the depth 20 mm, for the PUR-B1 specimen.

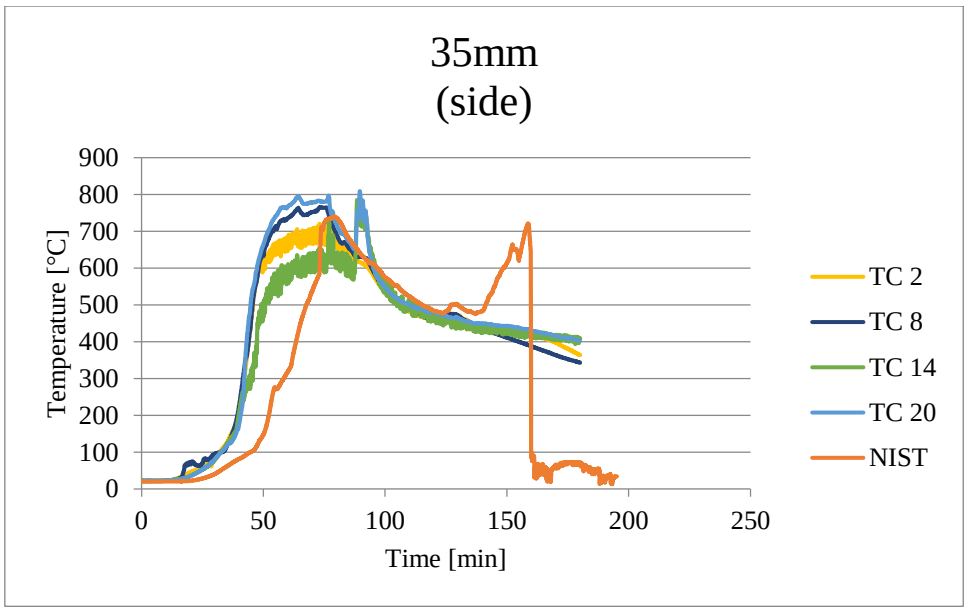

fig. D-40. All thermocouple temperatures at the depth 35 mm (bondline), for the PUR-B1 specimen.

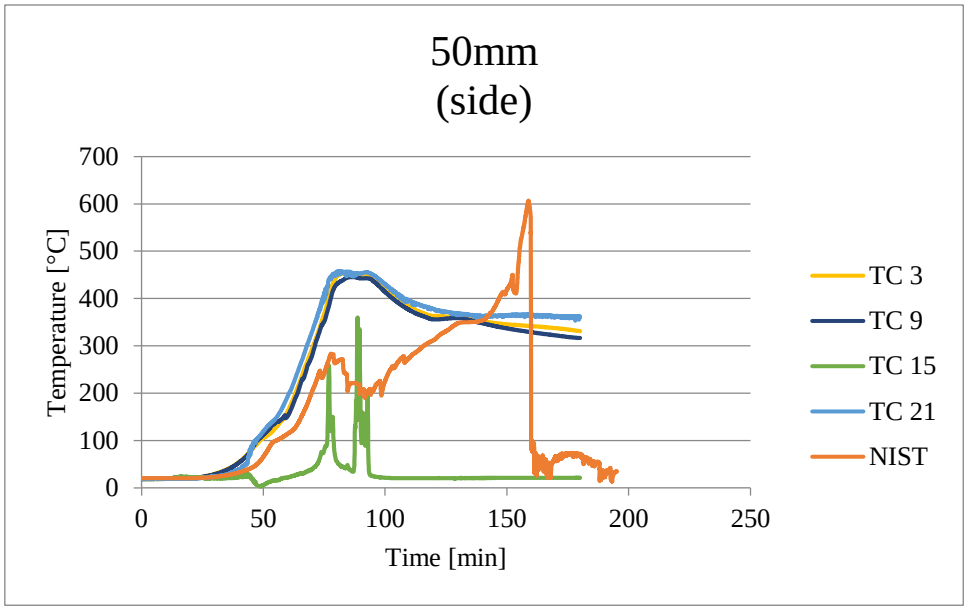

fig. D-41. All thermocouple temperatures at the depth 50 mm, for the PUR-B1 specimen.

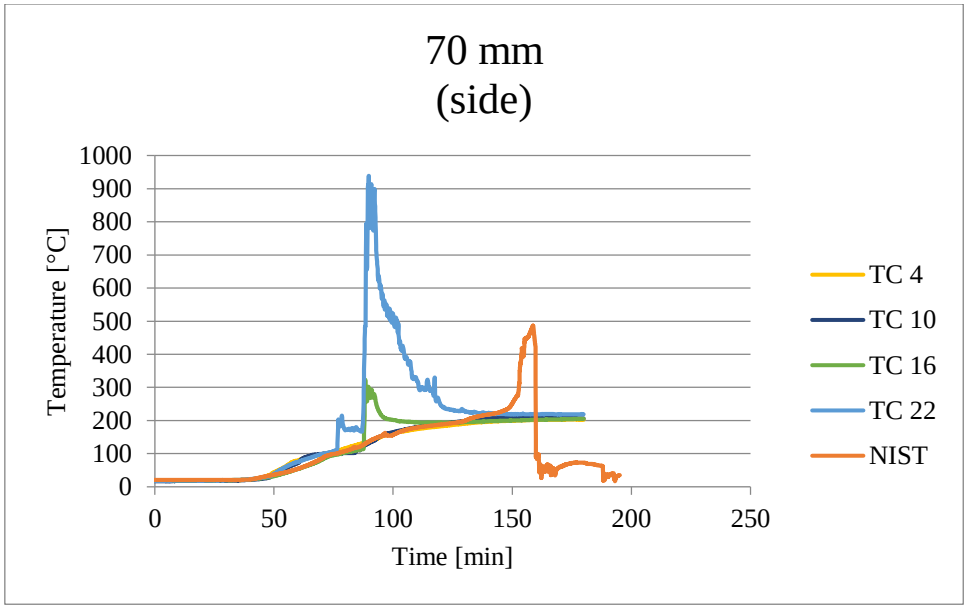

fig. D-42. All thermocouple temperatures at the depth 70 mm (bondline), for the PUR-B1 specimen.

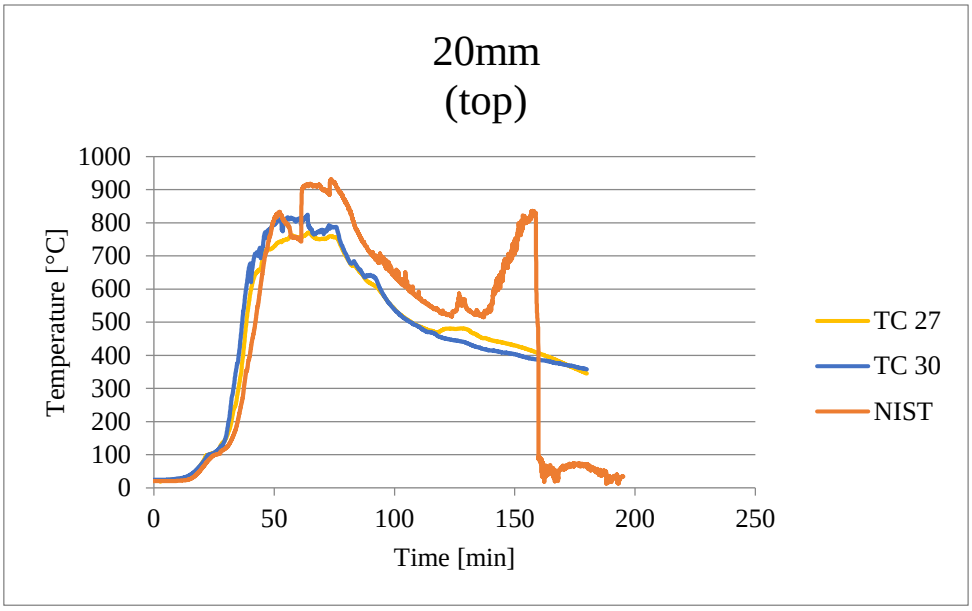

fig. D-43. All thermocouple temperatures at the depth 20 mm drilled from the top, for the PUR-B1 specimen.

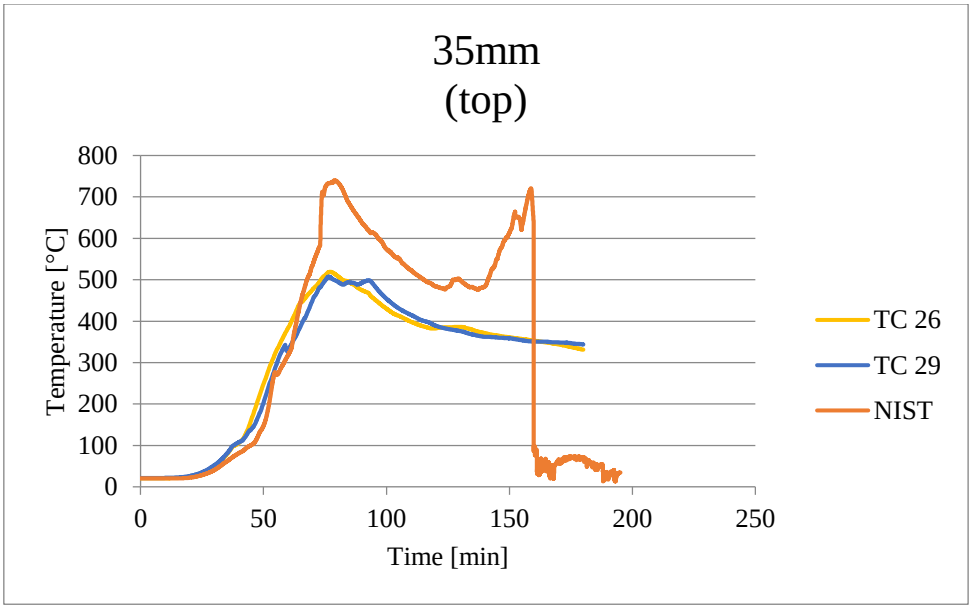

fig. D-44. All thermocouple temperatures at the depth 35 mm (bondline) drilled from the top, for the PUR-B1 specimen.

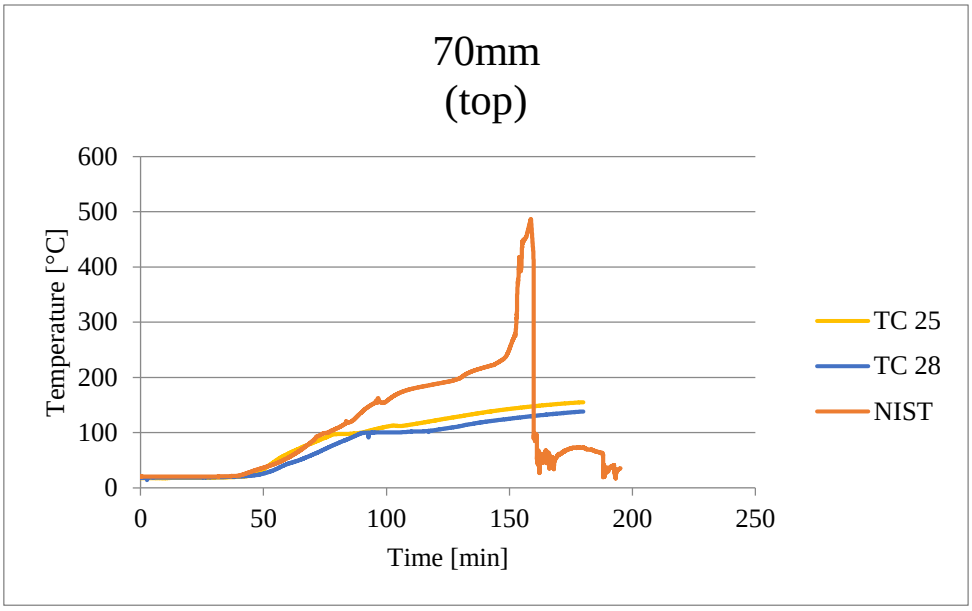

fig. D-45. All thermocouple temperatures at the depth 70 mm (bondline) drilled from the top, for the PUR-B1 specimen.

PUR-B2

In the PUR-B2 test thermocouples TC 7 and TC 3 were malfunctioning, which was noted during the test.

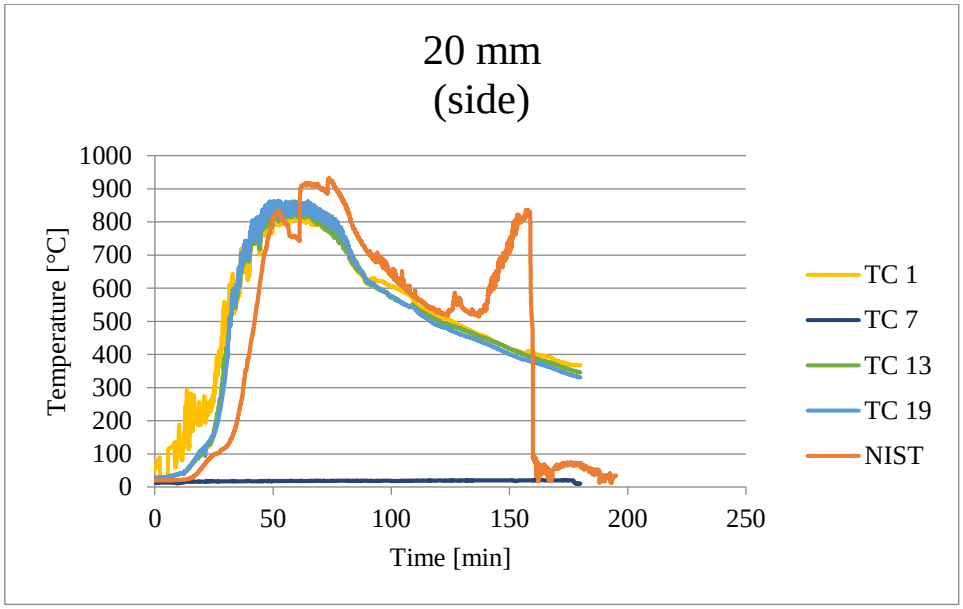

fig. D-46. All thermocouple temperatures at the depth 20 mm, for the PUR-B2 specimen.

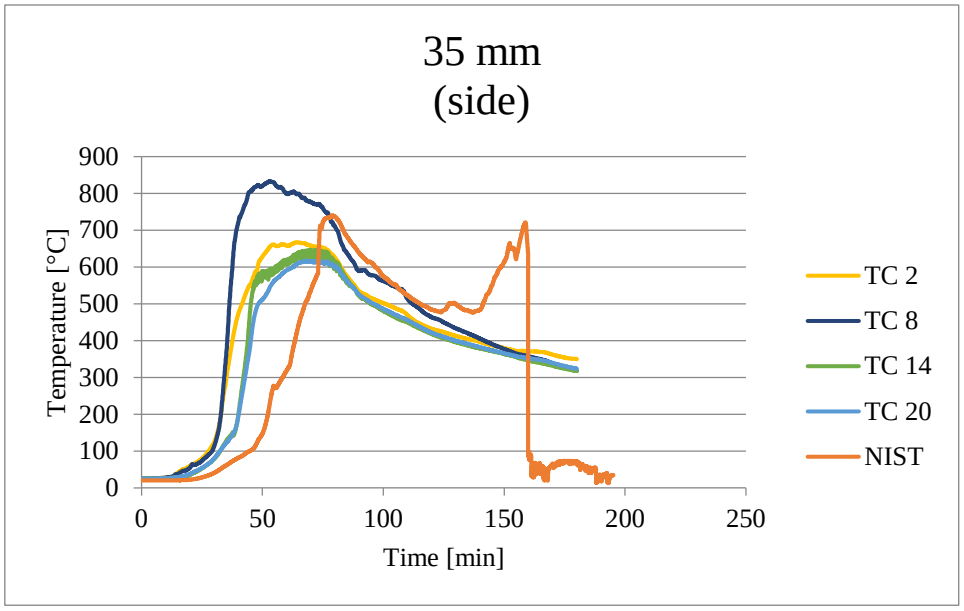

fig. D-47. All thermocouple temperatures at the depth 35 mm (bondline), for the PUR-B2 specimen.

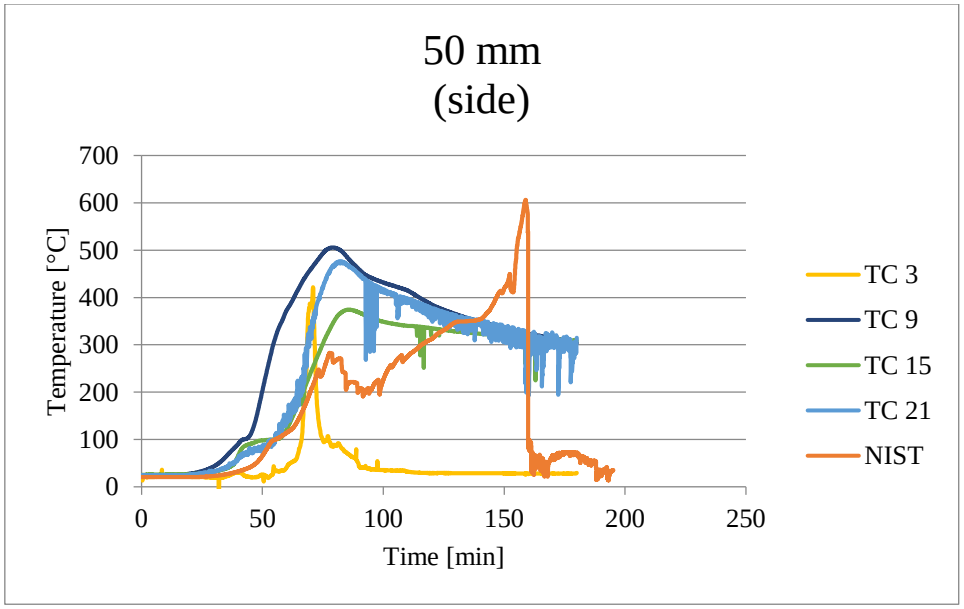

fig. D-48. All thermocouple temperatures at the depth 50 mm, for the PUR-B2 specimen.

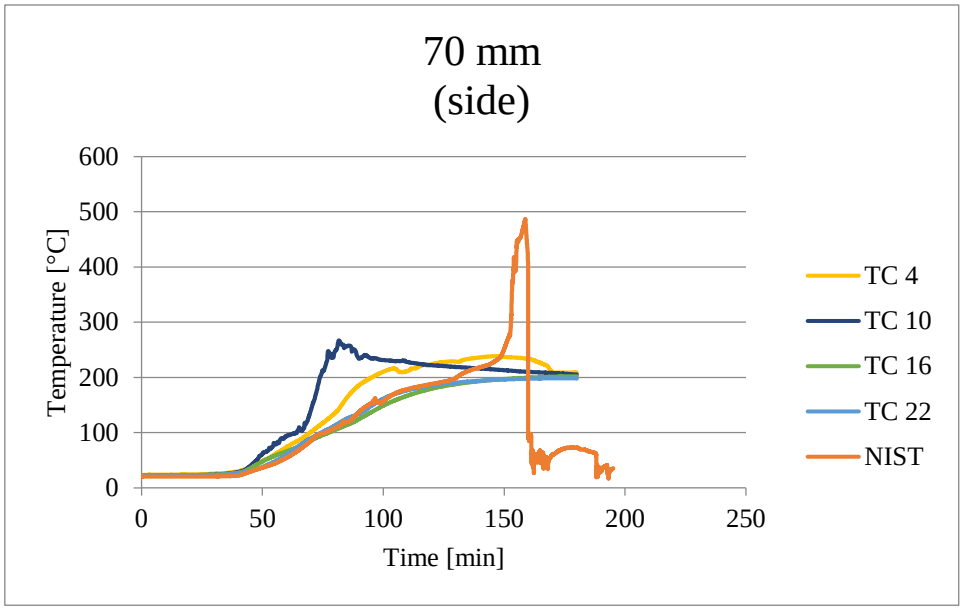

fig. D-49. All thermocouple temperatures at the depth 70 mm (bondline), for the PUR-B2 specimen.

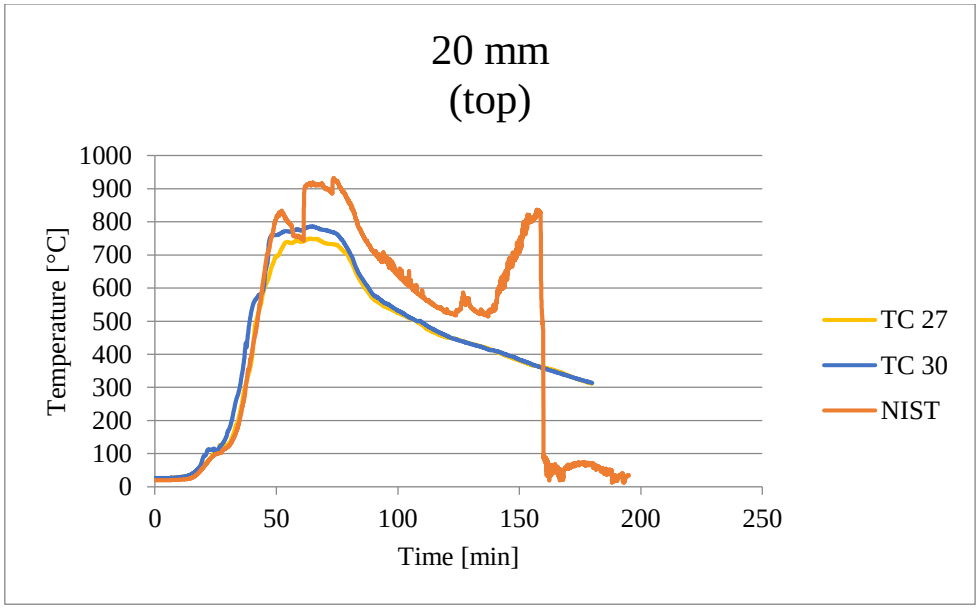

fig. 50. All thermocouple temperatures at the depth 20 mm, drilled from the top, for the PUR-B2 specimen.

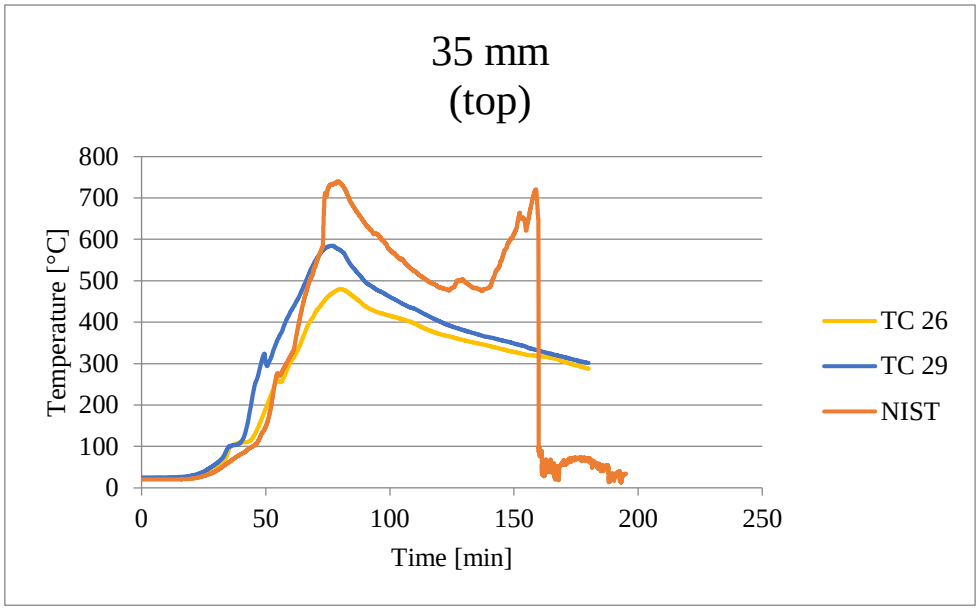

fig. D-51. All thermocouple temperatures at the depth 35 mm (bondline) drilled from the top, for the PUR-B2 specimen.

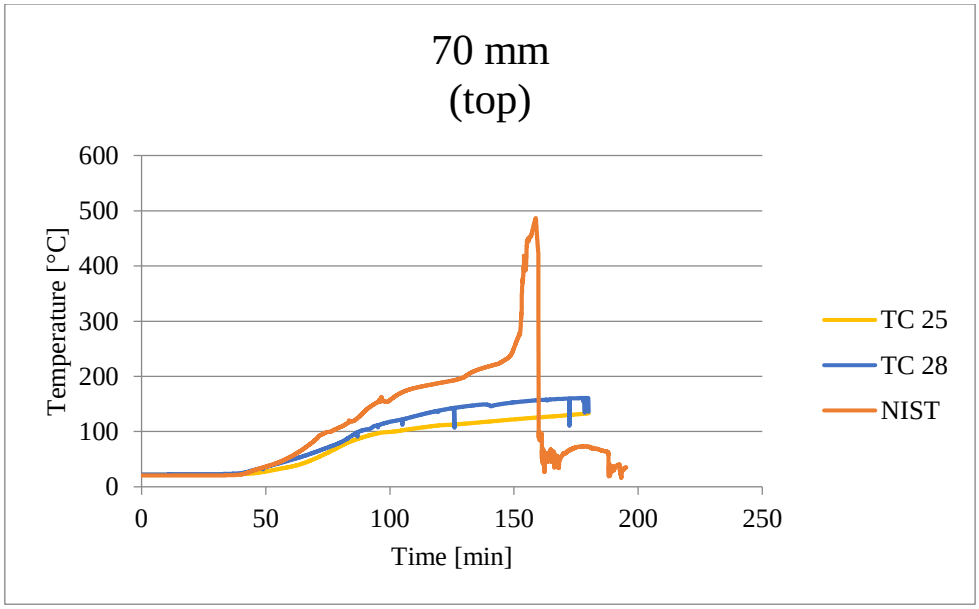

fig. D-52. All thermocouple temperatures at the depth 70 mm (bondline) drilled from the top, for the PUR-B2 specimen.

PRF-1

During the PRF-1 test, thermocouple 13 and 30 was registered as malfunctioning. However, it appears like TC 13 started working properly about 30 minutes into the test.

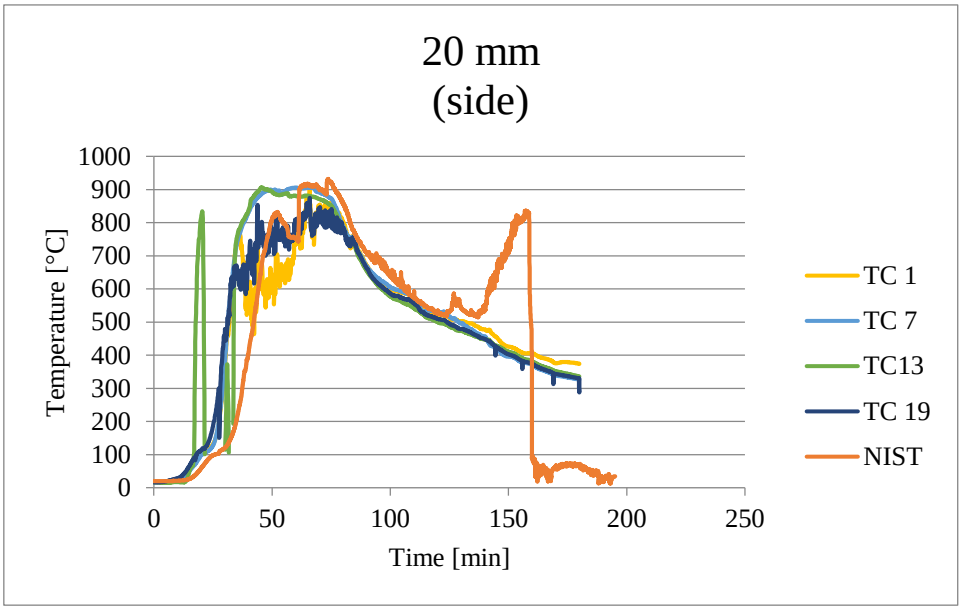

fig. D-53. All thermocouple temperatures at the depth 20 mm, for the PRF-1 specimen.

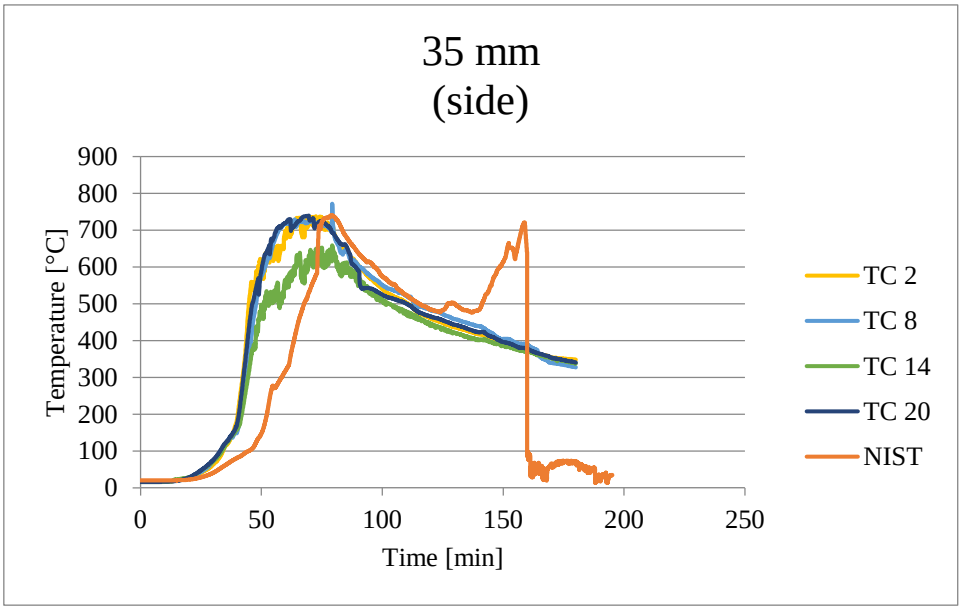

fig. D-54. All thermocouple temperatures at the depth 35 mm (bondline), for the PRF-1 specimen.

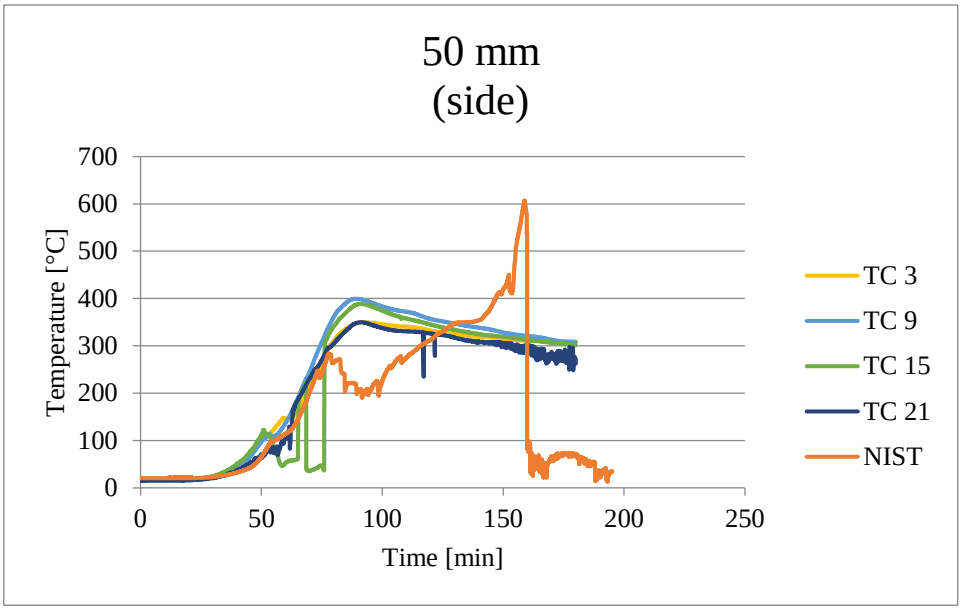

fig. D-55. All thermocouple temperatures at the depth 50 mm, for the PRF-1 specimen.

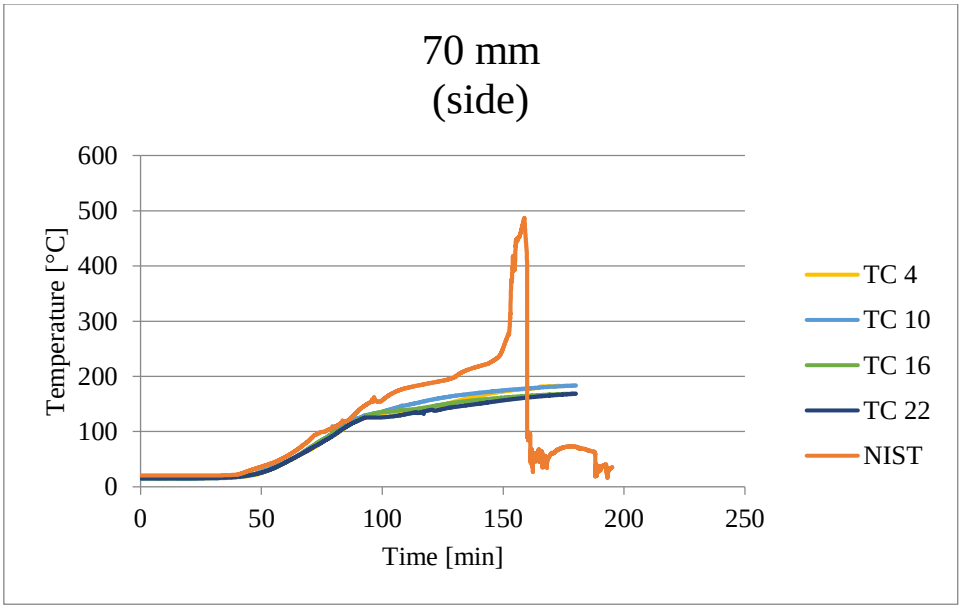

fig. D-56. All thermocouple temperatures at the depth 70 mm (bondline), for the PRF-1 specimen.

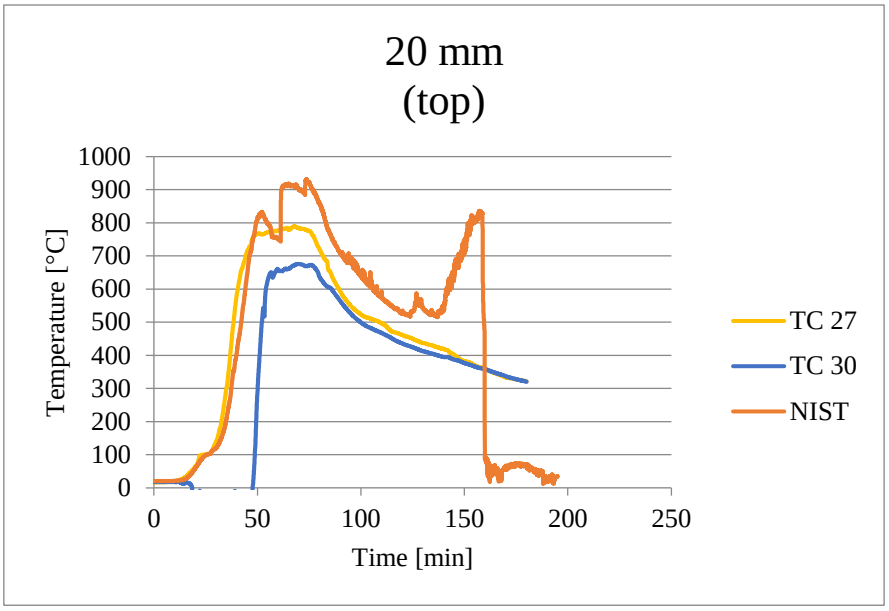

fig. D-57. All thermocouple temperatures at the depth 20 mm drilled from the top, for the PRF-1 specimen.

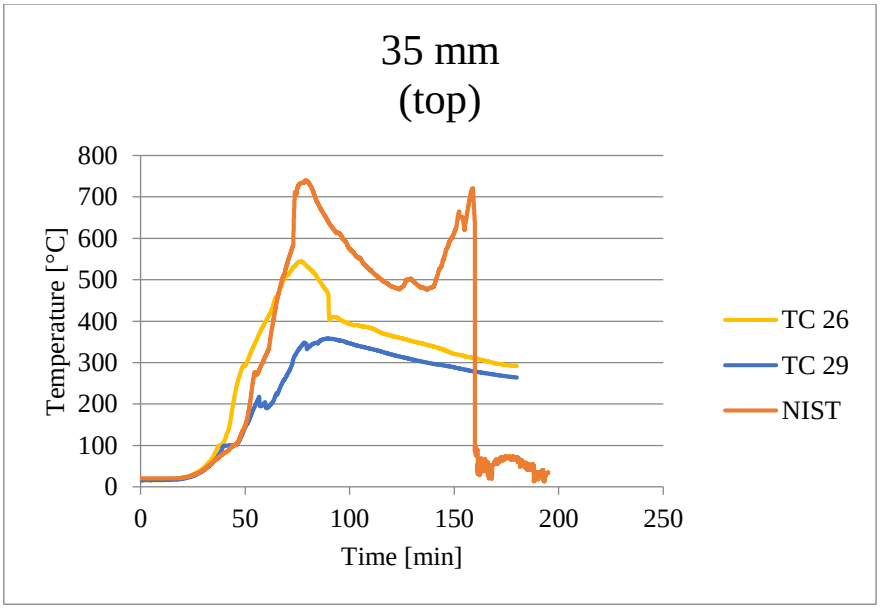

fig. D-58. All thermocouple temperatures at the depth 35 mm (bondline) drilled from the top, for the PRF-1 specimen.

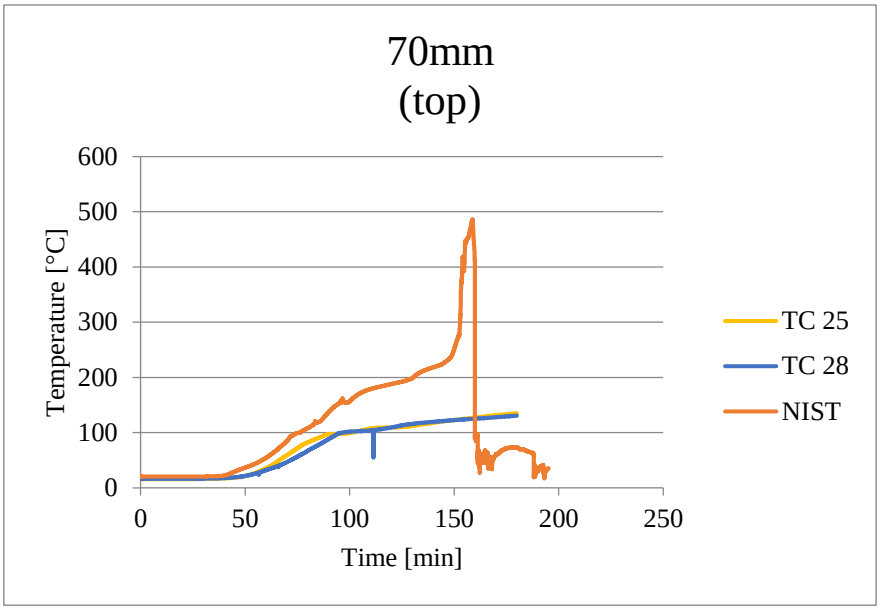

fig. D-59. All thermocouple temperatures at the depth 70 mm (bondline) drilled from the top, for the PRF-1 specimen.

PRF-2

Thermocouples 29 and 30 were malfunctioning during the PRF-2 test, and was noted during the test.

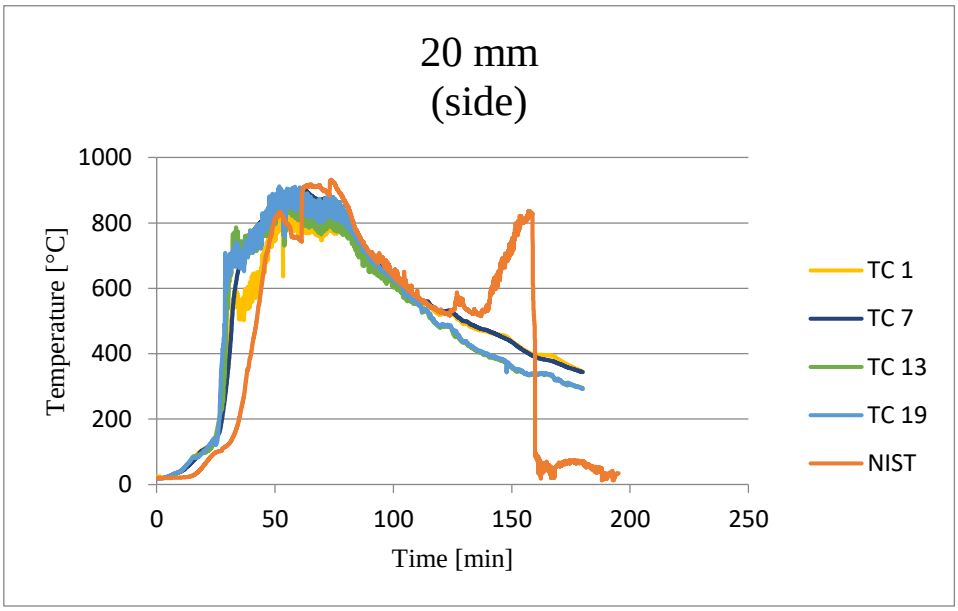

fig. D-60. All thermocouple temperatures at the depth 20 mm, for the PRF-2 specimen.

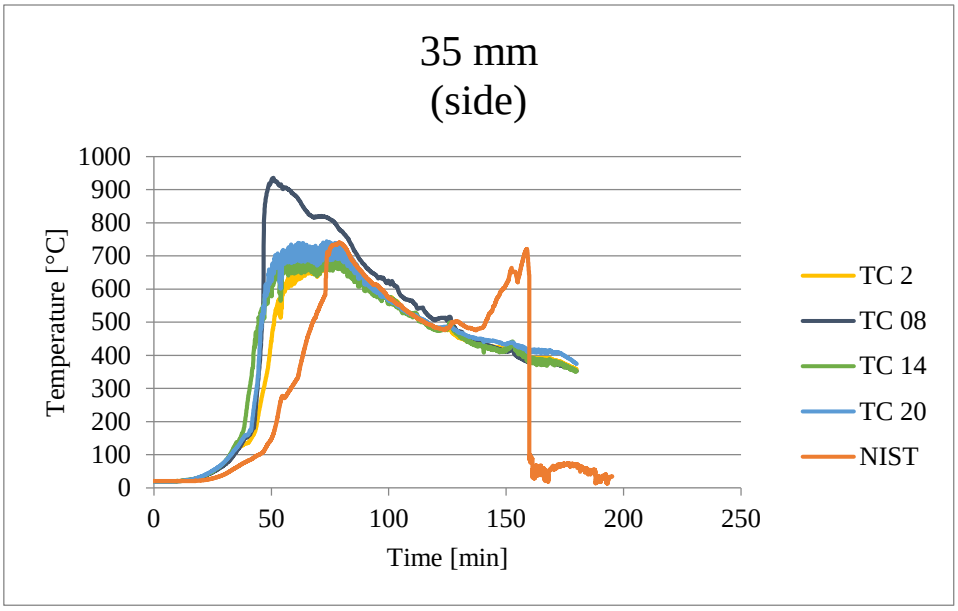

fig. D-61. All thermocouple temperatures at the depth 35 mm (bondline), for the PRF-2 specimen.

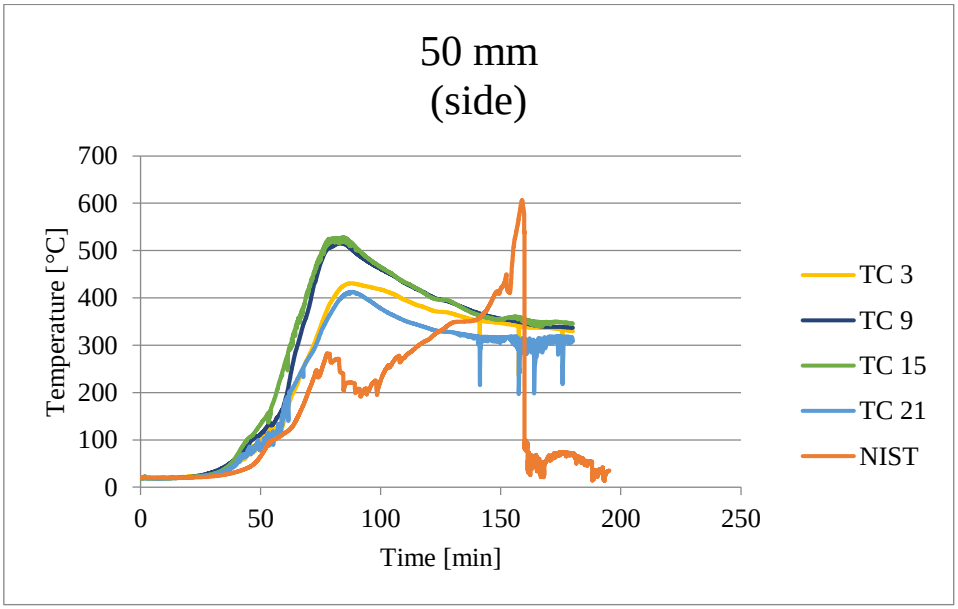

fig. D-62. All thermocouple temperatures at the depth 50 mm, for the PRF-2 specimen.

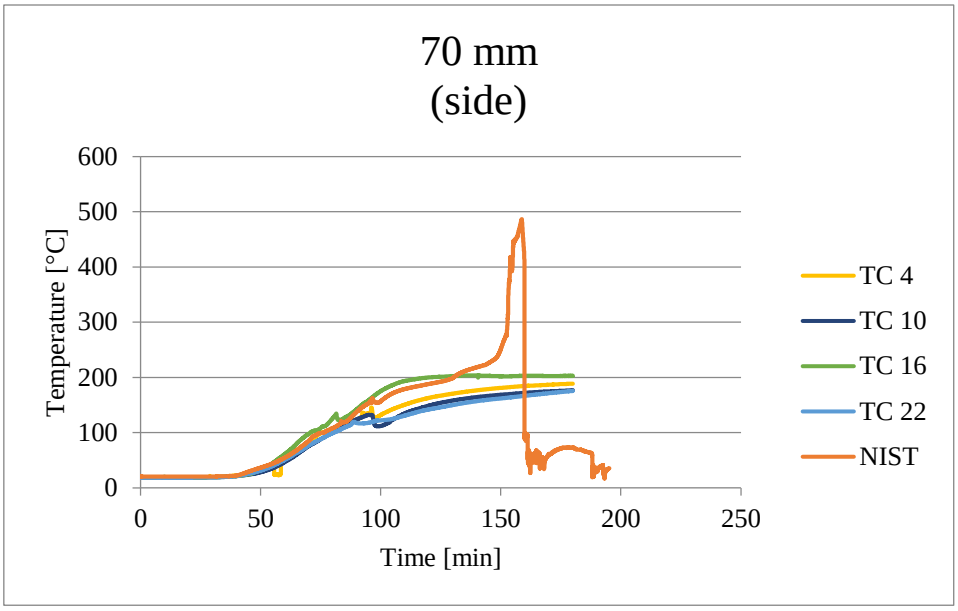

fig. D-63. All thermocouple temperatures at the depth 70 mm (bondline), for the PRF-2 specimen.

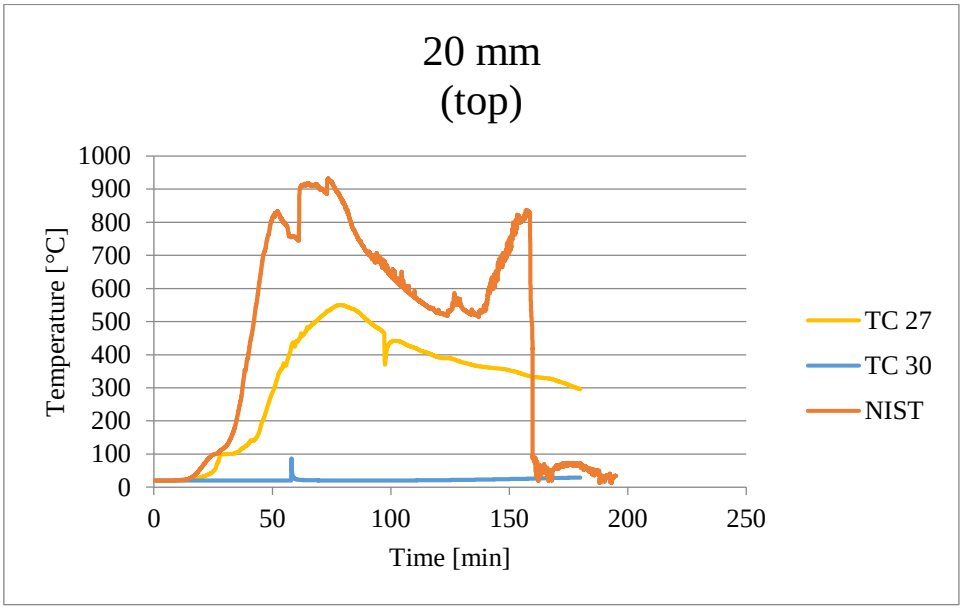

fig. D-64. All thermocouple temperatures at the depth 20 mm drilled from the top, for the PRF-2 specimen.

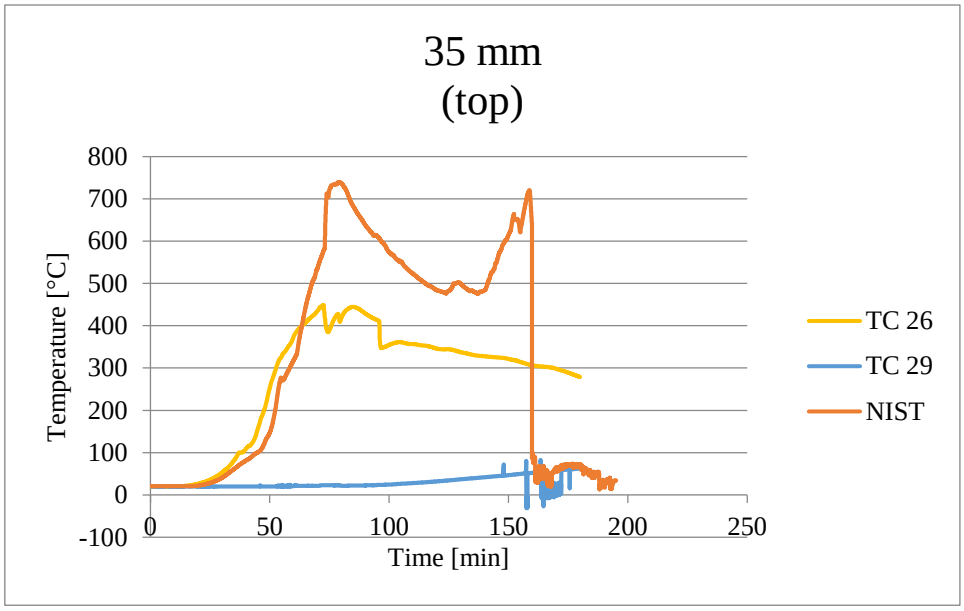

fig. D-65. All thermocouple temperatures at the depth 35 mm (bondline) drilled from the top, for the PRF-2 specimen.

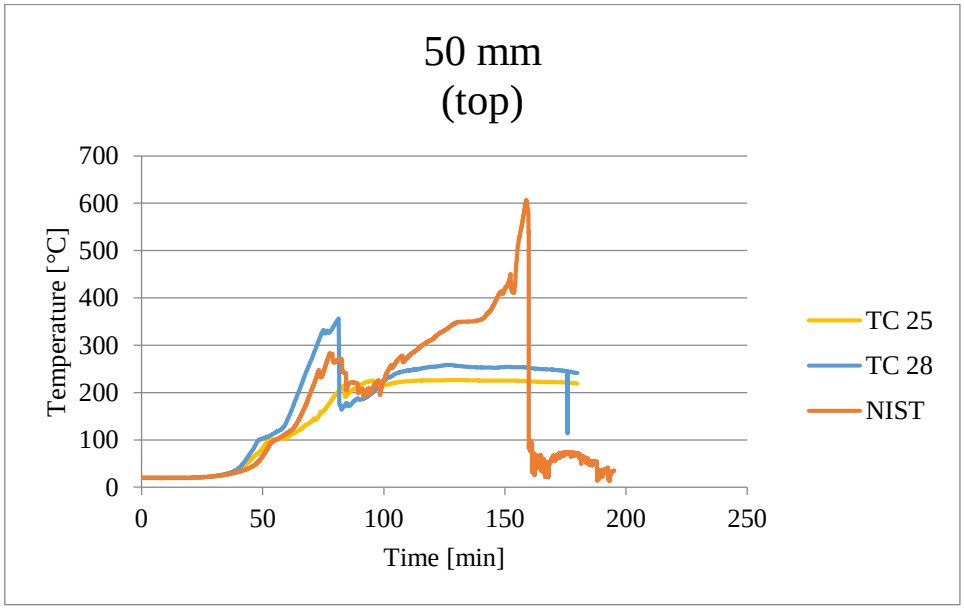

fig. D-66. All thermocouple temperatures at the depth 50 mm drilled from the top, for the PRF-2 specimen.

EPI-1

During the EPI-1 test, thermocouple 13 and 30 was registered as malfunctioning after approximately 100 minutes into the test.

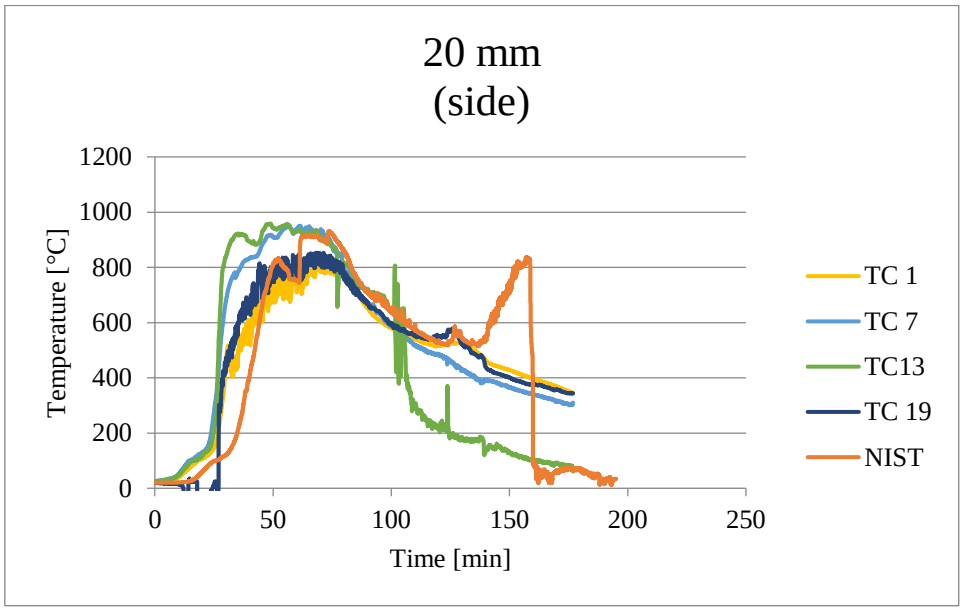

fig. D-67. All thermocouple temperatures at the depth 20 mm, for the EPI-1 specimen.

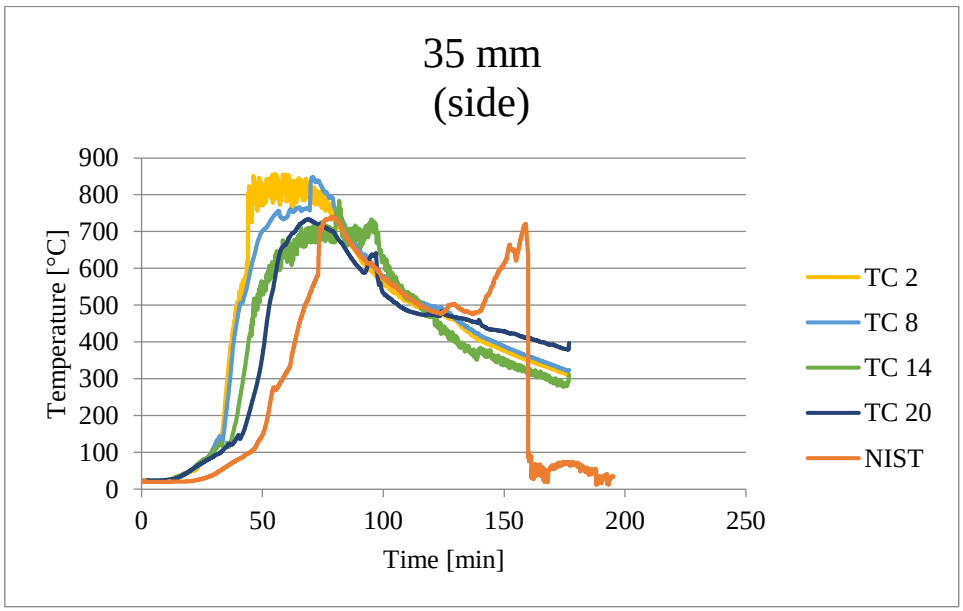

fig. 68. All thermocouple temperatures at the depth 35 mm (bondline), for the EPI-1 specimen.

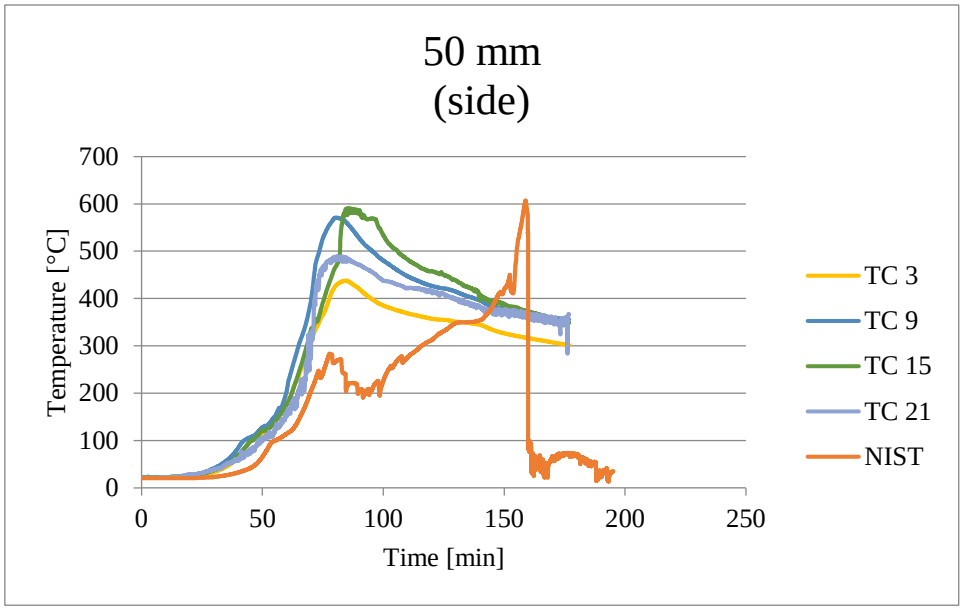

fig. D-69. All thermocouple temperatures at the depth 50 mm, for the EPI-1 specimen.

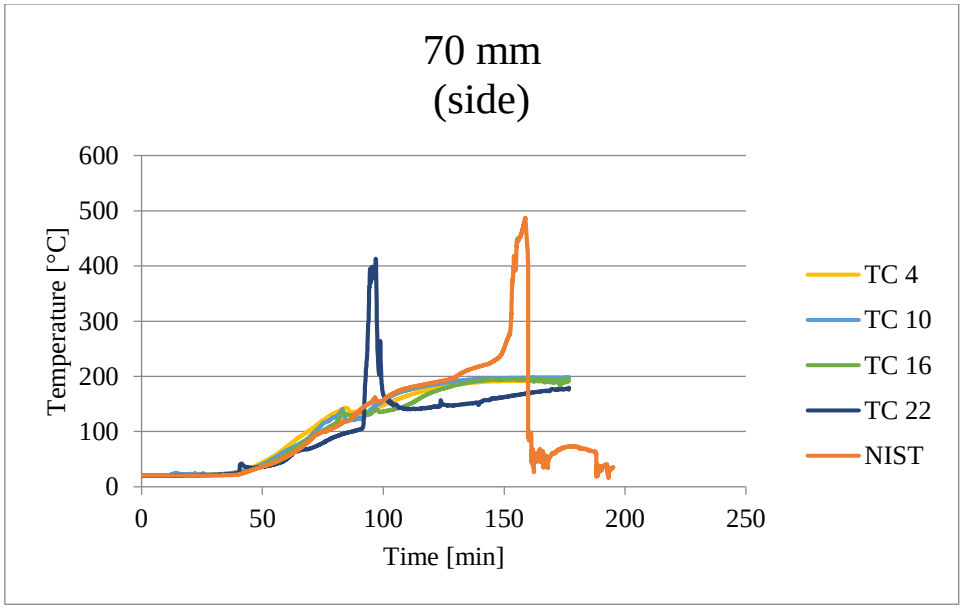

fig. D-70. All thermocouple temperatures at the depth 70 mm (bondline), for the EPI-1 specimen.

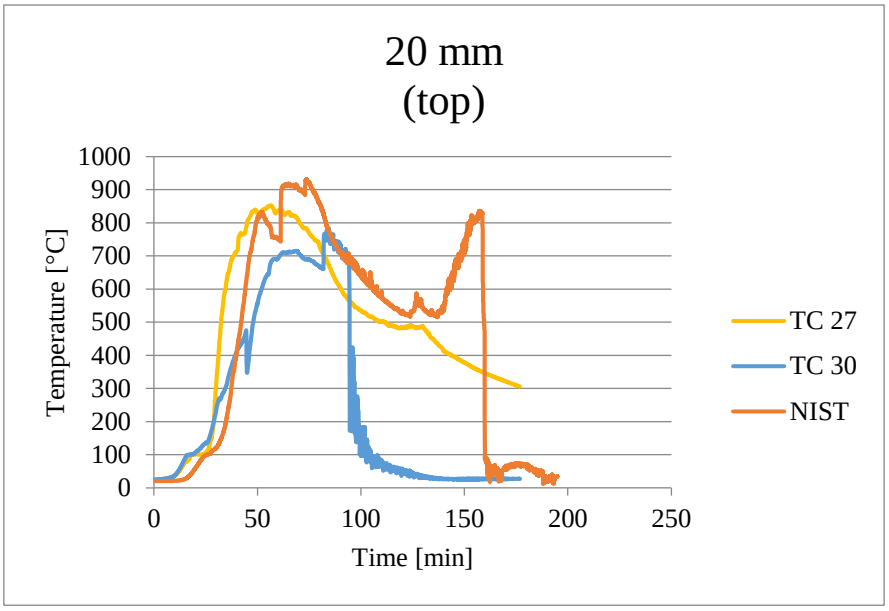

fig. D-71. All thermocouple temperatures at the depth 20 mm drilled from the top, for the EPI-1 specimen.

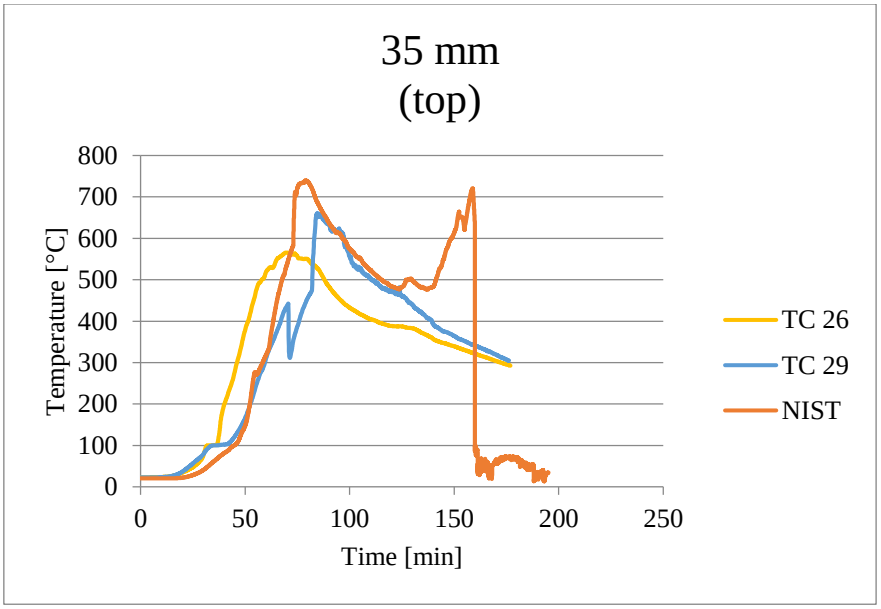

fig. D-72. All thermocouple temperatures at the depth 35 mm (bondline) drilled from the top, for the EPI-1 specimen.

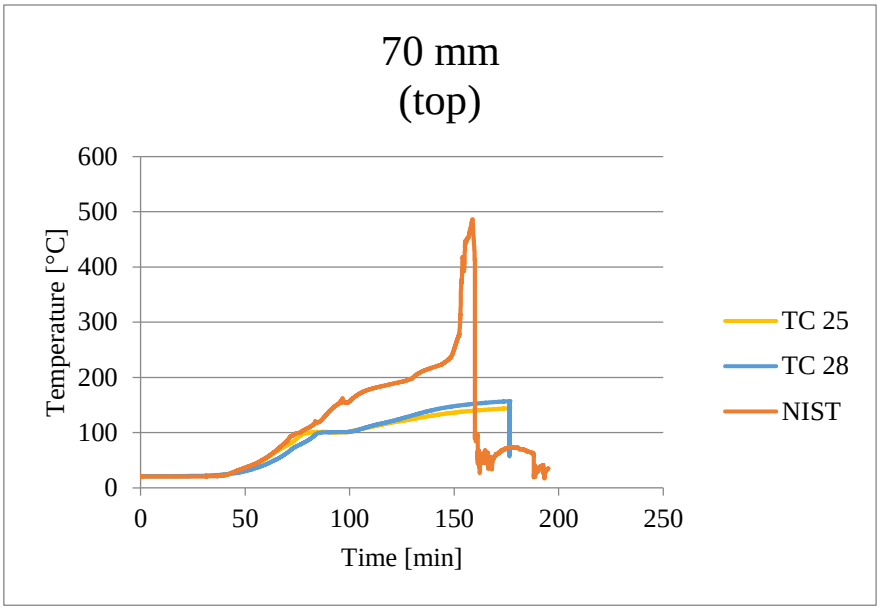

fig. D-73. All thermocouple temperatures at the depth 70 mm (bondline) drilled from the top, for the EPI-1 specimen.

EPI-2

For the EPI-2 test, TC 13 was malfunctioning in the initial phase, but was fixed after approximately 54 minutes into the test.

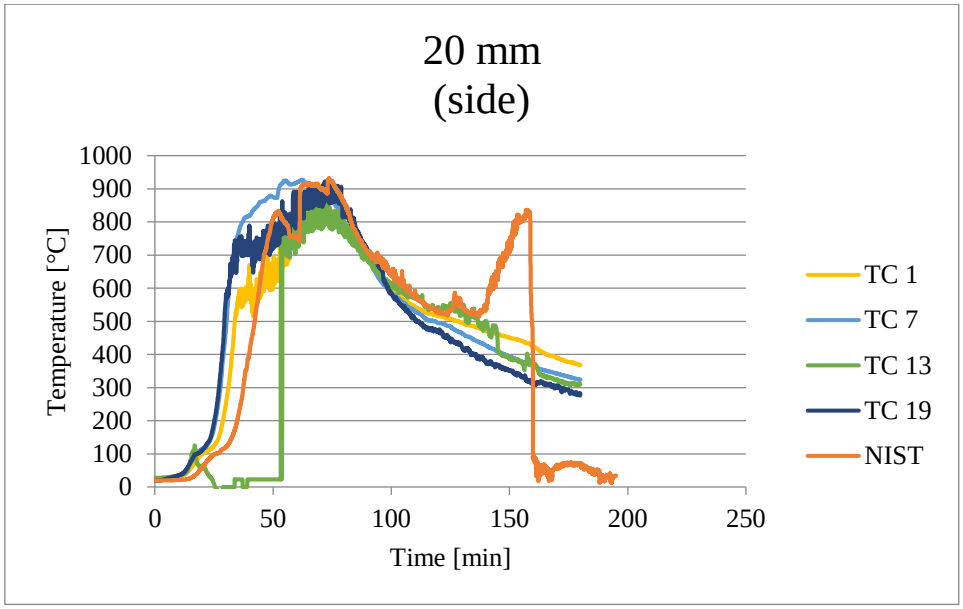

fig. D-74. All thermocouple temperatures at the depth 20 mm, for the EPI-2 specimen.

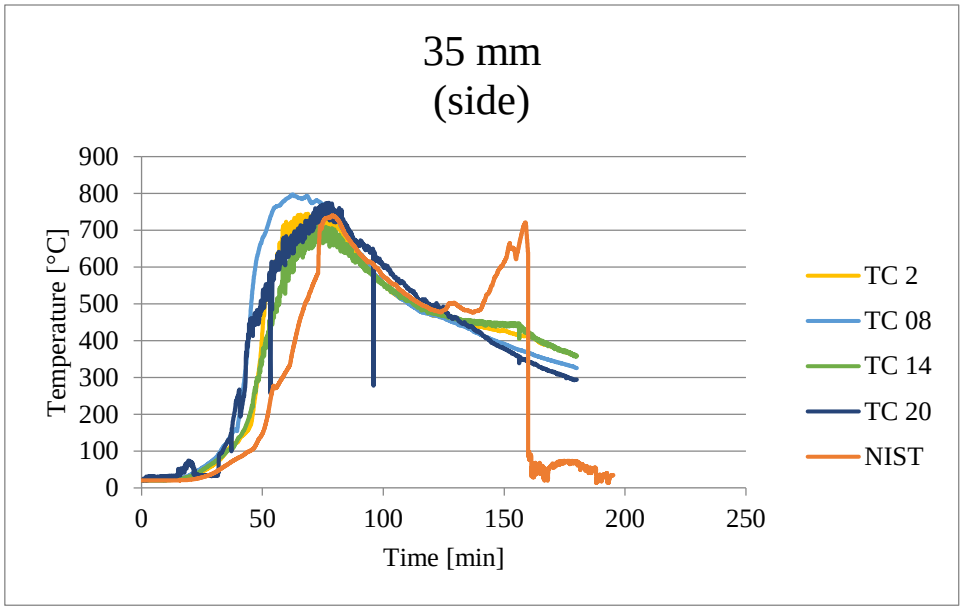

fig. D-75. All thermocouple temperatures at the depth 35 mm (bondline), for the EPI-2 specimen.

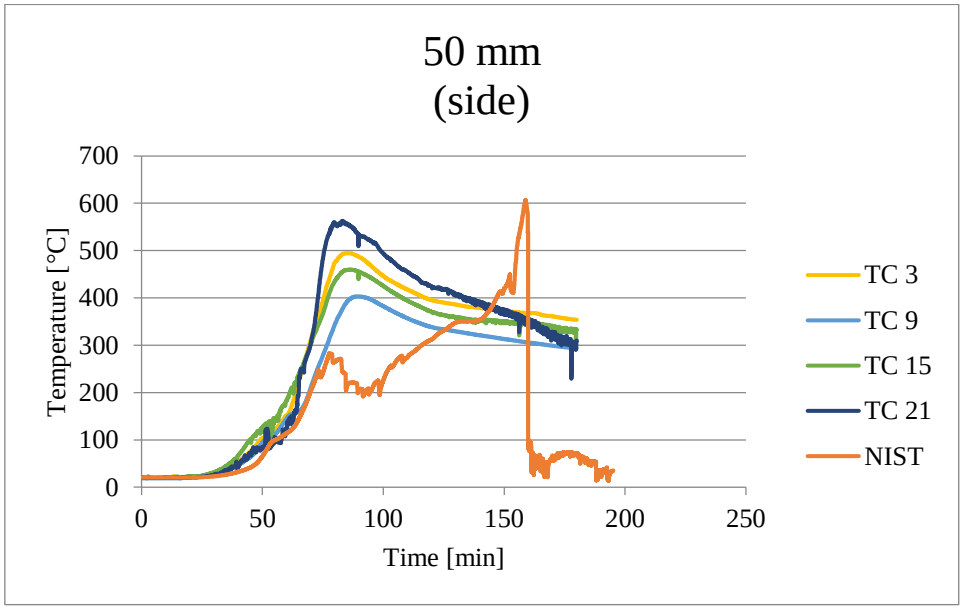

fig. D-76. All thermocouple temperatures at the depth 50 mm, for the EPI-2 specimen.

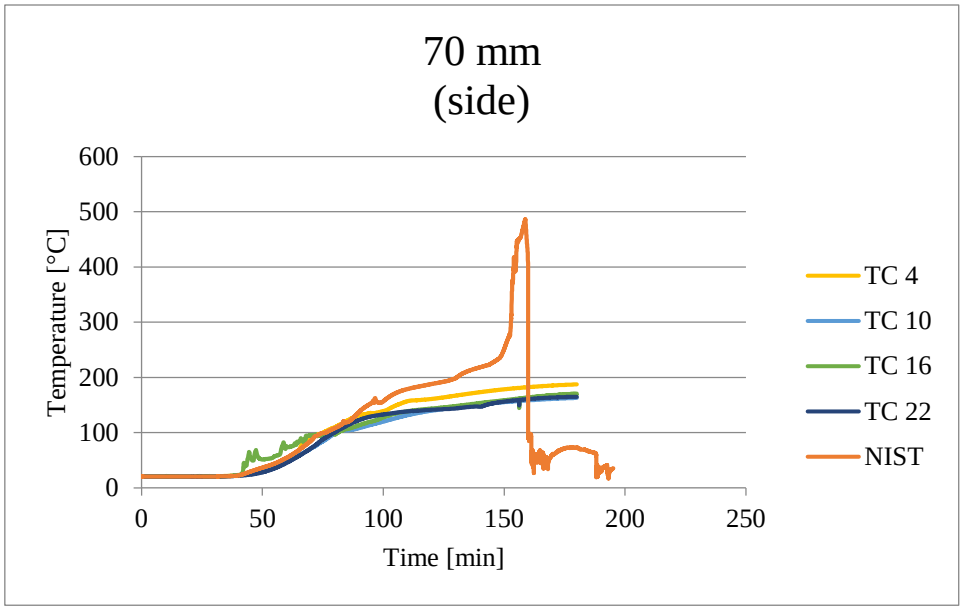

fig. D-77. All thermocouple temperatures at the depth 70 mm (bondline), for the EPI-2 specimen.

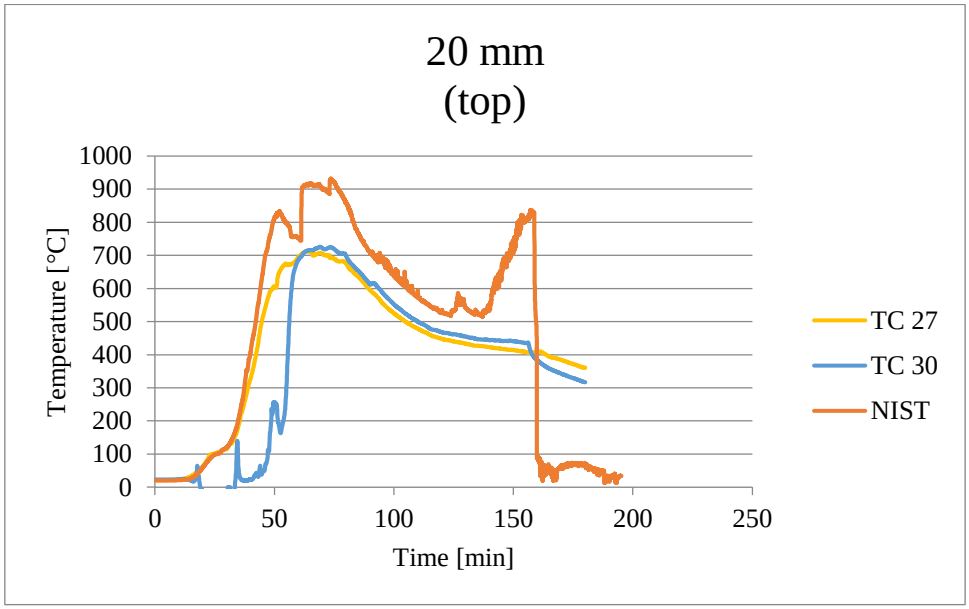

fig. D-78. All thermocouple temperatures at the depth 20 mm drilled from the top, for the EPI-2 specimen.

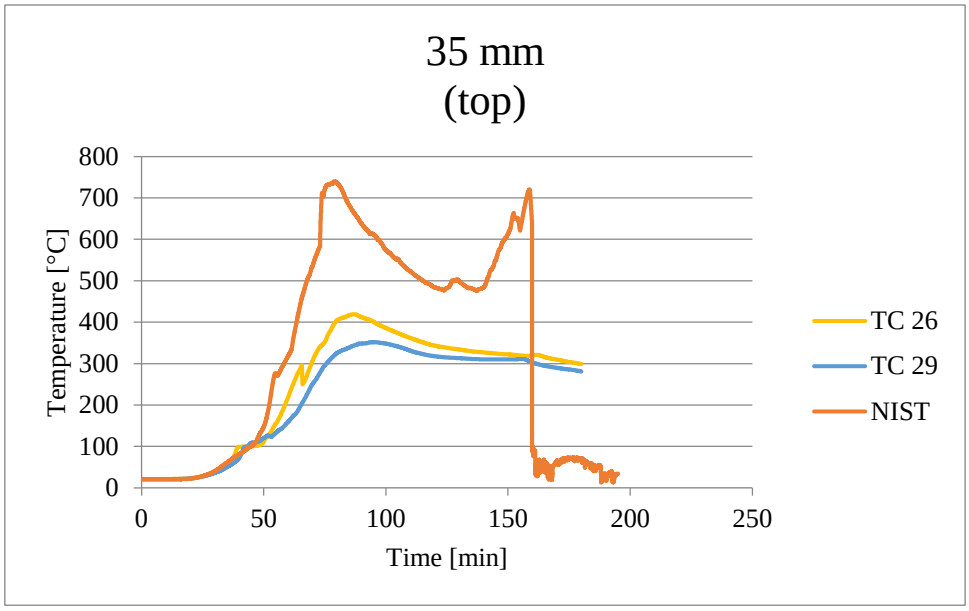

fig. D-79. All thermocouple temperatures at the depth 35 mm (bondline) drilled from the top, for the EPI-2 specimen.

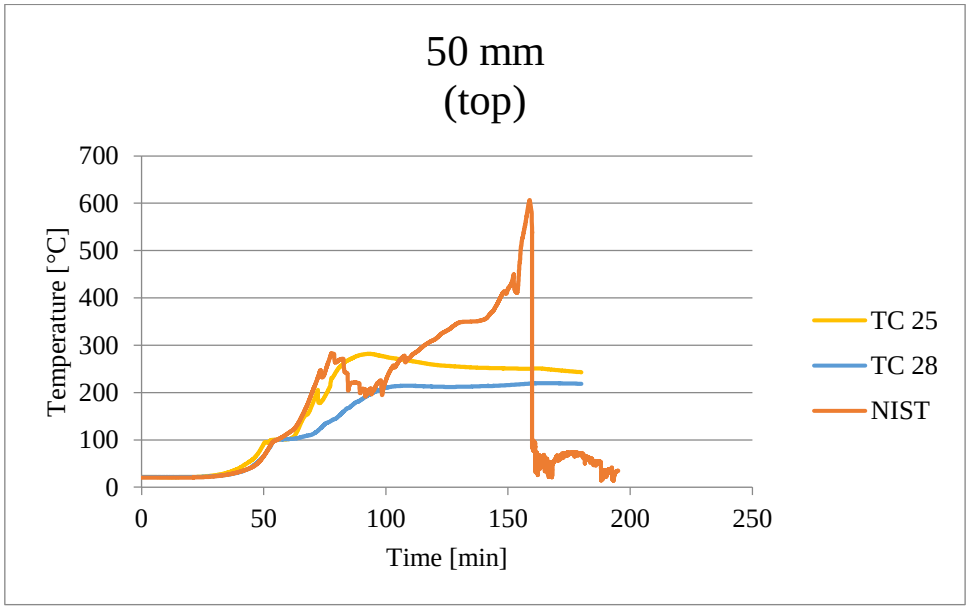

fig. D-80. All thermocouple temperatures at the depth 50 mm drilled from the top, for the EPI-2 specimen.

MF-1

For the MF-1 test, thermocouple 3 and 4 was registered as malfunctioning.

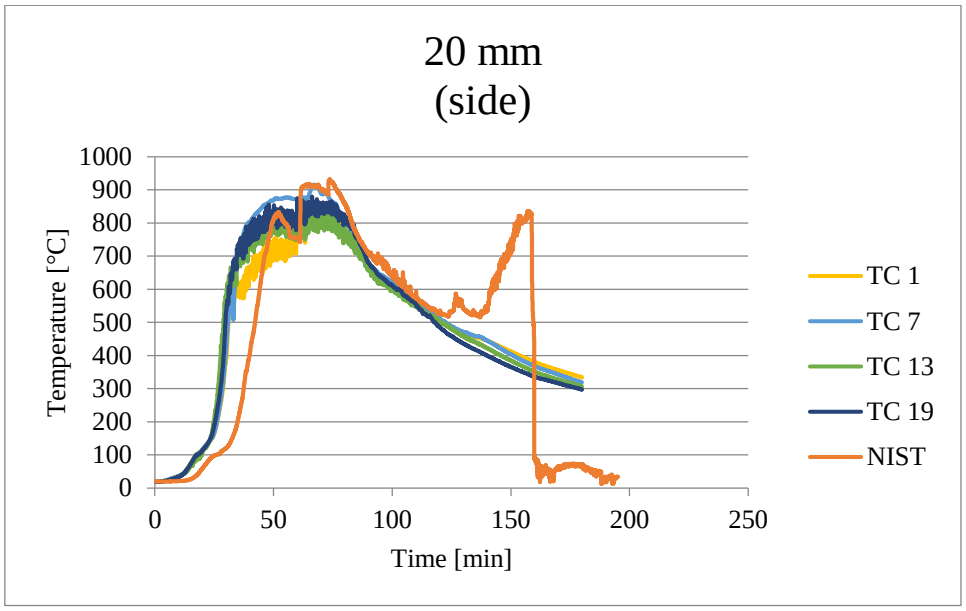

fig. D-81. All thermocouple temperatures at the depth 20 mm, for the MF-1 specimen.

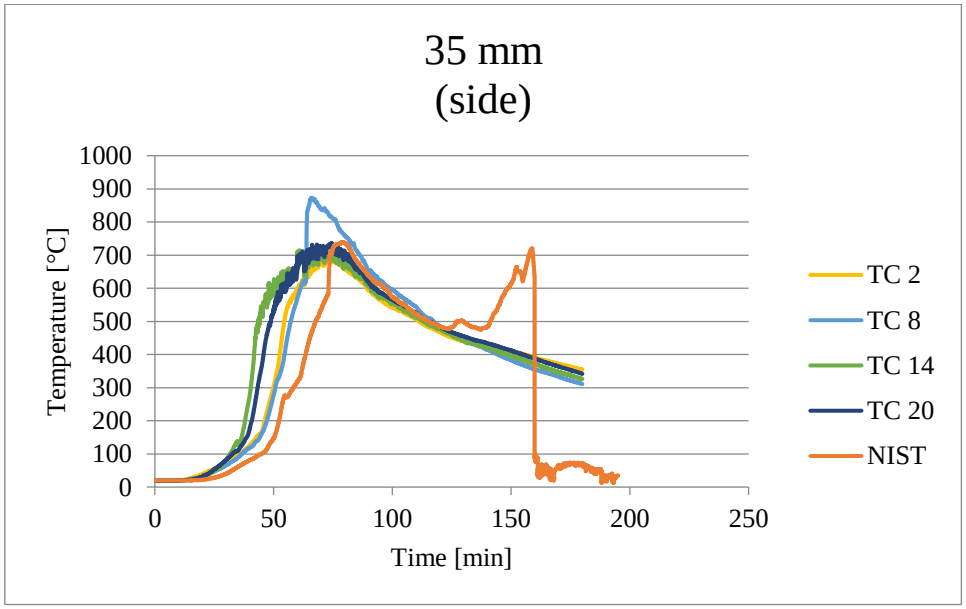

fig. D-82. All thermocouple temperatures at the depth 35 mm (bondline), for the MF-1 specimen.

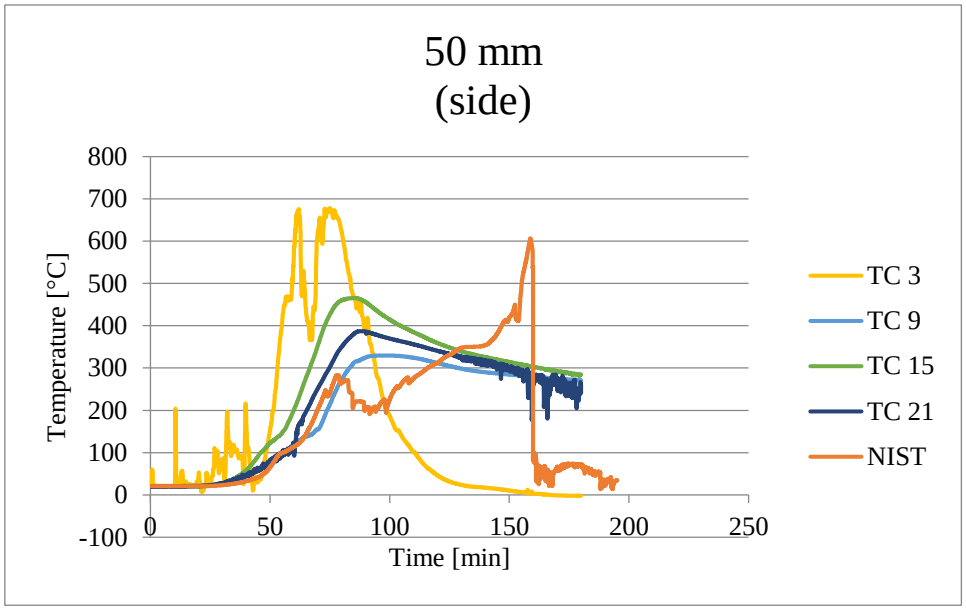

fig. D-83. All thermocouple temperatures at the depth 50 mm, for the MF-1 specimen.

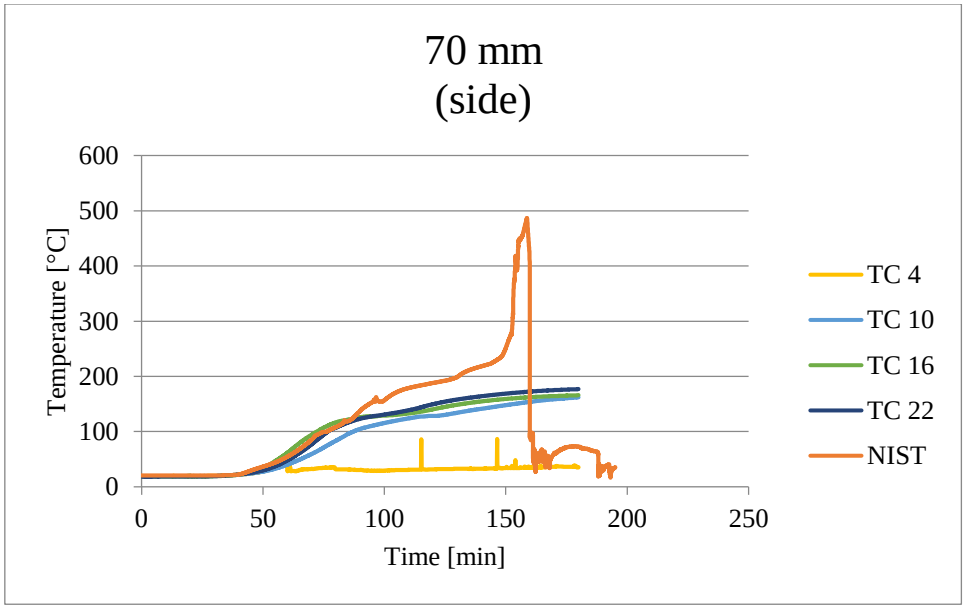

fig. D-84. All thermocouple temperatures at the depth 70 mm (bondline), for the MF-1 specimen.

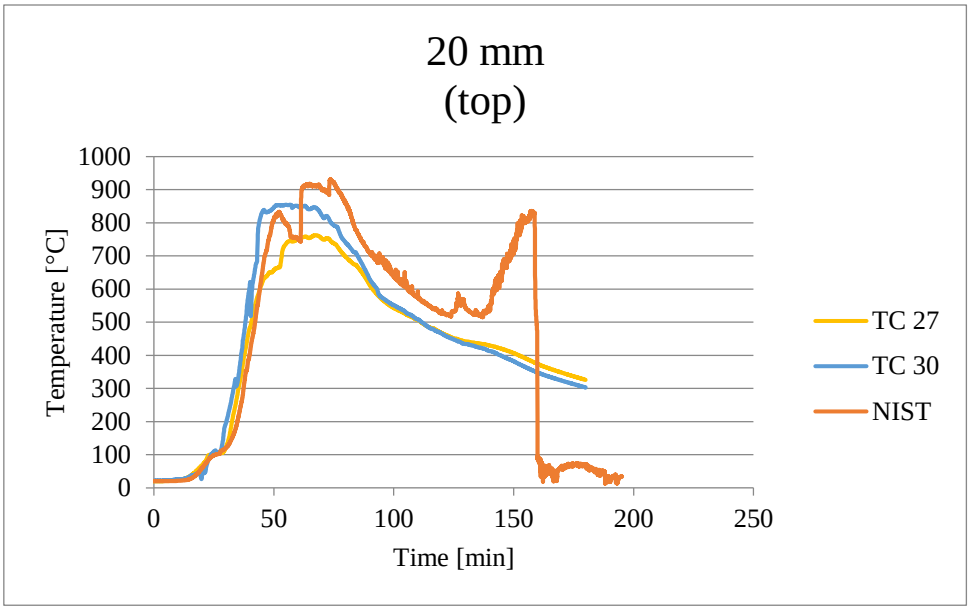

fig.D-62. All thermocouple temperatures at the depth 20 mm drilled from the top, for the MF-1 specimen.

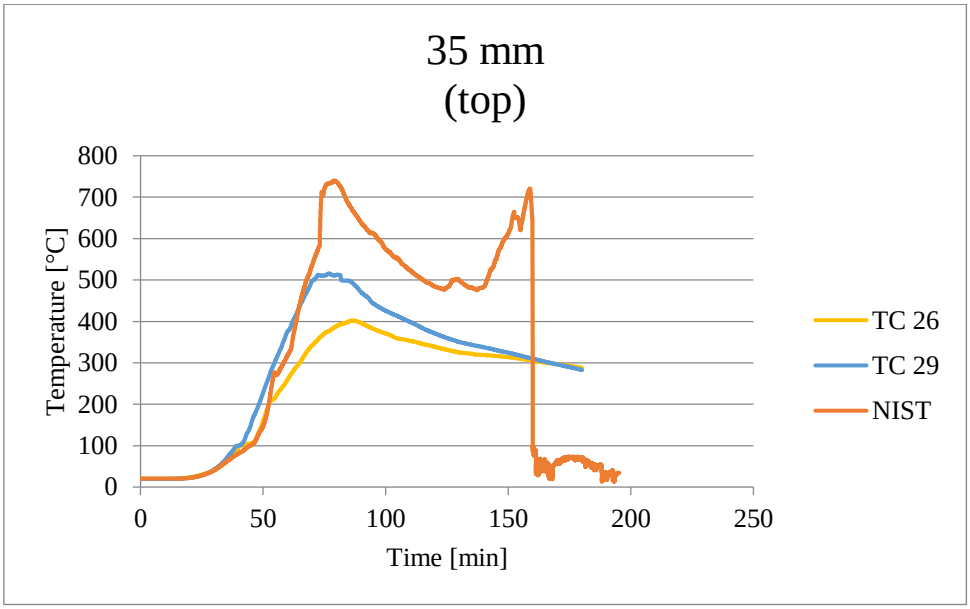

fig.D-63. All thermocouple temperatures at the depth 35 mm (bondline) drilled from the top, for the MF-1 specimen.

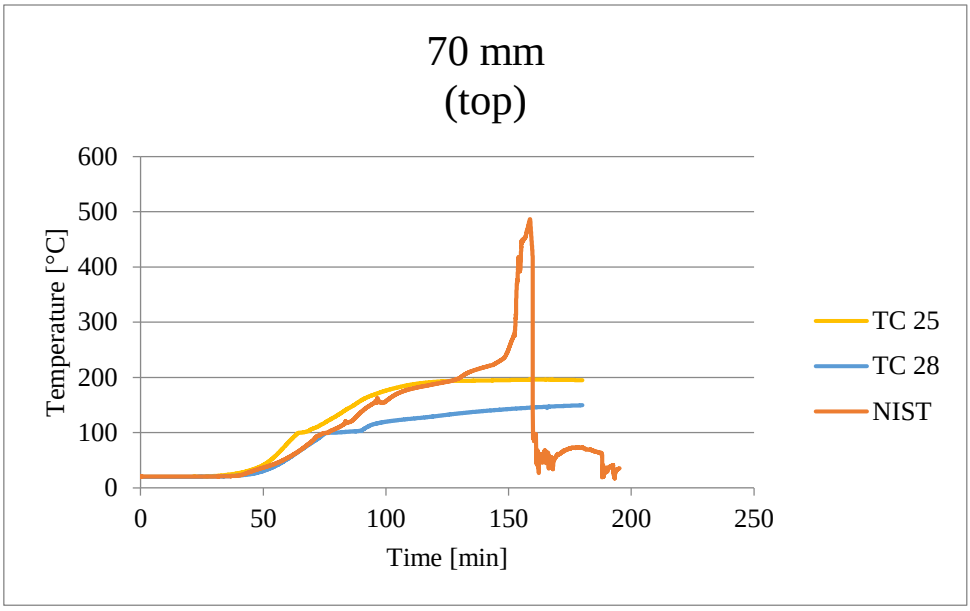

fig.D-64. All thermocouple temperatures at the depth 70 mm drilled from the top, for the MF-1 specimen.

MF-2

During the MF-2 test, thermocouple 27 was registered as completely non-responsive.

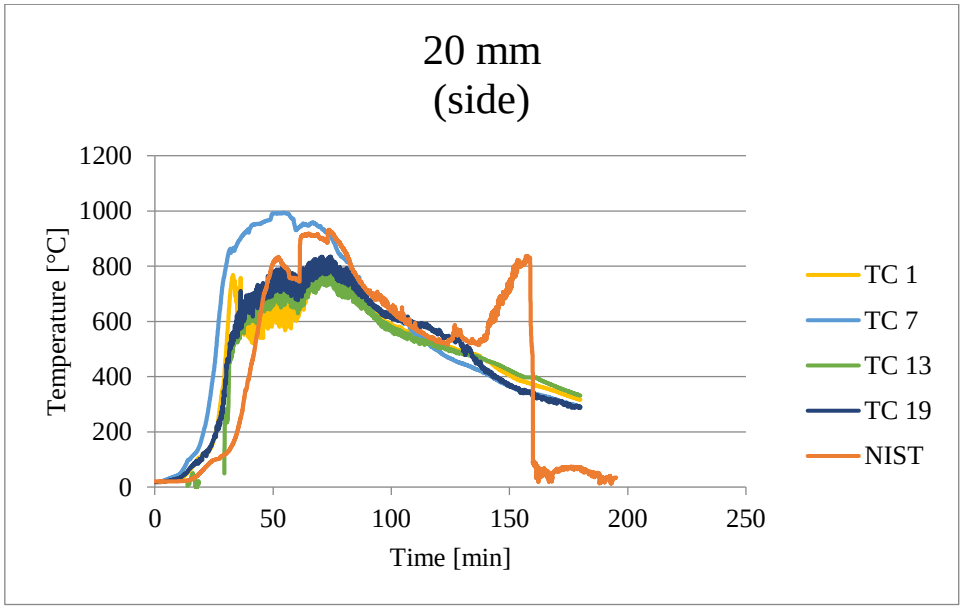

fig. D-65. All thermocouple temperatures at the depth 20 mm, for the MF-2 specimen.

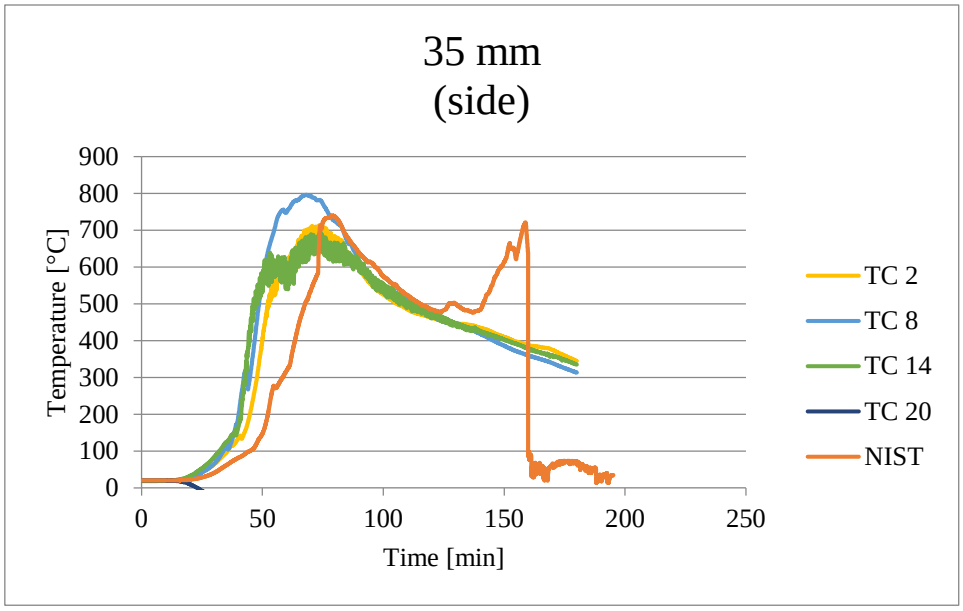

fig. D-66. All thermocouple temperatures at the depth 35 mm (bondline), for the MF-2 specimen.

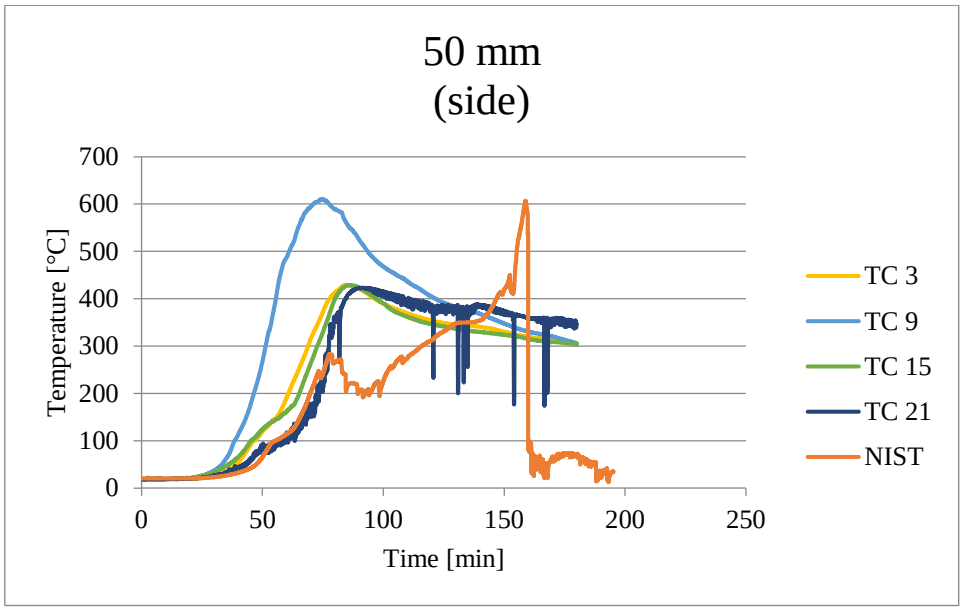

fig. D-67. All thermocouple temperatures at the depth 50 mm, for the MF-2 specimen.

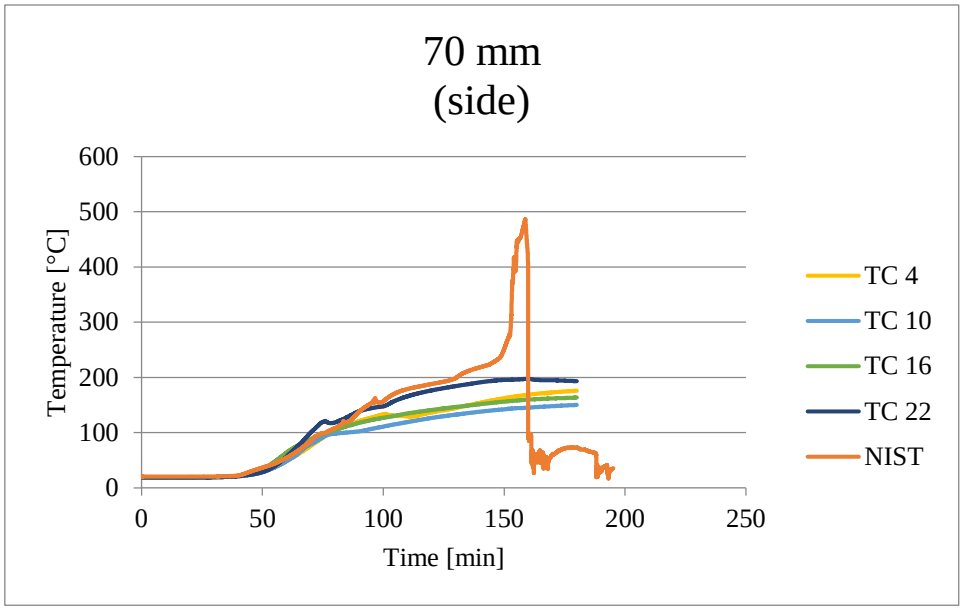

fig. D-68. All thermocouple temperatures at the depth 70 mm (bondline), for the MF-2 specimen.

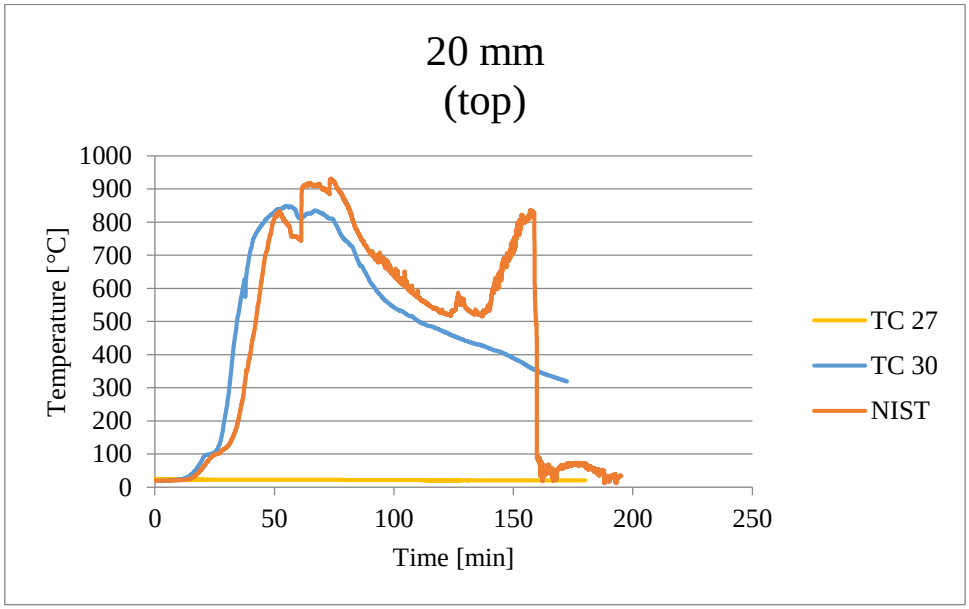

fig. D-69. All thermocouple temperatures at the depth 20 mm drilled from the top, for the MF-2 specimen.

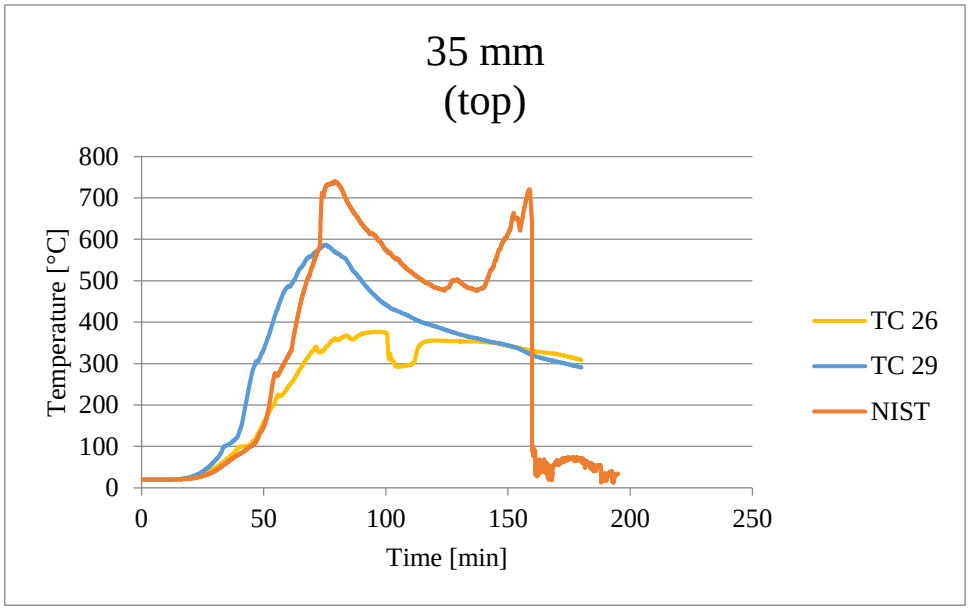

fig. D-70. All thermocouple temperatures at the depth 35 mm (bondline) drilled from the top, for the MF-2 specimen.

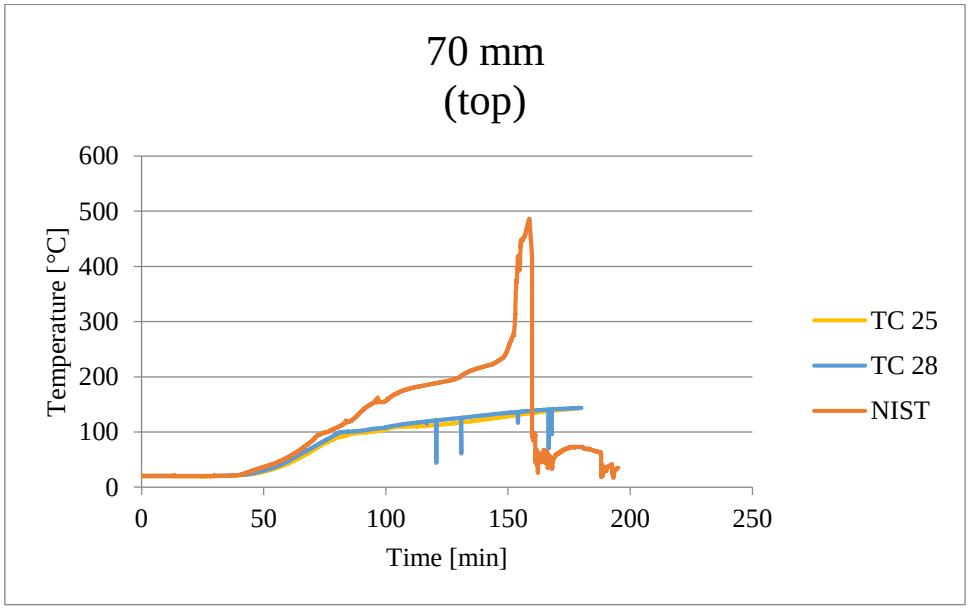

fig. D-71. All thermocouple temperatures at the depth 70 mm (bondline) drilled from the top, for the MF-2 specimen.

Appendix E – Charring rates

In this Appendix, the calculated average charring rates over time for all the specimen are presented, together with tabulated values and average charring depth over time.

PUR-A1

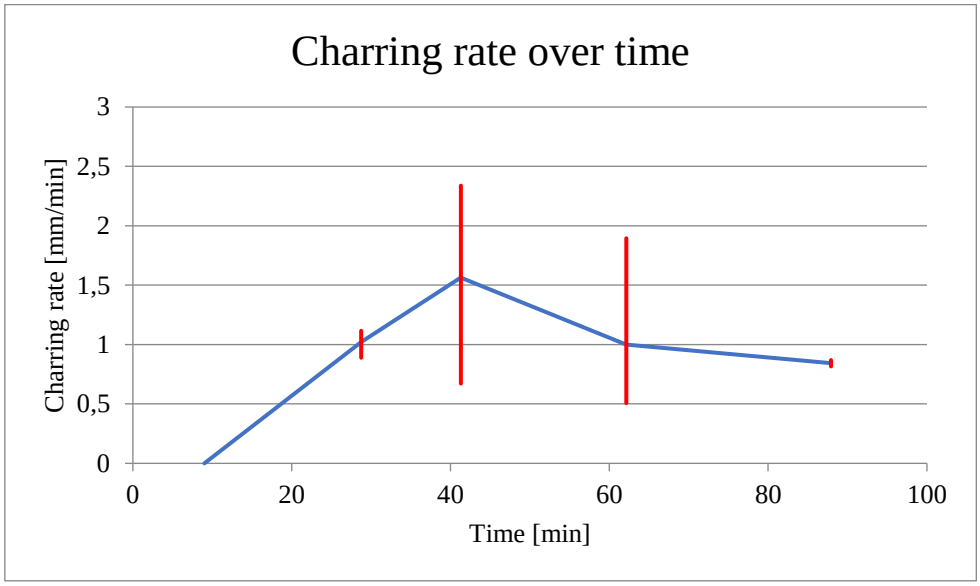

fig. E-1. Individual average charring rate over time for the PUR-A1 specimen. min and max intervals of each calculated average are marked in red.

Table E-1. Calculated mean, min and max values for the charring rate of PUR A1, for each measuring series.

Charring rate [mm/min]				
TC Group	**Minimum**	**Mean**	**Maximum**	**Std. Dev.**
1	0.67	1.21	1.89	0.51
2	0.51	1.03	1.68	0.48
3	0.60	1.17	2.34	0.76
4	-	-	-	-
Overall:		1.14		

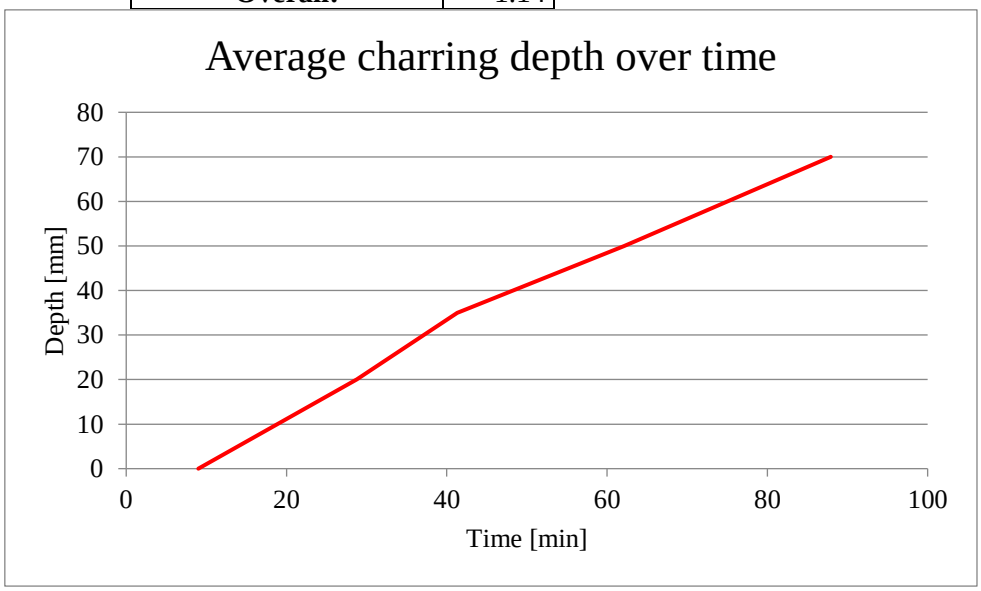

fig. E-2. Average charring depth over time for the PUR-A1 specimen.

PUR-A2

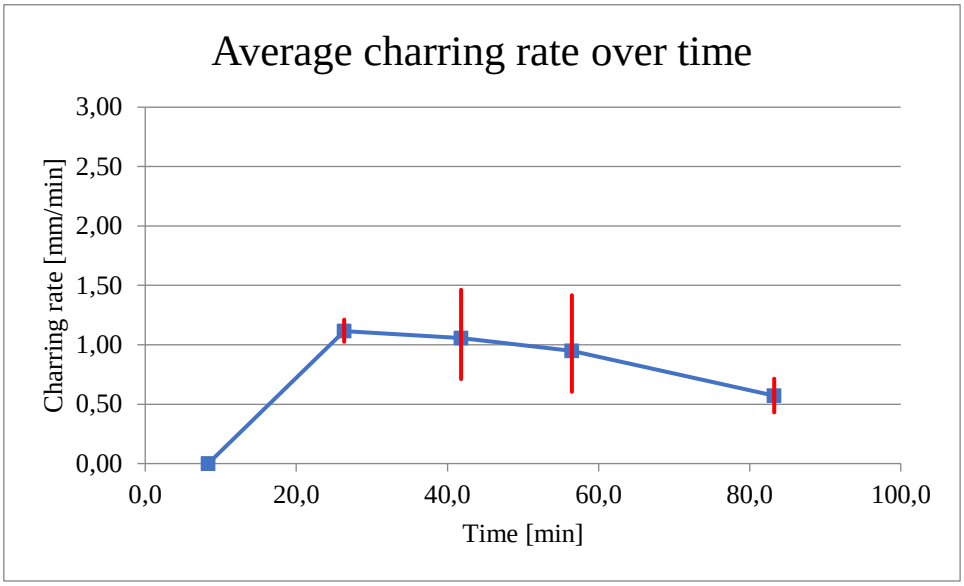

fig. E-3. Individual average charring rate over time for the PUR-A2 specimen. min and max intervals of each calculated average are marked in red.

Table E-2. Calculated mean, min and max values for the charring rate of PUR A2, for each measuring series.

Charring rate [mm/min]				
TC Group	**Minimum**	**Mean**	**Maximum**	**Std. Dev.**
1	0.71	0.89	1.21	0.23
2	0.71	0.96	1.11	0.15
3	0.60	1.03	1.46	0.35
4	0.43	0.99	1.42	0.41
Overall:		0.97		

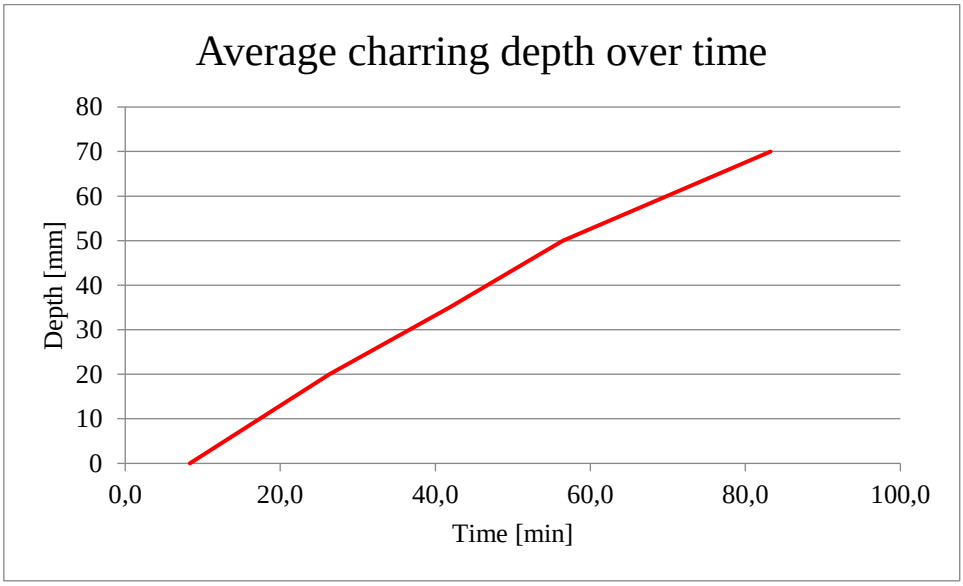

fig. E-4. Average charring depth over time for the PUR-A2 specimen.

PUR-B1

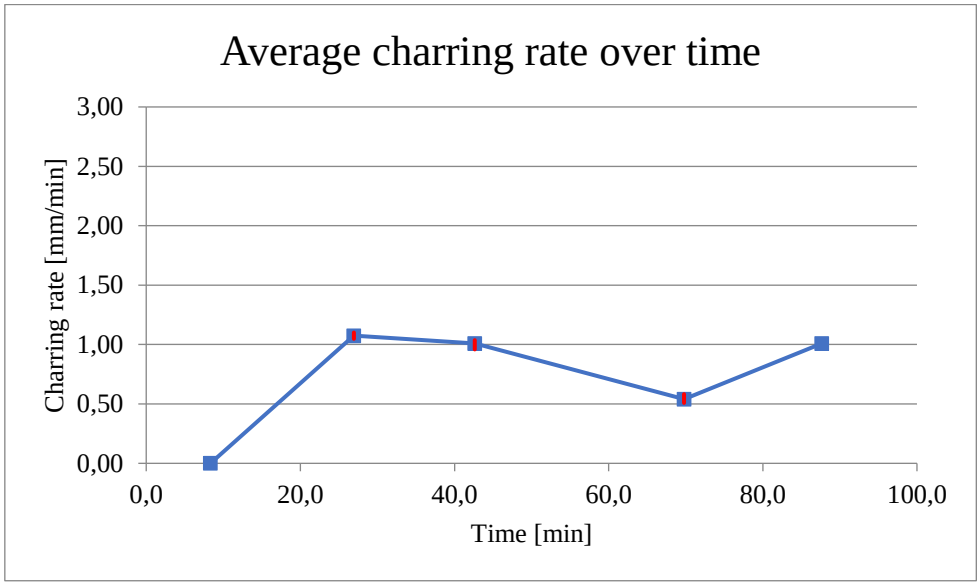

fig. E-5. Individual average charring rate over time for the PUR-B1 specimen. min and max intervals of each calculated average are marked in red.

Table E-3. Calculated mean, min and max values for the charring rate of PUR-B1, for each measuring series

Charring rate [mm/min]				
TC Group	**Minimum**	**Mean**	**Maximum**	**Std. Dev.**
1	0.53	0.78	1.04	0.25
2	0.51	0.87	1.08	0.26
3	0.96	1.03	1.10	0.07
4	0.58	0.92	1.05	0.19
Overall:		0.90		

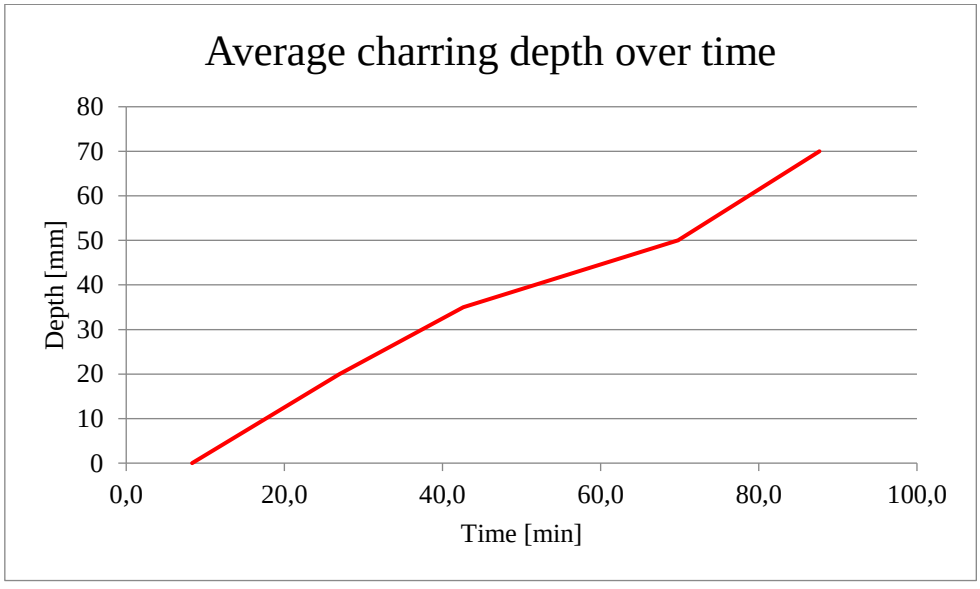

fig. E-6. Average charring depth over time for the PUR-B1 specimen.

PUR-B2

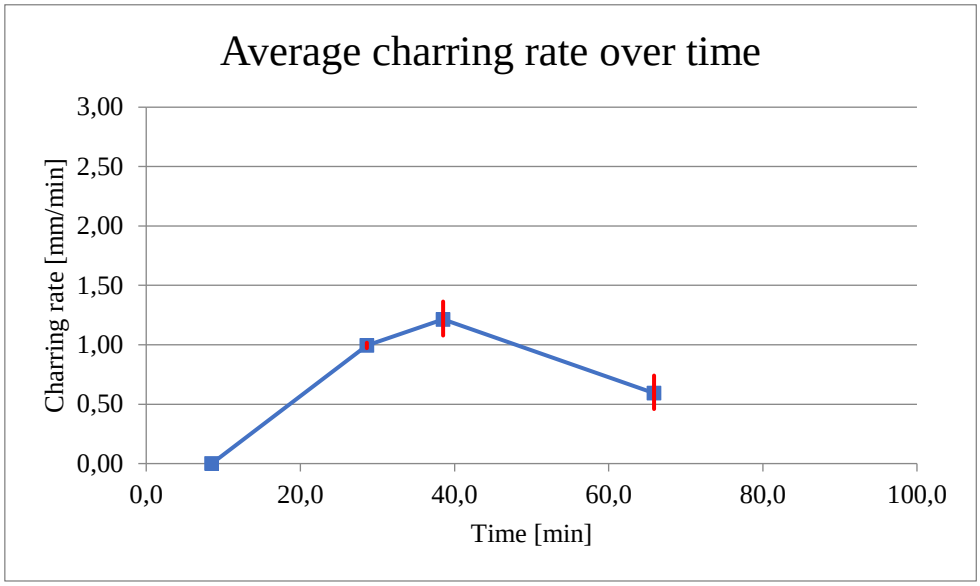

fig. E-7. Individual average charring rate over time for the PUR-B2 specimen. min and max intervals of each calculated average are marked in red.

Table E-4. Calculated mean, min and max values for the charring rate of PUR-B2, for each measuring series

Charring rate [mm/min]				
TC Group	**Minimum**	**Mean**	**Maximum**	**Std. Dev.**
1	-	1.32	-	-
2	0.74	1.05	1.36	0.31
3	0.46	0.85	1.08	0.28
4	0.58	0.88	1.10	0.22
Overall:		1.03		

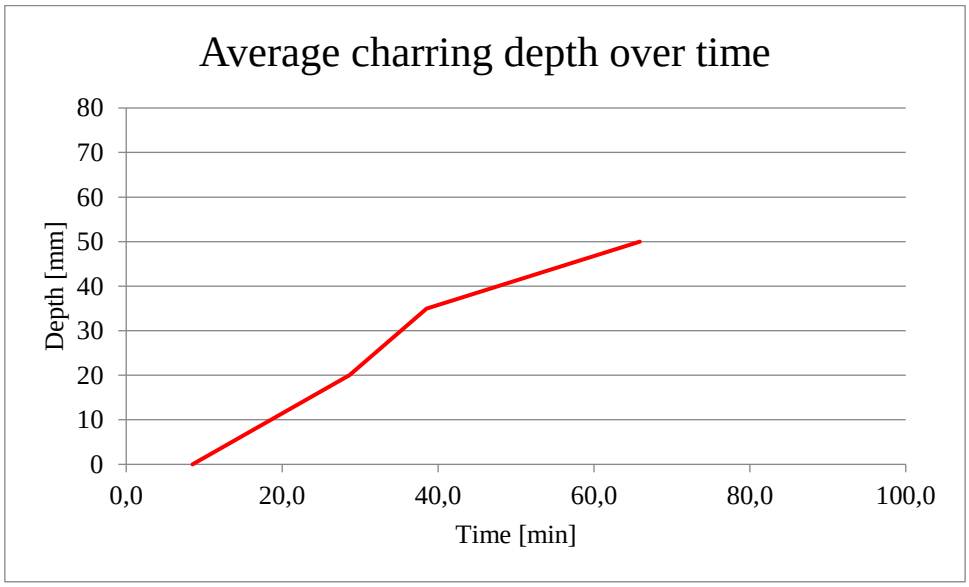

fig. E-8. Average charring depth over time for the PUR-B2 specimen.

PRF-1

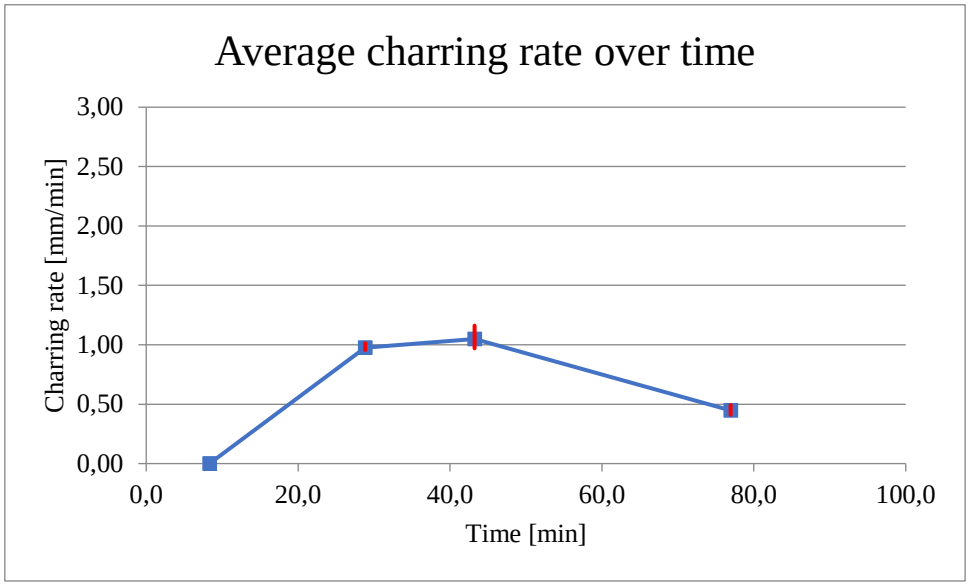

fig. E-9. Individual average charring rate over time for the PRF-1 specimen. min and max intervals of each calculated average are marked in red

Table E-5. Calculated mean, min and max values for the charring rate of PRF-1, for each measuring series.

Charring rate [mm/min]				
TC Group	**Minimum**	**Mean**	**Maximum**	**Std. Dev.**
1	0.41	0.84	1.16	0.32
2	0.49	0.83	1.02	0.24
3	0.47	0.72	0.97	0.25
4	0.41	0.82	1.04	0.29
Overall:		0.80		

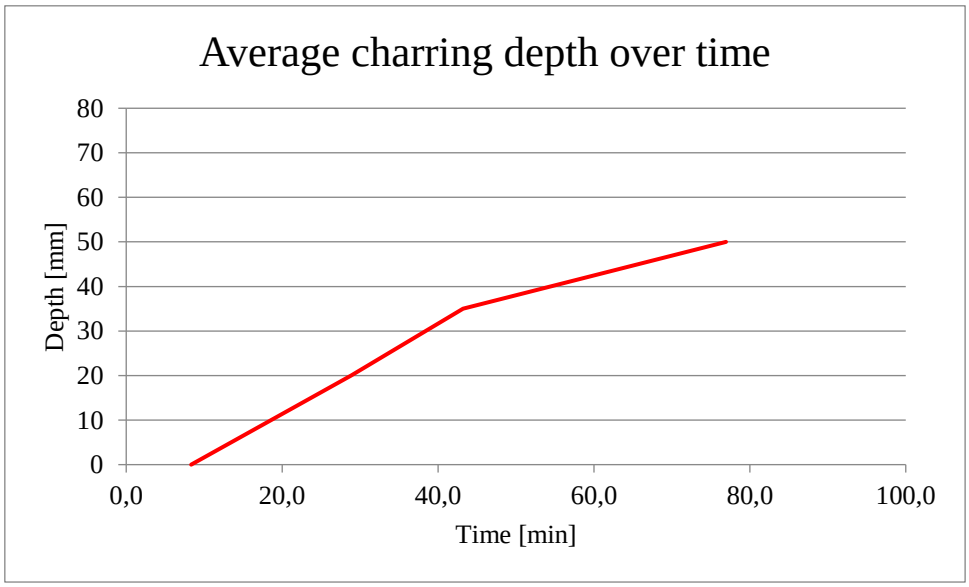

fig. E-10. Average charring depth over time for the PRF-1 specimen.

PRF-2

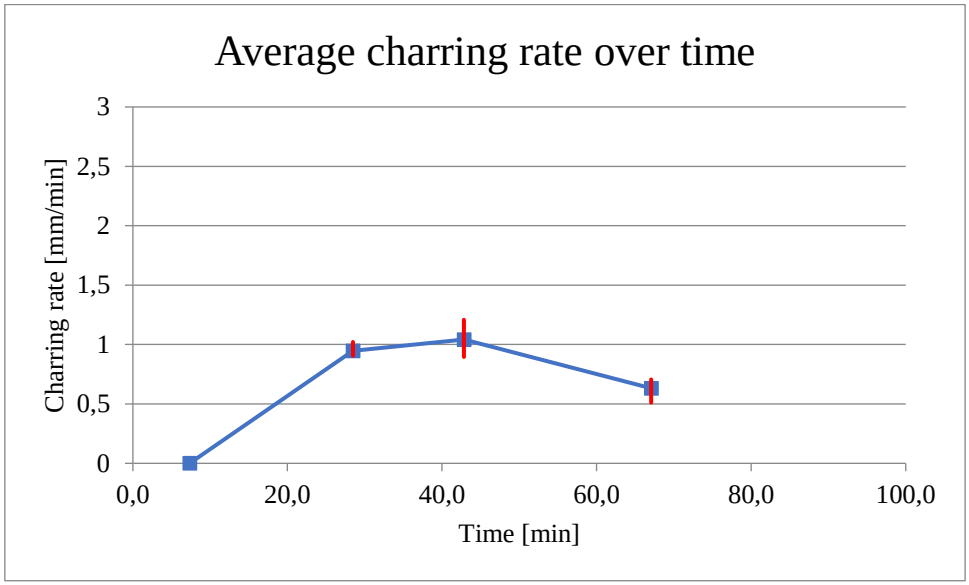

fig. E-11. Individual average charring rate over time for the PRF-2 specimen. min and max intervals of each calculated average are marked in red

Table E-6. Calculated mean, min and max values for the charring rate of PRF-2, for each measuring series.

Charring rate (MIN) [mm/min]				
TC Group	**Minimum**	**Mean**	**Maximum**	**Std. Dev.**
1	-	0.91	-	-
2	0.71	0.88	1.02	0.13
3	0.68	0.95	1.21	0.22
4	0.51	0.81	1.02	0.22
Overall:		0.89		

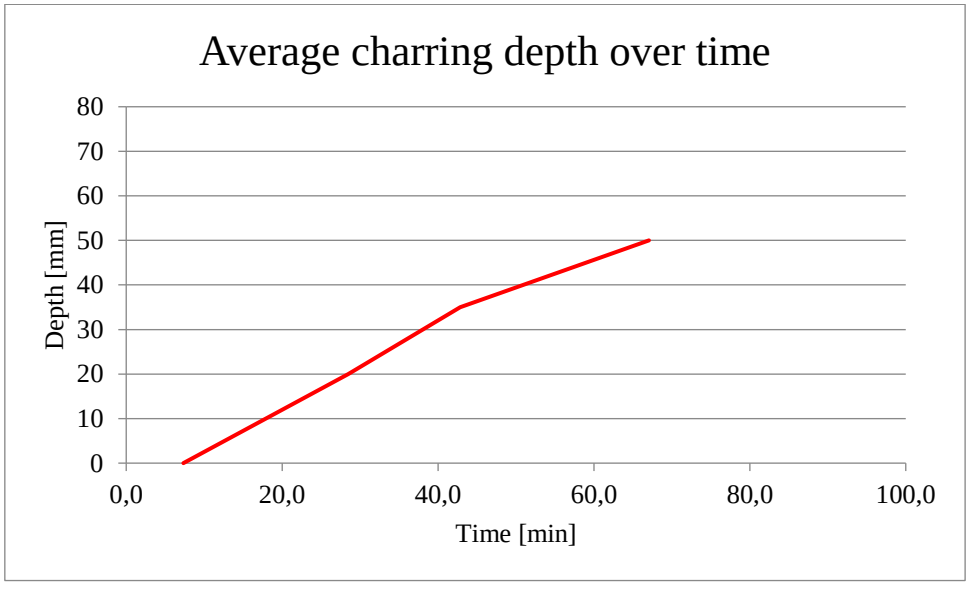

fig. E-12. Average charring depth over time for the PRF-2 specimen.

EPI-1

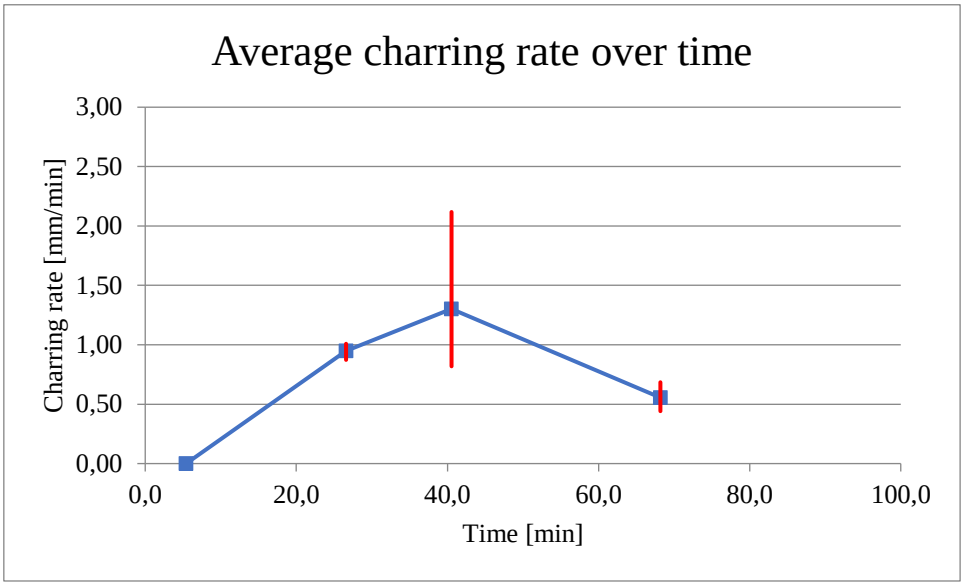

fig. E-13. Individual average charring rate over time for the EPI-1 specimen. min and max intervals of each calculated average are marked in red

Table E-7. Calculated mean, min and max values for the charring rate of EPI-1, for each measuring series.

Charring rate [mm/min]				
TC Group	**Minimum**	**Mean**	**Maximum**	**Std. Dev.**
1	0.44	1.14	2.12	0.71
2	0.53	0.95	1.32	0.33
3	0.57	0.83	0.96	0.18
4	0.68	0.75	0.82	0.07
Overall:		0.92		

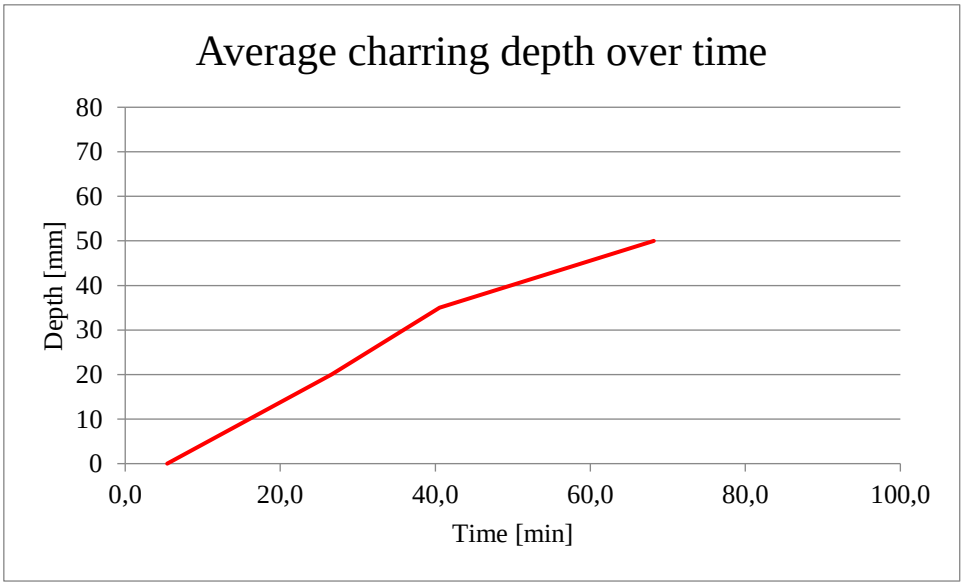

fig. E-14. Average charring depth over time for the EPI-1 specimen.

EPI-2

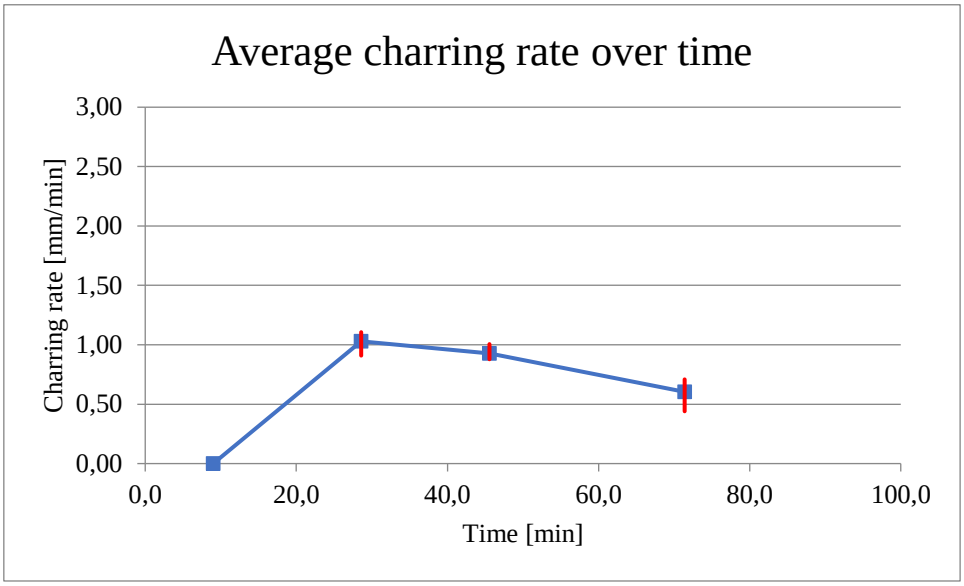

fig. E-15. Individual average charring rate over time for the EPI-2 specimen. min and max intervals of each calculated average are marked in red.

Table E-8. Calculated mean, min and max values for the charring rate of EPI-2, for each measuring series.

Charring rate (MIN) [mm/min]				
TC Group	**Minimum**	**Mean**	**Maximum**	**Std. Dev.**
1	0.71	0.83	0.91	0.09
2	0.44	0.84	1.07	0.28
3	0.71	0.80	0.88	0.09
4	0.56	0.87	1.11	0.23
Overall:		0.83		

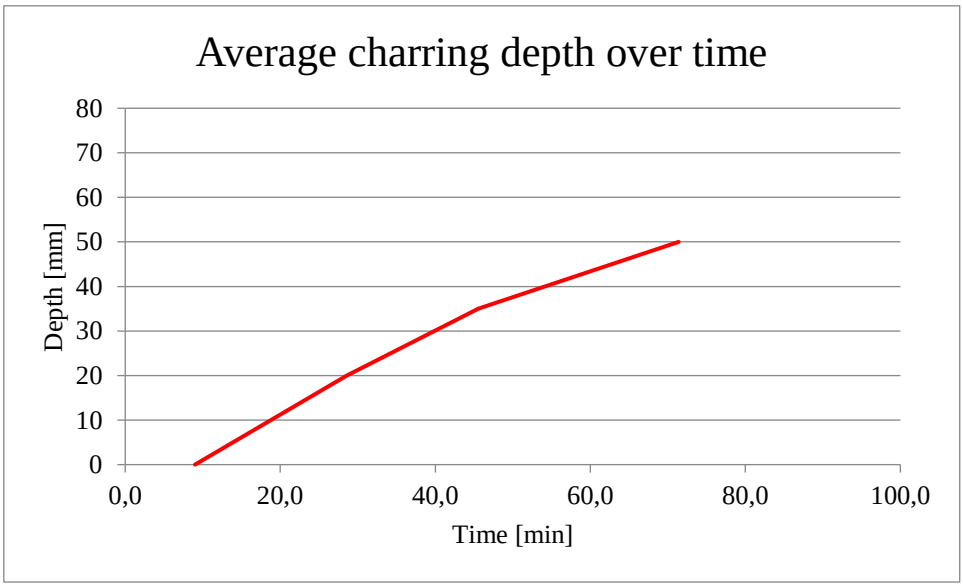

fig. E-16. Average charring depth over time for the EPI-2 specimen.

MF-1

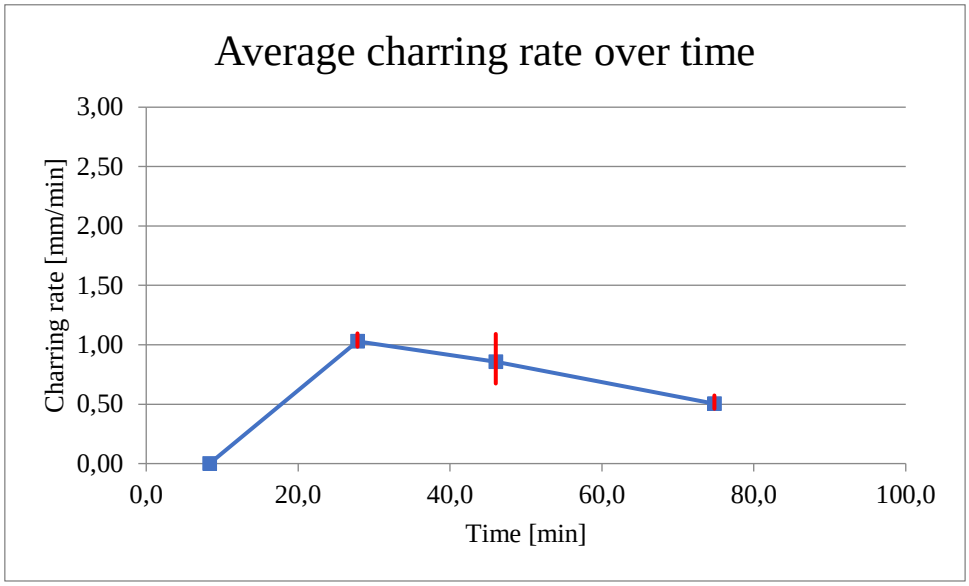

fig. E-17. Individual average charring rate over time for the MF-1 specimen. min and max intervals of each calculated average are marked in red.

Table E-9. Calculated mean, min and max values for the charring rate of MF-1, for each measuring series.

Charring rate [mm/min]				
TC Group	**Minimum**	**Mean**	**Maximum**	**Std. Dev.**
1	0.71	0.85	0.98	0.14
2	0.46	0.71	1.00	0.22
3	0.57	0.92	1.10	0.25
4	0.48	0.82	1.04	0.25
Overall:		0.83		

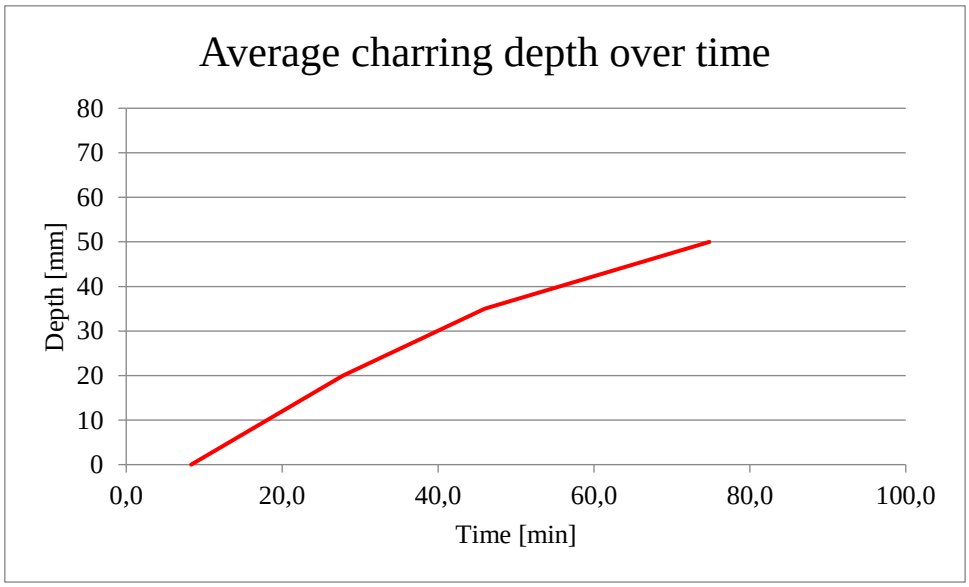

fig. E-18. Average charring depth over time for the MF-1 specimen.

MF-2

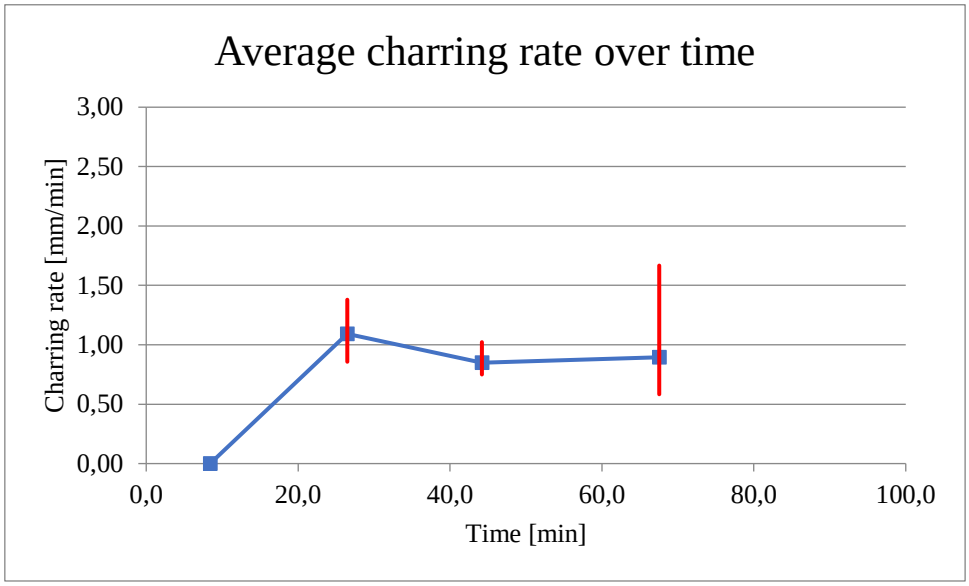

fig. E-19. Individual average charring rate over time for the MF-2 specimen. min and max intervals of each calculated average are marked in red

Table E-10. Calculated mean, min and max values for the charring rate of MF-2, for each measuring series.

Charring rate [mm/min]				
TC Group	**Minimum**	**Mean**	**Maximum**	**Std. Dev.**
1	0.71	0.83	1.04	0.15
2	0.78	1.27	1.67	0.37
3	0.58	0.80	1.02	0.22
4	0.62	0.74	0.86	0.12
Overall:		0.91		

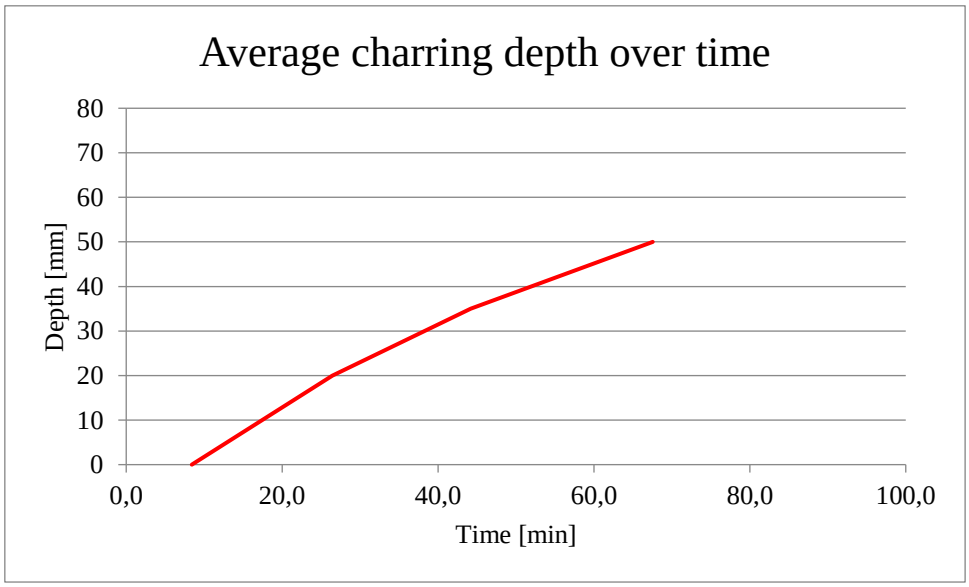

fig. E-20. Average charring depth over time for the MF-2 specimen.

Appendix F – Observational timelines

In this appendix, visual observations from the recorded video material will be presented for all the tests. The screen shots from the video material has been selected after events that has been of interest to the authors. Events such as increase in flames and smoke, charcoal falling and delamination of lamellas. Therefore, some timelines include more pictures than others where not much signs of such events occurs.

Timeline for PUR-A1

Initial stage of delamination

Image of the first lamella in the initial stage of the fire after 16 minutes.

The test with PUR-A1 started to show signs of delamination when a smaller part delaminated after approximately 51 minutes and within a minute later a major part of the first lamella delaminated.

First delamination

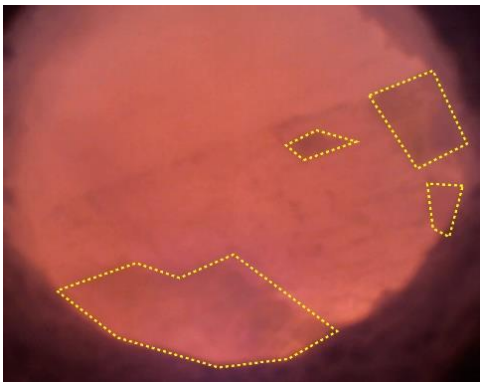

Reignition

Shortly after the first delamination the intensity of smoke and flames increases inside the furnace and reignition of the wood was shown.

Second delamination

After approximately 2 hours and 43 minutes a second layer of the specimens are delaminating from the element.

Timeline for PUR-A2

Initial stage

Initial stage of the first lamella before any major changes occurred. This picture represents the beginning of the test after approximately 17 minutes.

First delamination

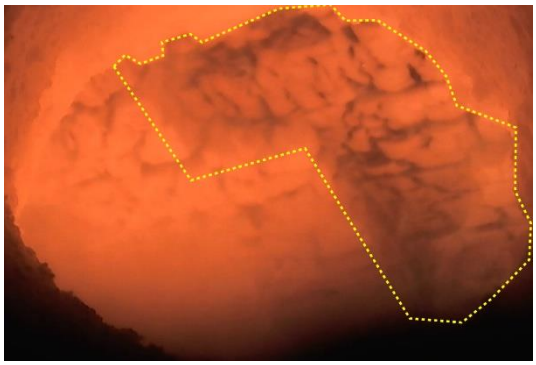

After approximately 42 minutes smaller parts of lamellas are falling off, and 2 minutes later a larger part of the first lamella falls off as well. After this an increase in flames occurred as well as turbulence of gases.

After 48 minutes further delamination of the first lamella occurred. Shortly after this an increased intensity of smoke and flames occurred and more parts of the first lamella were gone.

Second delamination

After a while of low activity on the screen small parts of the second lamella fell of around 2 hours and 48 minutes. The newly exposed wood in the furnace began to burn, contributing to flames and increased glowing on the wood.

Second delamination

After 2 hours and 58 minutes a highly increased intensity of light, glowing parts as well as flames occurred after a period of darkness. On the specimen way up from the furnace observations showed that a larger part delaminated in the down left corner of the picture.

Timeline for PUR-1B

Initial stage

After 17 minutes of the initial stage of PUR-1B the pyrolysis was in progress and the charcoal layer has started to form.

After 41 minutes, a smaller local part of the lamella has fallen off, see mark ups on picture. No major signs of change of the fire development were observed.

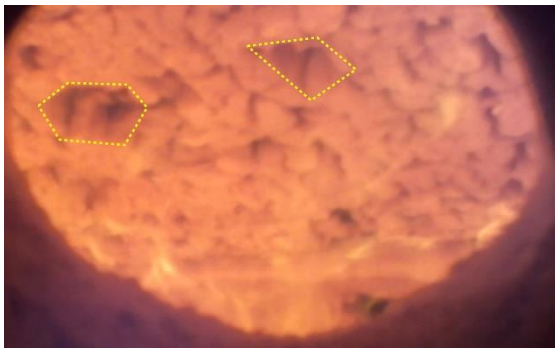

Decay phase

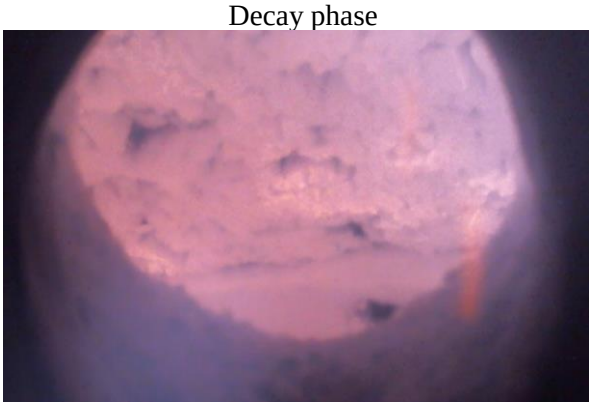

Flaming inside the furnace are no longer visible in the camera, this after 1 hour and 35 minutes. While the brightness inside the furnace was slowly reducing in intensity.

Timeline for PUR-2B

Initial stage

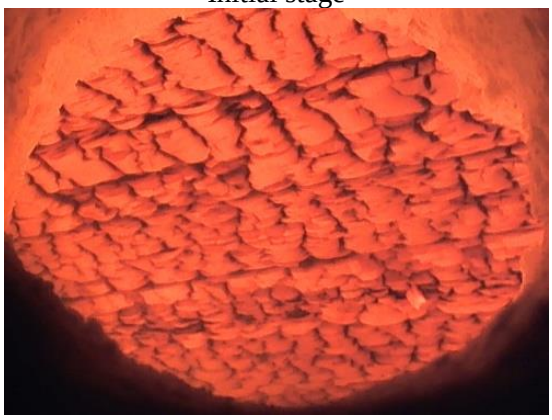

After 17 minutes of the initial stage PUR-2B the pyrolysis was in progress and the charcoal layer has started to form.

Decay phase

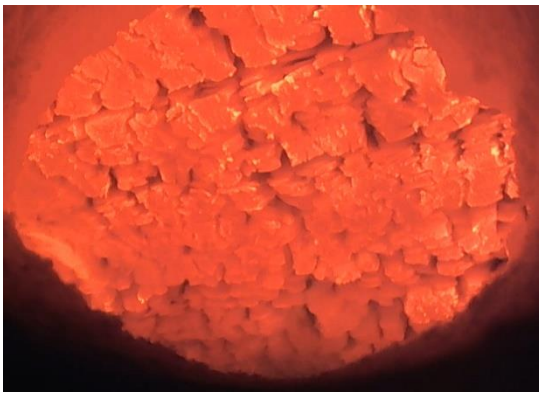

Flaming inside are no longer visible in the camera after 1 hour and 22 minutes. The specimen was still glowing but the brightness was slowly being reduced.

Timeline for PRF-1

Initial stage

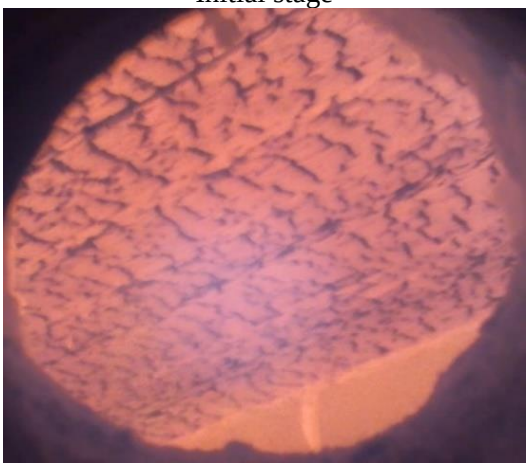

After 15 minutes the initial stage has started to take form. Flames was visible as well as the charcoal layer were in build-up progress.

Small signs of delamination

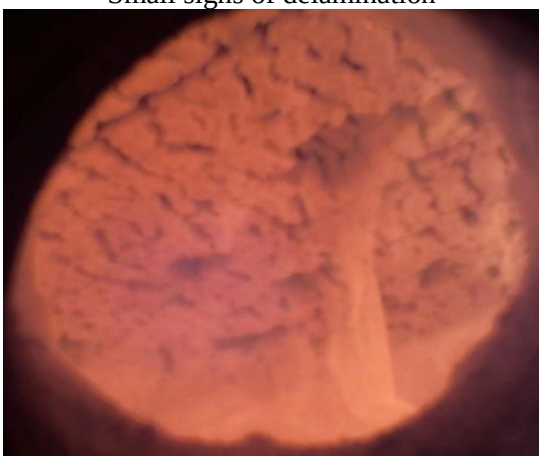

Small signs of delamination was appearing on the specimen when a small piece of the lamella fell off after approximately 40 minutes of time.

Small signs of delamination

After 1 hour and 27 minutes another small piece fell off, in that time period the the video material no longer showed visible flames on the screen and the brightness in the furnace were slowly turning to black.

Timeline for PRF-2

Initial stage

After 16 minutes the initial stage started to show flames within in the screen and the charcoal layer has started to form.

After 1 hour and 25 minutes there were no bigger signs of that delamination had occurred. Only small pieces of charcoal has fallen off. Flames are no longer occurring within the screen and the brightness in the furnace are slowly turning to completely black conditions.

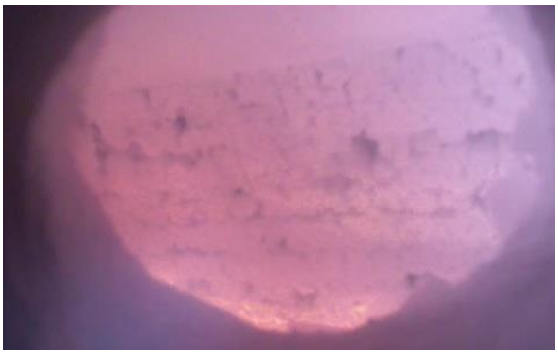

Timeline for EPI-1

Initial stage

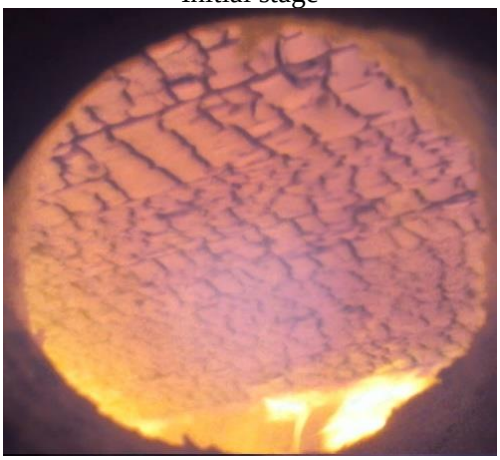

Initial stage of the fire showed the progress of the timber turning into a charcoal layer and a increase in flames, this 16 minutes into the test.

Small local parts of delamination

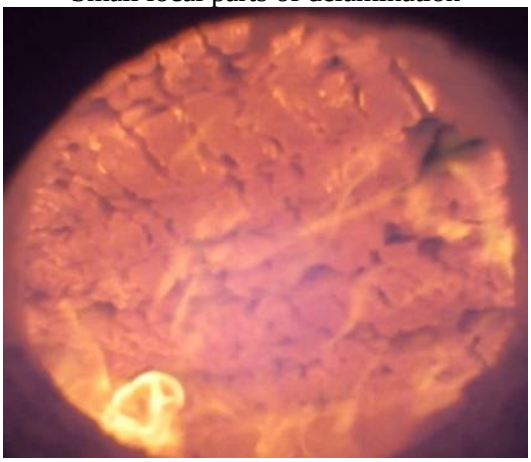

Partly and local signs of delamination of first lamella were shown after 1 hour and 15 minutes. Smaller pieces of charcoal have fallen off.

Decay phase

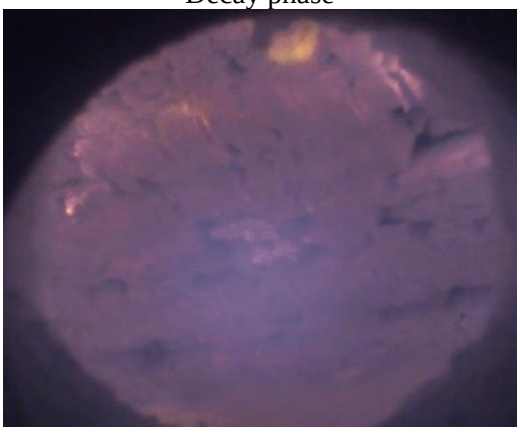

Flames inside the furnace started to decrease in intensity and the light are slowly turning down. This after 1 hour and 33 minutes into the test.

Timeline for EPI-2

Initial stage

The initial stage of the charcoal and fire after approximately 17 minutes.

Small and local parts of the first lamellas started to fall off around 1 hour and 16 minutes.

First stage of delamination

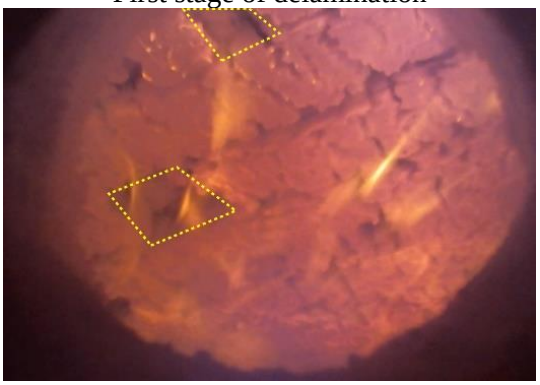

Second stage of delamination

Approximately 1 hour and 30 min into the test a larger part delaminated in the first lamella. This was the last visible stage caught on camera before it became too dark in the furnace.

Timeline for MF-1

Initial stage

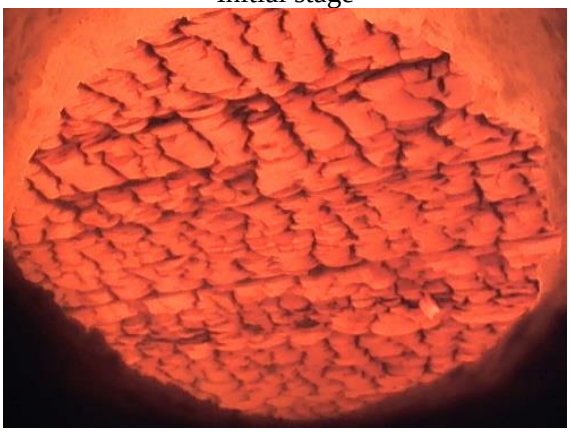

After 18 minutes of the initial stage of MF-1 the pyrolysis was in progress and the charcoal layer has started to form.

Decay phase

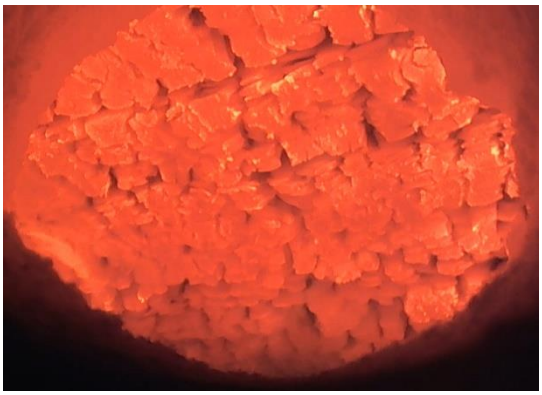

1 hour and 18 minutes into the test the flames are less common in the view of the video material. The specimen was glowing bright but the brightness was slowly turning down and after approximately 1 hour and 40 minutes the specimen are no longer clearly visible in the video until the end of the test.

Timeline for MF-2

Initial stage

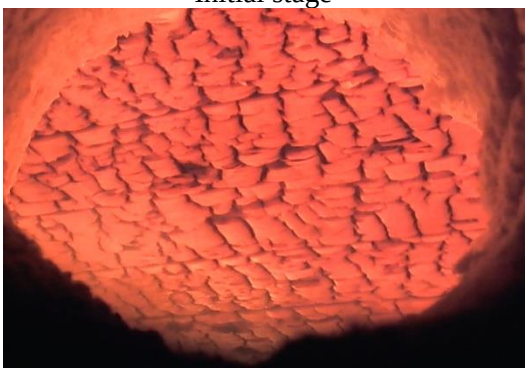

After 16 minutes of the initial stage MF-2 the pyrolysis was in progress and the charcoal layer has started to form.

Smaller pieces falls off

Approximately after 40 minutes a smaller piece delaminated from the lamella. No noticeable change on the fire development were observed.

Decay phase

The brightness inside the furnace were getting lower and slowly turning into a black image, this after 1 hour and 30 minutes.

Appendix G – Photos

In this appendix, a collection of pre- and post-test pictures are presented as well as some pictures of the furnace setup. The pre-test pictures show specimen deviations and defects that could have influenced the experiment outcomes. The post-test pictures show the final state of the specimen after fire exposure, with the charring pattern and damage to the specimen. This is just a small sample of pictures of some of the specimen that the authors deemed more significant and important, and is meant to serve as an overall example of the quality of the specimen as well as the differences in outcome of the experiments. For access to more picture material of individual specimen the authors can be contacted.

Pre-test

fig. G-1. The fire exposed side of specimen PUR-A1. As these specimen were cut from larger original element from the previous full-scale test, the boards of each lamella were not evenly distributed.

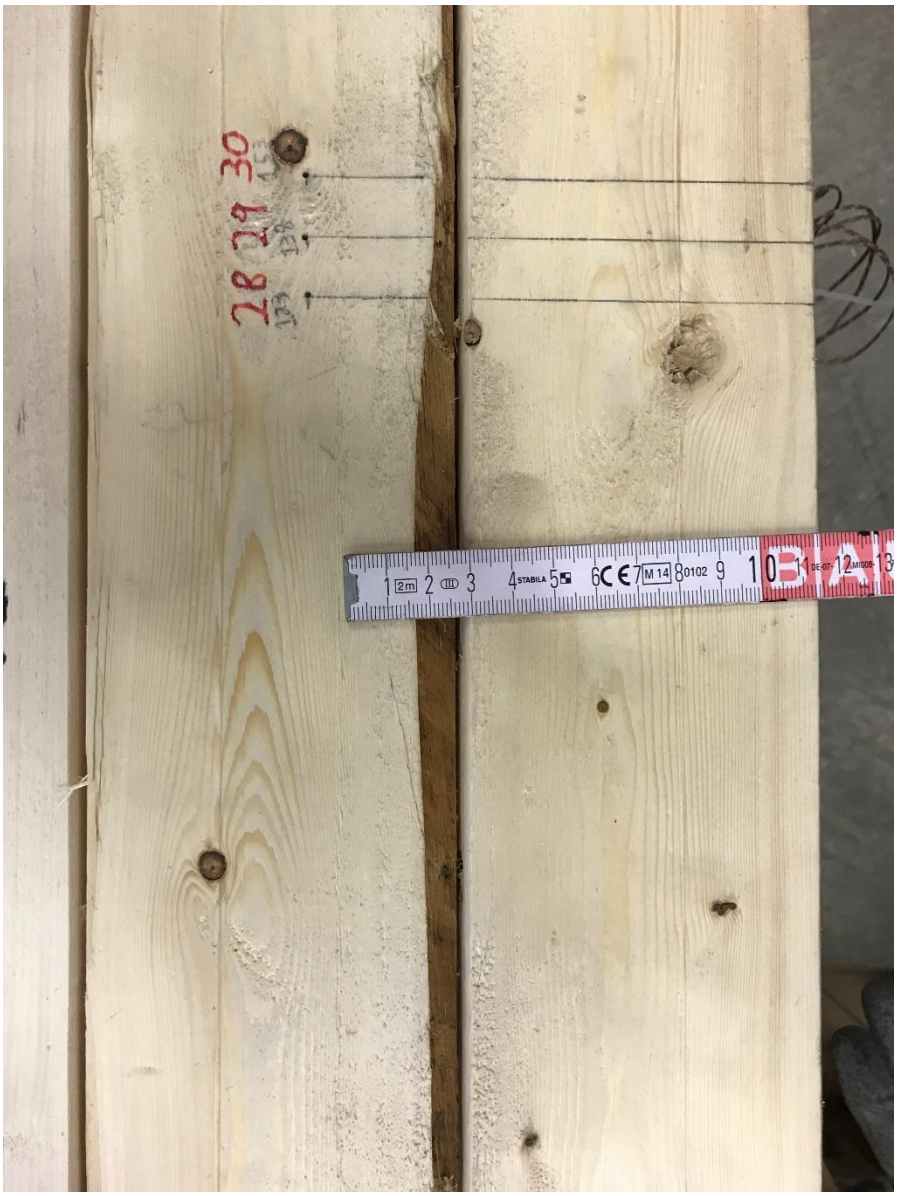

fig. G-2. Top side of EPI-1 specimen. Some boards of the specimen were of very poor quality, with defects such as the one above.

fig. G-3. A thin but long crack in the fire side of the MF-2 specimen.

fig. G-4. A larger crack in between boards of the fire side of the PUR-B1 specimen.

fig. G-5.Fire side of MF-1 specimen. For some specimen, the gaps between some boards of the surface lamellas was quite severe.

fig. G-6. Top side of EPI-2 specimen during experiment. In the initial heating phase of tests, moisture-rich smoke could be observed through the more severe gaps of the top layer of some specimen.

fig. G-7. A board of poor quality in the second lamella from the top of specimen EPI-1, resulting in two openings in the front side.

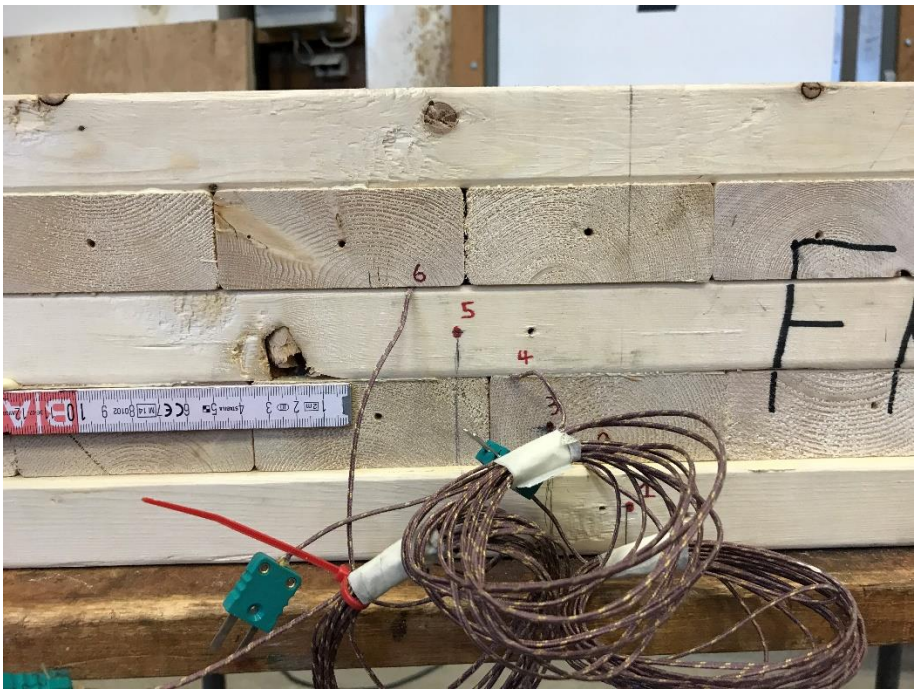

fig. G-8. A larger knot in the third lamella of the EPI-2 specimen.

fig. G-9. Section view of specimen PUR-B2. No specimen was entirely plane shaved, and some were in fact extremely uneven like shown in this picture.

Post-test

fig. G-10. Specimen PUR-A2 the day after test. The entire first lamella is missing, as it delaminated during the test. Larger portions of the second lamella are missing, exposing fresh wood underneath. Some of these pieces delaminated in the furnace, others fell off after removing the specimen from the furnace.

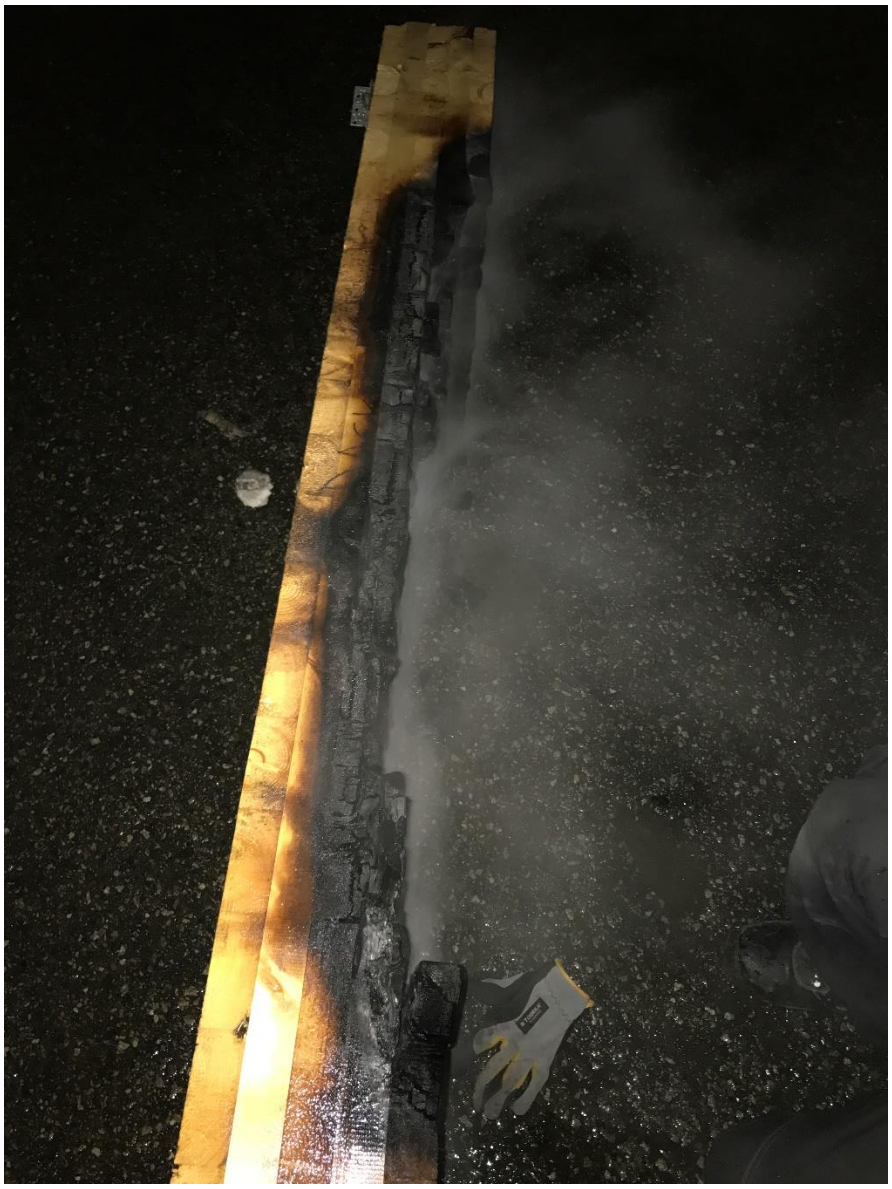

fig. G-11. Specimen PUR-A1 directly after extinguishing of fire. The first lamella is completely gone and delaminated during the test. A second delamination occurred during the test, and most of the second lamella is therefore missing as well.

fig. G-12. The EPI-1 specimen the day after testing. Larger pieces of the first lamella fell off during the test, but complete delamination was not observed.

fig. G-13. The PRF-1 specimen, the day after the test. Very small pieces of char fell off the specimen during the test, but no delamination was observed. Overall the PRF-specimen performed well in the tests, with a steady and predictable fire development.

fig. G-14. Fire side of the MF-2 specimen the day after the test. The MF-specimen, just like the PRF-specimen, performed very well in the tests, and only minimal pieces of char fell off during tests.

Setup

fig. G-15. Front view of the furnace.

fig. G-16. Inside view of the furnace showing burners, observation tube, exhaust as well as a specimen mounted on top of the furnace.

fig. G-17. Typical example for the opening where the test specimens are placed, surrounded by insulation as well as steel beams.

fig. G-18. Steel beams with ceramic insulation placed on the top of the furnace.

fig. G-19. Plate thermometers placed on the furnace door. Missing from the picture is a thermocouple mounted in the vicinity of the plate thermometer collecting data of the gas temperature.

fig. G-20. On the left-hand side of the picture the inflow of air and nitrogen setup can be observed. Next to this setup on the right side the video camera setup can be slightly seen.

fig. G-21. Nitrogen bottles placed on line for easy access and use during execution of the tests.

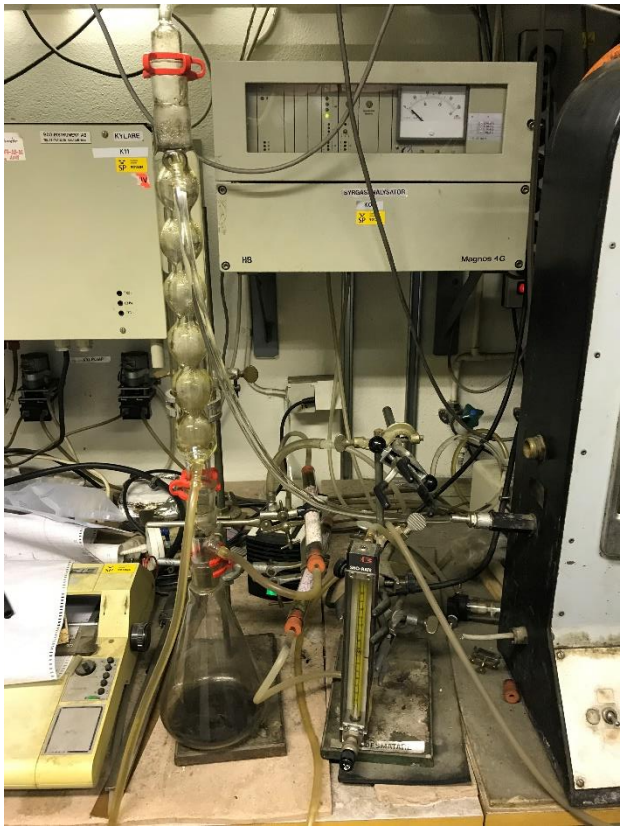

fig. G-22. Measuring equipment for the oxygen level inside the furnace.

fig. G-23. Alar adjusting the burners inside the furnace from a control panel.

fig. G-24. Plastic bags located in front of the furnace for collection of falling charcoal from specimens during lift off from the furnace.

fig. G-25. The head of the heat flux meter.

fig. G-26. Heat flux meter placed in a piece of wood for easy use during the experiments.

fig. G-27. Beam beside the specimen with a hole for the heat flux meter to be mounted in when in the furnace. In this picture Anton is placing a stopper to avoid fire and/or gases to spread up when heat flux meter is not used.

fig. G-28. Location of the heat flux meter while inside the furnace..